Joint Transportation Research Program   Civil Engineering

1-1-2011

Long-Term Behavior of Integral Abutment Bridges

Robert J. Frosch
Purdue University - Main Campus, frosch@purdue.edu

Matthew D. Lovell
Purdue University - Main Campus, mdlovell@purdue.edu

Draft Final Report

FHWA/IN/JTRP-2011/XX

LONG-TERM BEHAVIOR OF INTEGRAL ABUTMENT BRIDGES

by

Robert J. Frosch
Principal Investigator
Professor of Civil Engineering

and

Matthew D. Lovell
Graduate Research Assistant

School of Civil Engineering
Purdue University

The contents of this report reflect the views of the authors, who are responsible for the facts and the accuracy of the data presented herein. The contents do not necessarily reflect the official views or policies of the Indiana Department of Transportation or the Federal Highway Administration at the time of publication. This report does not constitute a standard, specification, or regulation.

Purdue University
West Lafayette, IN 47907
April 2011

ACKNOWLEDGEMENTS

TABLE OF CONTENTS

LIST OF TABLES

LIST OF FIGURES

CHAPTER 1. INTRODUCTION AND BACKGROUND

1.1. INTRODUCTION

Integral abutment bridges, a type of jointless bridge, are the construction option of choice when designing highway bridges in many parts of the country. Traditionally, highway bridges are constructed so the superstructure and substructure are separate units divided by expansion joints (Figure 1.1a). As the structure undergoes expansion and contraction due to volumetric strains caused by temperature, shrinkage, and creep; these joints allow the superstructure to move independently from the rigid substructure. However, because of many issues caused by expansion joints, it is desirable to remove the joints altogether. Rather than providing an expansion joint to separate the substructure from the superstructure, an integral abutment bridge is constructed so the superstructure and substructure are continuous (Figure 1.1b). The abutment is supported by a single row of piles which must account for the longitudinal movement previously accommodated by the joints.

(a) Conventional Construction

(b) Integral Construction
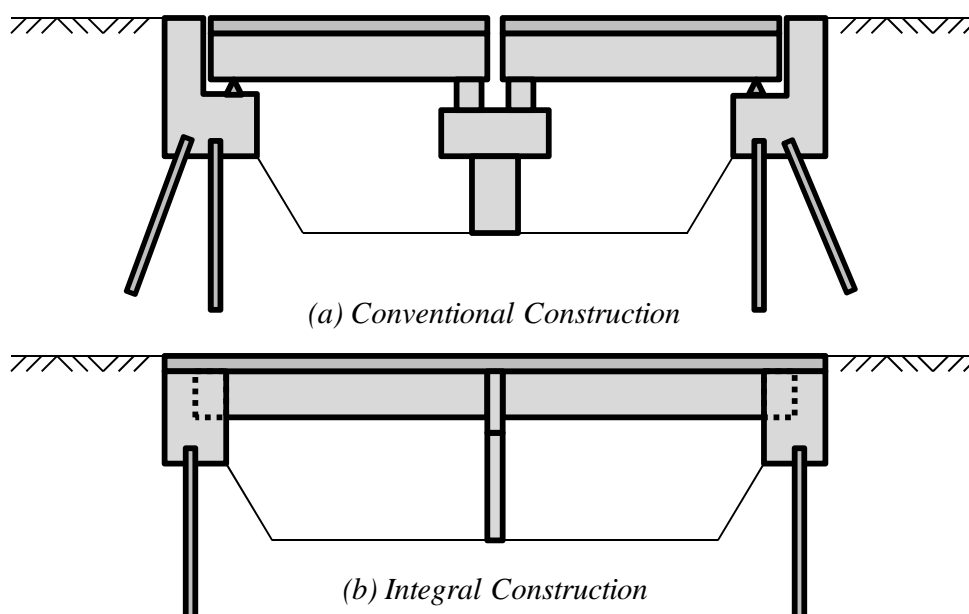
Figure 1.1: Methods of Construction

1.2. OVERVIEW OF INTEGRAL ABUTMENT BRIDGES

The primary advantage of an integral abutment bridge is that it is jointless (expansion joints are eliminated). The elimination of these joints removes the potential for corrosion of the superstructure, bearings, and substructure as caused by joint leakage and lowers both the initial cost of construction and overall life-cycle costs (Kunin and Alampalli 2000). Because a jointless bridge is seamless from end to end, the potential for snow-plow damage is eliminated, and the riding quality is dramatically improved as compared to the conventional method of construction. In addition, studies have shown that integral abutment bridges provide improved seismic performance (Talbott 2008; Wasserman and Walker 1996) and tend to produce a more efficient and simpler design (Burke 1993).

Although integral abutment bridges provide many advantages over jointed bridges, a variety of issues must be considered when designing these types of structures. Once the bridge becomes continuous during construction, expansion and contraction of the deck must be accommodated by the abutment and supporting piles rather than through expansion joints. This movement, which is a function of bridge length, causes high lateral displacement demands on the supporting piles. Traditionally, the demand on the piles has been estimated by the following equation:

$$\Delta L = \alpha(\Delta T)L \tag{1.1}$$

where:

ΔL = temperature induced change in bridge length, in.

α = coefficient of thermal expansion, 1/°F

ΔT = change in temperature, °F

L = total length of structure, in.

As the bridge undergoes seasonal cycles, the movement also causes soil pressure to develop behind the abutment. In addition to the development of lateral earth pressures, settlement of the soil behind the abutment can occur causing structural distress of the approach slab (Arsoy 1999). It is also unclear if structures with large skew angles tend to move out-of-plane due to soil-structure interaction effects. Because of this complex behavior, engineers have historically relied on rough judgment and experience to design these structures, rather than firm analytical approaches. Designs have been based on conservative limits of skew and length which differ

from region to region. More recently, studies have been conducted to expand the understanding of the behavior of these structures.

1.3. Previous Research

It is apparent that the parameter controlling the geometric limitations imposed on integral abutment bridges is the lateral deformation capacity of the supporting abutment piles. Correspondingly, much of the research conducted regarding integral abutment bridges is focused on various aspects affecting the behavior of the piles. Research has included the development of modeling techniques for the behavior of piles and interaction with surrounding soil (Greimann et al. 1984, Abendroth et al. 1989), full scale component testing for typical pile sections to determine lateral deformation and strength capacity (Greimann et al. 1987, Arsoy et al. 2002, Chovichien 2004, Talbott 2008), development of methods to analytically represent the abutment soil and describe corresponding effects on the structural system and demands on the piles (Duncan and Mokwa 2000, Rollins and Cole 2006), and full scale monitoring of in-service integral abutment bridges (Girton et al. 1993, Lawver et al. 2000, Chovichien 2004, Brena et al. 2007, Talbott 2008). To expand on the aforementioned research, the following section briefly highlights selected activities and findings of the four mentioned areas of investigation.

1.3.1. Analytical Modeling of the Behavior of Piles

Greimann et al (1984) conducted research focused on developing analytical methods to model piles in integral abutment bridges. The worked involved developing Winkler soil springs to represent soil surrounding the piles. As a result of his work, methods were developed to model piles loaded laterally in varying densities of sand and stiffnesses of clay.

Abendroth et al. (1989), building on the work accomplished by Greimann et al. (1984), produced a method to determine an equivalent column to represent the effects of soil surrounding the pile on the pile's behavior. Using this simplified modeling technique, designers can create simplified models to represent the behavior of piles in integral abutments for varying soil conditions. Methods for elastic and inelastic analysis are provided.

1.3.2. Experimental Component Testing of Pile-Abutment Connection

To follow up the research conducted by Greimann et al. (1984), Greimann et al. (1987) conducted one-tenth scale and full scale pile field tests. The experiments involved lateral loading

of piles and measuring strains and displacements of the piles. The study resulted in confirmation and modification of analytical modeling guidelines.

Arsoy et al. (2002) conducted a series of tests on three different potential pile sections: one HP10x42, one 14 in. concrete filled tube (CFT14), and one 12 in. prestressed concrete pile. The test program subjected the piles to lateral load cycles caused by realistic displacements as caused by annual temperature differentials for a period of 75 years. The purpose was to evaluate the expected life of integral bridges under typical working conditions. The study recommended that HP piles be used in weak axis bending (weak axis perpendicular to the centerline of structure) to limit the stresses imposed on the abutment. For the displacement demand, the HP pile showed no degradation over the simulated 75 year period.   Prestressed concrete piles were not recommended for use in integral abutment bridges.   The test setup was unable to accommodate the CFT 14.

Chovichien (2004) conducted full scale tests of several pile sections that are typically used in integral abutment bridges. The pile sections included six HP sections and three concrete filled tubes (CFT). The HP piles were tested in weak axis, strong axis, and 45° axis bending. The sections were tested for lateral deformation and strength capacity.   Using additional analytical modeling, Chovichien (2004) developed maximum lateral deformation recommendations for typical pile sections and various soil conditions used in integral abutment bridges. In general, 2 in. was determined as the maximum lateral deformation capacity for typical pile sections used in integral abutment bridges. Chovichien (2004) also recommended that piles be used in weak axis bending.

Talbott (2008) built on the work conducted by Chovichien (2004) by testing additional HP pile sections in the same manner. It was determined from these additional tests that two damage limits could be defined for HP sections: zero damage limit and acceptable damage limit. The zero damage limit corresponds to allowable lateral deformation that corresponds to no damage of the pile. This limit corresponds and agrees with the 2 in. that was defined by Chovichien (2004). The acceptable damage limit corresponds to damage that results in less than a 5% loss of load carrying capacity. It was determined that this corresponds to an allowable deformation for HP sections typically used in integral abutment bridges of 4 in.

1.3.3. EFFECTS OF ABUTMENT SOIL

Duncan and Mokwa (2000) performed an investigation of current models for predicting passive earth pressure and their applicability to abutments and laterally loaded pile caps. Based

on the study, it was determined the best method for predicting the lateral earth pressure was the log-spiral method. In addition, Duncan and Mokwa developed a method to model the load path of passive earth pressure so a designer could determine pressures in between static and full passive based on displacement into the fill.

Rollins and Cole (2006) have also investigated the cyclic lateral load behavior of pile caps. Their work involved testing of seven full scale pile caps. Four of the tests included backfill at different compacted levels. The results of their research provide insight on methods required to model backfill material and is applicable to integral abutment bridges.

1.3.4. FULL-SCALE MODELING OF INTEGRAL ABUTMENT STRUCTURES

Girton et al. (1993) conducted a field investigation of two integral abutment structures for a period of two years: the Boone River Bridge, a 324.5 ft prestressed girder bridge with a 45° skew and the Maple River Bridge, a 320 ft steel-girder bridge with a 30 degree skew. The research program involved monitoring the longitudinal displacement of the abutments, temperatures of the deck, and pile strains; however, direct measurements were not made regarding transverse movements. A longitudinal analytical model (simple frame) was developed using the equivalent column methods developed by Abendroth (1989), and the results were compared with those measured in the field. Additionally, a transverse model (simple frame) was coupled with strain measurements on selected piles to predict transverse movements. It was determined that the equivalent column method proposed by Abendroth (1989) adequately represent the longitudinal behavior of the pile. Girton et al. (1993) also notes that a designer should be careful to account for lateral movement of a skewed structure, but recommendations to determine a magnitude for transverse movement are not provided.

Lawver et al. (2000) conducted a field monitoring program of a 216.5 ft prestressed girder bridge with no skew for roughly two and a half years. The structure was highly instrumented to monitor temperature, lateral displacement of the abutment, pile strains, earth pressure, and pier movement. A live load test was also conducted as a part of the investigation. Many observations were made regarding the behavior of integral abutment bridges. Of particular interest, it was noticed that the abutment experienced a net inward movement for each annual cycle.

Brena et al. (2007) conducted a three year monitoring program of a 270 ft steel plate-girder bridge with zero skew. The structure was highly instrumented with pile strain gages, inclinometers, and earth pressure cells. Based on the investigation, various conclusions were

developed on the behavior of integral abutment bridges. It was determined that abutments experience rigid body motion where both rotation and translation occur. This behavior results in lower moments in piles that are typically designed fixed against rotation. It was also noted that the bridge experienced 60% of the displacements predicted by unrestrained thermal shrinkage.

A field investigation performed by Chovichien (2004) included three integral abutment structures. The monitoring program included a 152 ft steel-girder bridge with 25° skew, a 367 ft prestressed girder bridge with 8° skew, and a 990 ft prestressed girder bridge with 13° skew. The monitoring program for each of these structures began in Summer 2000, Summer 2003, and Spring 2000, respectively. Talbott (2008) continued the monitoring program for the 367 ft prestressed girder structure. These investigations highlighted general behavior of integral abutment structures including longitudinal movement of abutments, lateral earth pressures, and pile deflected shapes. The first two structures have continuing monitoring and will be included and discussed further as a part of this study.

1.4. INDOT STANDARDS

Because, the standards of integral abutment construction have traditionally been based on engineering judgment, the design practices of integral abutment bridges vary from state to state. This investigation will focus on the recommendations by the Indiana Department of Transportation (INDOT). According to the Indiana Design Manual (2010) (Appendix E), Indiana requires that integral abutment bridges be used provided the geometric limitations listed in Table 1.1 are met:

Table 1.1: INDOT Limitations for Integral Abutment Bridges

Structure Type	Highway Alignment Across Bridge	Maximum Skew (degrees)	Maximum Bridge Length (ft)	Maximum Zero Point (ft)
Reinforced Concrete Slab	No Restrictions	No Restrictions	500	250
Structural Steel	Tangent Only*	30	500	250
Prestressed Concrete	No Restrictions	30	500	250

The horizontal alignment may be curved as long as curved beams are not used.

Upon meeting these limitations, integral abutment bridge design becomes simple; requiring the designer to following some basic recommendations. The supporting foundations is required to be a single row of piles, of which, only two types can be used: steel H-piles oriented in weak axis or concrete filled steel pipe piles. The piles, provided the structure meets the above limitations, can be designed considering only gravity loads. To design the interior bents, it is assumed that longitudinal forces are negligible and can be ignored. Finally, to aid in the design of the abutment, INDOT has provided two design details. In Detail "A" (Figure 1.2), the superstructure rests directly on the foundation piles prior to the continuous casting of the deck and abutment. In Detail "B" (Figure 1.3), the abutment is cast in two segments. A "pile cap" is first constructed, and the beams rest on temporary bearings. A second lift of the abutment is poured continuously with the deck. As long as the proposed structure meets the geometric limitations, virtually no other considerations need to be made regarding the design of these structures. If a structure is desired to be an integral abutment bridge but does not meet the geometric limitations, exceptions can be provided as follows:

"The maximum length indicated may be increased, subject to approval by the Structural Services Office manager, if a rational analysis of induced pile loads indicates that the piles are not overloaded." (INDOT Design Manual 2010).

While exceptions to the general limitations are allowed, no guidance is provided as to what is considered a rational analysis. Furthermore, there is uncertainty in the design community as to what is required to properly analyze an integral abutment bridge.
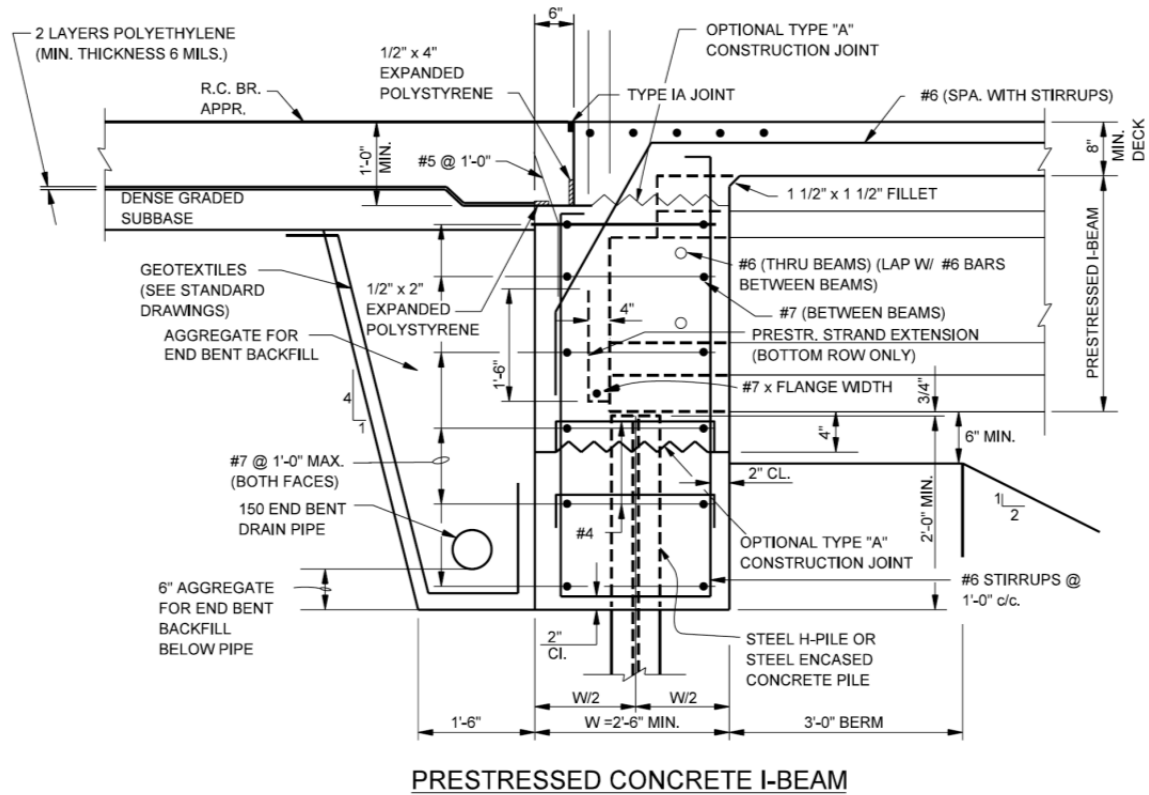
Figure 1.2: INDOT Suggested Detail "A"
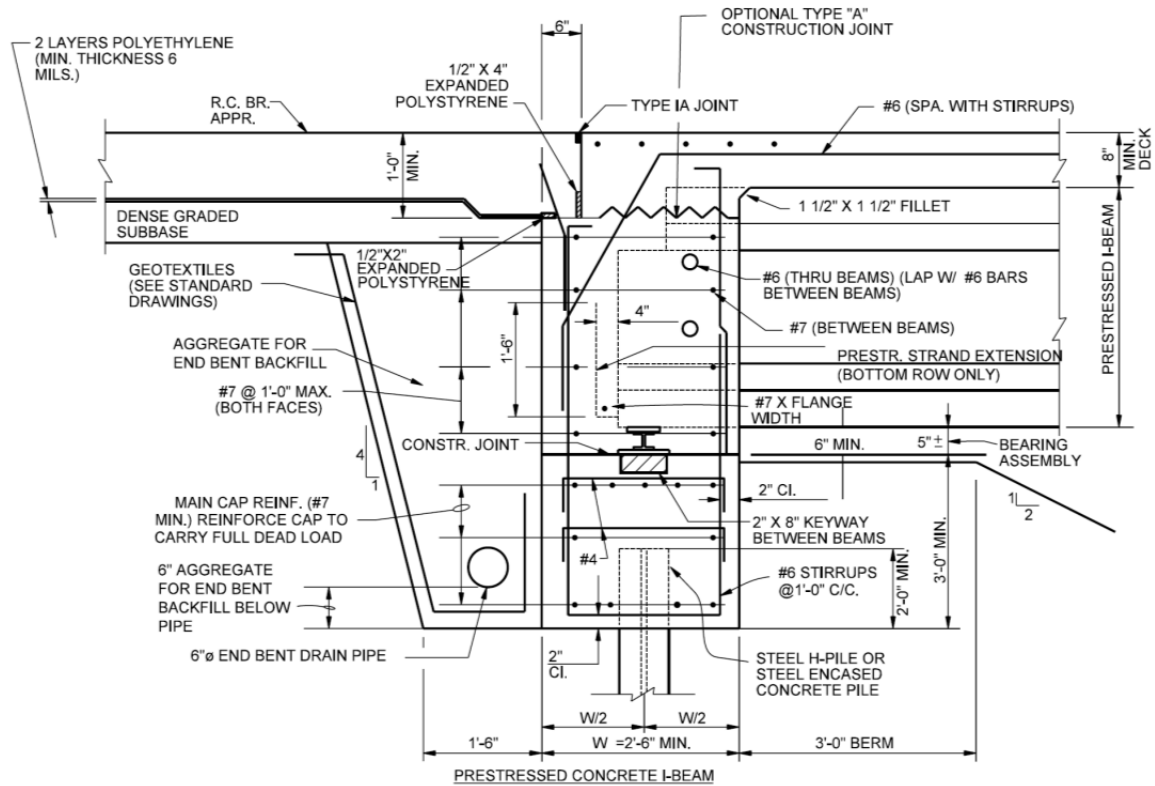
Figure 1.3: INDOT Suggested Detail "B"

1.5. LIMITATIONS OF CURRENT KNOWLEDGE

While considerable work has been accomplished to-date, many questions remain regarding the behavior of integral abutment bridges, specifically the deformation demand for the supporting piles. In particular, a large gap exists in the understanding of the long-term behavior of integral abutment bridges and corresponding demand on the supporting piles. Nearly all field studies involving monitoring the behavior of integral abutment bridges have been short term, less than 3 to 4 years. One particular unknown regarding long-term behavior involves the effects of the build-up of lateral earth pressure. It is commonly believed that as the bridge cycles through seasonal movements, soil pressures will continue to build behind the abutments. This phenomenon, known as ratcheting (Horvath 2004), causes the abutments to creep inward resulting in a permanent shortening of the bridge. There is concern that this phenomenon may cause a buildup of stresses high enough to cause structural distress.

Additionally, a great deal of work has been conducted to determine the capacity of piles, but the demand imposed on the piles is relatively unknown. Typically, the demand imposed on

the piles is simply assumed to be equivalent to unrestrained thermal shrinkage of the bridge superstructure. While this assumption may appear to be conservative, this method does not account for the potential of soil ratcheting. Furthermore, the effects of skew are unknown and are not accounted for using this procedure. Therefore, the long-term lateral deformation demand imposed on the abutment piles must be understood to adequately design these structures.

1.6. OBJECTIVE AND SCOPE

The advantages provided by the use of integral abutment bridges lends to a desire for their extended use and applicability. However, the long-term effects, specifically those of skew, must be understood. Therefore, the objective of this study is to develop an understanding of the long-term behavior of integral abutment bridges such that their use and applicability can be extended and rational design models can be developed. To that end, the following research will be conducted:

- Evaluate the effect of bridge length on the long-term behavior of integral abutment bridges including investigation of the ratcheting mechanism.
- Evaluate the effect of bridge skew on the long-term behavior of integral abutment bridges.
- Develop design recommendations that define geometric limitations (length and skew) of this bridge type.
- Develop analysis procedures that properly model short-term and long-term behavior.

CHAPTER 2. FIELD MONITORING PROGRAM

2.1. INTRODUCTION

      To understand the in-service behavior of integral abutment bridges, a field monitoring program was implemented consisting of three structures: Southbound I-65 over SR-25, SR-18 over the Mississinewa River, and US-231 over AEP Railway Spur (Table 2.1). These structures were highly instrumented to determine the movement of the abutments when subjected to seasonal volumetric strains. This chapter contains a description of the three structures, explanation of each corresponding instrumentation plan, and results of the collected data. Appendix A contains selected drawings from the plans for each of the three structures.

Table 2.1: General Bridge Details

	Southbound I-65 over SR-25	SR-18 over Mississinewa River	US-231 over Railway Spur
Total Length (ft)	152	367	221
Span Lengths (ft)	2@76	62, 3@81, 62	69.5, 82, 69.5
Skew Angle (deg)	25	8	33.8
Girder Type	W36x150	Prestressed Concrete Bulb Tee	Prestressed Concrete Type III I-Beams
Number of Girders	7	5	7
Pile Type	HP12x53 / 14.5" Steel Pipe Pile	14" Steel Pipe Pile	14" Steel Pipe Piles
Number of Piles	6 HP / 4 Pipe Each Abutment	5 Each Abutment	7 Each Abutment
Date Instrumented	Summer 2000	Summer 2003	Fall 2006

2.2. SOUTHBOUND I-65 OVER SR-25

      INDOT Bridge #I-65-176-5543C (I-65 over SR-25) in Tippecanoe County was selected to investigate the general behavior of integral abutment bridges. It is located in Lafayette, IN, 15 miles from Purdue University. The bridge (Figure 2.1) is one of the first structures to be instrumented to monitor long-term behavior of an integral abutment bridge. In late 1999 and

early 2000, the structure was impacted, and several girders were damaged. During the rehabilitation, it was decided that the superstructure would be replaced, raised, and made integral with the supporting abutments. During this conversion, an instrumentation plan was developed and implemented to specifically investigate the daily and seasonal behavior of the end bent (Durbin 2001). Because the structure is within the geometric limitations as defined by the Indiana Design Manual, it is an excellent candidate to investigate general behavior of integral construction.

The structure is 152 ft in length consisting of two equal spans. The superstructure is built on a 25 degree skew with respect to the substructure, and seven W36x150 girders support an 8 in. deck. An elevation and plan view of the structure are shown in Figure 2.2 and Figure 2.3 respectively.

Figure 2.1: Northbound I-65 over SR-25
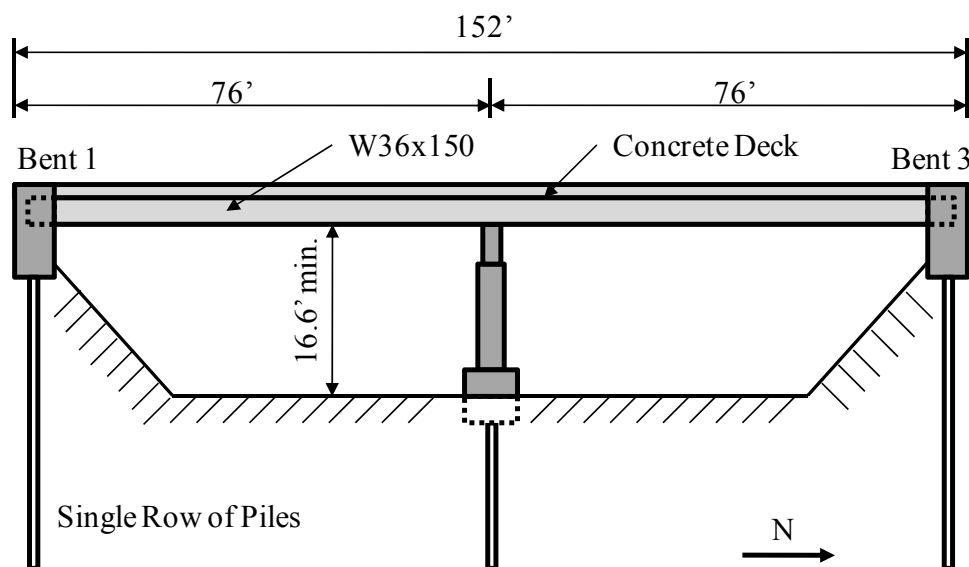
Figure 2.2: Elevation View of Southbound I-65 over SR-25

(Durbin, 2001)
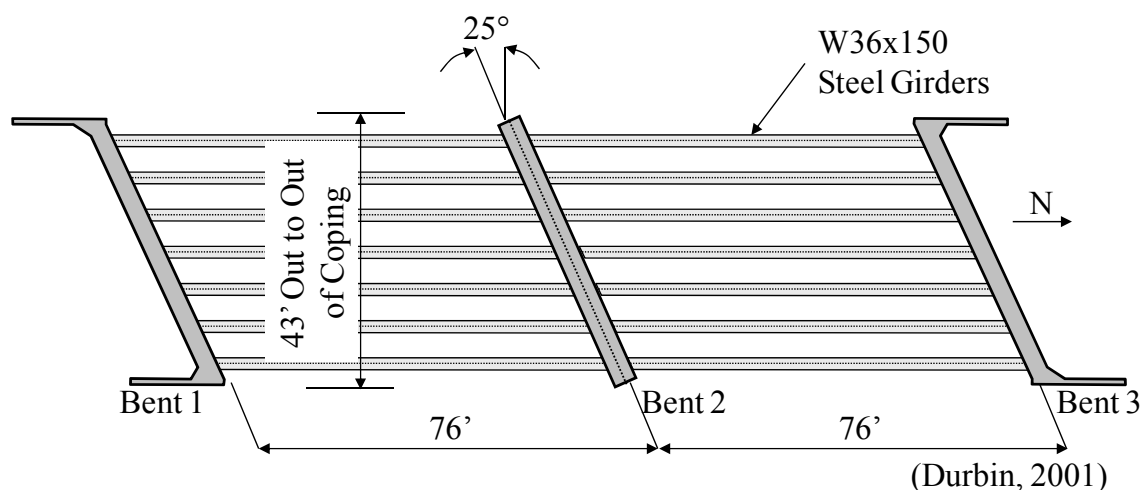
Figure 2.3: Plan View of Southbound I-65 over SR-25

Because the structure was converted to an integral abutment, the abutments have unique features. Each abutment is supported by two types of piles: six new HP12x53 piles oriented along the axis of the bent (Figure 2.5) and four existing 14.5 in. diameter steel pipe piles with a wall thickness of 0.25 in. (CFT 14.5x0.25) filled with concrete. The piles have an approximate length of 42 ft. Soil boring information, pile design, and pile driving records are presented in a separate report by Chovichien (2004). A typical cross section of the abutment and a plan view of the location of the separate piles are shown in Figure 2.4 and Figure 2.5, respectively.
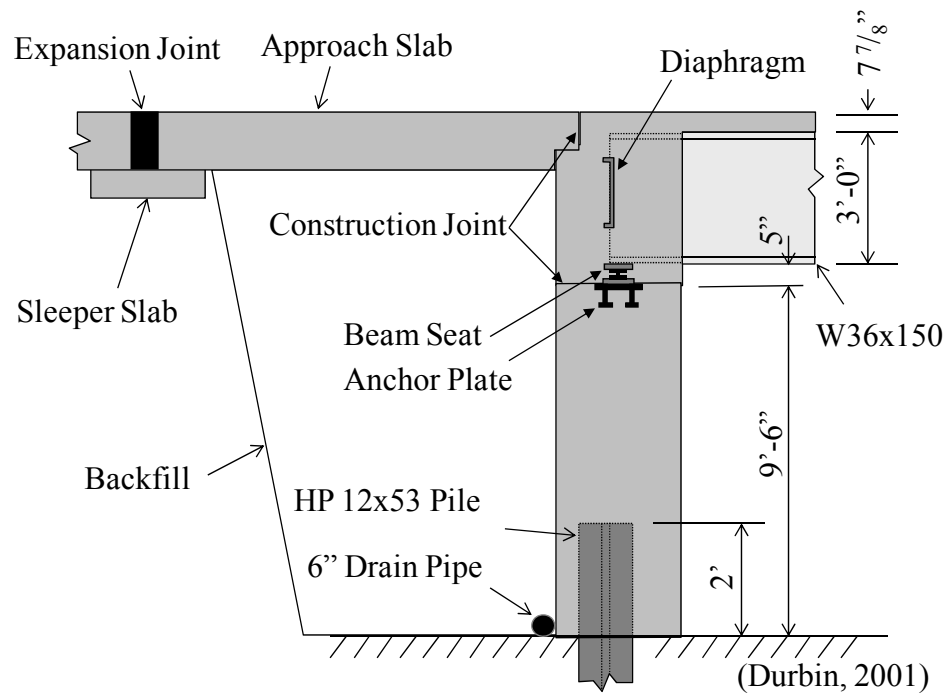
Figure 2.4: Typical Cross-section of I-65 over SR-25 Abutment
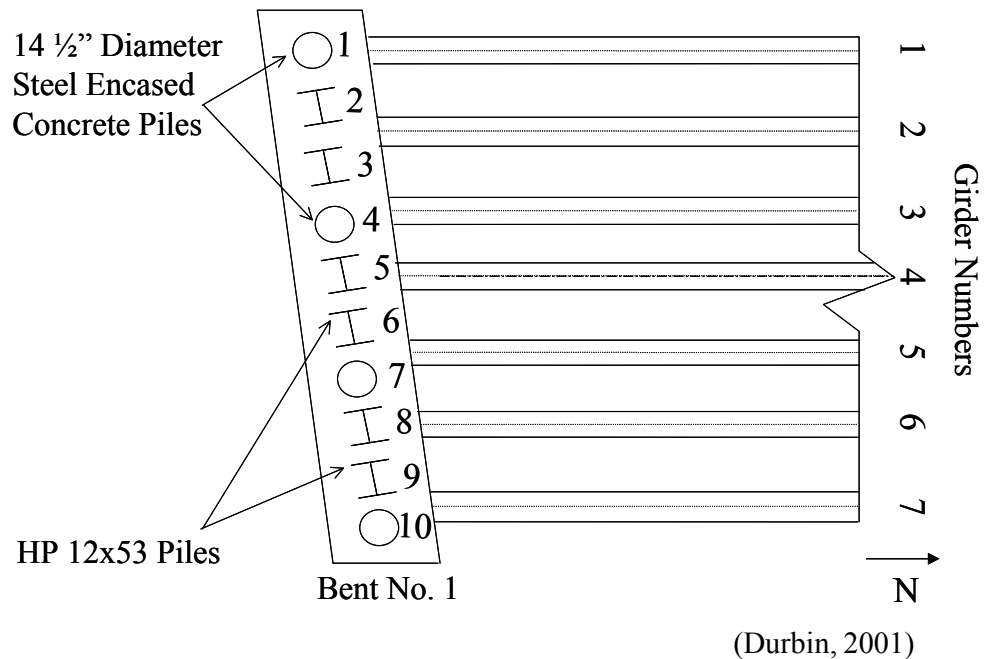
Figure 2.5: Plan View of Location of Piles for I-65 over SR-25

2.2.1. STRUCTURAL MATERIALS

2.2.1.1. CONCRETE

The structure was constructed in two phases: the substructure and the superstructure. The abutment was cast in two separate lifts in which the first lift was comprised of the pile cap supporting the beams and the second was cast continuously with the deck. The mixes for the first and second cast followed general INDOT practice and were INDOT Class A concrete ($f_c{}' =$ 3500psi) and INDOT Class C ($f_c{}' =$ 4000psi), respectively.

2.2.1.2. PILES

Each abutment is supported by a single row of ten piles. Four steel pipe piles filled with concrete (CFT14.5x0.25) were retained from the previous structure. Information regarding the material makeup of these piles was unable to be located. It is assumed, according to standard INDOT practice, that the piles comply with ASTM A252, Grade 2 or 3. The six newly installed piles are HP12x53 and complied with AASHTO M183 and ASTM A6.

2.2.2. INSTRUMENTATION

To understand the behavior of the Southbound I-65 over SR-25 structure, an instrumentation plan was implemented to monitor ambient temperature, abutment movement, pile strains, and lateral earth pressure.

2.2.2.1. ABUTMENT INSTRUMENTATION

The primary focus of this investigation was to measure the movement of the south abutment. To achieve this objective, the abutment was instrumented with linear potentiometers to measure longitudinal and transverse movement of the abutment, strain gages on selected piles at the base of the abutment to measure biaxial bending of the piles, strain gages at the interface of the girders and abutments to determine bending stresses, and earth pressure cells to measure lateral earth pressure. The locations of these instruments are shown in Figure 2.6, and the cross section A-A is shown in Figure 2.7. Information regarding specific gages is provided by Durbin (2001).
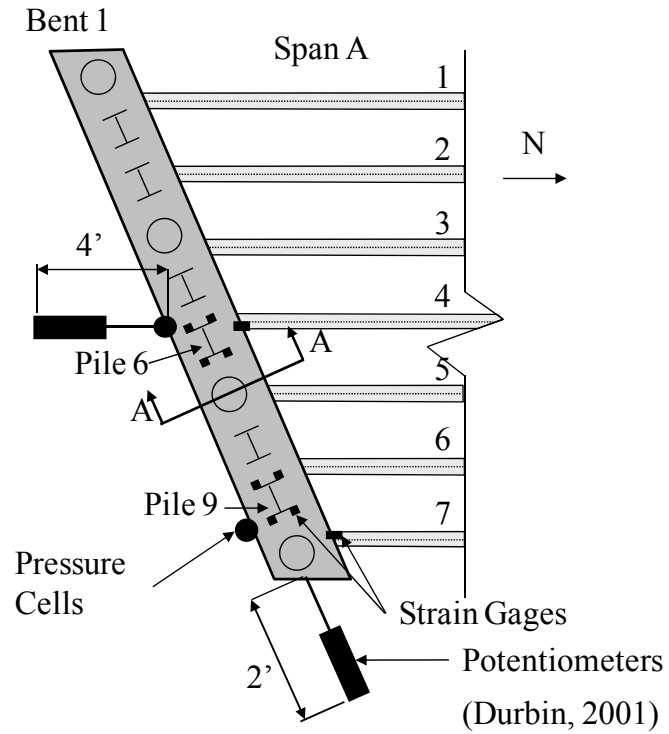
Figure 2.6: Plan View of I-65 over SR-25 Instrumentation Plan
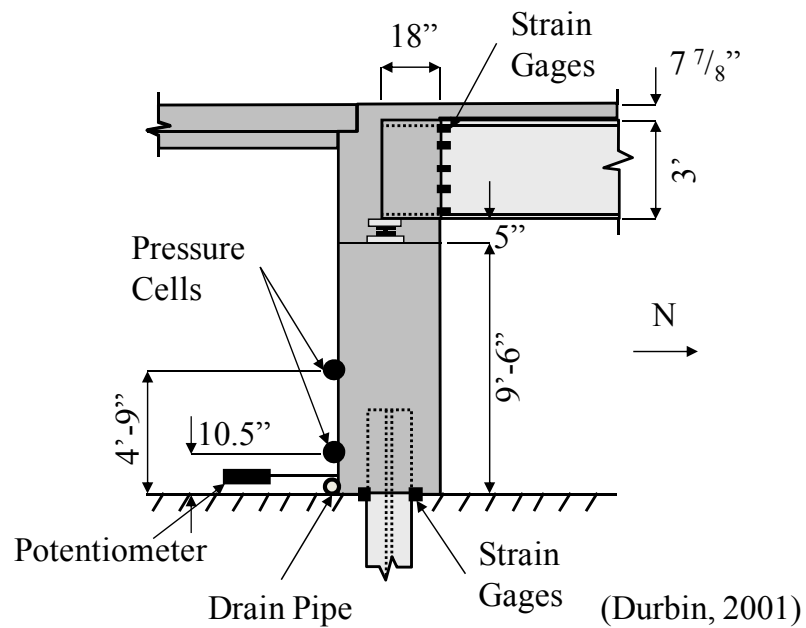
Figure 2.7: Cross-section A-A of I-65 over SR-25 Instrumentation Plan

2.2.3. DATA COLLECTION

A Campbell Scientific model CR10X datalogger with two AM416 multiplexers was used as the data acquisition system for this structure. The program was set to collect readings every hour beginning in September of 2000. Initial readings for all gages were taken at the beginning of the monitoring program and readings have continued from September 2000 thru February 2010.

2.2.3.1. PROBLEMS

During the life of this monitoring program, several problems have occurred with the data collection system:

- The earth pressure cells located on the east side of the abutment produced readings that were erroneous from the time of construction. The earth pressure cells that remain are located in the center of the abutment: one 4'-9" above the base of the abutment (Pressure Cell #1) and the other 10.5" above the base of the abutment (Pressure Cell #3).
- A power outage occurred in May of 2002. Because the initial values were stored on the system, all initial readings were lost. Initial readings, therefore, are estimated.
- The linear potentiometers produced erratic data. In February 2005, readings for these instruments were discontinued, and data was discarded.
- In February 2005, the temperature record was inadvertently discontinued.
- Nearly all of the strain gages on the piles have malfunctioned.
- In January 2006 and July 2007, the program for the data acquisition system was rewritten in an attempt to correct noise issues. The measured values of the recorded earth pressure show a significant quantitative change in January 2006.
- In May 2007, an ambient temperature gage was installed to reinitiate the temperature record.

2.2.4. RESULTS

Due to issues encountered in the monitoring program of I-65 over SR-25, much of the data collected is not useable for analysis. However, the temperature records and earth pressure readings can be used to explain some of the general behavior of this structure.

2.2.4.1. TEMPERATURE

  Ambient shade temperature was collected using a thermocouple placed underneath the structure (Figure 2.8). Though there is a break in the collected temperature record, the record is shown to be consistent. Table 2.2 shows critical temperature values including construction temperature, max high, max low, average summer temperature, and average winter temperature.
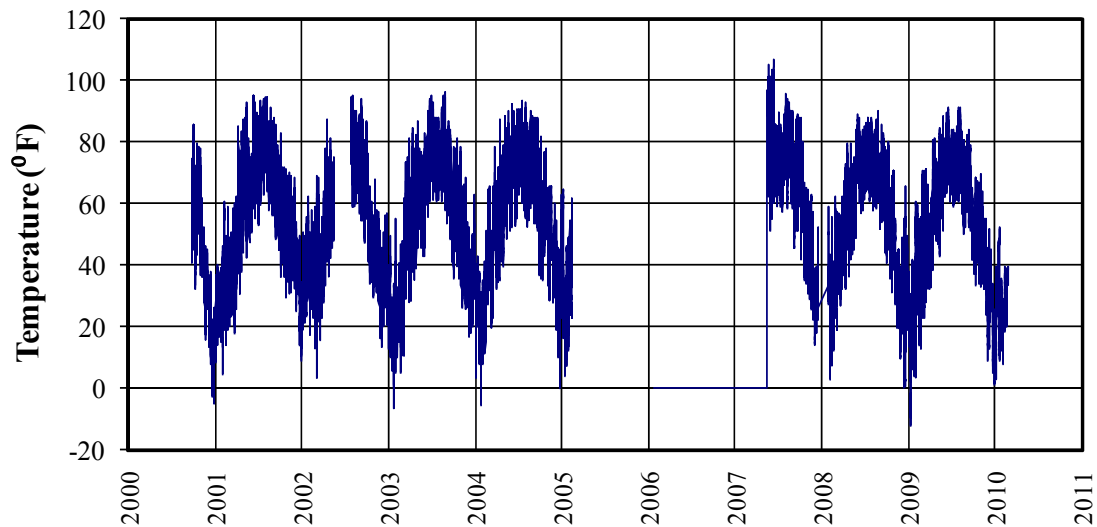
Figure 2.8: I-65 over SR-25 Temperature Record

Table 2.2: Critical Temperature Records for I-65 over SR-25

Record	Temperature (°F)
Construction Temperature	58
Average Summer Temperature	90
Average Winter Temperature	10
Maximum High Temperature	107
Maximum Low Temperature	-12

2.2.4.2. EARTH PRESSURE

  Lateral earth pressure was collected to determine the effect of the backfill on the abutment. Figure 2.9 shows the location of the two functioning gages. Because the initial values were lost and a significant change occurred in the magnitude of pressure upon the updating of the data acquisition program in January 2006, quantitative results should be met with some skepticism. However, the general behavior of the pressure record is considered to be valid. The

collected values shown are assumed to be qualitative. The pressure records for the two pressure cells are shown in Figure 2.10 and Figure 2.11, respectively.
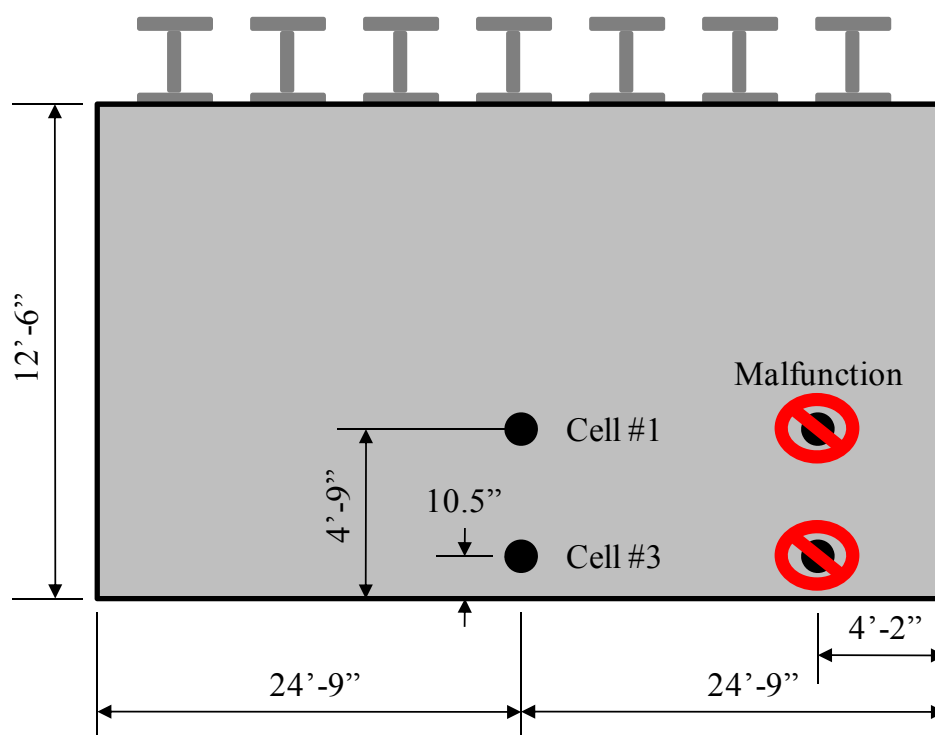
Figure 2.9: Abutment Pressure Cell Locations for I65 over SR-25
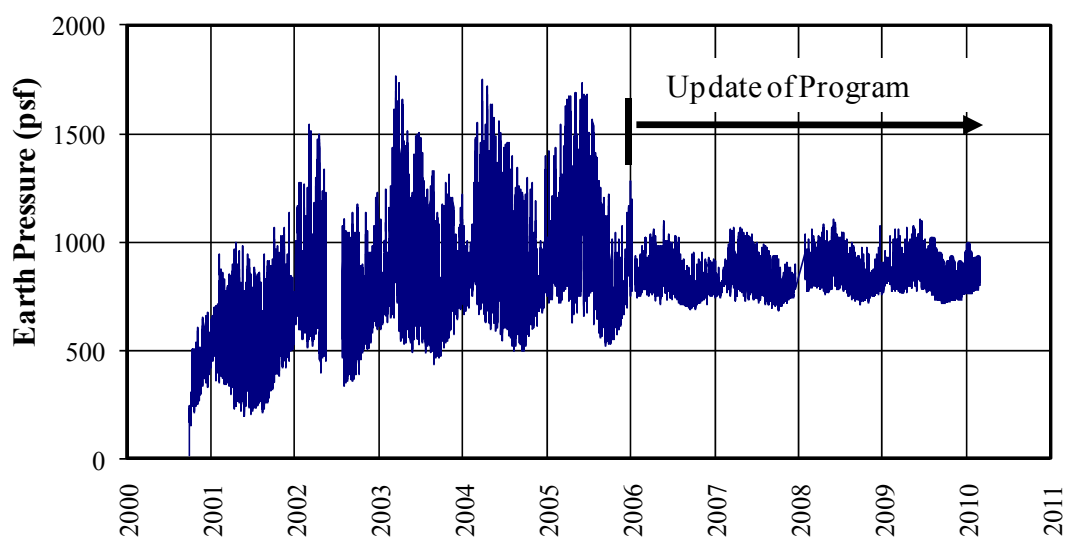
Figure 2.10: Record of Pressure Cell #1 – Center / Top of I-65 over SR-25
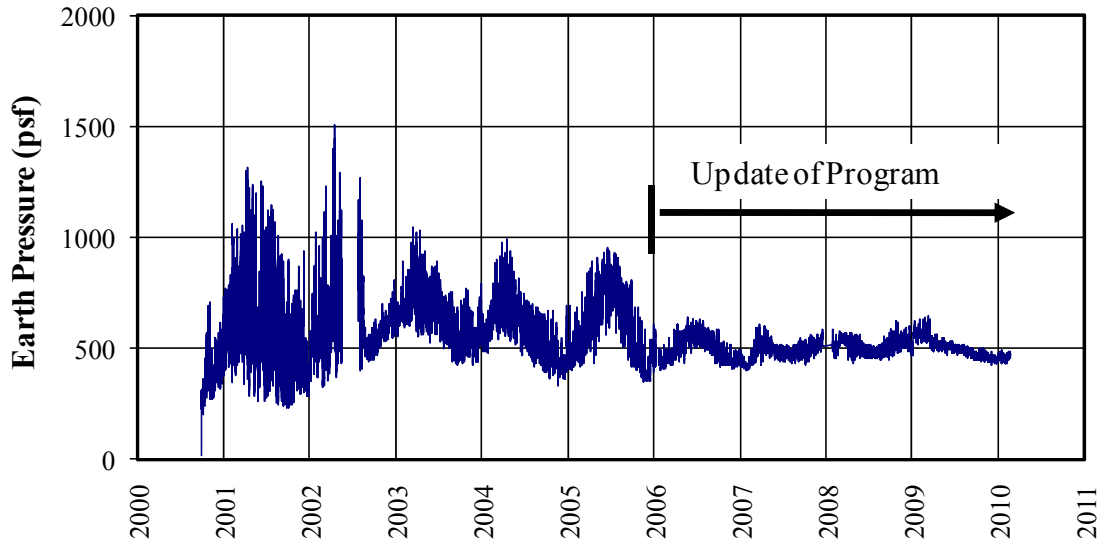
Figure 2.11: Record of Pressure Cell #2 – Center / Bottom of I65 - over SR-25

2.2.5. EVALUATION OF RESULTS

It appears that, according to Figure 2.10 and Figure 2.11, Southbound I-65 over SR-25 is exhibiting the traditionally assumed cyclic behavior of an integral abutment bridge. The superstructure is being loaded by a consistent yearly temperature differential of approximately 80 degrees Fahrenheit. Conventionally, an estimated lateral demand for the supporting piles would be calculated as follows:

$$\Delta L = \alpha(\Delta T)\frac{L}{2} \tag{2.1}$$

where:

ΔL = temperature induced change in bridge length, in.

α = coefficient of thermal expansion, 1/°F

= assumed $5.5 \cdot 10^{-6}\ \frac{1}{°F}$ (Wight and MacGregor 2009)

ΔT = change in temperature, °F

L = total length of structure, in.

$$\Delta L = \left(5.5 * 10^{-6}\frac{1}{°F}\right)(80°F)\left(\frac{152\,ft}{2}\right)\left(\frac{12in.}{1ft}\right) = 0.40in. \tag{2.2}$$

This cyclic temperature response drives a similar cyclic earth pressure response. However, upon inspecting the two earth pressure records, two phases of behavior seem to be occurring. During the first few years of the structure's life, there is a general trend of gradual, residual pressure increase. After two to four years of service, the earth pressure values seem to reach a "steady state." The pressures are ceasing to increase, but rather oscillate between consistent summer and winter pressures (Figure 2.12). The magnitudes of the recorded values can be validated through evaluation and comparison with simplified analysis procedures.
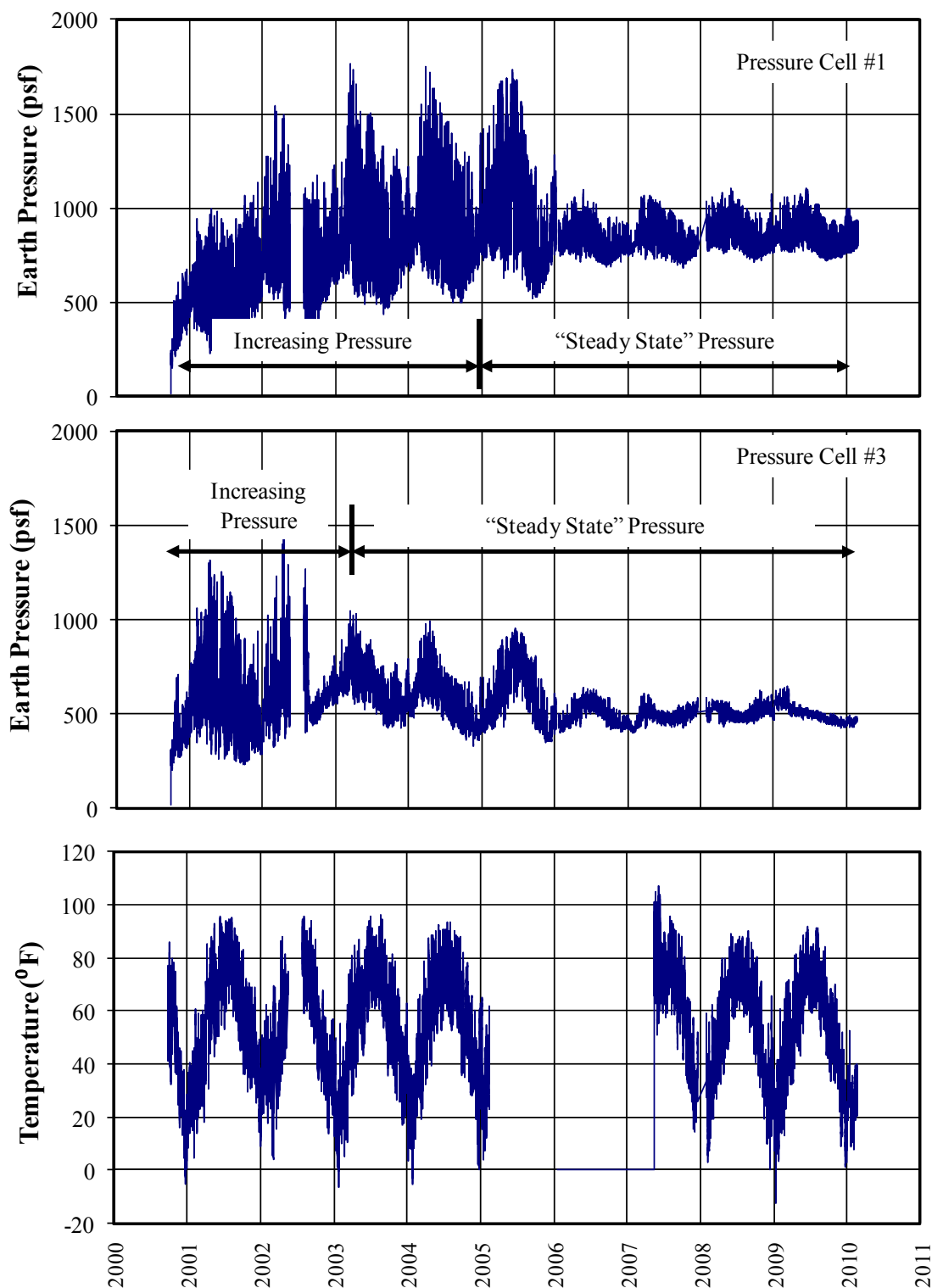
Figure 2.12 General Behavior of I-65 over SR-25

According to lateral earth pressure theory, lateral earth pressure, σ_h, is a function of vertical overburden pressure, σ_v.

$$\sigma_h = K\sigma_v = K\gamma H \tag{2.3}$$

where:

K = Coefficient of Lateral Earth Pressure

γ = Unit weight of soil (pcf)

H = Depth below ground surface (ft)

There are three separate conditions for the coefficient of lateral earth pressure depending on the movement of the soil-supporting structure: active state – when the structure is moving away from the retained soil, passive state – when the structure is moving toward the retained soil, and at rest state. The active state of passive pressure is always the lower bound, and correspondingly, the passive state is an upper bound of lateral earth pressure. According to the Rankine Theory for Passive Earth Pressure, the active and passive coefficients are calculated as follows:

$$K_a = \tan^2\left(45 - \frac{\varphi}{2}\right) \tag{2.4}$$

and

$$K_p = \tan^2\left(45 + \frac{\varphi}{2}\right) \tag{2.5}$$

where:

K_a = Active state coefficient of thermal expansion

K_p = Passive state coefficient of thermal expansion

φ = Angle of internal friction (degrees)

The earth pressure cells have a depth of 7'-9" and 11'-7.5", respectively. Assuming a unit weight for the soil behind the abutment of 120 pcf and an angle of internal friction of 30 degrees, the

measured active and passive earth pressures can be compared to their approximated theoretical values (Table 2.3).

The theoretical active and passive lateral earth pressure values are based on bounding pressures at limiting movements of the abutment. However, the classical theories of lateral earth pressure theory do not give recommendations on the necessary movement to develop these pressures. However Coduto (2001) recommends lateral movement equal to 0.2% and 2% of the height abutment is required to achieve the active and passive lateral earth pressures, respectively. These values correspond to movements equal to 0.3 in. and 3 in.

Comparing the calculated active pressure values to the measured values reveal that the measured values are actually less than the theoretical values. According to theory, this is impossible. Assuming the soil properties are approximately correct, the results show a gap is possibly forming behind the abutment. Inspecting the results for passive earth pressure, the measured values are much less than the theoretical full passive state. This makes sense because the maximum estimated abutment movement is approximately 0.4 in., which is much less than the 3 in. estimated by Coduto (2001). Based on these results, soil pressures should be bounded by zero and the passive pressure. The active pressure should not be considered a lower bound for these types of structures since outward movement can produce gaping. The passive pressure is an upper bound and the actual maximum pressure depends on the movement of the abutment into the backfill. Consequently, the overall bridge length plays a major role and for this structure a maximum of 61% of passive pressure was observed.

Table 2.3: Theoretical and Measured Lateral Earth Pressures for I-65 over SR-25

Gage	EP1		EP3	
	Theory	**Measured**	**Theory**	**Measured**
Depth (ft)	7.75		11.625	
φ (degrees)	30		30	
γ (pcf)	120		120	
σ_h (psf)	930		1395	
K_a	0.33		0.33	
K_p	3		3	
σ_{va} (psf)	307	min = 250	460	min = 275
σ_{vp} (psf)	2790	max = 1700	4185	max = 1300

2.3. S<small>R-18 OVER</small> T<small>HE</small> M<small>ISSISSINEWA</small> R<small>IVER</small>

INDOT Bridge #18-27-4518D (SR-18) (Figure 2.13) in Grant County was also selected to investigate the general behavior of integral abutment bridges. It is located in Marion, IN, less than one mile east of downtown Marion. In late fall 2003, the previous structure carrying SR-18 over the Mississinewa River was converted to an integral abutment bridge. Virtually, the entire structure was replaced. At the time of construction, this structure exceeded the maximum length criteria as recommended by INDOT for integral abutment bridges. Consequently, the SR-18 Bridge became an excellent candidate to investigate the effects of length. As part of a previous study, the bridge was instrumented to investigate the seasonal behavior of integral abutment bridges with particular focus on the effects of length (Chovichien 2004).

The structure spans the Mississinewa River and is 367 ft in length with an 8° skew angle. The superstructure consists of five 60 in. prestressed bulb-tee beams centered with the structure and equally spaced at 10'-2" supporting an 8 in. concrete deck. An elevation and plan view of the structure are shown in Figure 2.14 and Figure 2.15, respectively. Selected plan drawings are shown in Appendix A. Appendix B shows the soil borings taken around the structure.

Figure 2.13: SR-18 over The Mississinewa River
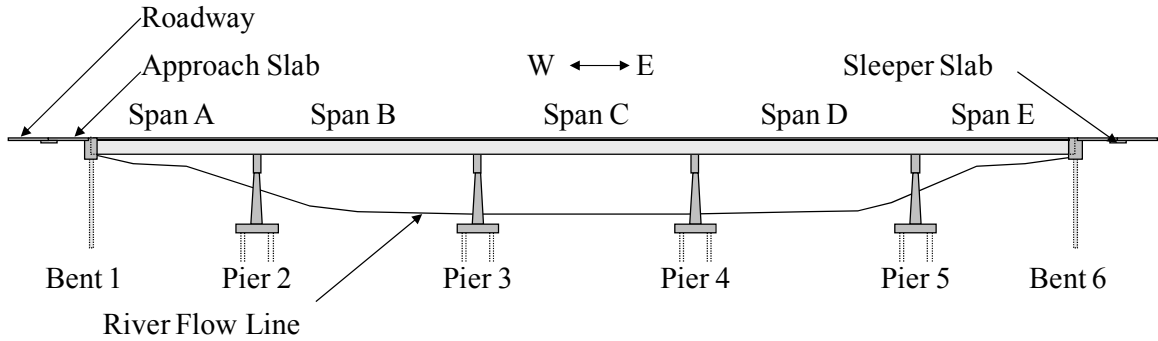
Figure 2.14: Elevation View of SR-18 over The Mississinewa River
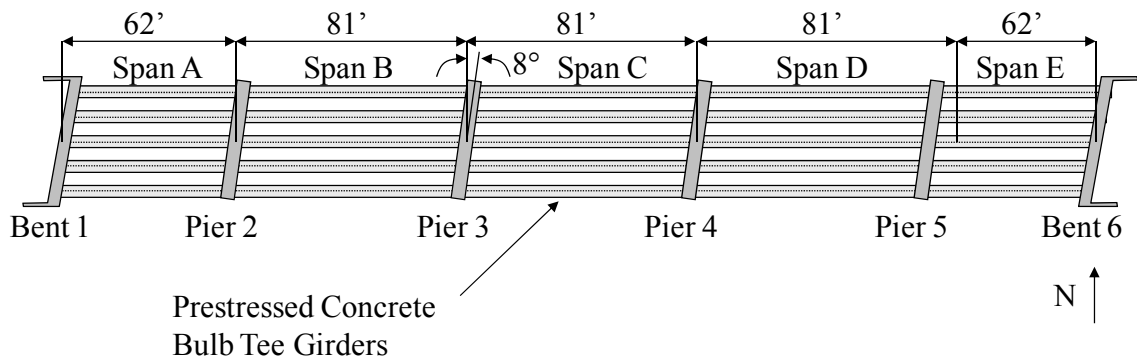
Figure 2.15: Plan View of SR-18 over The Mississinewa River

When the structure was retrofitted, the entire substructure was replaced. The piles were designed according to INDOT specifications which require the consideration of only axial load. Each abutment is supported by ten 14 in. steel pipe piles with 0.312 in. wall thicknesses (CFT 14.5x0.312) filled with concrete. The piles have an average length of 20.8 ft and 27 ft for Bent 1 and Bent 2, respectively. Soil boring information, pile design, and pile driving records are presented in a separate report by Chovichien (2004). A typical cross section of the abutment is shown in Figure 2.16.
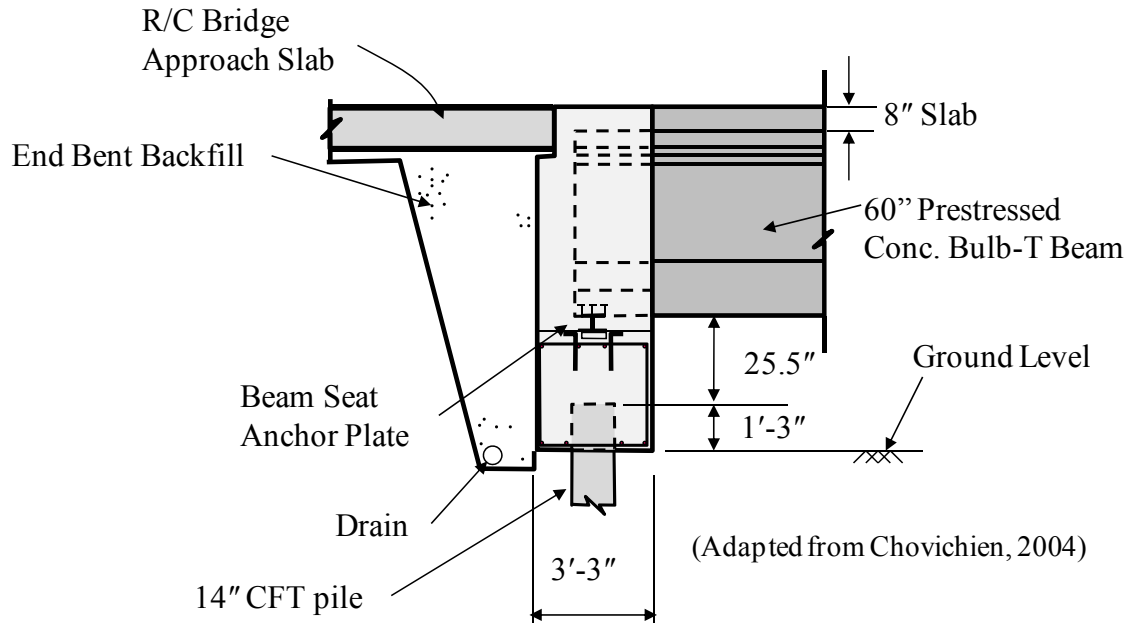
Figure 2.16: Typical Cross-section of Abutment for SR-18 over The Mississinewa River

2.3.1. STRUCTURAL MATERIALS

2.3.1.1. CONCRETE

The structure was constructed in two phases: the substructure and the superstructure. The abutment was cast in two separate lifts, in which the first lift was comprised of the pile cap supporting the beams, and the second was cast continuously with the deck. The mixes for the first and second cast followed general INDOT practice and were INDOT Class A concrete ($f_c^{'}$ = 3500psi) and INDOT Class C ($f_c^{'}$ = 4000psi), respectively.

2.3.1.2. PILES

Each abutment is supported by a single row of ten piles. The piles are CFT14x0.312 steel pipe shells meeting ASTM A252, Grade 2 and are filled with Class A concrete.

2.3.2. INSTRUMENTATION

To understand the behavior of the SR-18 over the Mississinewa River structure, an instrumentation plan was implemented to monitor ambient temperature, abutment movement, and lateral earth pressure.

2.3.2.1. ABUTMENT INSTRUMENTATION

The primary focus of the instrumentation of SR-18 was to determine the effects of length on the behavior of an integral abutment bridge. Therefore, each abutment was instrumented to monitor movements over the life of the structure. To those means, each abutment was instrumented with convergence meters to measure longitudinal movement of the abutment, strain gages on selected piles at the base of the abutment to measure biaxial bending of the piles, strain gages along the depth of Pile 6 on Bent 1 to monitor the deflected shape, tilt meters to measure the angle of tilt of the abutment, and earth pressure cells to measure lateral earth pressure. The locations of the instruments attached to the abutment are shown in plan-view in Figure 2.17, and elevation view in Figure 2.18. The location of the strain gages along the depth of Pile 6 in Bent 1 is shown in Figure 2.19. Information regarding specific gage information is provided by Chovichien (2004).
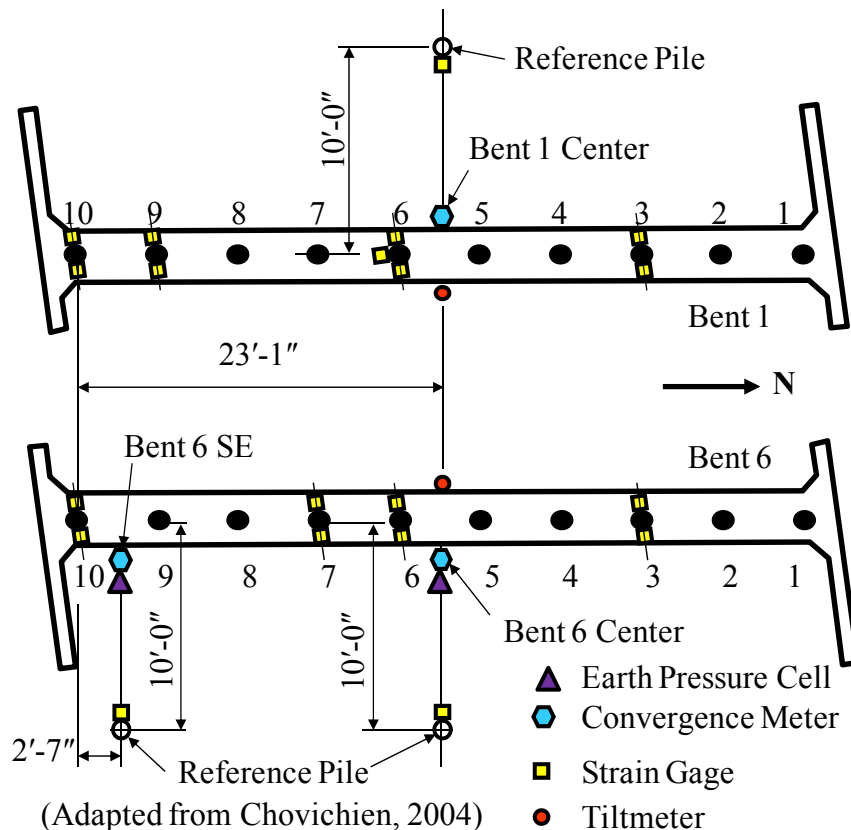
Figure 2.17: Plan View of SR-18 Abutment Instrumentation

R/C Bridge
Approach Slab

End Bent Backfill

Earth Pressure Cell

Convergence Meter

8″ Slab

60" Prestressed Conc.
Bulb-T Beam

3″

Ground Level

1′-3″

Strain Gage

Drain

Tiltmeter

3′-3″

14″ CFT pile

Reference Pile

Strain Gages

(Adapted from Chovichien, 2004)

10′
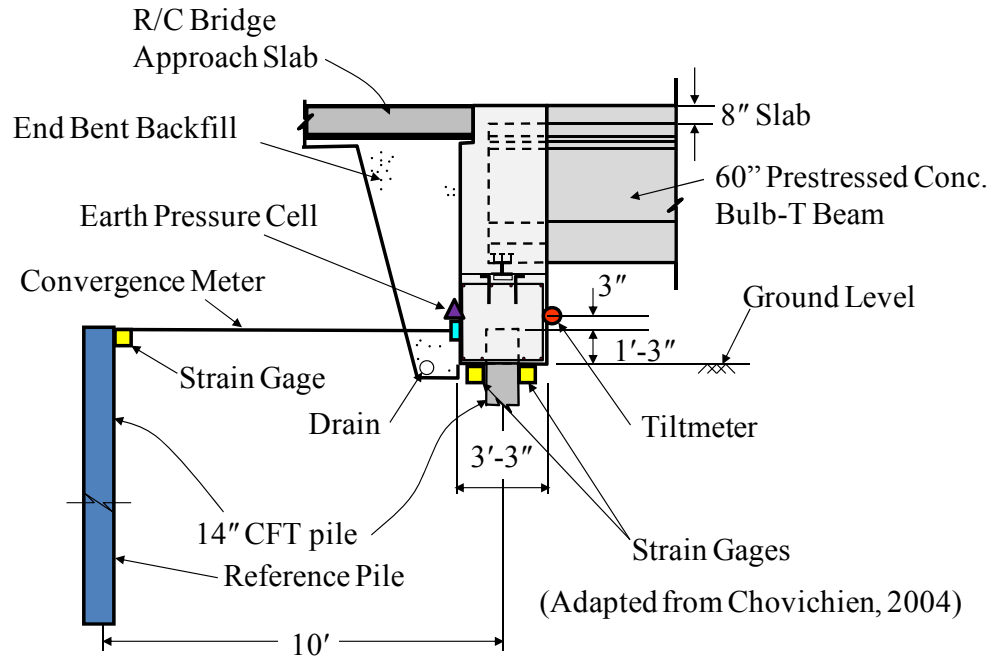
Figure 2.18: Elevation View of SR-18 Abutment Instrumentation

N

Abutment

Ground
Level

1′-3″

8°

90°

Parallel to
Roadway

Centerline of
Abutment

Strain Gage

5 spaces at 4′=20′

Plan

(Chovichien, 2004)

Pile

Elevation
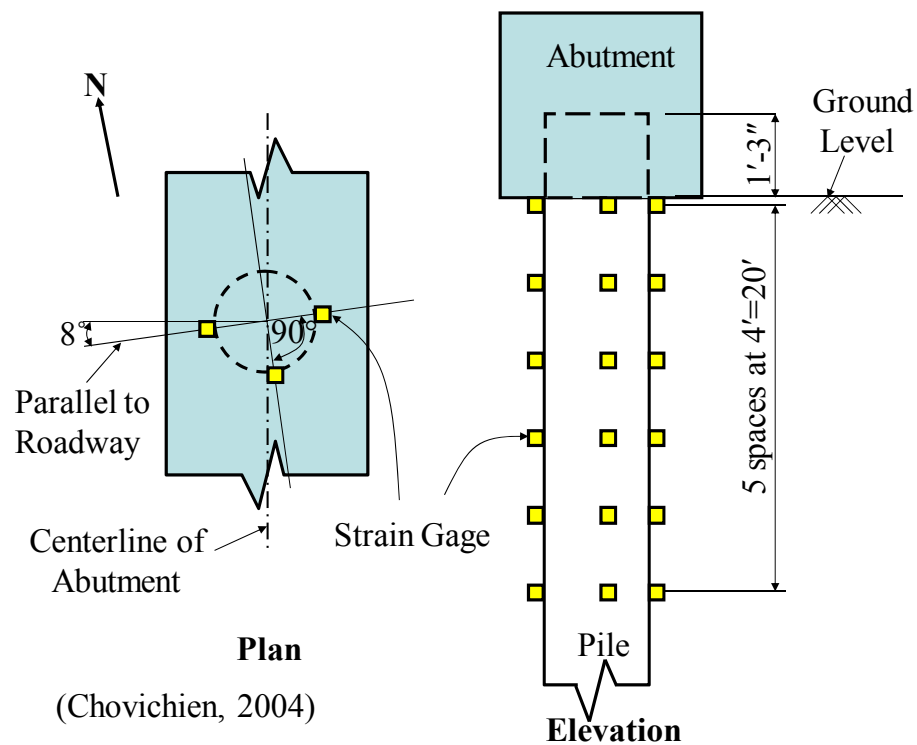
Figure 2.19: Location of Pile Strain Gages on Pile 6, Bent 1, on SR-18

2.3.3. DATA COLLECTION

The data acquisition system for this instrumentation plan was a Geokon Model 8020 Micro-10 datalogger with Model 8032 multiplexers. The system was installed and data collection began in June of 2003. Collection has continued since 2003 collecting hourly. Data provided is shown through February 2010.

2.3.3.1. PROBLEMS

The tilt meters for SR-18 produced erratic and erroneous data. This data was, therefore, not used for analysis.

2.3.4. RESULTS

2.3.4.1. TEMPERATURE

Ambient shade temperature was collected using a temperature gage placed underneath the structure (Figure 2.20). As shown, the temperature record is very consistent over the duration of the research program. Table 2.4 shows critical temperature values including construction temperature, max high, max low, average summer temperature, and average winter temperature.
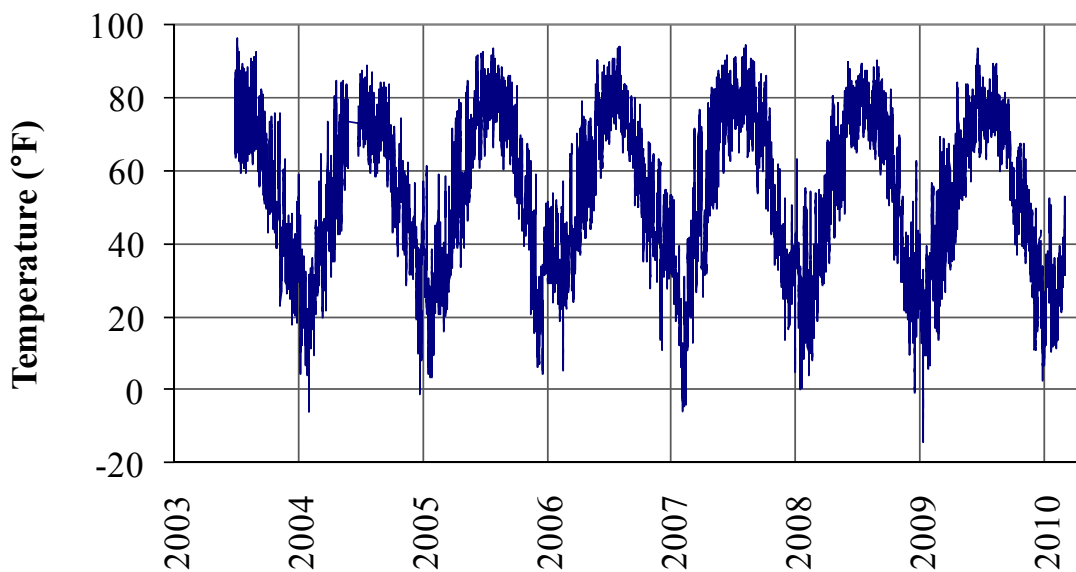
Figure 2.20 SR-18 Temperature Record

Table 2.4: Critical Temperatures for SR-18

Record	Temperature (°F)
Construction Temperature	65
Average Summer Temperature	90
Average Winter Temperature	20
Maximum High Temperature	96
Maximum Low Temperature	-11

2.3.4.2. CONVERGENCE METERS

      Convergence meters were installed at each abutment to monitor longitudinal movement as the bridge was subjected to seasonal temperatures. The three collected displacement records are shown in Figure 2.21. The records are shown together to highlight the similarities.
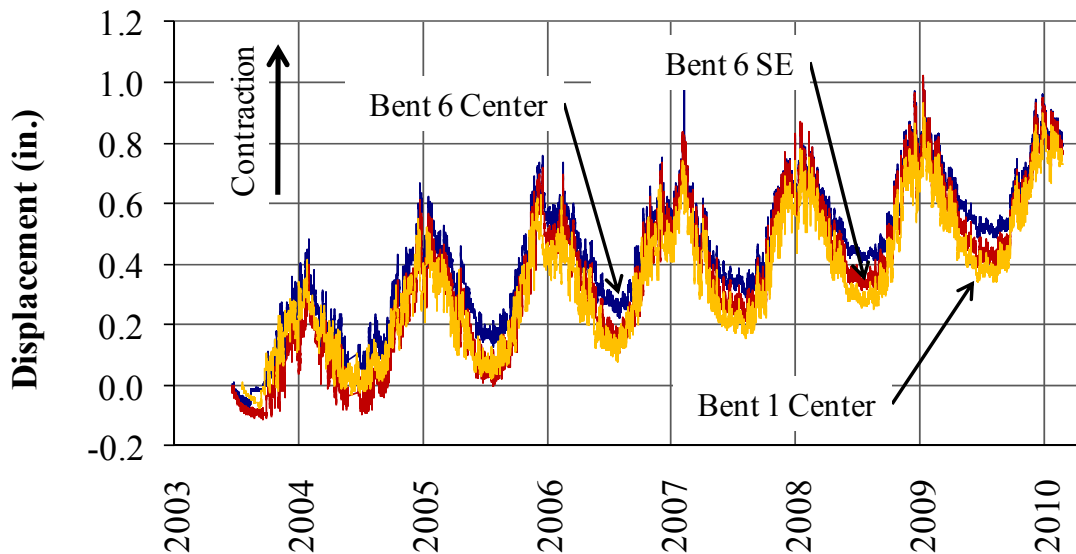
Figure 2.21: Collected Displacement Records for SR-18

2.3.4.3. EARTH PRESSURE

      Lateral earth pressure was measured to determine the effect of the backfill on the abutment. The pressure records for the two pressure cells are shown in Figure 2.22. The records are shown together to highlight their similarities.
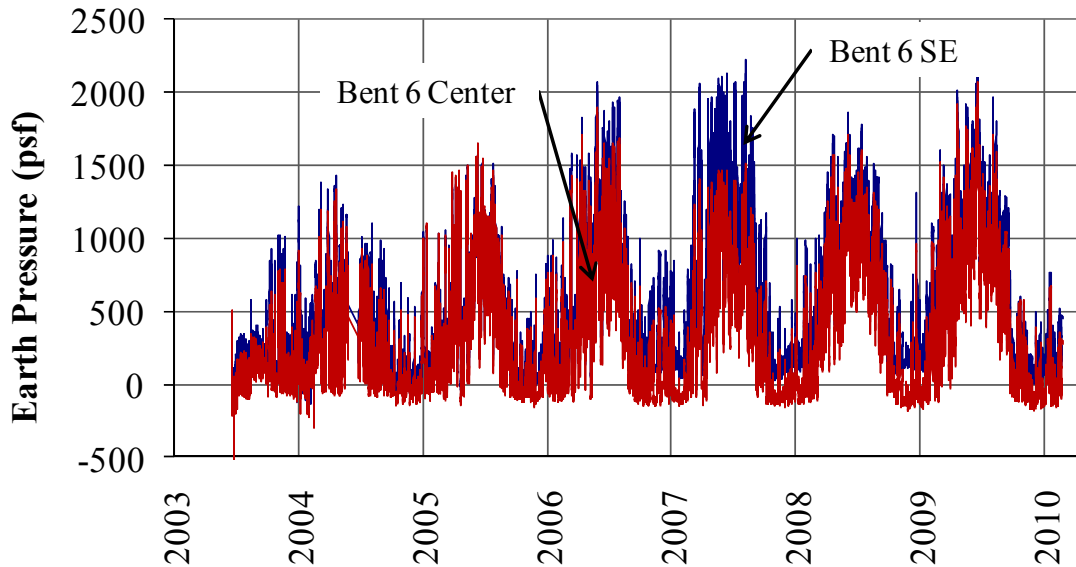
Figure 2.22: Earth Pressure Records for SR-18

2.3.4.4. PILE STRAIN GAGES

Pile strains were collected along the depth of the center pile of Bent 1. The pile was instrumented with strain gages on three faces; two along the longitudinal axis of the structure and one at 90 degrees to the longitudinal axis as shown in Figure 2.19. The gages started at the interface of the abutment and pile and continued down the length of the pile at 4 ft increments. The output of the strain gages provided a discretized strain profile along the length of the pile. This information can be integrated to determine and approximate the deflected shape. The recorded strain profiles for Pile 6 are shown for the first peak of contraction and first valley of expansion as well as the final peak and valley to highlight the differences in the life of the structure. The strain and stress values for the east side of the pile are shown in Figure 2.23 and those for the west side are shown in Figure 2.24. For the two later dates, the top strain gage on both the east and west side malfunctioned. Looking at the general trend of the strain measurements, the values were estimated.
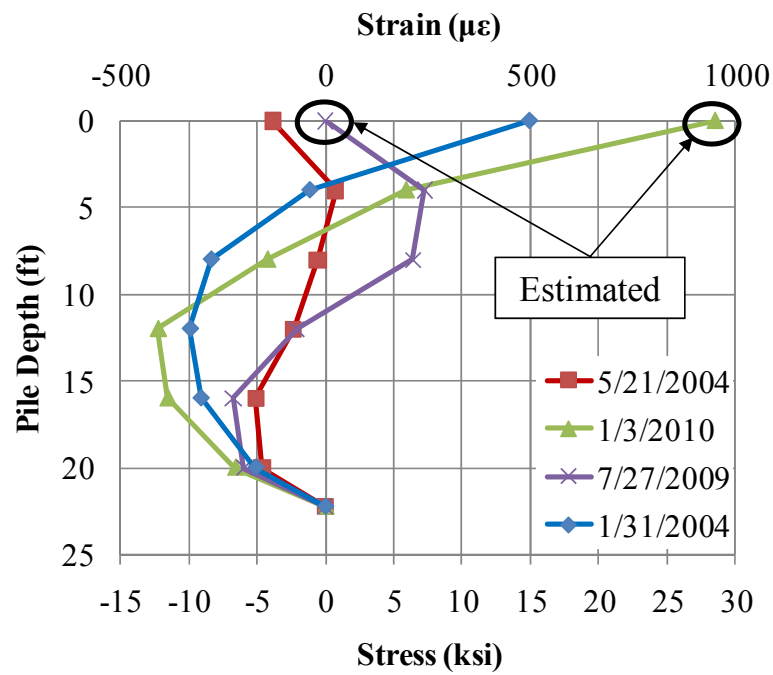
Figure 2.23: Recorded Strain Values for the East Side of Pile 6, Bent 1 for Selected Days
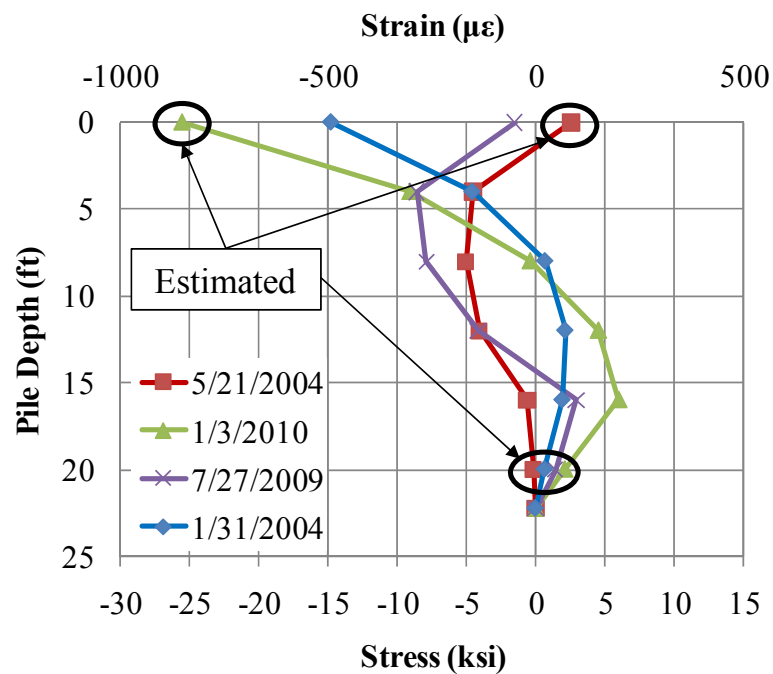
Figure 2.24: Recorded Strain Values for the West Side of Pile 6, Bent 1 for Selected Days

2.3.5. EVALUATION OF RESULTS

To develop an understanding the behavior of SR-18 over the Mississinewa River, the temperature, displacement, and earth pressure measurements can be analyzed and compared. Initially, a visual inspection of the data reveals some insight regarding the behavior (Figure 2.25). Though the three displacement records, along with the two earth pressure records, are at different locations on the structure (different end bent and different horizontal location on the end bent), the measurements are virtually identical. Conclusively, one can interpret two significant points from this finding: first, the structure is behaving symmetrically, and second, the low skew angle is not causing out-of-plane behavior. Inspecting the measured displacements, it is apparent that both abutments are experiencing an annual net inward movement. However, it seems that the inward movement is decreasing each consecutive year.
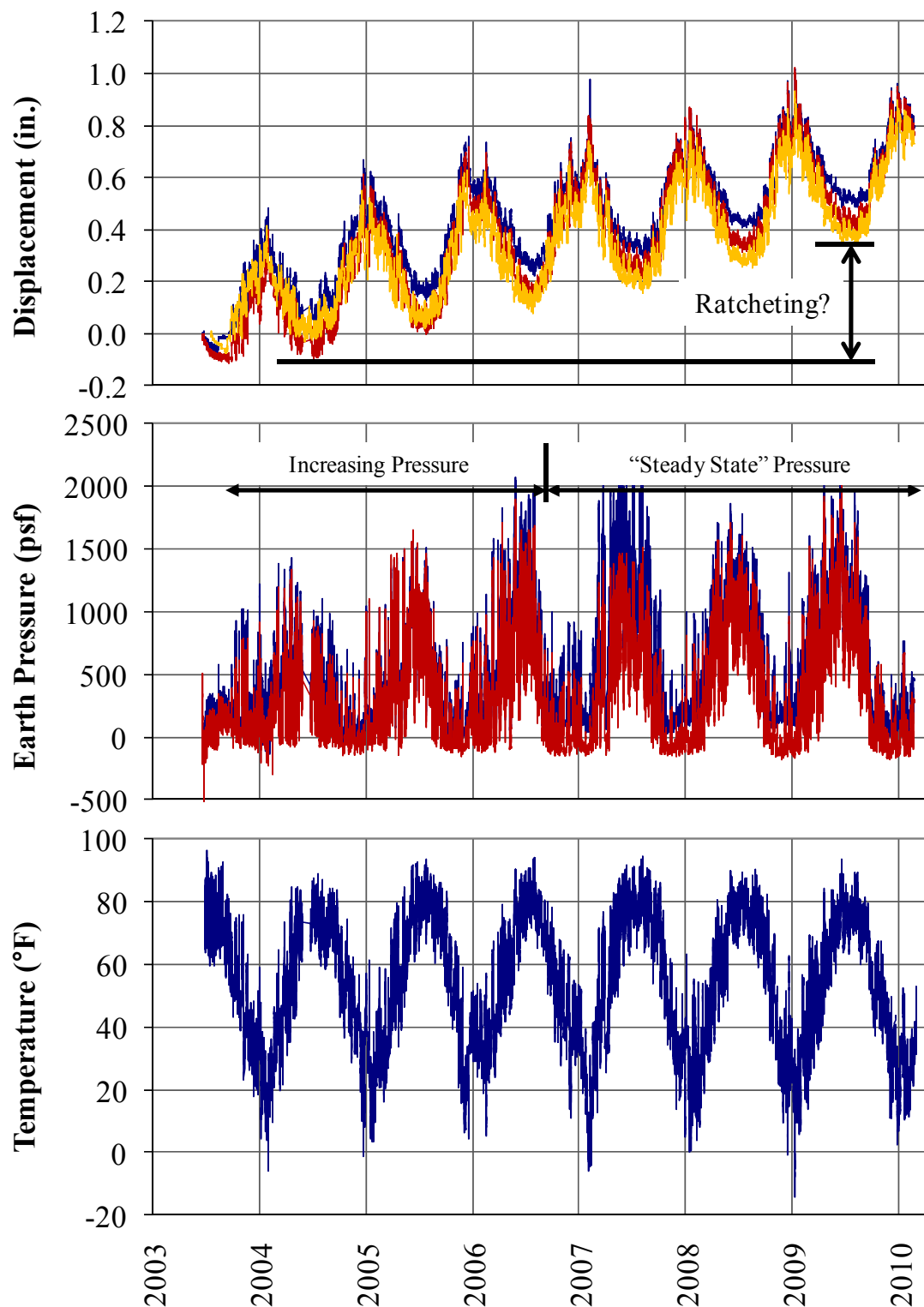
Figure 2.25: Evaluation of Collected Data from SR-18

The superstructure is being loaded by a yearly consistent temperature differential of approximately 80 degrees Fahrenheit. Following the conventional method, determining the estimated lateral demand for the supporting piles would be calculated using Equation 2.1.

$$\Delta L = \left(5.5*10^{-6}\frac{1}{°F}\right)(80°F)\left(\frac{367\,ft}{2}\right)\left(\frac{12in.}{1ft}\right) = 0.97in. \tag{2.6}$$

However, the annual cycle measured by the convergence meters shows a total movement equal to 0.6 in. Because the prediction is based on unrestrained thermal shrinkage, this difference may be attributed to soil restraint and pile stiffness. It is interesting to note that the simplified formula closely predicts the long-term displacement of the structure. Further investigation is required to determine if this is a coincidence.

SR-18 seems to exhibit similar behavior to that of I-65 over SR-25. The earth pressure records reveal that, initially, pressures increase year to year. Then, much like I-65, SR-18 reaches a "steady state" cycle of lateral earth pressure. The pressure records also reveal the lateral earth pressure behind the abutment reduces to zero during the contraction phase. This can be explained by the formation of a gap between the backfill and abutment during times of greatest contraction. Using the depth of the gage at 8.75 ft and assuming a unit weight of 130 pcf and internal angle of friction of 30 degrees for the backfill, the following compares the measured magnitudes of lateral earth pressure with classical lateral earth pressure theory (Equation 2.3 through Equation 2.5).

$$\sigma_{ha} = K_a\sigma_v = 0.33(120\,pcf)(8.75\,ft) = 350\,psf \tag{2.7}$$

$$\sigma_{hp} = K_p\sigma_v = 3(120\,pcf)(8.75\,ft) = 3150\,psf \tag{2.8}$$

The pressure data for SR-18 reveals very similar information to that of I65 over SR-25. The measured values of pressure for the active state are much less than the theoretical values, which agrees with the formation of a gap between the backfill and the abutment. The measured passive pressure is also less than the theoretical values. Again, the necessary movement to reach passive pressure is assumed to be 2% of the height of the abutment, which is approximately 2 in. This displacement is much greater than the measured movements. Therefore, the abutment pressures do not reach the full passive values and are approximately only 63% of full passive pressure.

Inspecting the displacement measurements combined with the earth pressure measurements reveals greater insight regarding the overall behavior of the structure. It is noticed that the net displacement of each abutment is continually inward. However, the pressures have increased over time. For this behavior to occur, there must be settlement of the soil behind the abutment. As the pressure record continues and reaches "steady state" behavior, the displacement continues to move inward. In order for the increasing earth pressure to cause continued inward abutment movement, as a ratcheting phenomenon suggests, the pressure would need to increase each year. Obviously, the pressures do not increase. In fact, the largest inward displacements occur at a time when the earth pressures are low or zero. This behavior suggests there is a different driver for the continual inward movement that occurs from year to year.

Using the procedure as outlined by Chovichien (2004), the strain measurements were used to approximate the deflected shape of the center pile in Bent 1. First, the curvature of the pile (Figure 2.26) was calculated using the following:

$$\phi = \frac{\varepsilon_{east} - \varepsilon_{west}}{O.D.} \tag{2.9}$$

where:

φ = curvature, rad/in.

ε_{east} = strain on the east side of the pile, in./in.

ε_{west} = strain on the west side of the pile, in./in.

O.D. = outer diameter of pile, 14 in.
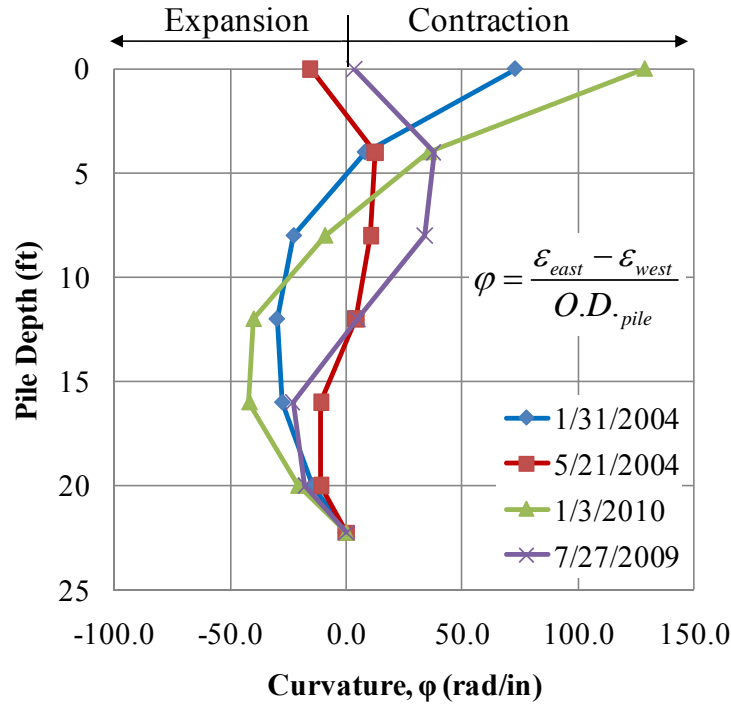
Figure 2.26: Approximated curvature for SR-18, Pile 6, Bent 1 on Selected Dates

Using the approximated curvature, the deflected shape was then calculated by integrating the moment of the area under the curvature diagram. The pile was assumed to have a pin-end at the base of the pile and assumed to be fixed from rotation but free to translate at the top. Also, the top deflection of the pile was set to match the measure displacement from the corresponding convergence meter and the bottom of the pile was assumed to have zero displacement. Because the base of the pile was assumed to allow rotation, the original deflected shape had to be adjusted to account for the end conditions. The rotation allowed by the pin was determined by assuming the convergence meter to be correct at the top of the pile and dividing the displacement by the height of the pile. This rotation was subtracted from the interpolated displacement along the length of the pile to produce the deflected shape. The calculated deflected shape is shown for the first and last measured phases of contraction and expansion (Figure 2.27). It is clear that the pile bends in double curvature and has throughout the structure's life-cycle. Also, the evidence of residual inward movement is apparent. In fact, on the last phase of expansion (7/27/09), it is shown that nearly 0.4 in. of movement remains as compared to the pile returning to its initial position during the first phase of expansion. However, the yearly movement is approximately

similar. This would be expected if the driver of seasonal movement is temperature, and the residual movement is caused by some other phenomenon.
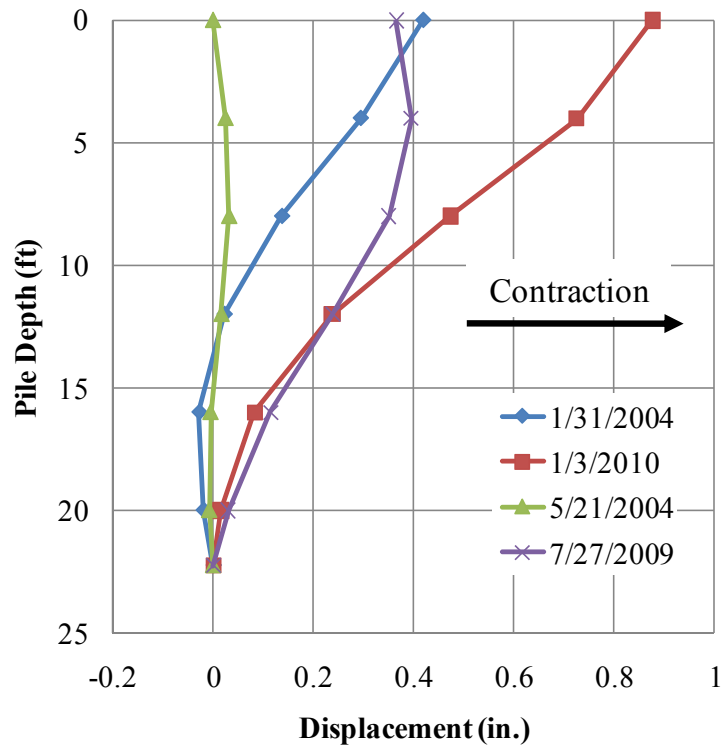
Figure 2.27: Calculated Pile Deflection for SR-18 Pile 6, Bent 1

2.4. US-231 OVER RAILROAD SPUR

INDOT Bridge #231-74-2699 (US-231) (Figure 2.28) in Spencer County was selected to investigate the general behavior of integral abutment bridges while specifically evaluating the effects of skew. The structure, completed in late fall 2006, is located two miles north of Rockport, IN. US-231 exceeds the current maximum skew angle as mandated by INDOT, and therefore, is a prime candidate to investigate the effects of high skew angles on these types of structures. The structure spans the AEP railroad spur and is 221 ft in length with a 33.8 degree skew angle. The superstructure consists of seven Type III Prestressed I-beams centered with the structure and equally spaced at 6'-8" supporting an 8 in. concrete deck. The superstructure is also built with a four degree cross-slope. An elevation and plan view of the structure are shown in Figure 2.29 and Figure 2.30, respectively. Seledcted drawings from the plans for US231 are

shown in Appendix A.   Appendix C contains the locations and results of a subsurface investigation.

Figure 2.28: US-231 over AEP Railroad Spur
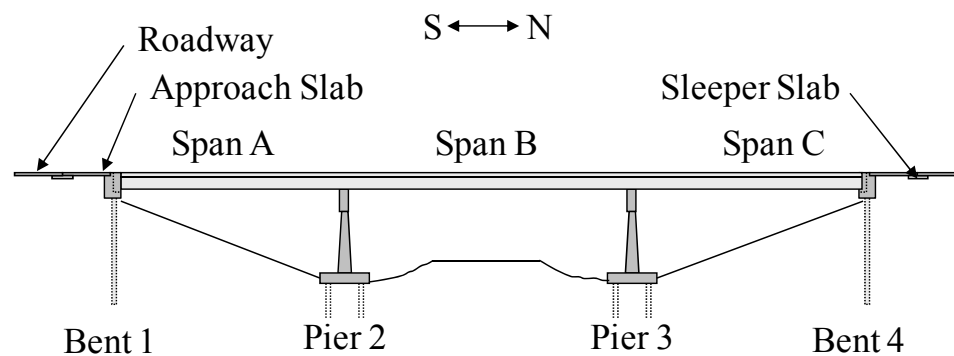
Figure 2.29: Elevation View of US-231
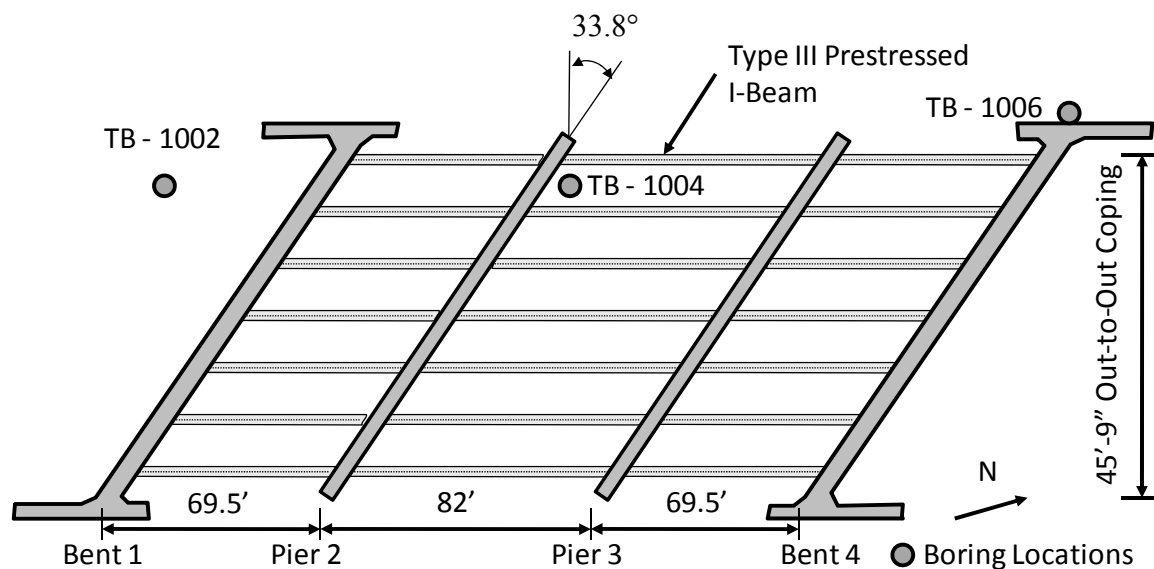
Figure 2.30: Plan View of US-231

The substructure for US-231 was constructed in two phases. First, an initial lift of the abutment was cast to construct a pile cap for the supporting piles. The second lift was cast simultaneously with the deck. A cross-section of the abutment for US-231 is shown in Figure 2.31. The height of the abutment varies across the width of the structure due to the cross slope of the superstructure. At the east end, the abutment is 8.36 ft, and at the west it is 6.51 ft tall. The bent cap was supported by seven 14 in. steel pipe piles with 0.312 in. wall thicknesses (CFT 14.5x0.312) filled with concrete. The piles also serve as the pedestals for the prestressed girders. The piles have an average length of 80.9 ft and 81.2 ft for Bent 1 and Bent 4, respectively. The piles were designed according to INDOT specifications which require the consideration of only axial load. Two soil borings were performed at the location of each of the end bents of this structure. The in-situ soil profile is shown in Table 2.5. To attain the necessary elevation of the structure, over 54 feet of fill was placed above the existing ground elevation. The fill material is known, according to INDOT standards, as B-Borrow and has the following description:

"*B-Borrow, used for special filling, is required to be of acceptable quality, free from large or frozen lumps, wood, or other extraneous matter. Sand, gravel, crushed stone, air cooled blast furnace slag, granulated blast furnace slag, or other approved materials are used for B Borrow. The material is required to contain no more than 10 % passing the No. 200 sieve and be*

otherwise suitably graded. The use of an essentially one-size material is not allowed, unless approved." (INDOT Design Manual, 2010)

Based on this requirement, the material properties can be quite variable and the specific material must be known to quantify.
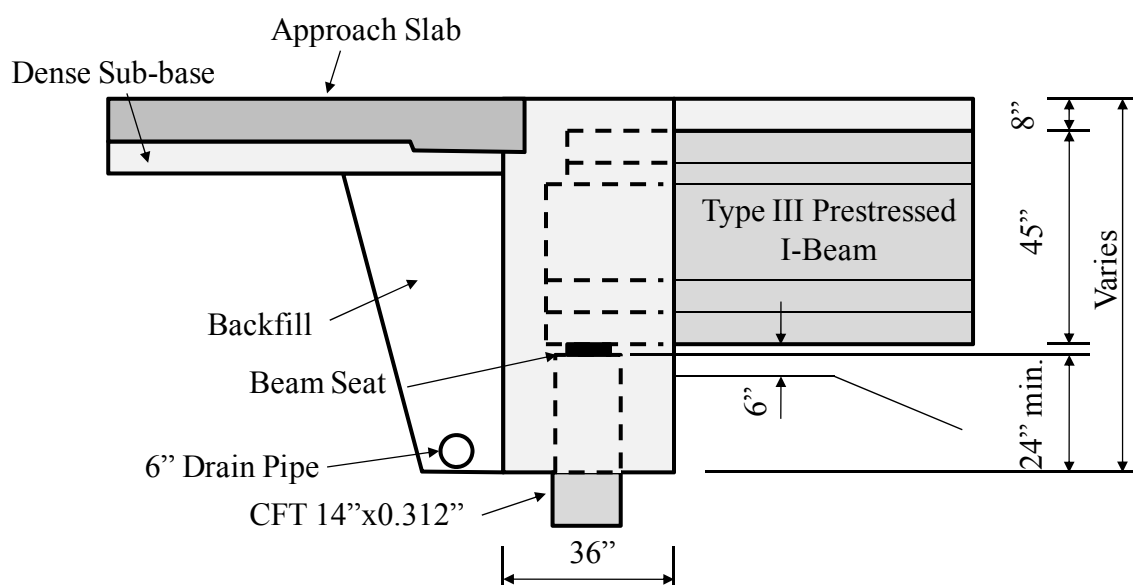
Figure 2.31: Typical Cross-section of Abutment for US-231

Table 2.5: In-situ Soil Profile for US-231

Soil Type	TB-1002	TB-1006	TB-1004	Average	Layer Thickness (ft)
Bottom of Abutment	418	418	418	418	-
Existing Surface / Compacted Fill	387	388	388	388	31.0
Brown Clay Top Soil	386	387	387	387	1.0
Very Stiff Silty Clay Loam	372	380	380	377	9.4
Medium Stiff to Stiff Silty Clay Loam ▽	364	365	365	365	12.6
Gravelly Sand Medium Dense / Pile Bottom	337.3	337.3	337.3	337	27.3
SUM					81.3

2.4.1. STRUCTURAL MATERIALS

2.4.1.1. CONCRETE

The structure was constructed in two phases: the substructure and the superstructure. The abutment was cast in two separate lifts, in which the first lift was comprised of the pile cap supporting the beams, and the second was cast continuously with the deck. The mixes for the first and second cast followed general INDOT practice and were INDOT Class A concrete $\left(f_c^{'} = 3500\,psi \right)$ and INDOT Class C $\left(f_c^{'} = 4000\,psi \right)$, respectively.

2.4.1.2. PILES

Each abutment is supported by a single row of seven piles. The piles are CFT14x0.312 steel pipe shells meeting ASTM A252, Grade 2 filled with Class A concrete.

2.4.2. INSTRUMENTATION

To understand the behavior of the US-231 over the AEP railroad spur, an instrumentation plan was implemented to monitor ambient temperature, abutment movement, pile strains, and lateral earth pressure.

2.4.2.1. ABUTMENT INSTRUMENTATION

The primary focus of the instrumentation of US-231 was to monitor both in-plane and out-of-plane movement of the abutments as the structure undergoes seasonal movements. Therefore, each abutment was instrumented to monitor movements over the life of the structure. The following Geokon vibrating wire gages were used:

- Model 4425 Convergence Meter – To measure longitudinal and transverse movement of each abutment.
- Model 4700 Temperature Gage –To measure ambient temperature.
- Model 4800 Earth Pressure Cell – To measure lateral earth pressure behind each abutment.
- Model 6350 Tiltmeter – To measure the angle of inclination of each abutment.
- Model 4100 Pile Strain Gage – To measure pile strains along the length of selected piles.

The locations of these instruments in plan view are shown in Figure 2.32. An elevation view of the instrumentation is shown in Figure 2.33.
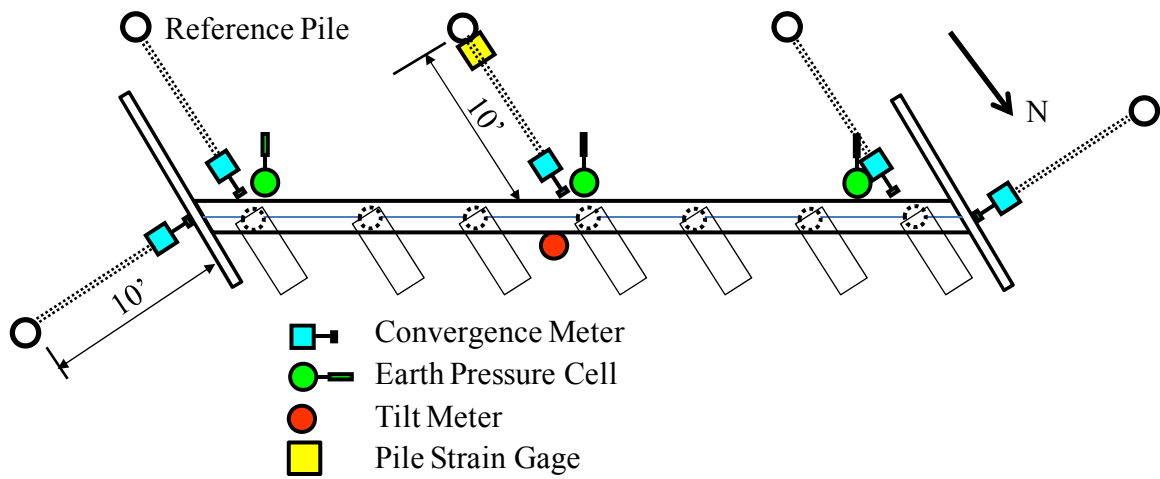
Figure 2.32: Plan View of US-231 Instrumentation
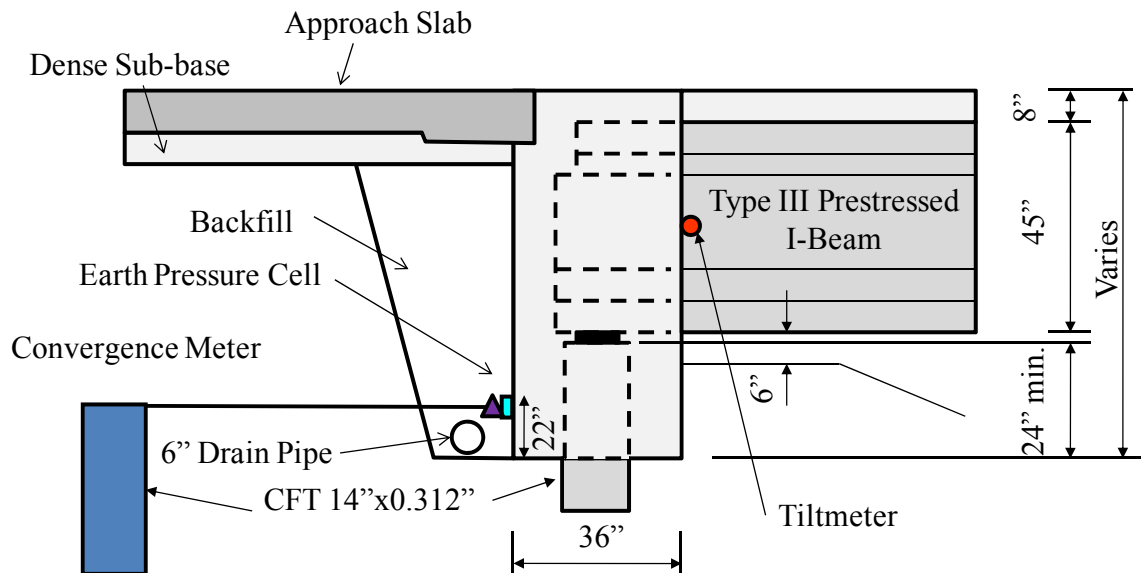
Figure 2.33: Elevation View of US-231 Instrumentation

2.4.3. DATA COLLECTION

The data acquisition system for this instrumentation plan was a Geokon Model 8020 Micro-10 datalogger with Model 8032 multiplexers. The system was installed, and data

collection began in August of 2006. Collection has continued since 2006 collecting hourly. Data provided is shown through February 2010.

2.4.3.1. PROBLEMS

Several problems occurred in the collection of data:

1. Several gages were incorrectly wired which resulted in a loss of data from February 2007 until May of 2007.
2. A noise issue occurred during May 2007 through August 2007 due to an abnormal power malfunction. The resulting data shows an unnatural shift in most the recorded data.
3. The tiltmeters installed on both abutments produced erratic and erroneous data. Therefore, their results have been disregarded.
4. Nearly all of the pile strain gages malfunctioned during the life of the structure.
5. On July17, 2009, the south abutment data acquisition system suffered a power surge and all gages were lost.

2.4.4. RESULTS

2.4.4.1. TEMPERATURE

Ambient shade temperature was collected using a temperature gage placed underneath the deck (Figure 2.34). As shown, the temperature record is very consistent over the duration of this study. Table 2.6 shows critical temperature values including construction temperature, max high, max low, average summer temperature, and average winter temperature.
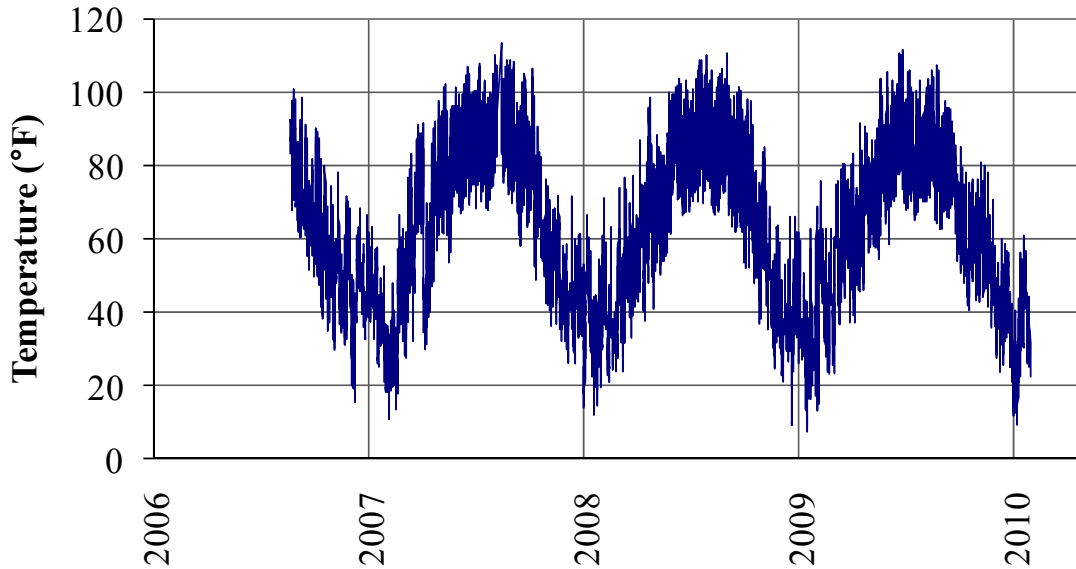
Figure 2.34: Temperature Record for US-231

Table 2.6: US-231 Critical Temperature Values

Record	Temperature (°F)
Construction Temperature	65
Average Summer Temperature	100
Average Winter Temperature	20
Maximum High Temperature	108
Maximum Low Temperature	9

2.4.4.2. CONVERGENCE METERS

Convergence meters were installed at each abutment to monitor the longitudinal and transverse movement as the bridge is subjected to seasonal temperatures. There are three convergence meters at each abutment to measure longitudinal movement, as well as to capture rotation of the abutment. One convergence meter was also placed at each of the four corners of the structure to measure transverse movement and monitor out-of-plane movement. The measured displacements are shown in Figure 2.35 thru Figure 2.38. The values have been zeroed on the date the deck was cast. Upon inspecting the results of the convergence meters along the longitudinal axis of the structure, it is apparent that the overall trend of the north and south abutments are the same. For both the north and south abutment, the displacement at the center of

each respective abutment is approximately the same. However, the acute corner of the south abutment displaces approximately 0.1 in. more than the acute corner of the north abutment. The same is true of the obtuse corners. This difference is assumed to be negligible. For the out-of-plane convergence meters, it is noted that rapid jumps occur in the measurements toward the end of 2006. If these are assumed to be erroneous, the out-of-plane measurements are virtually the same. Considering these results, it is apparent that each of the structure's abutments is behaving approximately the same. As a result, because the last few months of collected data for the south abutment were lost, future analysis of the data will be conducted from movements measured at the north abutment.
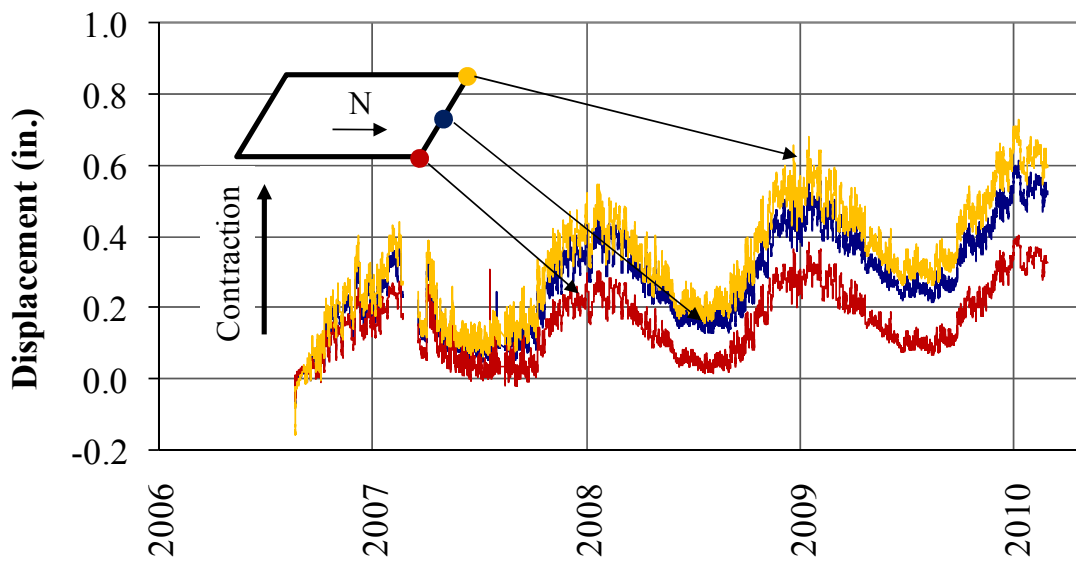
Figure 2.35: Longitudinal Movement of the US-231, North Abutment
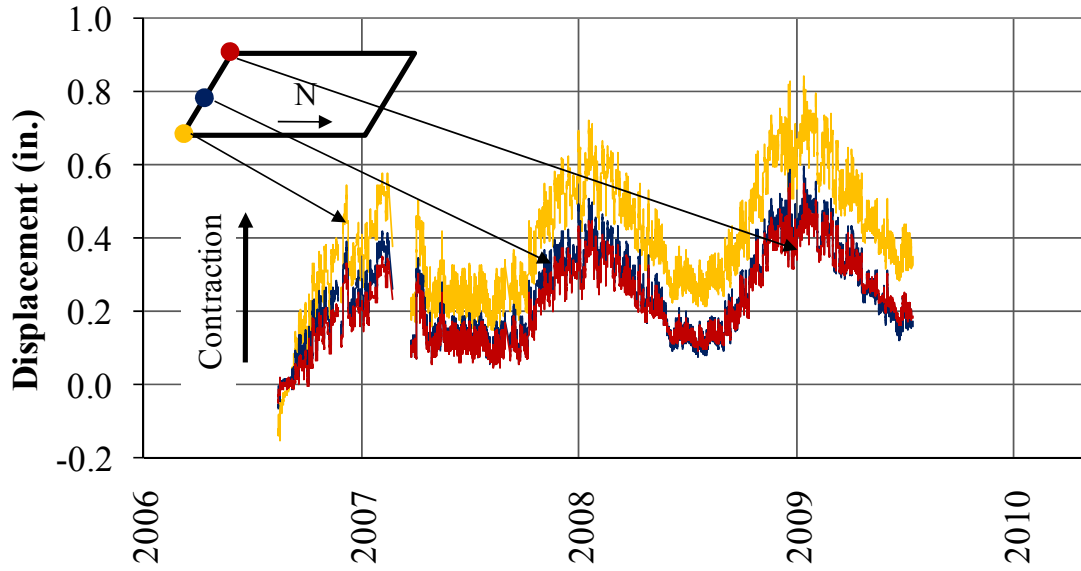
Figure 2.36: Longitudinal Movement of US-231, South Abutment
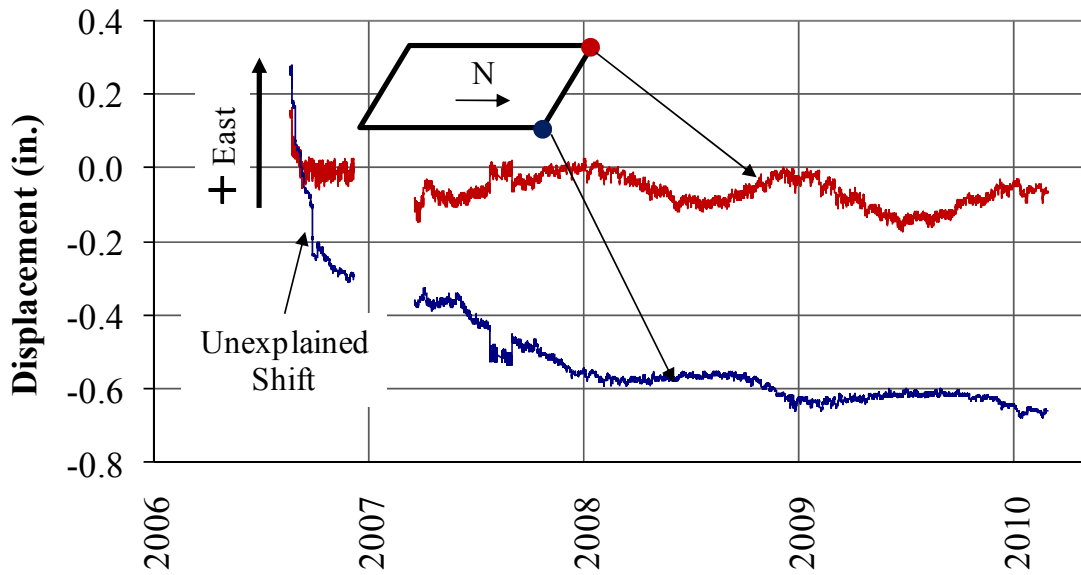
Figure 2.37: Transverse Movement of US-231, North Abutment
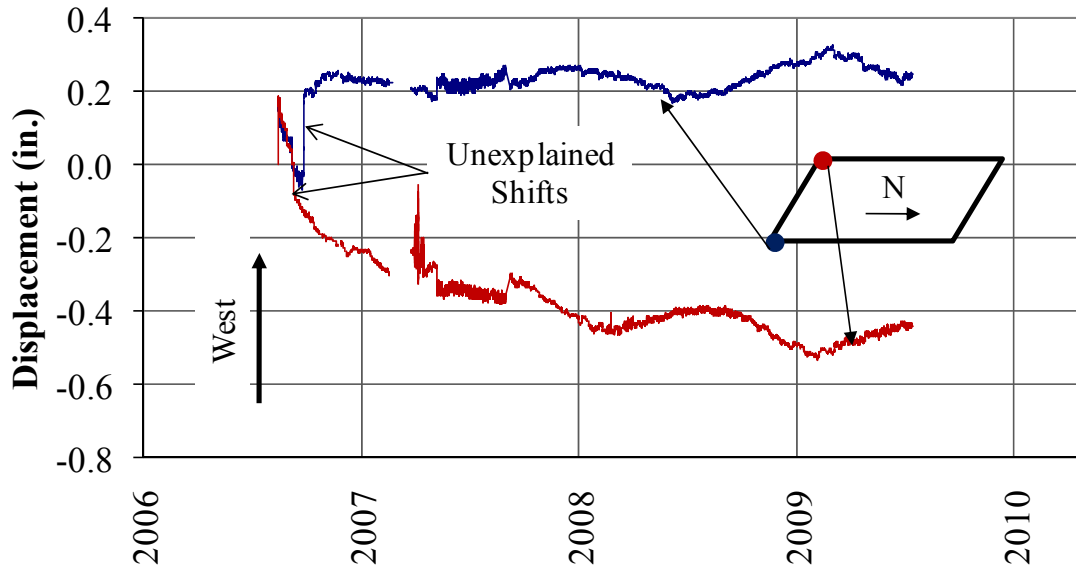
Figure 2.38: Transverse Moment of US-231, South Abutment

2.4.4.3. EARTH PRESSURE

Lateral earth pressure was collected to determine the effect of the backfill on the abutment. The instrumentation program resulted in an earth pressure cell being located at each location of a longitudinal convergence meter. The pressure records for the two groups of pressure cells, north and south, are shown in Figure 2.39 and Figure 2.40, respectively. The records are shown together to highlight their similarities. As can be seen, the pressure is approximately equivalent at each abutment. Therefore, pressure records from the north abutment will be used for future analysis as data was lost for the south following July 2009. It should be noted that the record for the pressure on the south abutment displays a jump in data for the summer of 2007. As discussed previously, this is believed to be an error in data collection. Furthermore, pressures less than zero are not physically possible.
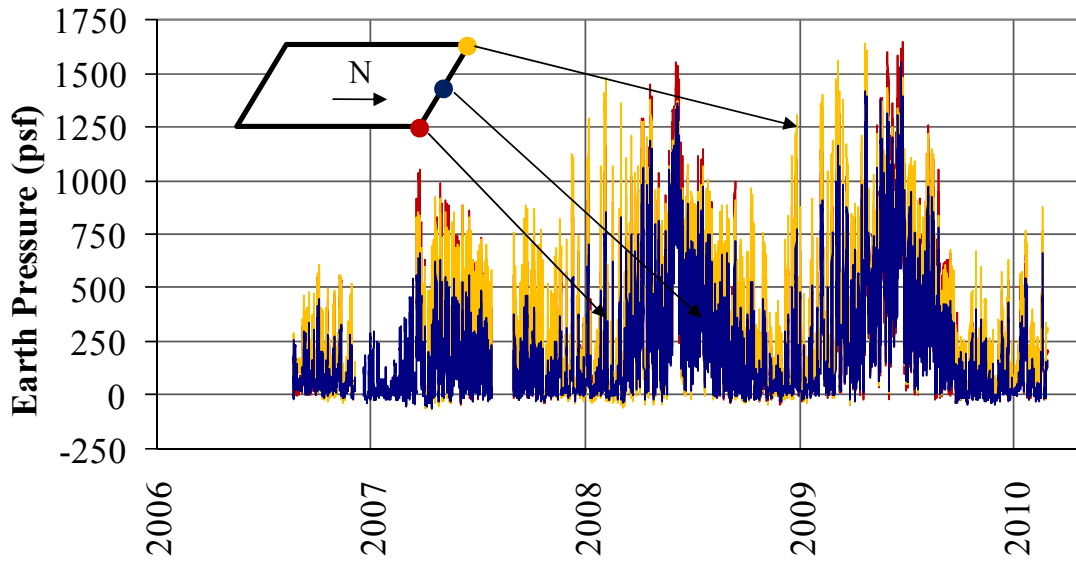
Figure 2.39: Lateral Earth Pressure for US-231, North Abutment
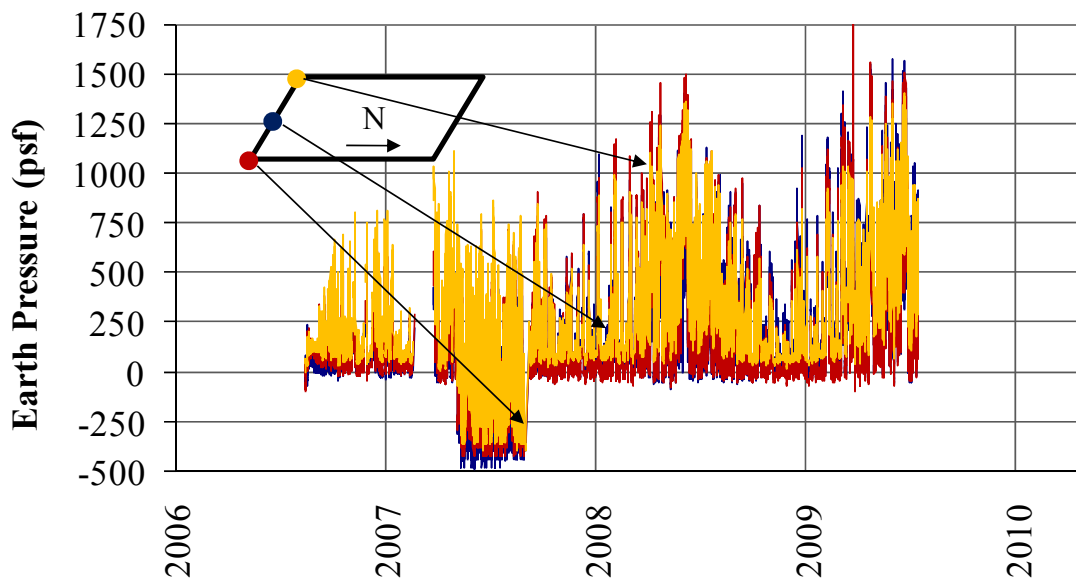
Figure 2.40: Lateral Earth Pressure for US-231, South Abutment

2.4.5. EVALUATION OF RESULTS

Using the temperature, displacement, and earth pressure measurements, a general understanding of the behavior of US-231 over the AEP railroad spur can be developed. Initially,

a visual inspection of the data reveals some insight regarding the behavior (Figure 2.41). Upon first glance, it is evident that US-231 exhibits many behaviors similar to those of SR-18. First, a net inward movement as the structure is cycled through various seasons is evident. Also, similar to SR-18, the net-inward displacements for US-231 reduce in magnitude each consecutive year. As mentioned previously, each abutment is behaving approximately symmetrically. However, differing from SR-18, it is apparent that the abutment is rotating in addition to translating longitudinally. As the structure contracts annually, the skew angle is reduced. Simply stated, the structure is attempting to "straighten" itself out throughout its life-cycle. The more the abutment contracts, the more the abutment undergoes this behavior. However, the amount of rotation is negligible: equaling less than a fraction of a degree toward the end of the record. The superstructure is being loaded by a yearly consistent temperature differential of approximately 80 degrees Fahrenheit. Following the conventional method, determining the estimated lateral demand for the supporting piles would be calculated according to Equation 2.1.

$$\Delta L = 5.5*10^{-6} \frac{1}{°F} (80°F) \left(\frac{221\,ft}{2} \right) \left(\frac{12\,in.}{1\,ft} \right) = 0.58\,in. \tag{2.10}$$

The first inward cycle measured by the convergence meters shows, on average, a displacement equal to 0.4 in. Because the calculation in Equation 2.10 is based on unrestrained thermal shrinkage, the difference can be attributed to soil restraint and pile stiffness. However, as the life of the structure progresses, the displacement of the center of the abutment reaches the predicted amount. Furthermore, the displacement of the acute angle corner displaces beyond the calculated amount toward the end of the record. In this case, the prediction closely estimates the actual displacement. It is unclear if this is a coincidence, and requires additional investigation. However, it is clear that the skew of the structure is causing additional displacement in the longitudinal direction. Specifically both acute corners of the structure displace more that the the obtuse corner meaning that the abutment is rotating. This is a significant mode of behavior for skewed structures.
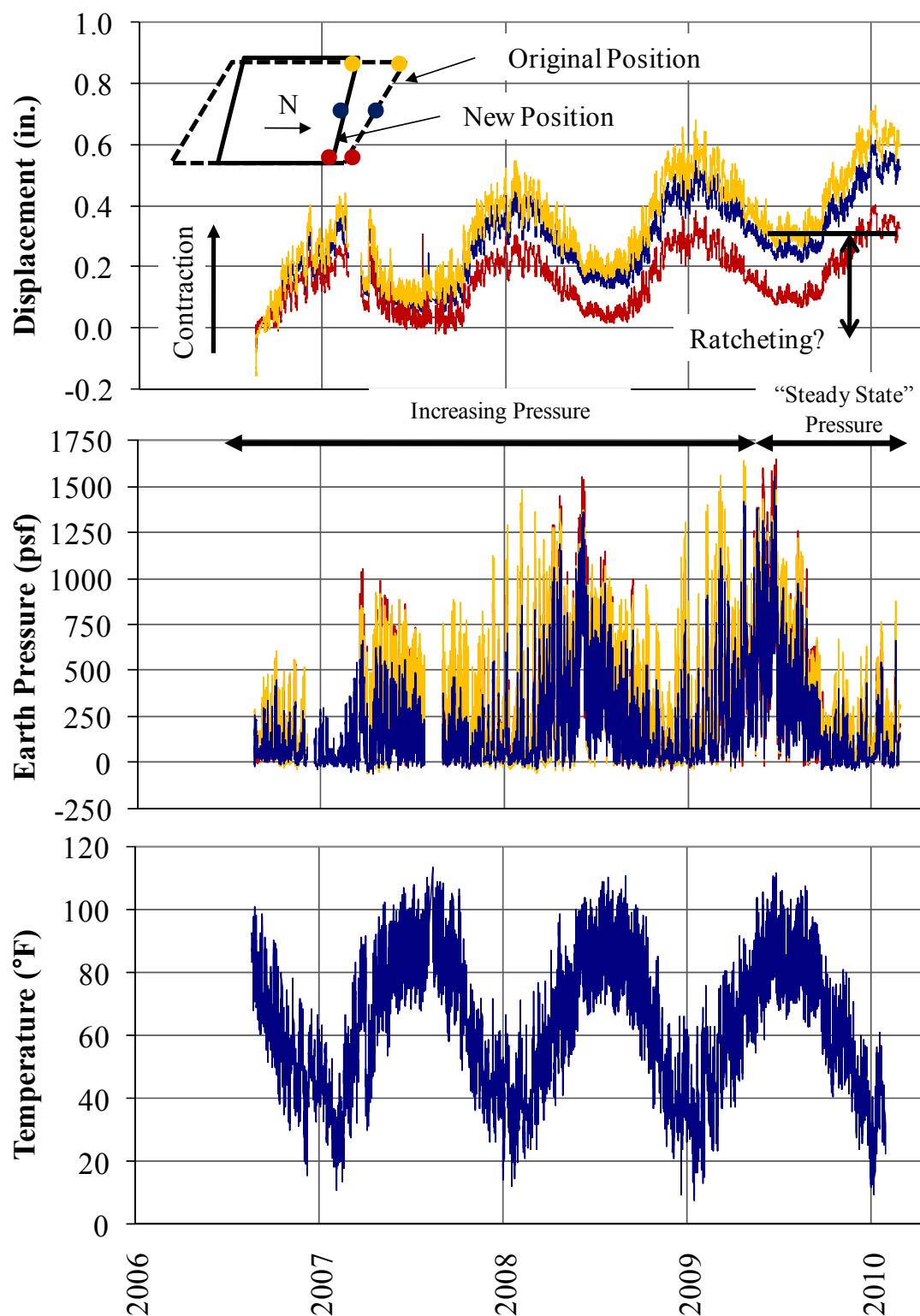
Figure 2.41: Evaluation of Collected Data from US-231

US-231 also seems to exhibit similar pressure behavior to that of SR-18. While is it unclear if the earth pressures have reached a steady-state, it is clear that the increase in pressure is decreasing from year to year. The end of the record is the approximate amount of time when other structures have begun steady state behavior. The pressure records also reveal that the lateral earth pressure behind the abutment reduces to zero during the contraction phase. Again, this is explained by the formation of a gap between the backfill and the abutment during times of greatest contraction. Using the depth of the gage at 4.64 ft and assuming a unit weight of 130 pcf and internal angle of friction of 30 degrees for the backfill, the measured magnitudes of lateral earth pressure can be compared with classical lateral earth pressure theory (Equation 2.3 through Equation 2.5).

$$\sigma_{ha} = K_a \sigma_v = 0.33(120\,pcf)(4.64\,ft) = 300\,psf \qquad (2.11)$$

$$\sigma_{hp} = K_p \sigma_v = 3(120\,pcf)(4.64\,ft) = 1700\,psf \qquad (2.12)$$

The pressure data for US-231 reveals very similar information to that of I65 over SR-25 and SR-18. The measured values of pressure for the active state are less than the theoretical values which agrees with the formation of a gap between the backfill and the abutment. The measure passive pressure is also less than the theoretical values; however, in this case it is fairly close to that estimated by theory. Again, the movement necessary to reach passive pressure is assumed to be 2% of the height of the abutment, which is approximately 1.5 in. which is significantly more than the measured movements (0.6 in.). Consequently it is expected that the abutment pressures should not reach full passive pressure. The fact that the pressures experienced here are approaching the full passive pressures which wasn't observed in the other structures may be explained by several reasons. First, the abutment is rotating which may cause an increased pressure especially at the acute corner which experiences greater displacement. Greater pressures are observed throughout the history at this location. Second, the backfill used in this structure may have a tendency to produce higher pressures at smaller displacements. Therefore, full passive pressure is reached at lower displacements.

Inspecting the displacement measurements combined with the earth pressure measurements provides even greater insight regarding the overall behavior of the structure. Similar to the SR-18 structure, it is noticed that the abutments of US-231 experience a net inward movement throughout the structure's life. However, the earth pressures have increased over time. For this behavior to occur, there must be settlement of the soil behind the abutment. As the

pressure record continues and starts to enter "steady-state", the displacement continues to move inward. As previously discussed for SR-18, for the increasing earth pressure to cause the inward abutment movement, the pressure would need to increase each year which is not the case. This structure again supports that a different mechanism is driving the inward movement.

2.5. CONCLUSIONS

Based on the measured data, several conclusions can be provided regarding the general behavior of integral abutment bridges:

1. The superstructure of an integral abutment bridge, when subjected to seasonal temperature differentials, expands and contracts. However, over a structure's life-cycle, a net inward displacement occurs (contraction). The annual magnitude of inward displacement decreases each consecutive year until a steady-state develops and the net inward movement stops. Considering the behavior of SR18, it appears that a steady state response occurs following approximately seven years.

2. Lateral earth pressures behind abutments initially increase from year to year. This increase occurs for approximately four years. Following this time frame, a steady-state develops where increasing pressures do not develop. A gap typically forms behind the abutment during the contraction phase reducing the lateral earth pressure to zero. Considering that the maximum inward displacement of the structure occurs at a time where the inward pressure is zero, it is evident that lateral earth pressure does not cause continuing inward movement of the structure.

3. Supporting piles continue to bend in double curvature throughout the life of the structure. The piles also indicate a net inward movement of the abutment. For Indiana, the average maximum temperature differential is approximately 70 degrees Fahrenheit.

4. Temperature differentials cause the cyclic behavior of the abutment movement; however, temperature differentials are not responsible for the net inward movement.

5. For skewed structures, rotation of the abutment occurs in addition to longitudinal movement.

6. While simple thermal contraction (Eq. 1.1) significantly overestimates the annual displacement of the structure caused by thermal movement, this value closely estimates the maximum inward movement of the structure over its life-cycle. It should be noted that this correspondence may be coincidence and needs further evaluation regarding its applicability.

CHAPTER 3. ANALYSIS OF FIELD RESULTS

3.1. INTRODUCTION

To evaluate the data collected from the field investigation in Chapter 2 and expand the understanding of the behavior of integral abutment bridges, analytical models were developed. Two and three dimensional models were developed for the SR-18 structure, and a three dimensional model was developed for the US-231 structure. Because of the limited collected data from the I-65 structure, an analytical model was not developed. For both SR-18 and US-231, simplified models were created using standard finite elements with assumed linear elastic behavior. The primary variables that needed to be considered were the conditions of the soil surrounding the piles and abutments, as well as the loading forces. To simplify soil modeling, equivalent springs were developed that represented the lateral earth resistance for both the abutment and piles. Regarding the loading, temperature records recorded from the field investigation were converted to equivalent strains and applied to the superstructure. To capture the net inward structural movement, shrinkage strains were also applied to the superstructure. Using the measured seasonal movements of each structure, the analytical models were calibrated by adjusting the loading and soil parameters to match the measured movements of each structure. This chapter provides a description of the models for each structure as well as the corresponding results.

3.2. STRUCTURAL ELEMENTS

The analytical models were developed using SAP 2000 (CSI 2009), a finite element program designed for structural analysis and design. Using built-in elements, a simplified analytical model was developed for each structure. The beams and piles were modeled using frame elements. The deck of the superstructure and the abutments were modeled in two ways: for the 2-D model they were modeled using a frame element while for the 3-D model, they were modeled using shell elements. For the 3-D models, the abutment was modeled as a thick shell element as opposed to a thin shell element which was used for the deck. To capture continuity between the deck and the girders, rigid links were attached to the centroids of each element.

Detailed descriptions of each element along with the corresponding characteristics of the modeled member are provided below.

3.2.1. GIRDERS

For each structure, the girders were modeled using a frame element. The frame element is a general beam-column formulation that includes biaxial bending, torsion, axial deformation, and biaxial shear deformations. For each respective structure, the properties of the actual beam members are shown below.

3.2.1.1. SR-18 BEAM PROPERTIES

The superstructure of SR-18 over the Mississinewa River Bridge consists of five 60 in. Indiana Bulb Tee beams. The dimensions and properties used to develop the frame elements for the beams are shown in Figure 3.1 and Table 3.1, respectively.
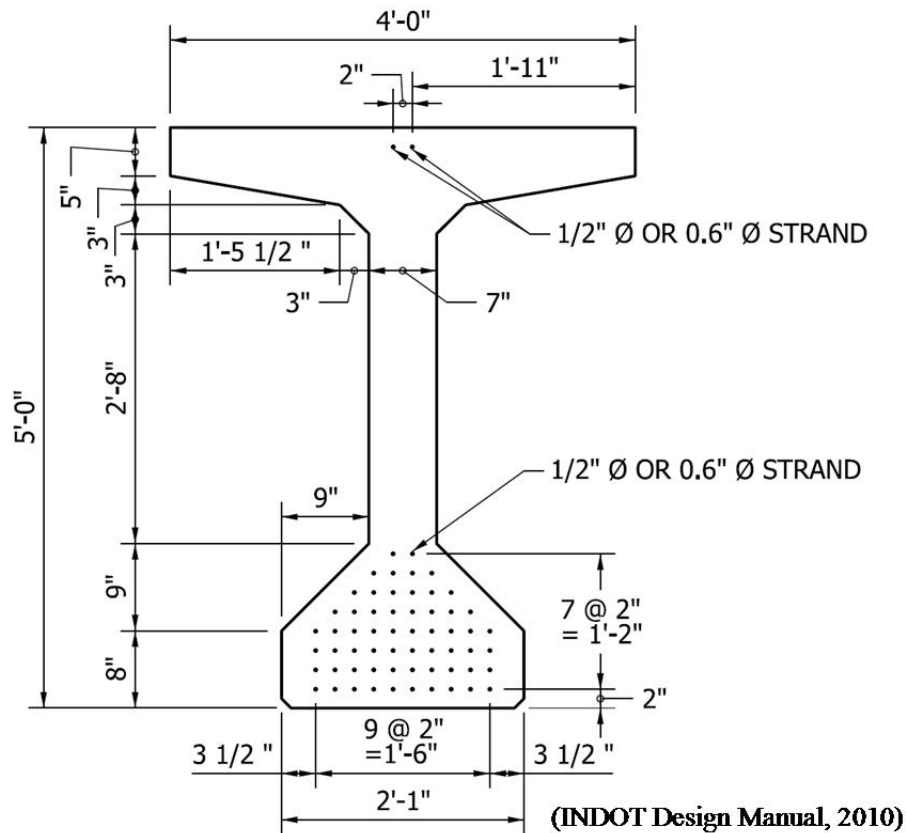
Figure 3.1: SR-18 Beam Cross Section

Table 3.1: SR-18 Beam Properties

Area of Beam, A_g	929.5 in.^{2}
Primary Axis Moment of Inertia, I_{11}	448036 in.^{4}
Secondary Axis Moment of Inertia, I_{22}	71156 in.^{4}
Design Concrete Compressive Strength, f_c'	6000 psi
Weight of Beam, w_g	971 plf

3.2.1.2. US-231 BEAM PROPERTIES

The superstructure for the US-231 structure consists of seven AASHTO Type III Prestressed I-Beams. The dimensions and properties used to develop the frame elements are shown in Figure 3.2 and Table 3.2, respectively.

(INDOT Design Manual, 2010)
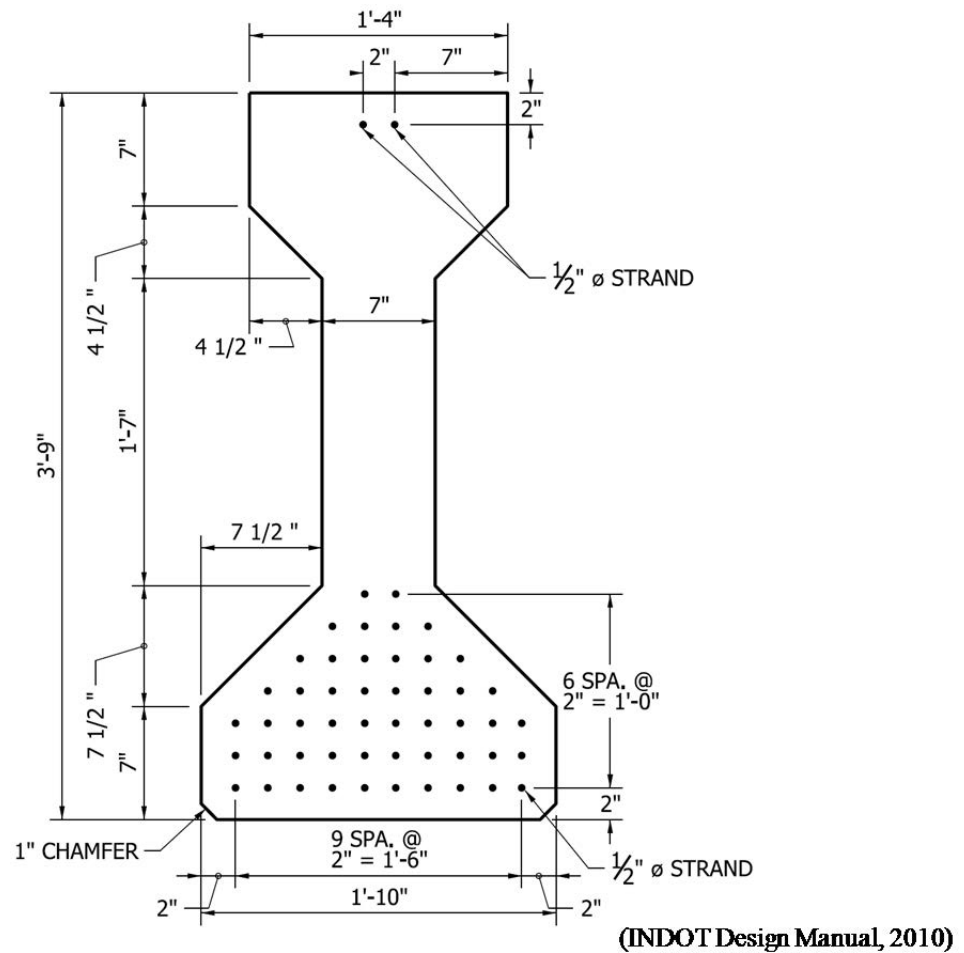
Figure 3.2: US-231 Beam Cross Section

Table 3.2: US-231 Beam Properties

Area of Beam, A_g	560 in.^{2}
Primary Axis Moment of Inertia, I_{11}	125390 in.^{4}
Secondary Axis Moment of Inertia, I_{22}	12217 in.^{4}
Design Concrete Compressive Strength, f_c'	5000 psi
Weight of Beam, w_g	683 plf

3.2.2. PILES

Each abutment for SR-18 and US-231 is supported by 14 in. pipe piles with a 0.312 in. wall thickness filled with concrete (CFT14x0.312). The sections were transformed into equivalent steel sections and the corresponding transformed properties were used in the analysis of both structures. Each pile consisted of ASTM A252, Grade 2 steel with a 35 ksi yield strength and concrete with a design compressive strength of 4000 psi. The modulus of elasticity of the steel and concrete is 29,000 ksi and 3,605 ksi respectively. To determine a transformed section for the concrete core, the modular ratio, *n*, was determined using Equation 3.1.

$$n = \frac{E_s}{E_c} \tag{3.1}$$

where:

E_s = Modulus of Elasticity of Steel, 29,000 ksi

E_c = Modulus of Elasticity of Concrete, $57\sqrt{f_c'} = 3605$ ksi

The modular ratio was used to transform the concrete core to an equivalent steel section (Figure 3.3). The transformed section's moment of inertia was then determined by the summation of the moment of inertias of the steel pipe and transformed core. The calculated effective pile properties are shown in Table 3.3.

$$I_{eff} = I_{pipe} + I_{trans} \tag{3.2}$$

$$I_{pipe} = \frac{\pi}{64}\left(O.D.^4 - I.D.^4\right) \tag{3.3}$$

$$I_{trans} = \frac{1}{4}\pi\left(\frac{I.D.}{2}\right)^3\left(\frac{I.D.}{2n}\right) \tag{3.4}$$

where:

O.D. = Outer Diameter of Pipe Pile

I.D. = Inner Diameter of Pipe Pile
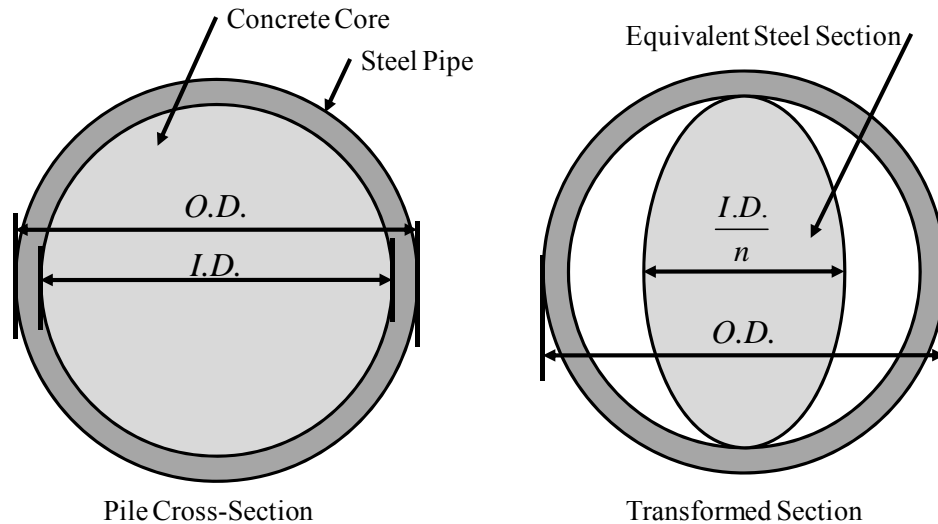
Figure 3.3: Transformed Section of Pile Cross-Section

Table 3.3: CFT14x0.312 Transformed Section Properties

Outer Diameter, O.D.	14 in.
Inner Diameter, I.D.	13.376 in.
Wall Thickness, t	0.312 in.
Effective Area, A_e	30.7 in.^{4}
Effective Moment of Inertia, I_e	507 in.^{4}

For the analysis of each structure, several assumptions were made regarding the piles. These assumptions are as follows:

- Piles are fixed at their base.
- The embedment of the pile into the abutment provides a rigid connection. Therefore, no differential rotation is permitted between the pile and the abutment.
- The piles are assumed to be perfectly vertical at the moment the structure becomes continuous.
- The piles lengths are constant and are considered as the average pile depth.

3.2.3. DECK

Both structures, SR-18 and US-231, contain 8 in. concrete decks on top of their respective girders. The concrete was 4000 psi concrete and is assumed to behave linear elastic. Two methods were used to analytically represent the concrete slabs depending on the method of analysis. Initially, a two dimensional analysis was developed for the SR-18 structure. The two dimensional model represented an interior section of the structure. Specifically, the superstructure for the two dimensional model consisted of two frame elements: one frame element to represent a single girder, and another frame element to represent the corresponding tributary area of concrete deck supported by that girder. Subsequently, three dimensional models were developed for both the SR-18 and US-231 structures. In contrast to the two dimensional model, these analytical models were developed to represent the entire structure. To represent the concrete deck, a four node shell element was implemented with a thin-plate formulation that neglects transverse shearing deformation. The concrete deck, in turn, was supported by frame elements that represent the girders. In both the two and three dimensional analyses, rigid links were provided to connect the deck elements to the supporting girders to account for continuity (Figure 3.4).
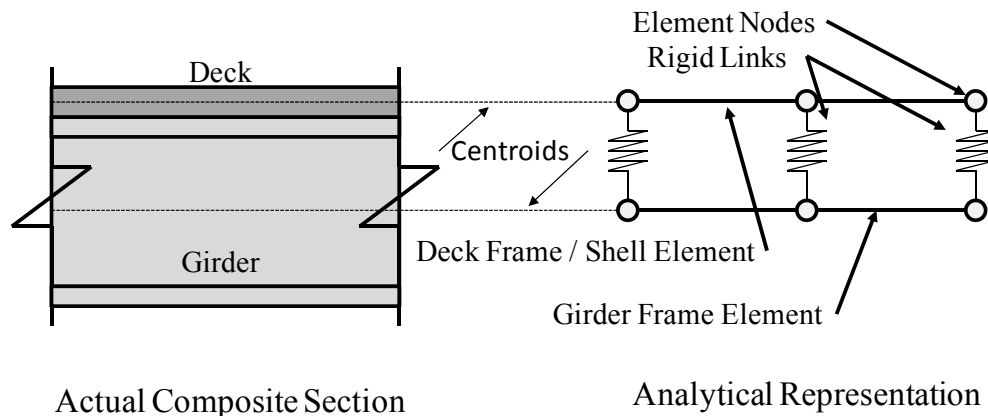
Figure 3.4: Analytical Representation of Composite Girder and Deck Connection

3.2.4. ABUTMENTS

The end bents for the two structures were modeled following the same procedures that were used to model the deck. A frame element was used to model the abutment in the two dimensional model of SR-18. For both three dimensional models, four node shell elements were

used. As opposed to the deck elements, a thick-shell element that incorporates the effects of transverse-shearing deformations was implemented. The connections of the abutment to the girder, deck, and piles were assumed to behave as rigid connections. The abutments were cast with 4000 psi concrete and assumed to behave linear elastic. For US-231, the abutment was modeled to account for a four degree cross-slope of the superstructure. Therefore, the abutment height of the US-231 structure is 101 in. on the west end of the structure and 63 in. on the east end. The average dimensions for the two abutments are shown in Table 3.4.

Table 3.4: Abutment Dimensions for Analytical Models

Structure	SR-18	US-231
Average Abutment Height	108.5 in.	82 in.
Abutment Thickness	39 in.	36 in.
Abutment Width	48 in.	45.75 in.
Skew Angle	8 deg	33.8 deg

3.3. SOIL ELEMENTS

The difficulty of modeling integral abutment bridges is primarily a result of soil-structure interaction. Both the behavior of the piles and abutments are a function of the supporting soil. To capture the effect of the supporting soil, recommendations of Griemann et al. (1984) were used to develop equivalent soil springs for piles, and various lateral earth pressure theories were used to develop springs behind the abutments. The springs were based on Winkler type mechanisms in which each spring is linear and each spring acts independently from the others (Coduto 2001).

3.3.1. PILE SPRINGS

The recommendations of Griemann et al. (1984) are based on the development of p-y curves. A p-y curve, shown in Figure 3.5, is a method commonly used to account for lateral resistance of soil on a pile as a function of the lateral displacement of the pile. The relationship is represented in units of force per length. The curve is a function of various parameters including soil type, moisture content, effective stress, stress history, and loading conditions (Welch and Reese 1972). The true soil response is typically non-linear, but can be represented by an elastic, perfectly plastic relationship. A representative response starts with an initial soil stiffness, $E_{si}(z)$, and continues until an ultimate soil resistance, P_{ult}, is reached. The value of the ultimate

resistance and initial soil stiffness vary with depth, therefore various curves must be developed along the length of the pile (Figure 3.6).
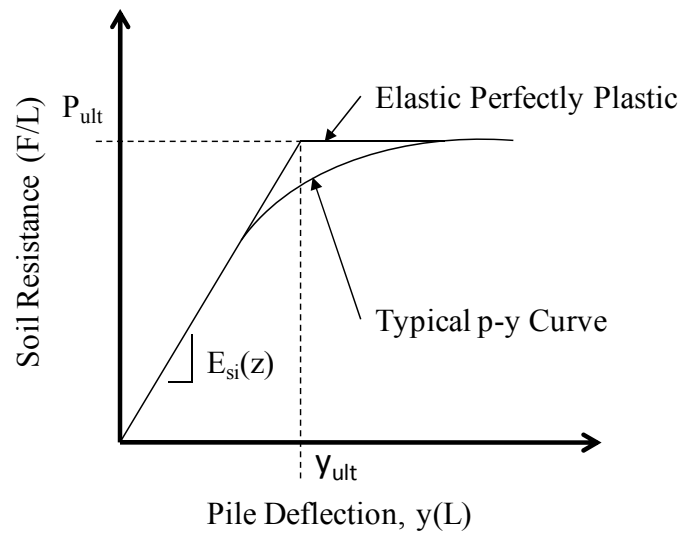
Figure 3.5: Typical p-y Curve
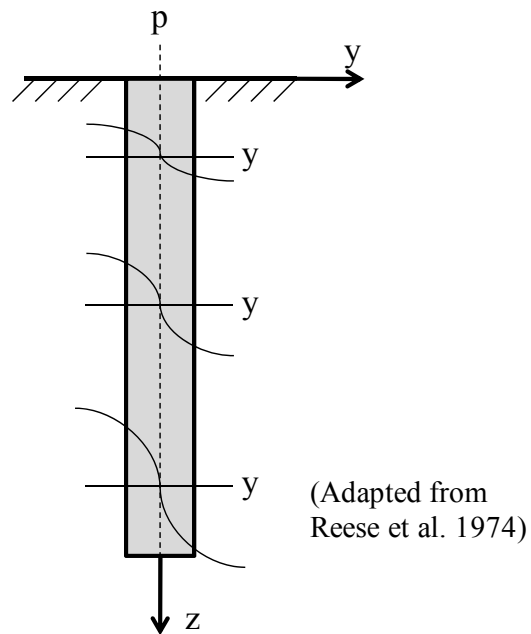
Figure 3.6: Lateral Pile Resistance (p-y curves) Along the Depth of a Pile

To account for various soil types, different expressions have been developed for sand and clay. Griemann et al. (1987) developed an expression for the ultimate soil resistance of clay. For soft and stiff clay, the initial soil modulus, $E_{si}(z)$, and the ultimate resistance, $p_u(z)$ are calculated as follows:

$$E_{si}(z) = \frac{p_u}{y_{50}}$$ (3.5)

$$p_u(z) = \min \left\{ \begin{array}{c} \left[3 + \frac{\gamma}{c_u} z + \frac{0.5}{B} z \right] c_u B \\ 9 c_u B \end{array} \right\}$$ (3.6)

For very stiff clay, the properties are as follows:

$$E_{si}(z) = \frac{p_u}{2 y_{50}}$$ (3.7)

$$p_u(z) = \min \left\{ \begin{array}{c} \left[3 + \frac{\gamma}{c_u} z + \frac{2}{B} z \right] c_u B \\ 9 c_u B \end{array} \right\}$$ (3.8)

where:

p_u = ultimate soil resistance, kip/ft

γ = unit soil weight, lbs/ft^3

c_u = shear strength, psf (Table 3.5)

B   = dimension the pile parallel to axis of bending, ft (Figure 3.7)

z   = depth of spring from soil surface, ft

y_{50} = displacement at one-half ultimate soil resistance, ft

      soft and stiff clay – $2.5 B \varepsilon_{50}$

      very stiff clay – $2.0 B \varepsilon_{50}$

      (Griemann et al. 1987)

ε_{50} = axial strain at one-half peak stress from tri-axial test

      soft clay – 0.02

      stiff clay – 0.01

      very stiff clay – 0.005

      (Reese and Van Impe. 2000)

Table 3.5: Undrained Shear Strength and Soil Modulus Parameters

Clay	Undrained Shear Strength, s_u (psf)	Average Shear Strength c_u, (psf)	Soil Modulus, k (lb/in.^{3})
Soft	250-500	375	30
Medium	500-1000	750	100
Stiff	1000-2000	1500	500
Very Stiff	2000-4000	3000	1000
Hard	4000-8000	6000	2000

Bending Axis   Bending Axis   Bending Axis

$B = b_f$ $B = d$ $B = $ O.D.

(a) Strong Axis Bending   (b) Weak Axis Bending   (c) Symmetric Axis

(Chovichien 2004)
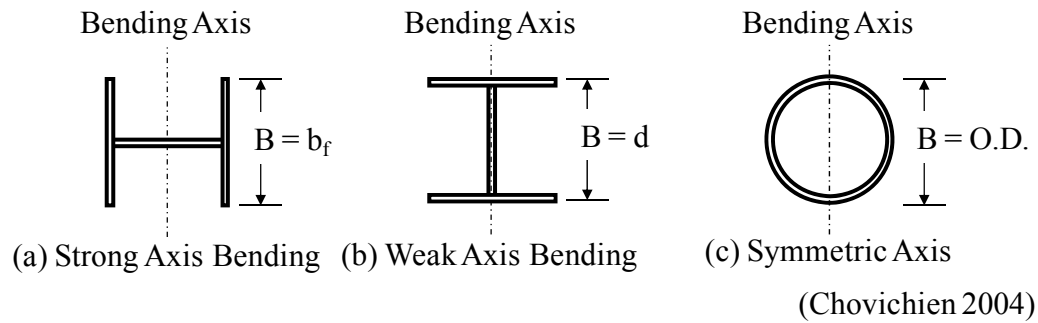
Figure 3.7: Definition of B for Griemann p-y Curve Expression

Griemann et al. (1984) also proposed the following expressions for the initial soil modulus and maximum resistance for sand.

$$E_{si}(z) = \frac{J\gamma}{1.35} z \qquad (3.9)$$

$$p_u(z) = 3\gamma B(K_p) z \qquad (3.10)$$

where:

J   =   200 for loose sand ($\varphi = 30°$)

             600 for medium sand ($\varphi = 35°$)

             1500 for dense sand ($\varphi = 40°$)

φ =   internal angle of friction, degrees

γ =   unit weight of soil, pcf

z   =   depth below ground surface, ft

B   =   dimension of pile parallel to axis of bending, ft (Figure 3.7)

K_p =   coefficient of passive earth pressure,

$$\tan^2\left(45° + \frac{\phi}{2}\right) \text{ according to Rankine Theory}$$

To convert the computed p-y curves into an elastic, perfectly plastic spring, the desired spring spacing is determined. The spring stiffness is calculated by multiplying the spring spacing by the soil modulus at that desired depth (Equation 3.11). The spring is limited by the ultimate resistance which is similarly computed (Equation 3.12).

$$k_{soil} = s \cdot E_{si}(z_i) \tag{3.11}$$

$$P_u = s \cdot p_u(z_i) \tag{3.12}$$

where:

k_{soil} = elastic stiffness of pile spring, kip/ft

$E_{si}(z_i)$ = soil modulus at desired spring depth z_i, kip/ft^2

s = spacing of soil springs, ft

P_u = Ultimate Soil Resistance, kip

$p_u(z_i)$ = ultimate soil resistance at desired depth z_i, kip/ft

The displacement at which resistance no longer increases can be back calculated by dividing the ultimate pile resistance by the soil stiffness as follows:

$$\Delta_u = \frac{P_u}{k_{soil}} \tag{3.13}$$

A typical force-displacement relationship of a pile spring is shown in Figure 3.8
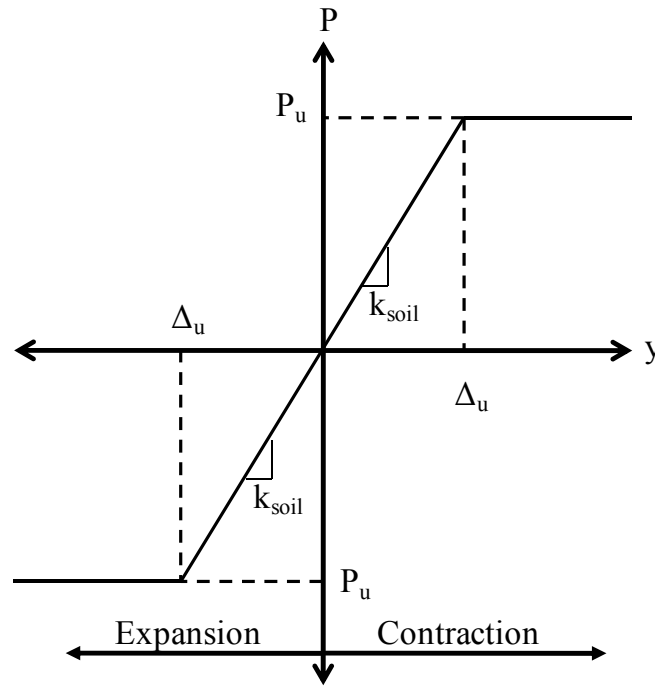
Figure 3.8: Typical Force-Displacement of a Pile Spring

Because each structure was built on a skew, it is important to ensure constant pile spring stiffness in all directions. To account for the skew of each structure, two pile springs, with equivalent stiffness, were applied at each elevation orthogonally to one another (Figure 3.9). In SAP2000, the stiffness of the spring works only in the axis the spring is assigned. Therefore, with this configuration, any direction of horizontal movement of the pile is resisted by equivalent soil stiffness.
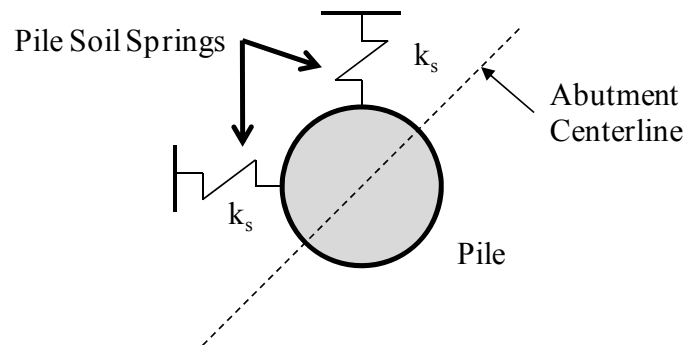
Figure 3.9: Soil Spring Configuration on Piles to Account for Skew Angle

3.3.2. ABUTMENT SPRINGS

Similar to the modeling technique for the soil surrounding the piles, the abutment fill was represented by a single spring with an approximated equivalent stiffness. However, much of the work on determining p-y curves for piles is not applicable to abutments. Rather, the abutment of an integral abutment bridge behaves similar to a typical retaining wall. Passive earth pressures are developed behind the abutment as the structure expands during summer months. During phases of contraction, the pressure measurements reveal that the abutment behaves differently, in which the lateral earth pressure reduces to zero. Therefore, passive earth pressure theories were implemented to develop springs to represent the soil's resistance to passive movement of the abutment. The soil was assumed to provide zero stiffness for movement away from the soil.

There are various theories available to determine passive earth pressure. Classical earth pressure theories include Rankine and Coulomb. Typically, these two theories are bounding values of the true passive earth pressure. Because Rankine neglects the effect of interface friction between the wall and supported backfill, the magnitude of passive pressure is under-predicted. On the other hand, Coulomb's theory includes the effects of interface friction but was not originally derived for passive earth pressures. According to Potyondy (1961), typical values of for the interface friction angle are at minimum 76% and 50% of the angle of internal soil friction for concrete against sand and clay, respectively. However, work by Duncan and Mokwa (2001) suggest that Coulomb's theory results in considerable error when the interface friction angle between the wall and supported backfill reaches 40% of the angle of internal soil friction. Therefore, Duncan and Mokwa (2001) recommend using the log-spiral theory for more accurately determining passive earth pressures as opposed the classical Rankine and Coulomb theories. Though more accurate, the log-spiral theory is much more complex. Because the backfill properties are usually not well defined, it would be advantageous to use a simple theory.

Based on the review of passive earth pressure theories, it was decided to implement both the log-spiral method and Rankine's theory to determine an estimation of the maximum lateral earth pressure. Rankine's theory was considered to evaluate the use of a simple theory while the log-spiral was considered to evaluate one that has been shown to be more accurate. These values were compared and evaluated regarding their effectiveness in representing the behavior of the structures evaluated as part of this study. Coulombs theory was not included in the analysis because of the extreme over-prediction of the passive earth pressure. While these passive earth pressure theories provide a theoretical maximum passive earth force, the theories do not provide

guidance on a load path required to reach that force. Two methods to obtain the load path are presented in Section 3.3.2.3.

3.3.2.1. RANKINE'S THEORY

Rankine theory is very simple to apply and works well for cohesionless soil which is typically used as backfill material. Rankine's theory, a lower bound theory, assumes that a wedge of soil forms behind a retaining wall when the wall is subjected to some movement (Figure 3.10). A solution is developed based on solving the statics of the soil weight, normal and friction forces along the slip plane, and the lateral resistance of the wall. If the retaining wall moves away from the supporting soil, an active condition is produced. The active condition is the lowest theoretical value of lateral earth pressure. The maximum value of lateral earth pressure is the passive case where the wall moves toward the supported fill. The pressures are then assumed to have a triangular distribution, with zero pressure at the surface and maximum pressure at the base of the wall.

H – Abutment Height
b – Abutment Width
P – Lateral Resisting Force
W – Weight of Soil
T – Interface Friction
N – Normal Force
φ – Internal Friction Angle
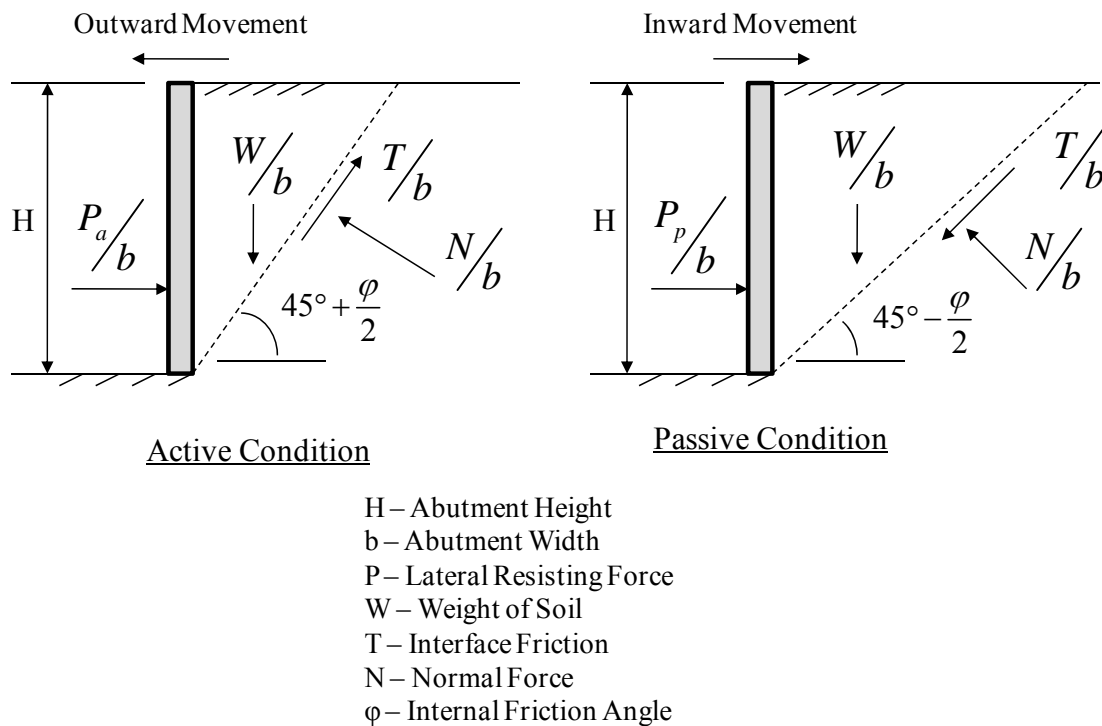
Figure 3.10: Rankine's Solution to Passive Earth Pressure

To determine the lateral earth pressure, σ_p, in the passive direction, the vertical effective stress is multiplied by a passive earth pressure coefficient determined from the static solution of the assumed failure plane.

$$\sigma_p(z) = \sigma_z^{'}(z)K_p \tag{3.14}$$

where:

$\sigma_z^{'}(z)$ = vertical effective stress at desired spring depth, ksf

$\qquad\qquad = \gamma^{'}z$

$\gamma^{'}$ = effective unit weight, pcf

z = depth of desired spring

K_p = passive earth pressure coefficient

$\qquad\qquad = \tan^2\left(45° + \dfrac{\varphi}{2}\right)$

φ = internal angle of friction, degrees

A total passive force is then determined by assuming a distribution of passive pressure behind the abutment wall. It is traditional to assume a triangular distribution. The maximum passive earth pressure is then calculated using Equation 3.15.

$$P_p = \frac{1}{2}(H)(b)\sigma_p(z) \tag{3.15}$$

where:

P_p = maximum passive earth force, kips

$\sigma_p(z)$ = passive lateral earth pressure at base of wall, ksf

b = width of abutment, ft

H = height of abutment, ft

3.3.2.2. LOG-SPIRAL THEORY

The log-spiral theory, discussed in detail by Terzaghi (1943) and Terzaghi et al. (1996), assumes a curved failure surface as opposed to the triangular wedge as assumed by Rankine's theory (Figure 3.11). The failure mechanism is assumed to consist of two zones, a Prandtl zone and Rankine zone. Soubra (2000) developed a kinematical approach to numerically solve the

log-spiral problem. Because the theory is an upper bound approach, the passive resistance is solved for various locations of a spiral center and continued until a minimum pressure is determined. A spreadsheet was developed to implement the method proposed by Soubra (2000) and used to determine the maximum passive resistance.
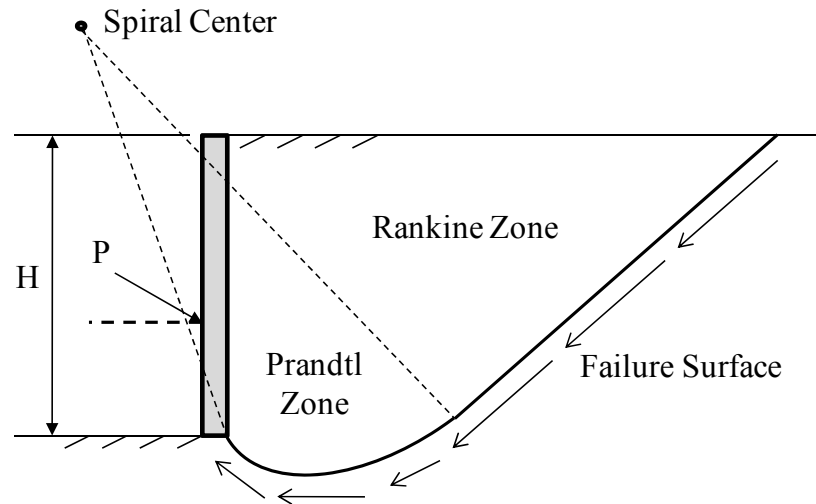
Figure 3.11: Assumed Failure Mechanism of Log-Spiral Theory

3.3.2.3. PASSIVE STIFFNESS

While Rankine's theory and the log-spiral method do not predict a load path required to attain the full passive pressure, other methods have been developed to define passive stiffness. Coduto (2001) recommends the required horizontal movement of a retaining wall to reach the passive condition is 2% of the wall's height for dense sand. Assuming the soil behaves elastic, perfectly plastic up to the full passive pressure, stiffness values can be determined for equivalent springs along the depth of the abutment. To determine the equivalent stiffness, the maximum passive pressure, from Rankine or Log-Spiral, is then divided by 2% of the wall height (Equation 3.16). The spring is assumed to act at the centroid of the assumed triangular stress block and perpendicular to the wall. A typical force-displacement relationship of a pile spring is shown in Figure 3.12. To capture the behavior measure in the field, specific cyclic behavior was assumed for the spring. Movement away from the fill (contraction) is assumed to be plastic. When the abutment begins an expansion phase, it is assumed the soil has filled in behind the wall and instantly provides stiffness. An example of the cyclic behavior of the abutment soil spring,

further referred to as a walking spring, is shown in Figure 3.13. To illustrate the walking spring shown in Figure 13, suppose an abutment starts at location A1. Assume that the structure heats up and expands to location B while encountering passive stiffness from the backfill, k_{abut}. If the structure contracts to point C, which is less than the previous expansion amount, the abutment will encounter the same backfill stiffness. Upon the next cycle of expansion, the abutment will travel in the direction of B with the same stiffness. Now assume that the structure contracts further than the previous expansion amount. While the structure moves past point A1 to an arbitrary point D, the backfill stiffness will be zero (representing a gap behind the abutment). The stiffness will remain zero until the structure begins to expand (from D to A1). Upon the expansion phase, the stiffness will again be k_{abut}.

$$k_{abut} = \frac{P_p}{0.02H} \qquad (3.16)$$

where:

k_{abut} =   lateral spring stiffness of abutment spring in passive direction, kip/ft

P_p =   maximum passive earth force, kips

H   =   height of abutment, ft
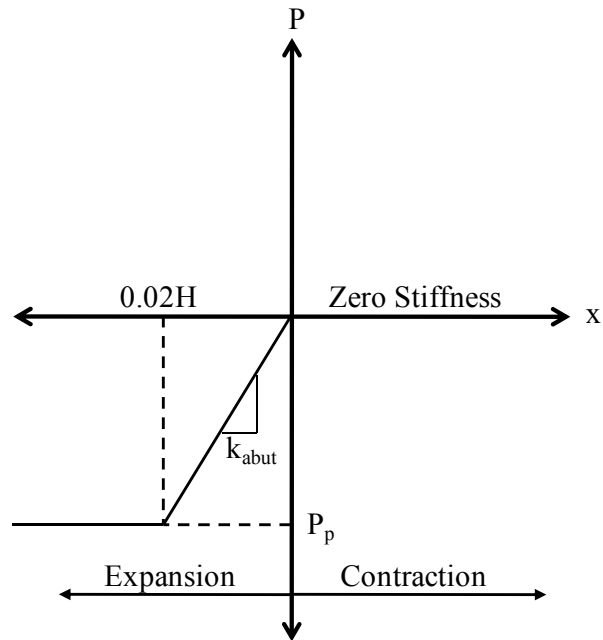
Figure 3.12: Typical Abutment-Soil Force-Displacement Relationship Using Rankine's Theory
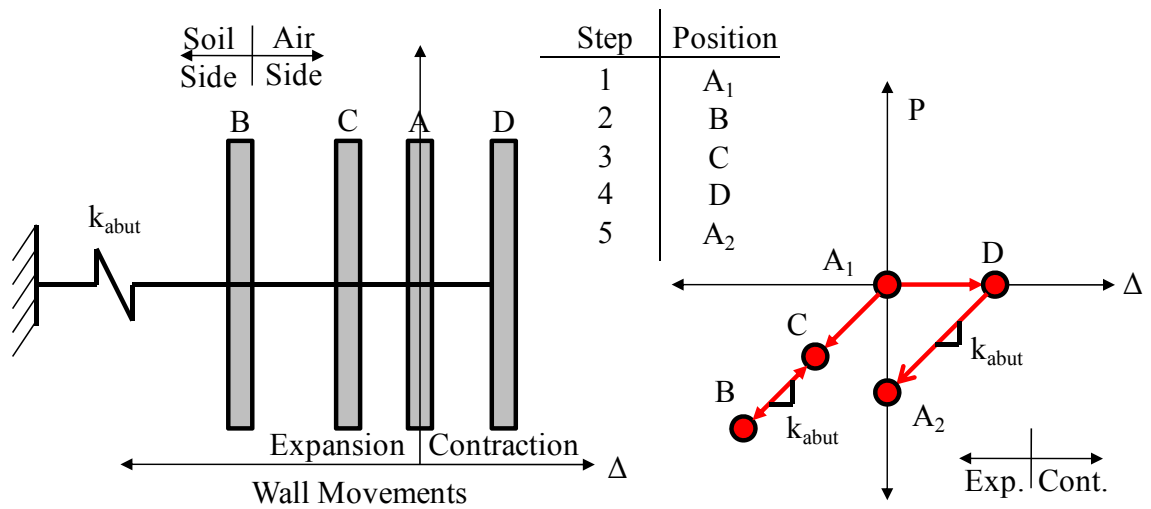
Figure 3.13: Walking Spring Cyclic Behavior

Another method to define a load path for passive pressure was developed by Duncan and Mokwa (2001). The method assumes a hyperbolic relationship to describe the force-displacement relationship of the backfill material:

$$P = \frac{y}{\dfrac{1}{K_{max}} + R_f \dfrac{y}{P_p}}$$ (3.17)

where:

P	= passive resistance, kip
y	= deflection, in.
K_{max}	= initial stiffness of backfill material / initial slop of curve, kip/in.
R_f	= failure ratio
P_p	= maximum passive earth resistance of backfill, kip

The failure ratio, as described by Duncan and Mokwa (2001), is the ratio of the ultimate passive pressure load divided by the hyperbolic asymptotic value of passive resistance. The value can be determined experimentally but usually ranges between 0.75 and 0.95. Based on recommendations by Duncan and Mokwa (2001), the failure ratio was assumed to be 0.85 in all calculations. The initial stiffness of the backfill material is calculated by solving an elastic solution for horizontal displacements of a uniformly loaded vertical rectangular area (plate) in an elastic half-space (Douglas and Davis 1964). The supporting backfill is represented by an equivalent initial Young's Modulus, E, and Poisson's ratio, ν. Values for Young's Modulus are given in Table 3.6, and Poisson's ratio is calculated using Equation 3.18. With an assumed applied load, deflections are calculated at two corners of the plate and averaged to determine values for K_{max}.

Table 3.6: Initial Values for Young's Modulus for Sand

Density	Initial Tangent Modulus, E_i (ksf)
Loose	200-400
Medium	300-500
Dense	400-600

(Duncan and Mokwa 2001)

$$v = \frac{1 - \sin(\phi)}{2 - \sin(\phi)} \tag{3.18}$$

where:

v = Poisson's ratio

φ = internal angle of friction, degrees

For use in the finite element analysis, an elastic, perfectly plastic relationship similar to that shown in Figure 3.12 was developed using the hyperbolic relationship. The hyperbolic curve continues until the ultimate passive resistance is reached. A simplified representation of the lateral pile stiffness was developed by ensuring the area under the simplified curve equaled the area under the hyperbolic prediction (Figure 3.14). As is shown in Figure 3.14, the elastic portion is a secant of the hyperbolic curve. Two areas are created between the two curves (A1 and A2). The location of the intersection of the two curves was adjusted until the areas were equal. The calculated stiffnesses were, therefore, lower at the beginning of the displacement range and higher toward the end of the displacement range. As opposed to the stiffness corresponding to the Rankine analysis, the displacement required to reach the full passive resistance is not dependant on the height of the abutment. The cyclic behavior of the abutment-soil spring was assumed to follow the same behavior of the previously defined walking spring (Figure 3.13). Again, this represents the assumed behavior of the backfill settling behind the abutment and instantly providing stiffness during an expansion phase.
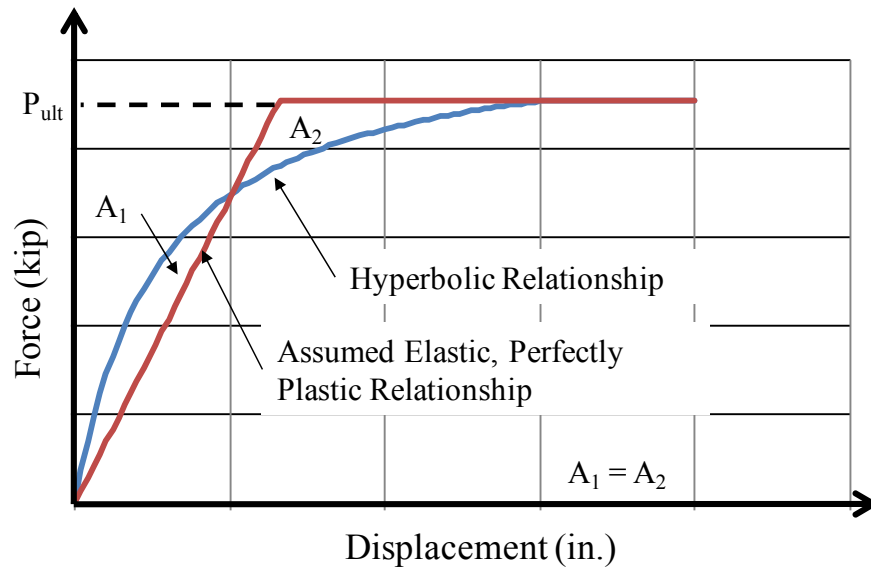
Figure 3.14: Approximated Elastic-Plastic Relationship for Abutment Soil

3.3.3. SR-18 SOIL SPRINGS

The soil surrounding the piles of SR-18 is classified as silt or clayey sand (soil borings for SR-18 are provided in Appendix B). However, models do not exist to produce soil springs for silts. For that reason, it was assumed that the soil surrounding the piles for SR-18 is a dry, medium density sand. The soil was assumed to have a unit weight of 120 pcf. The water table was measured as being below the bottom elevation of the piles. Using the previously describe method (Section 3.3.1), soil springs were developed. Table 3.7 shows stiffnesses for soil-springs spaced at 2 ft intervals along the depth of the pile. For the three-dimensional model, the entire structure was represented. Therefore, the values for a single pile were used in the three-dimensional analysis. However, the two dimensional model was developed to represent a section of the structure: a single girder, tributary area of deck, and two piles. Therefore, for use in the two-dimensional analysis, the values for two piles were used to account for the resistance of the soil against the two piles in the modeled section of the structure. For both analytical models of SR-18, the base, at 22 ft, was assumed to be fixed.

Table 3.7: Soil Spring Stiffnesses for SR-18 Piles

Pile Depth (ft)	Spring Stiffness (kip/in.)	
	Single Pile	Two Piles
0	0	0
2	18	36
4	36	71
6	53	107
8	71	142
10	89	178
12	107	213
14	124	249
16	142	284
18	160	320
20	178	356
22	Fixed	Fixed

Similarly, using the methods previously described (Section 3.3.2), soil-springs representing the backfill material were developed. Because the B-borrow backfill can have a variety of properties, the soil was assumed to be a densely compacted granular material. Table 3.8 shows the assumed properties of the fill.

Table 3.8: Soil Properties of SR-18 Abutment Fill

Soil Type	Unit Weight, γ (pcf)	Internal Friction Angle, φ (degrees)	Passive Earth Pressure Coefficient, K_p	
			Rankine (Eq. 3.14)	Log Spiral
Dense Sand	130	35	3.7	8.8

As discussed previously, two methods have been proposed to determine an equivalent stiffness of passive resistance for an abutment spring. The force-displacement properties of the representative springs are shown in Figure 3.15 and Figure 3.16. For both methods, the spring was located at the centroid of the assumed triangular stress distribution. Both methods were implemented, and the corresponding results in this chapter discuss the validity of each in regards to the structures evaluated in this study.
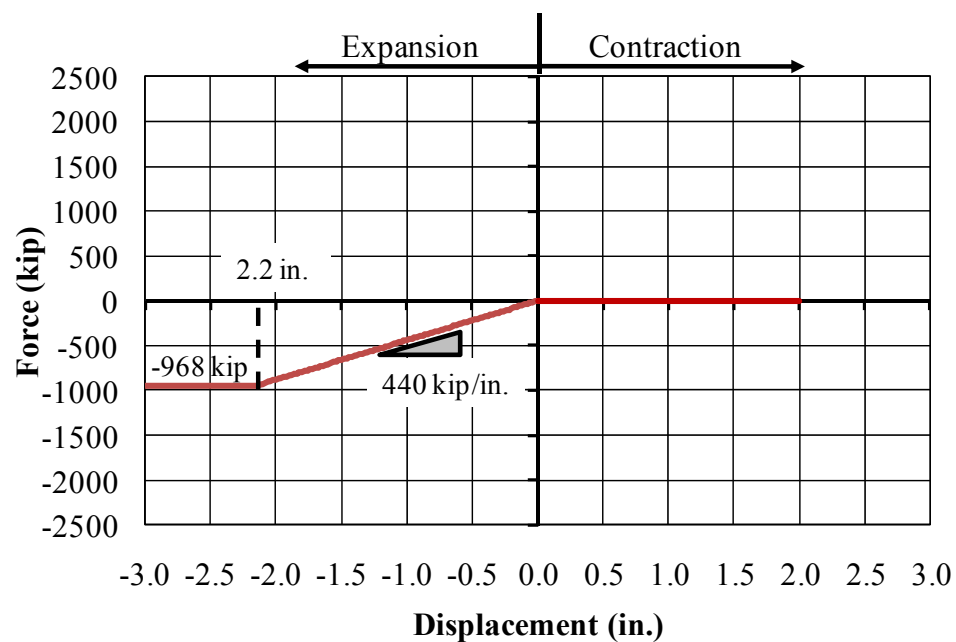
Figure 3.15: Abutment Spring - Rankine Theory
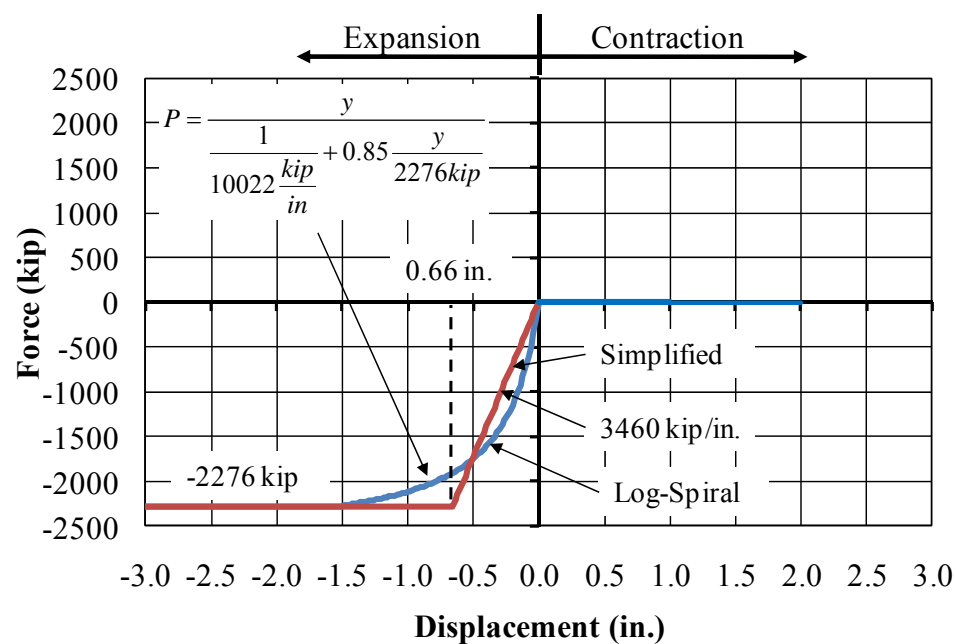
Figure 3.16: Abutment Spring - Log Spiral Method

3.3.4. US-231 Soil Springs

The US-231 sight required a large amount of fill to be placed for the construction of the bridge. The piles, 81 ft in total length, were therefore driven 50 ft into the existing soil. The top 31 ft were in the newly placed compacted fill. Table 3.9 contains the soil profile for the piles; the top 31 ft was assumed and the bottom 50 ft were obtained from the soil borings (illustrated in Appendix C). Following the procedures previously outlined, stiffnesses for soil springs spaced at 4.5 ft intervals along the depth of the pile were calculated (Table 3.10). It should be noted that the top and bottom layers of soil are coarse grained while the middle layer was clay. The base of the pile, at 81 ft, was assumed to be fixed.

Table 3.9: Soil Properties of Backfill and In-situ Soil for US-231

Soil Type	Depth (ft)	Thickness (ft)	γ_{eff} (pcf)	c_u (psf)	φ (deg.)
Existing Surface / Compacted Fill	0-30.7	30.7	120	-	30
Stiff Silty Clay Loam	30.7-53.7	23.0	125	1600	-
Gravelly Sand, Medium Dense	53.7-81.0	27.3	60	-	35

Table 3.10: Soil Spring Stiffness along the Depth of US-231 Piles

Pile Depth (Below Abutment) (ft)	Spring Stiffness (k/in.)
0.0	0
4.5	30
9.0	59
13.5	89
18.0	118
22.5	148
27.0	177
31.5	216
36.0	216
40.5	216
45.0	216
49.5	216
54.0	541
58.5	586
63.0	631
67.5	676
72.0	721
76.5	766
81.0	FIXED

Similar to the procedures used for SR-18, soil-springs representing the backfill material were developed using both Rankine Theory and the log-spiral method. Using the properties provided in Table 3.9, the passive earth pressures were calculated and are shown in Table 3.11. The force-displacement properties of the representative springs are shown in Figure 3.17 and Figure 3.18. For both methods, the spring was located at the centroid of the assumed triangular stress distribution. Both methods were implemented, and the corresponding results in this chapter discuss the validity of each prediction of the approach considering the structures evaluated in this study.

Table 3.11: Soil Properties for US-231 Abutment Fill

Soil Type	Unit Weight, γ (pcf)	Internal Friction Angle, φ (degrees)	Passive Earth Pressure Coefficient, K_p	
			Rankine (Eq. 1.34)	Log Spiral
Dense Sand	120	30	3.0	5.8
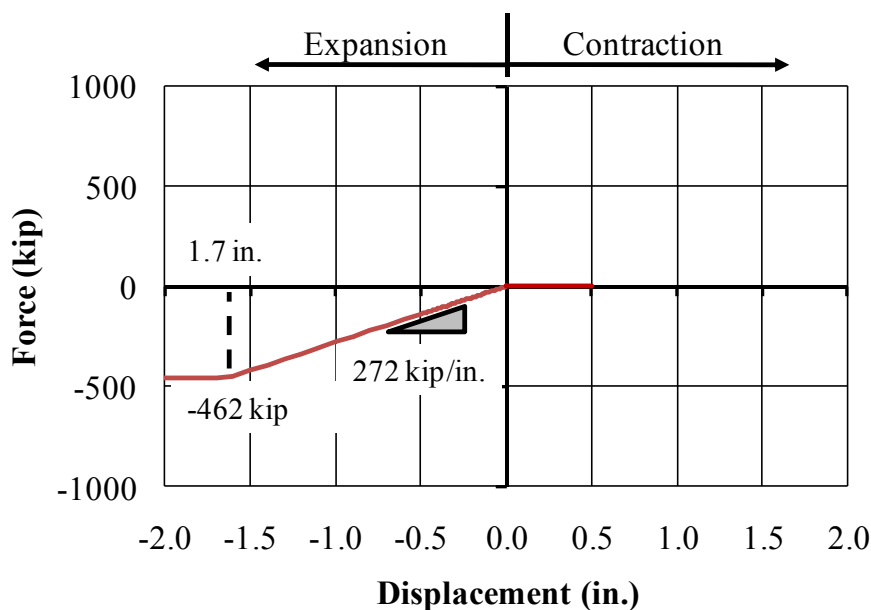
Figure 3.17: US-231 Abutment Spring - Rankine Theory
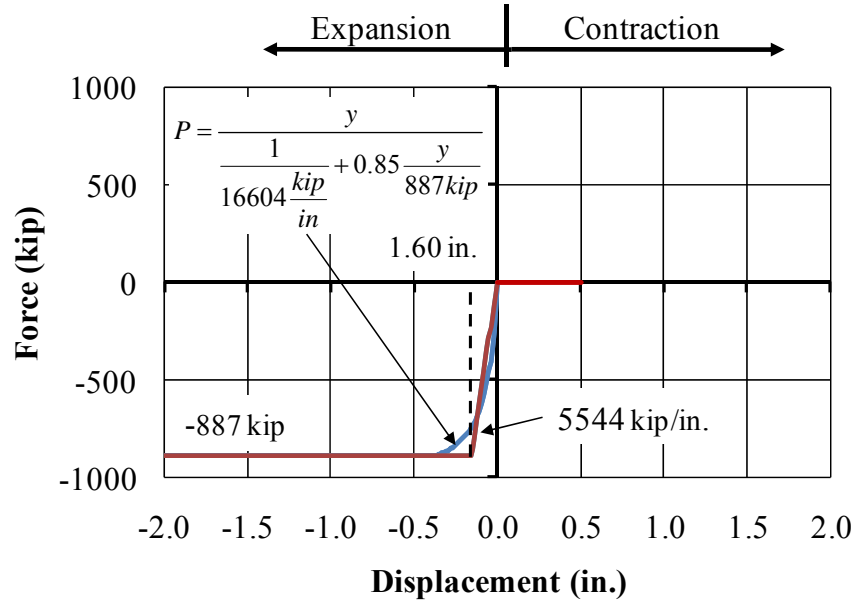
Figure 3.18: US-231 Abutment Spring - Log Spiral Method

3.4. LOADING SYSTEM

3.4.1. TEMPERATURE

The primary driving force behind the behavior of integral abutment bridges revolves around temperature differentials that the structure encounters from seasonal cycles. Using the collected ambient temperatures from the field investigation, average temperatures were selected at times of peak displacements. Using the ambient temperature when the structure was cast integral, temperature differentials were calculated. The temperature differentials were then converted to equivalent strains using the following expression:

$$\varepsilon_t = \frac{\Delta L}{L} = (\Delta T)\alpha \tag{3.19}$$

where:

ε_t = thermal induced strain, in./in.

ΔL = change in length, ft

L = total length, ft

ΔT = change in temperature, °F

α = coefficient of thermal expansion for concrete, $5.5 \cdot 10^{-6}$, 1/°F

The temperature strains applied to SR-18 and US-231 are shown in Table 3.12 and Table 3.13, respectively.

Table 3.12: SR-18 Temperature Strains

	Ambient Temperature (°F)	Differential Temperature (°F)	Strain (με)
Reference Temp. (Sept.)	65	0	0
Avg. Minimum Temp. (Jan.)	20	-45	-248
Avg. Maximum Temp. (July)	90	+25	138

Table 3.13: US-231 Temperature Strains

	Ambient Temperature (°F)	Differential Temperature (°F)	Strain (με)
Reference Temp. (Sept.)	65	0	0
Avg. Minimum Temp. (Jan.)	20	-45	-248
Avg. Maximum Temp. (July)	100	+35	193

3.4.2. SHRINKAGE

As discussed in Chapter 2, it is hypothesized that shrinkage, as opposed to the build-up of lateral earth pressure, causes net inward displacement of the abutment. ACI 209 (2008) presents several methods for predicting shrinkage strain in hardened concrete. The various models are based on different combinations of concrete properties and environmental conditions including compressive strength, cement content, water-cement ratio, relative humidity, and length of moist curing. Coincidentally, the properties and conditions for the deck of both the SR-18 and US-231 structures were the same and are shown in Table 3.14. A plot of the computed assumed shrinkage strains for the different models is shown in Figure 3.19.

Table 3.14: Properties of SR-18 and US-231 for Shrinkage Computations

Relative Humidity	50%
Time of Moist Curing of Deck	7 days
Volume to Surface Ratio of Deck	3.95 in.
Slump of Concrete	4 in.
Fine Aggregate Ratio	40%
Cement Content	658 lb / yd ^{3}
Air Content	6.5%
Concrete Compressive Strength	4000 psi
Water / Cement Ratio	0.44
Mean 28 Day Compressive Strength	5100 psi
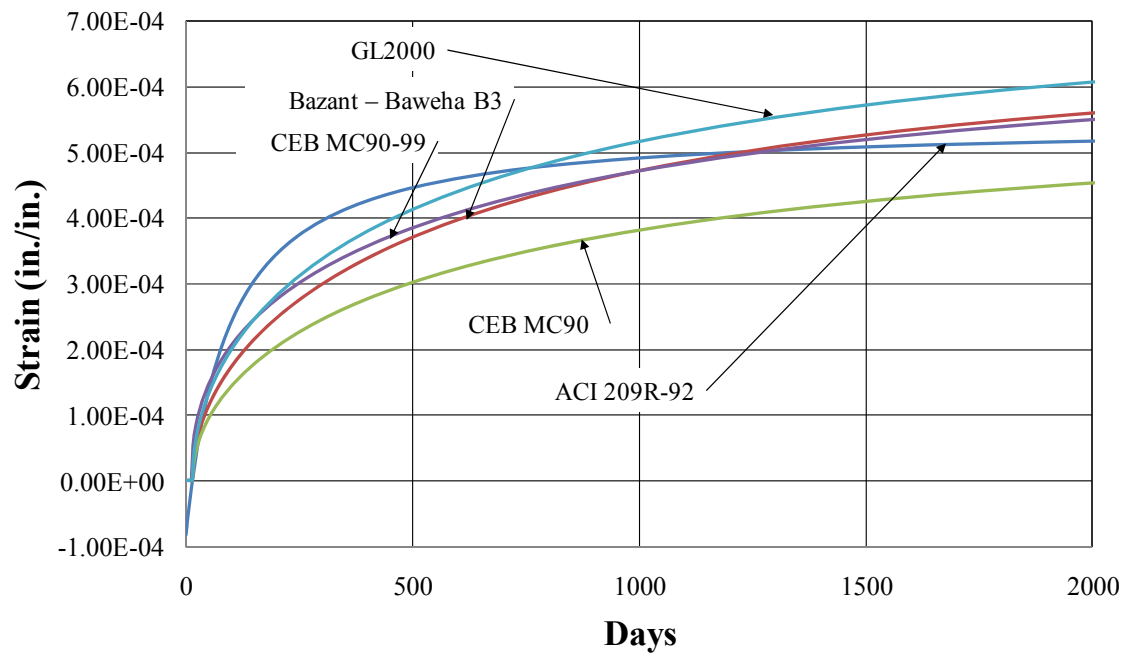
Figure 3.19: Prediction Models for Shrinkage Strains in SR-18 and US-231

3.4.3. TOTAL LOAD

To apply the total demand to the structure, both the thermal and shrinkage strains were assumed to follow the principle of superposition. A nonlinear staged loading sequence was input into SAP 2000, wherein each consecutive step accounted for the previous loading step. The analysis was nonlinear due to the need to recalculate the stiffness matrix after each loading stage, as well as allow for the use of a plastic abutment spring. However, the materials of both

structures were assumed to be linear-elastic. The temperature and shrinkage values calculated for both SR-18 and US-231 are shown in Table 3.15 and Table 3.16, respectively.

Table 3.15: Input Strain Values for SR-18 Loading Program

Stage	Date	Temperature (°F)				Shrinkage (με)		Total Strain (με)
		Measured	ΔT	Increment	Strain (με)	Cumulative	Increment	
0	Sept-03	65	0	-	-	-	-	**-**
1	Jan-04	20	-45	-45	248	-162	-162	**-410**
2	Jul-04	90	25	70	385	-238	-76	**309**
3	Jan-05	20	-45	-70	-385	-297	-59	**-444**
4	Jul-05	90	25	70	385	-336	-38	**346**
5	Jan-06	20	-45	-70	-385	-362	-26	**-411**
6	Jul-06	90	25	70	385	-384	-22	**363**
7	Jan-07	20	-45	-70	-385	-404	-20	**-405**
8	Jul-07	90	25	70	385	-418	-14	**371**
9	Jan-08	20	-45	-70	-385	-430	-12	**-397**
10	Jul-08	90	25	70	385	-441	-10	**374**
11	Jan-09	20	-45	-70	-385	-450	-9	**-394**
12	Jul-09	90	25	70	385	-458	-8	**376**
13	Jan-10	20	-45	-70	-385	-466	-7	**-392**
14	Jul-10	90	25	70	385	-472	-7	**379**

Table 3.16: Input Strain Values for US-231 Loading Program

Stage	Date	Temperature (°F)				Shrinkage (με)		Total Strain (με)
		Measured	ΔT	Increment	Strain (με)	Cumulative	Increment	
0	Sept-06	65	0	-	-	-	-	**-**
1	Jan-07	20	-45	-45	248	-162	-162	**-410**
2	Jul-07	100	35	80	440	-238	-76	**364**
3	Jan-08	20	-45	-70	-440	-297	-59	**-499**
4	Jul-08	100	35	80	440	-336	-38	**402**
5	Jan-09	20	-45	-70	-440	-362	-26	**-466**
6	Jul-09	100	35	80	440	-384	-22	**417**
7	Jan-10	20	-45	-70	-440	-404	-20	**-460**
8	Jul-10	100	35	80	440	-418	-14	**426**

3.5. ANALYSIS RESULTS

      Following the modeling techniques discussed, various loading cases were investigated to calibrate the models so that the predicted analytical response matched the measured behavior of the corresponding structures in the field. To calibrate the models, temperature and shrinkage strains were applied to the deck and girders in different combinations. Also, the various calculated soil springs were toggled on and off to evaluate their contribution to the overall behavior of the structure. An analysis matrix, shown in Table 3.17, reveals the different combinations of variables in the analysis. As opposed to the other analysis cases, Case 6 was only completed for the three-dimesional analysis. Sections 3.5.1 through 3.5.3 present the corresponding results as compared with the field measurements.

Table 3.17: Analysis Matrix

Analysis Case	Temperature Strains		Shrinkage Strains		Abutment Springs		Pile Springs
	Deck	Girder	Deck	Girder	Rankine	Log Spiral	
1	X	X					X
2	X	X	X	X			X
3	X	X	X				X
4	X	X	X		X		X
5	X	X	X			X	X
6	X	X	X			X	

3.5.1. SR-18 – TWO DIMENSIONAL

      The results of the five analysis cases for the SR-18 two-dimensional model are plotted along with the measured response from the abutment (Figure 3.20 through Figure 3.24). All load cases are also plotted together in Figure 3.25. The displacements of the analytical model and the measured field response are presented at the equivalent location of the convergence meters as described in Section 2.3.2.1. Upon reviewing the results from the various analysis cases, several findings were developed:

- Case 1 - Temperature strains cause a steady state cyclic movement of the abutment and do not result in net inward movement of the abutment.

- Case 2 – Application of shrinkage strains in addition to temperature strains captures the behavior of net inward movement. However, applying the sum of the temperature and shrinkage strains to the entire superstructure over-predicts the total inward movement. The total annual movement is also larger than that measured in the field. It was

determined, both by analysis and visual inspection, that the model that best predicted the rate and magnitude of shrinkage was the CEB MC90 prediction.

- Case 3 – Application of shrinkage strains to the deck only provide a more accurate prediction of the long-term inward movement of the structure. However, the total annual movement is still greater than that measured in the field.

- Case 4 – The addition of an abutment spring following Rankine theory has little effect on the behavior of the model, and virtually produces the same results as Case 3.

- Case 5 – Modeling the abutment spring using the log-spiral method dramatically reduced the total annual movement of the model. The displacements fit reasonably well.

- Case 4 and 5 – The stiffness of the abutment fill is a key value in understanding the entire response of the structure; however, the stiffness does not affect the maximum contraction which is the controlling demand for lateral deflection. Only the maximum expansion is affected. The method of determining an accurate stiffness to represent the backfill is virtually independent of the lateral earth pressure theory. What is significant is the method used to determine the displacement corresponding to passive pressure as this controls the spring stiffness. For this analysis, Case 4 and Case 5 represent approximate lower and upper boundaries, respectively. Case 4 uses the lower bound Rankine passive pressure along with a low stiffness spring suggested by the 2% displacement method. Case 5, on the other hand, uses an upper bound passive pressure compounded with a higher stiffness model. Rankin could provide similar results to the log-spiral if the spring stiffness is increased by decreasing the displacement assumed to reach full passive pressure.
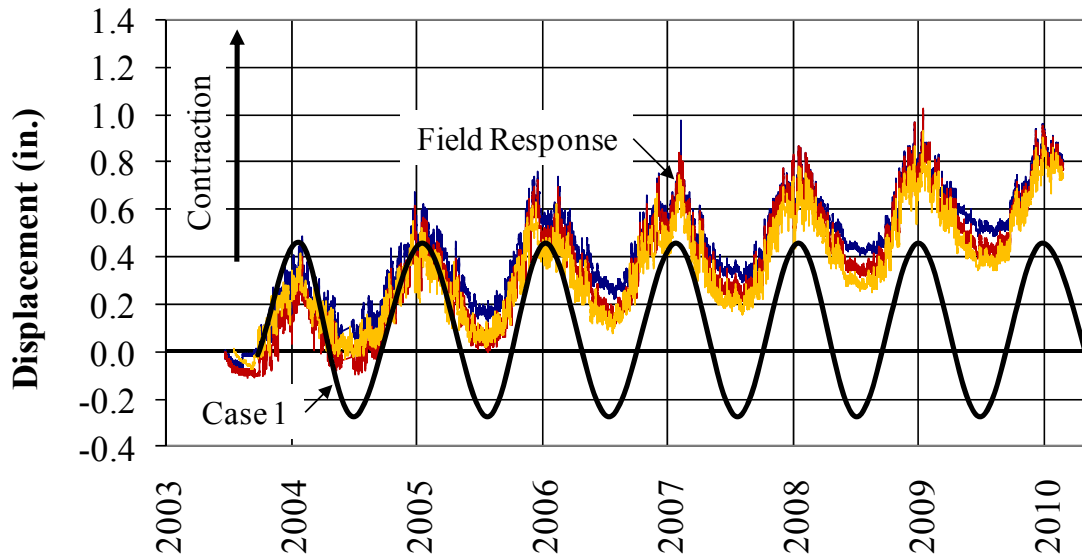
Figure 3.20: SR-18 Results of Two-Dimensional Structure – Case 1
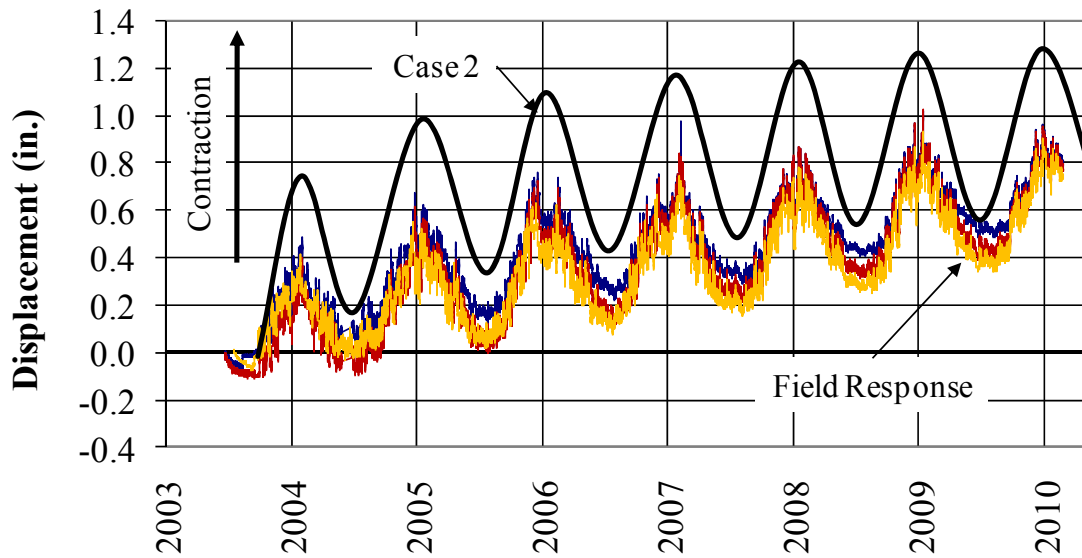
Figure 3.21: SR-18 Results of Two-Dimensional Structure – Case 2
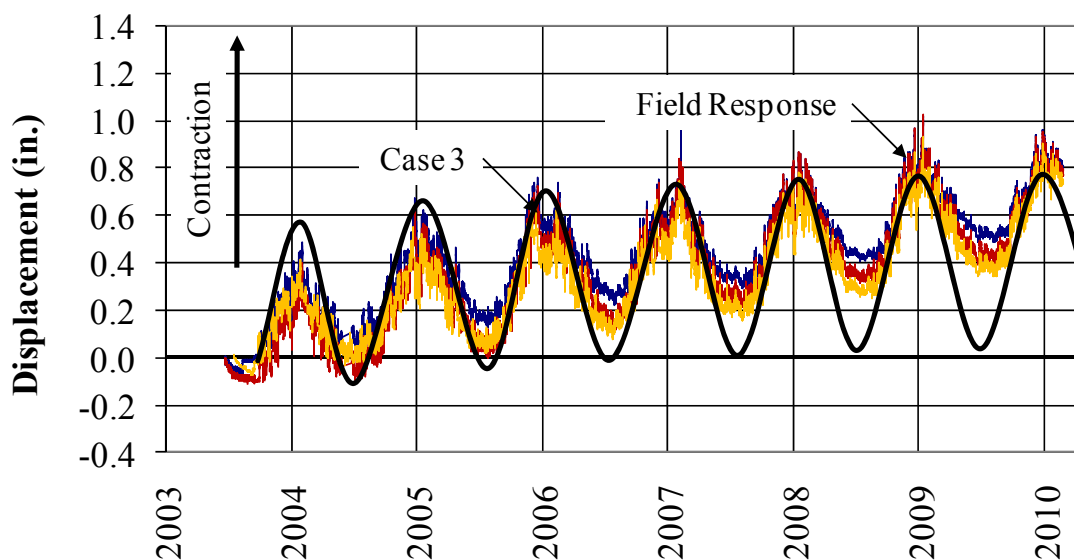
Figure 3.22: SR-18 Results of Two-Dimensional Structure – Case 3
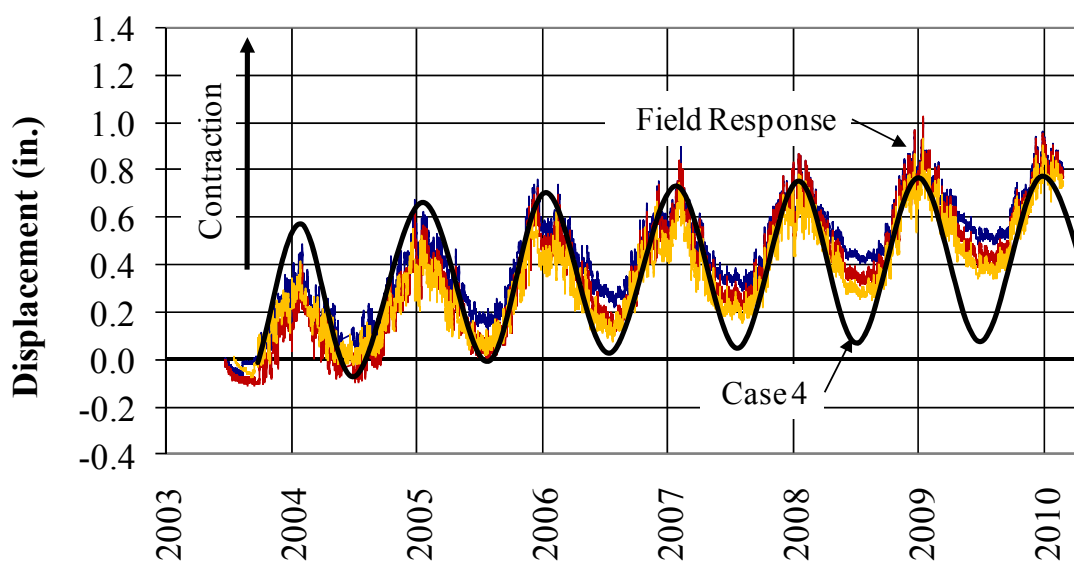
Figure 3.23: SR-18 Results of Two-Dimensional Structure – Case 4
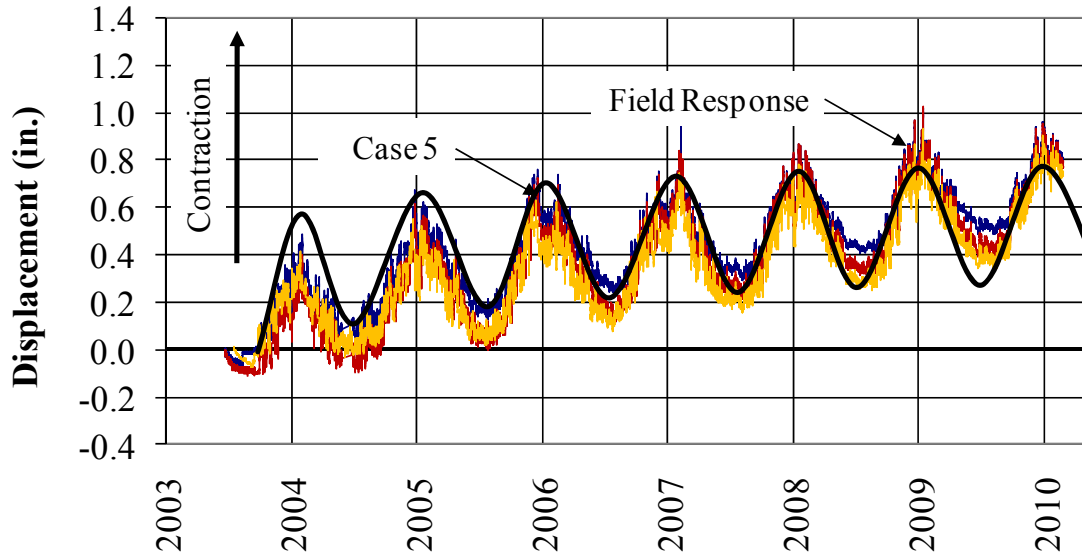
Figure 3.24: SR-18 Results of Two-Dimensional Structure – Case 5
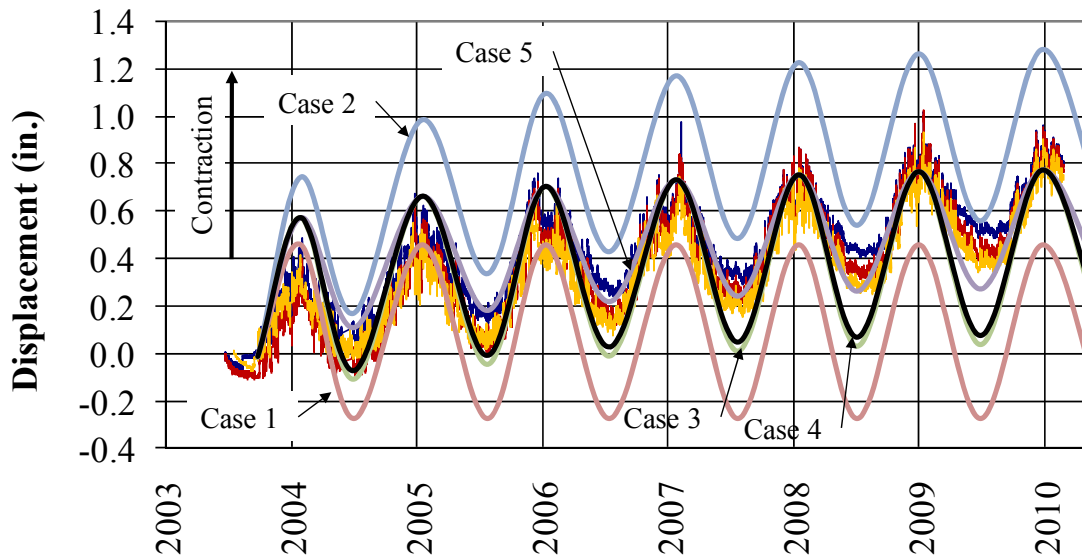
Figure 3.25: SR-18 Results of Two Dimensional Model

3.5.2. SR-18 – THREE DIMENSIONAL

The results of the six separate analysis cases for the SR-18 three-dimensional model are plotted along with the measured response from the abutment (Figure 3.26 through Figure 3.31). Also all load cases are shown together in Figure 3.32. The displacements of the analytical model and the measured field response are presented at the equivalent location of the convergence

meters as described in Section 2.3.2.1. Initially, it can be seen that the predictions from the three dimensional model are identical to the predictions of the two dimensional model. Therefore, the same findings for the two dimensional model can be applied to the three dimensional model. However, several additional findings unique to this model were observed. Primarily, Analysis Case 6 reveals that removing the pile springs provides a slightly more accurate prediction of the behavior of the structure. Figure 3.33 shows the predicted deflection of the pile for Case 5 and Case 6 along with the measured deflected shape. Assuming the measured shape is correct, the absence of soil stiffness produces a closer match. This indicates that the soil stiffness used adjacent to the pile is too stiff and could be softened. Alternately, removal of the springs provides very good response, and this can greatly simplify structure modeling.
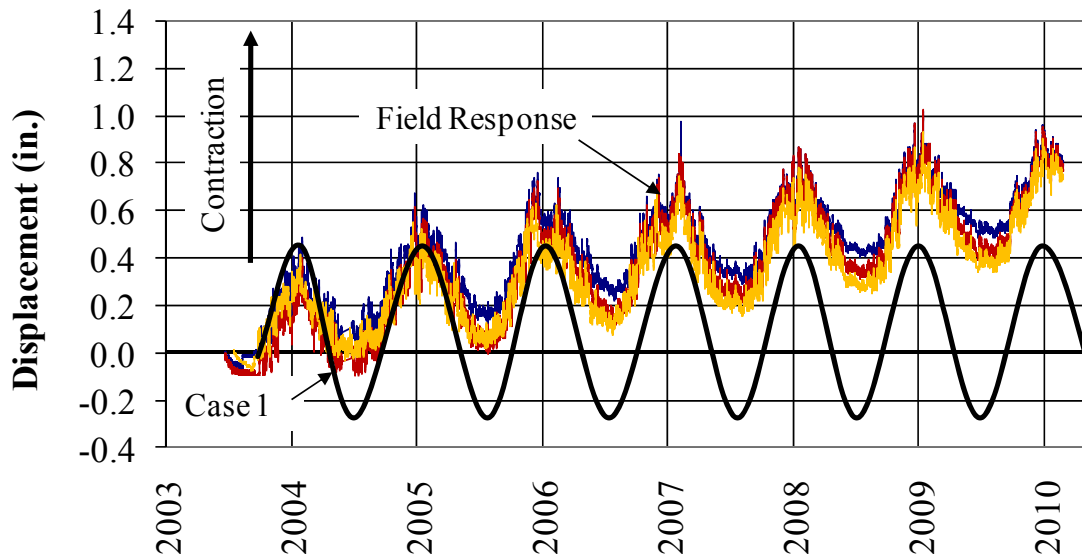
Figure 3.26: SR-18 Results of Three-Dimensional Structure – Case 1
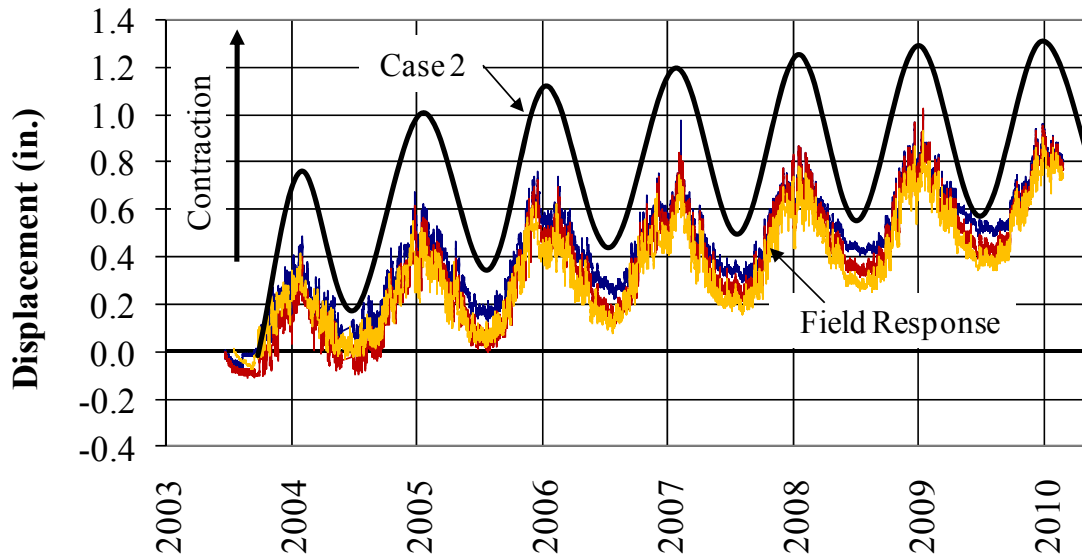
Figure 3.27: SR-18 Results of Three-Dimensional Structure – Case 2
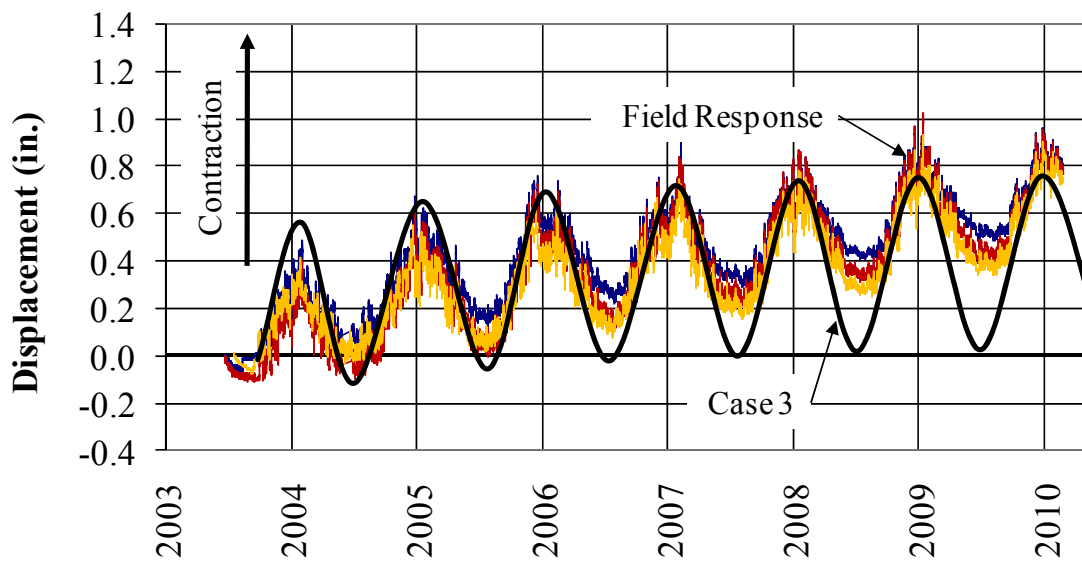
Figure 3.28: SR-18 Results of Three-Dimensional Structure – Case 3
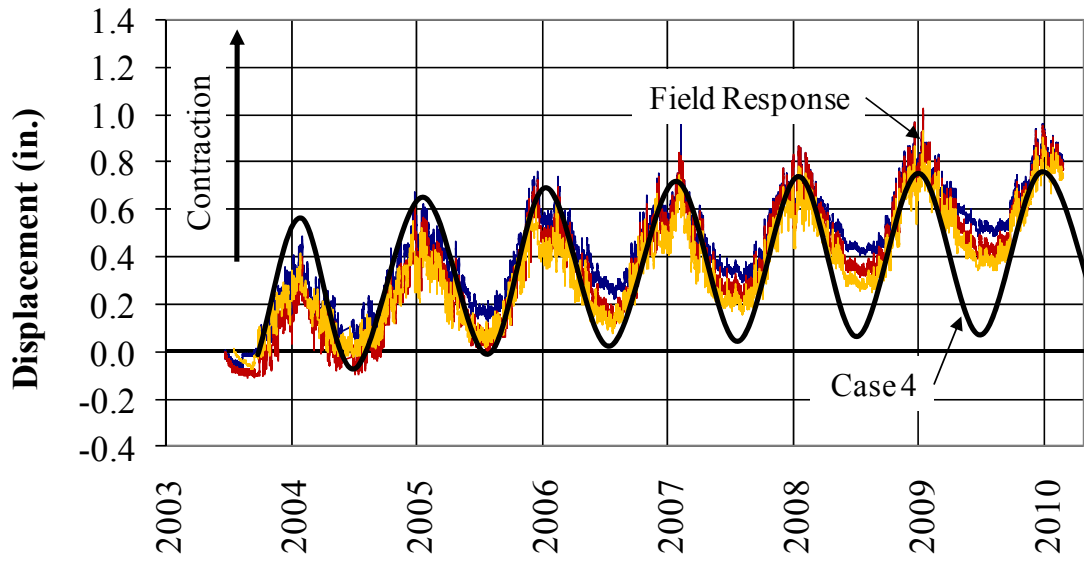
Figure 3.29: SR-18 Results of Three-Dimensional Structure – Case 4
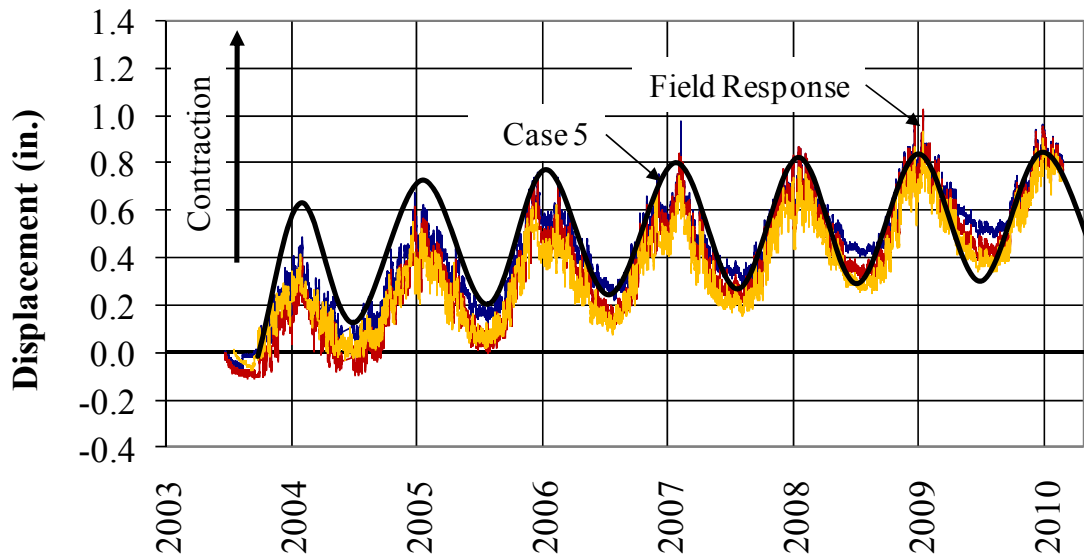
Figure 3.30: SR-18 Results of Three-Dimensional Structure – Case 5
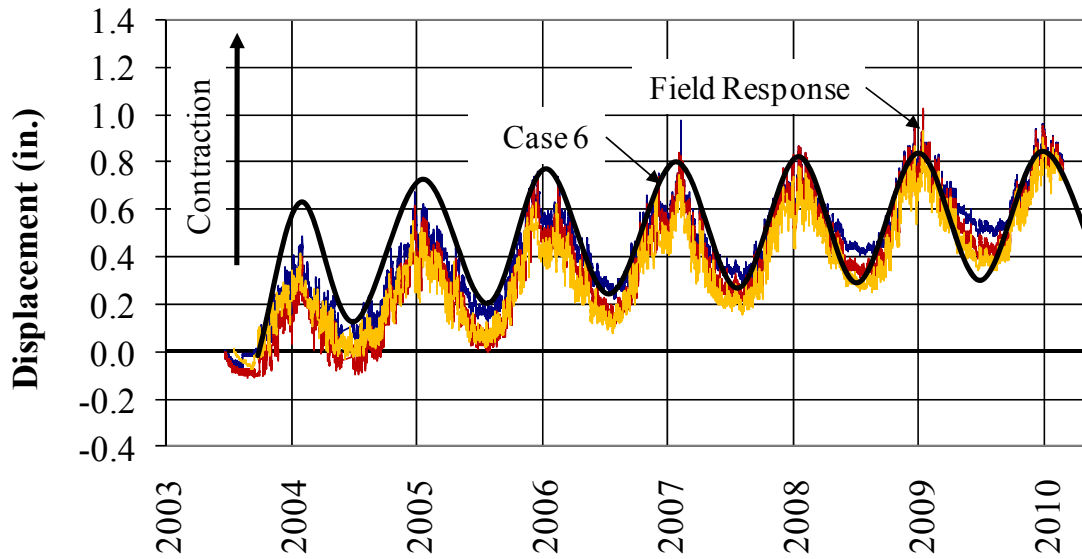
Figure 3.31: SR-18 Results of Three-Dimensional Structure – Case 6
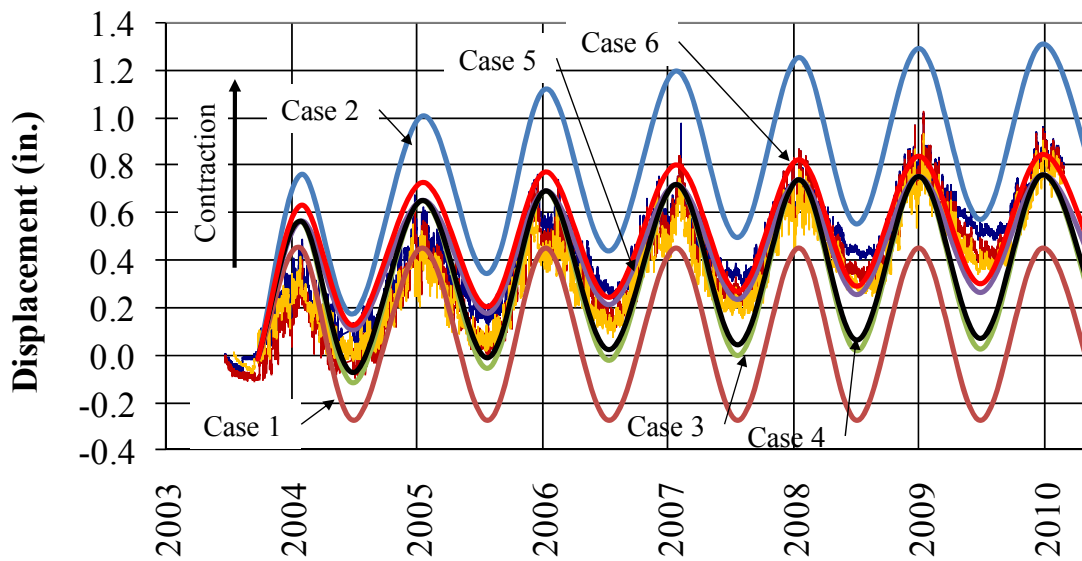
Figure 3.32: SR-18 Results of Three Dimensional Model
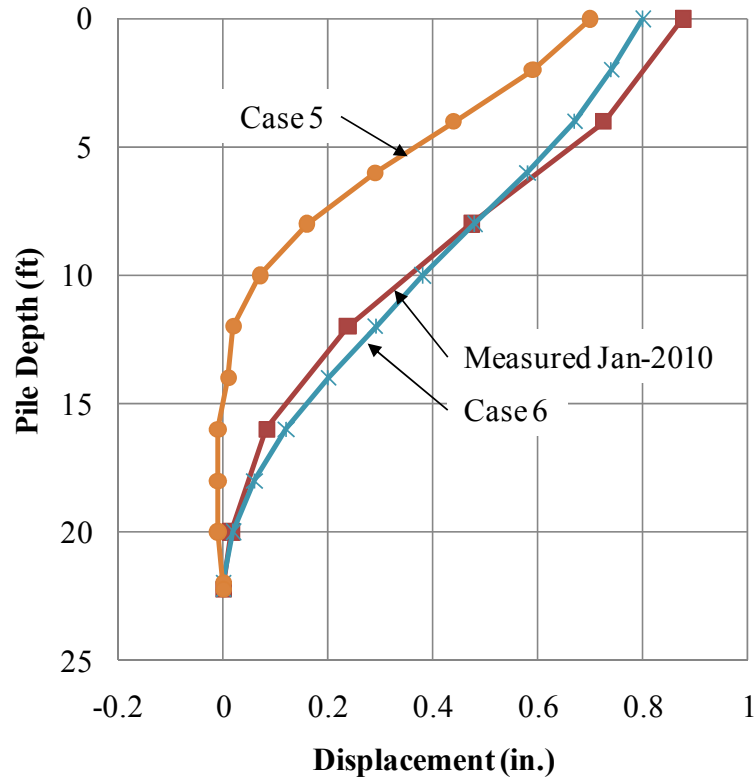
Figure 3.33: Predicted Pile Deflection for SR-18

3.5.3. US-231 – THREE DIMENSIONAL

The results of the six analysis cases for the US-231 three-dimensional model are plotted along with the measured response from the abutment in Figure 3.34 through Figure 3.39. The displacements of the analytical model and the measured field response are presented at the equivalent location of the convergence meters as described in Section 2.4.2.1. For all plots of transverse movement, the initial offset at the beginning of the model output is due to dead load. Upon reviewing the results from the various analysis cases, several finding were made. Some are similar to those for SR 18.

- Case 1 - Temperature strains cause a steady-state cyclic movement of the abutment and do not provide a net inward movement of the abutment. The skewed geometry of the structure causes a slight rotation of the abutment at peak displacements. During contraction phases, the model predicts that the skew angle is reducing while it is increasing for expansion phases. Temperature strains and bridge skew geometry do not have a significant effect on long-term out-of-plane movement.

- Case 2 – Application of shrinkage strains in addition to temperature strains captures the behavior of net inward movement. Applying the sum of the temperature and shrinkage strains to the entire superstructure, however, over-predicts the total inward movement. The total annual movement is also larger than that measured in the field. Transverse displacements are maintained small, but are slightly more than that provided by Case 1.

- Case 3 – Application of shrinkage strains to the deck only provide a more accurate prediction of the long-term inward movement of the structure. However, the total annual movement is still greater than that measured in the field. The transverse movement of the abutment is more closely predicted by the strain differential between the deck and the girder.

- Case 4 – The addition of an abutment spring following Rankine theory has little effect on the behavior of the model in the longitudinal direction. Transversely, the measurements are approximately the same as Case 3. However, a phase shift occurs in the response of displacements at the acute angle. It is important to note that the analytical model predicts that the acute corner moves more transversely than the obtuse corner. This is opposite from the field measurements.

- Case 5 – Modeling the abutment spring using the log-spiral method causes the skew of the structure to increase as the structure is expanding. The valleys do not match up as well as shown for SR-18. Also, the transverse prediction is close regarding the average magnitude, but the annual magnitude is much larger and has a phase shift. Also, it is noted that the acute corner is again predicted as having larger transverse movements as opposed to the obtuse corner from the field measurements.

- Case 6 – Removal of the soil springs from the piles exaggerates the conclusions from Case 5.
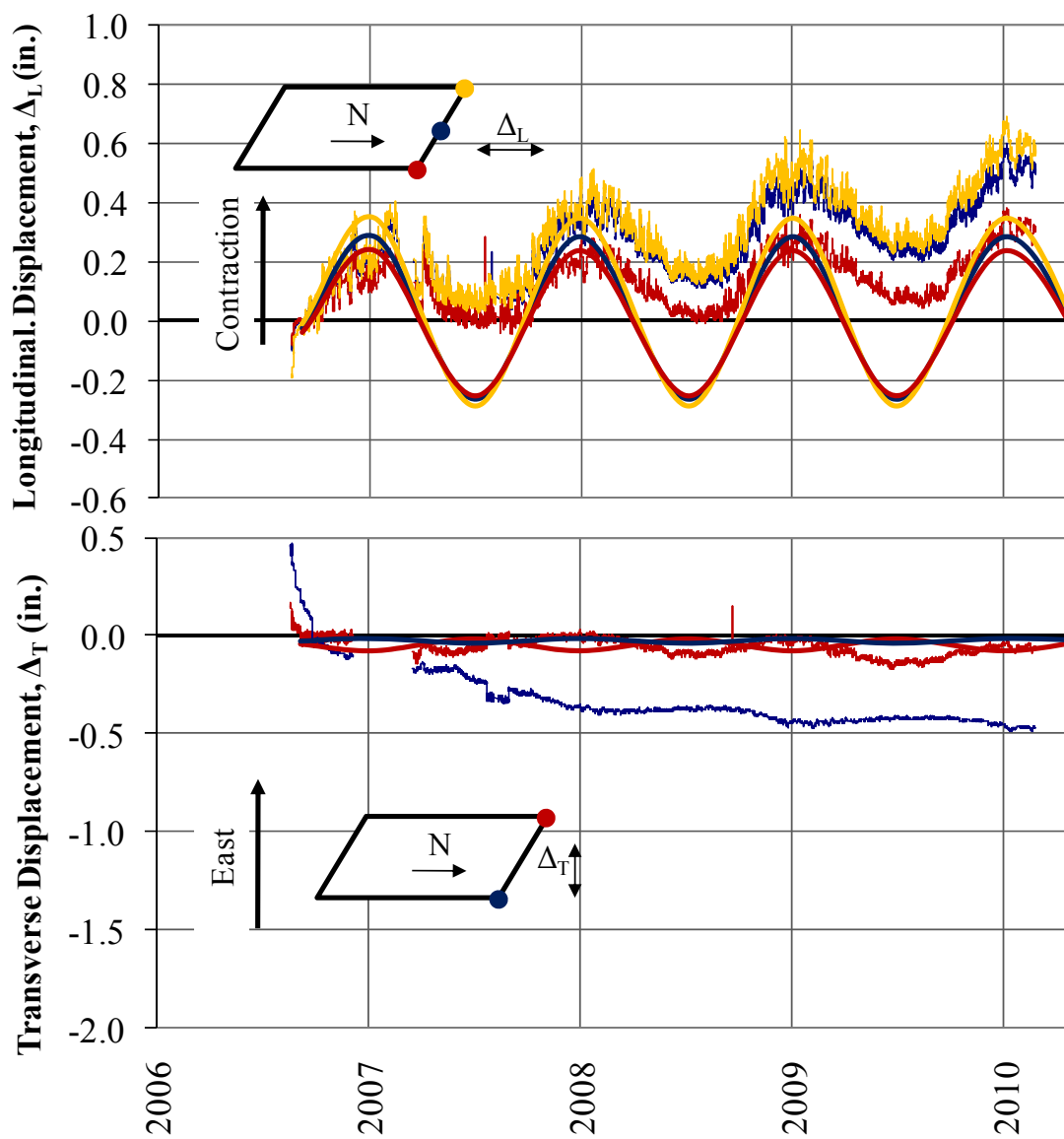
Figure 3.34: US-231 Case 1 Results
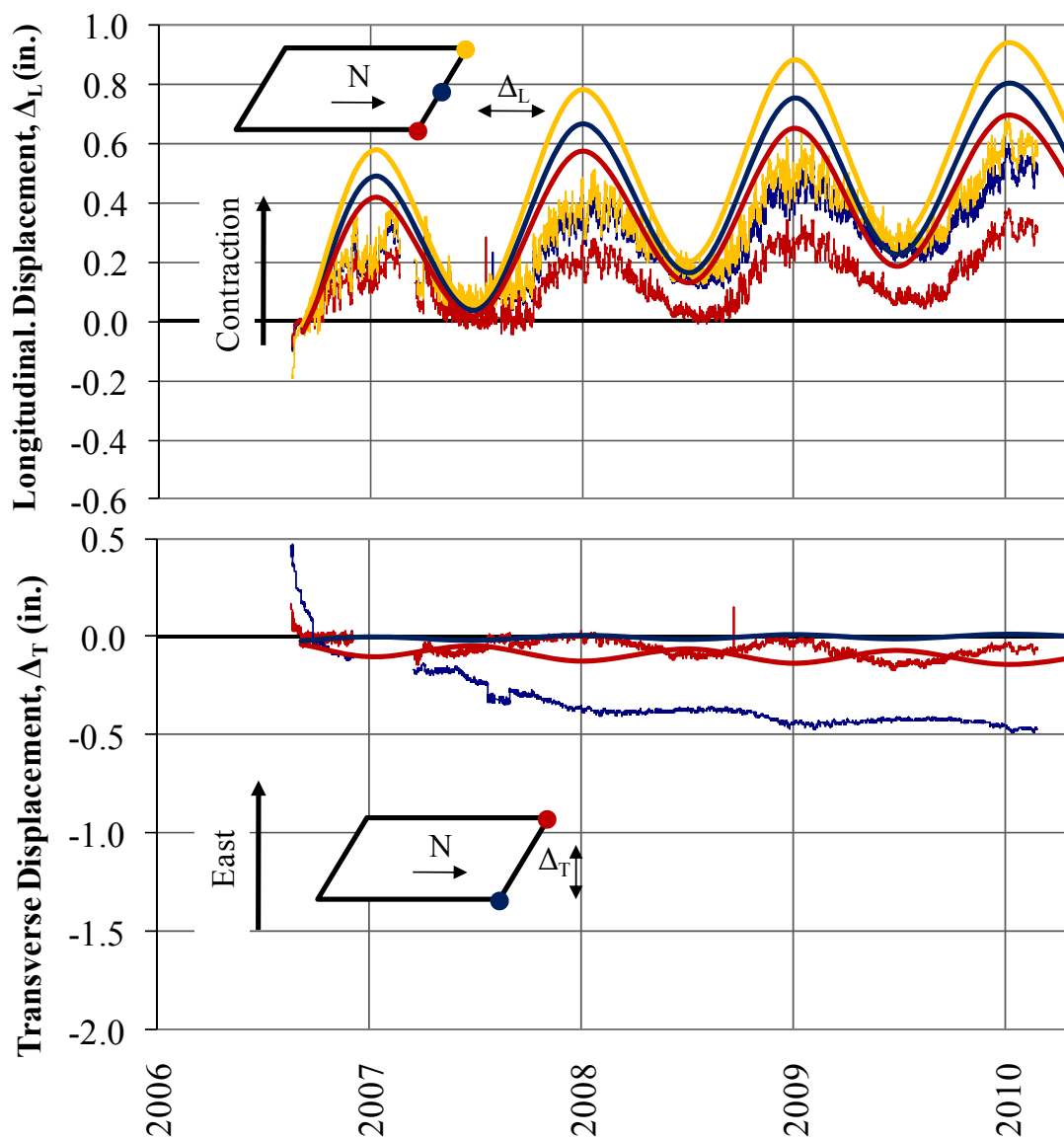
Figure 3.35: US-231 Case 2 Results
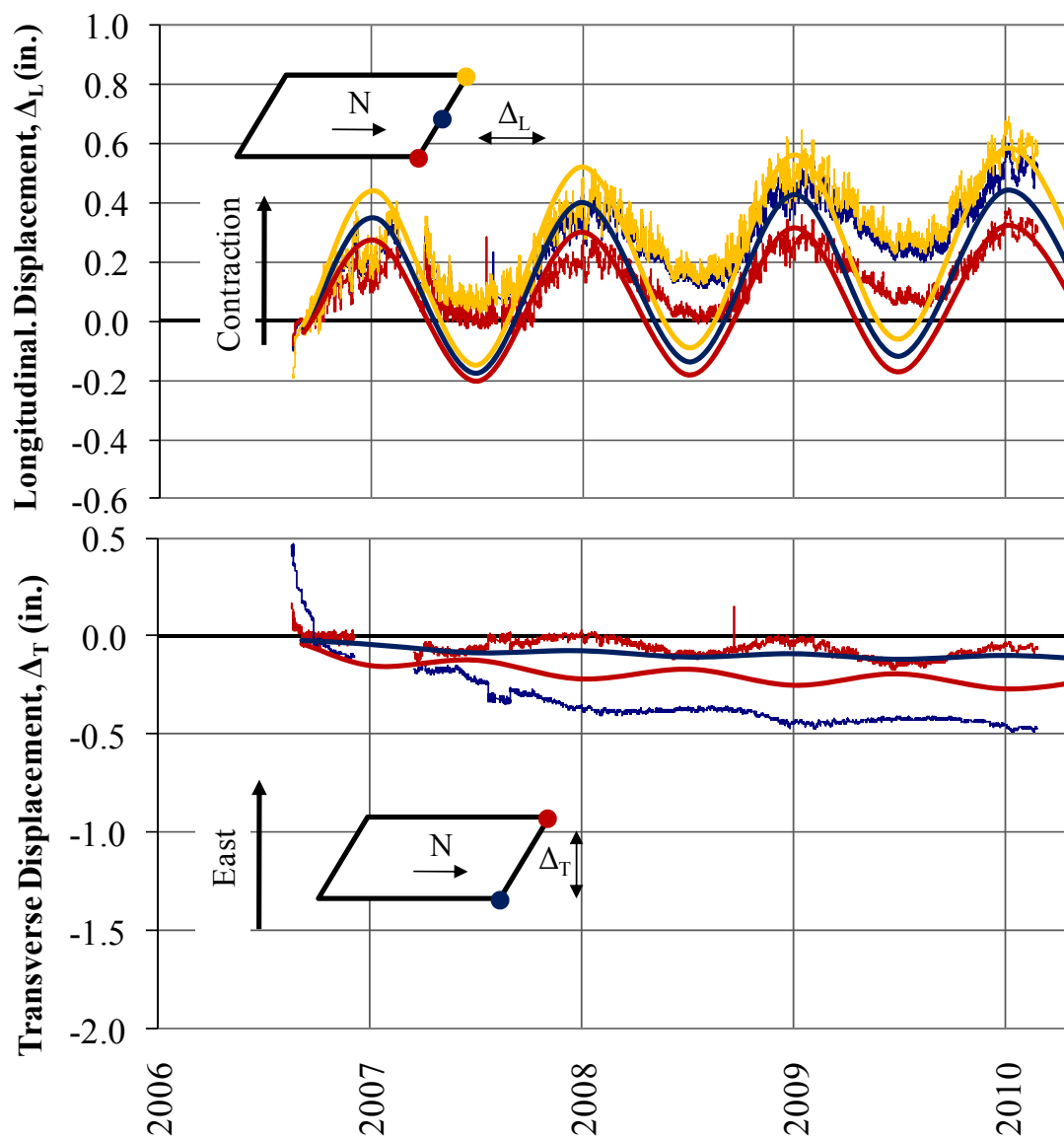
Figure 3.36: US-231 Case 3 Results
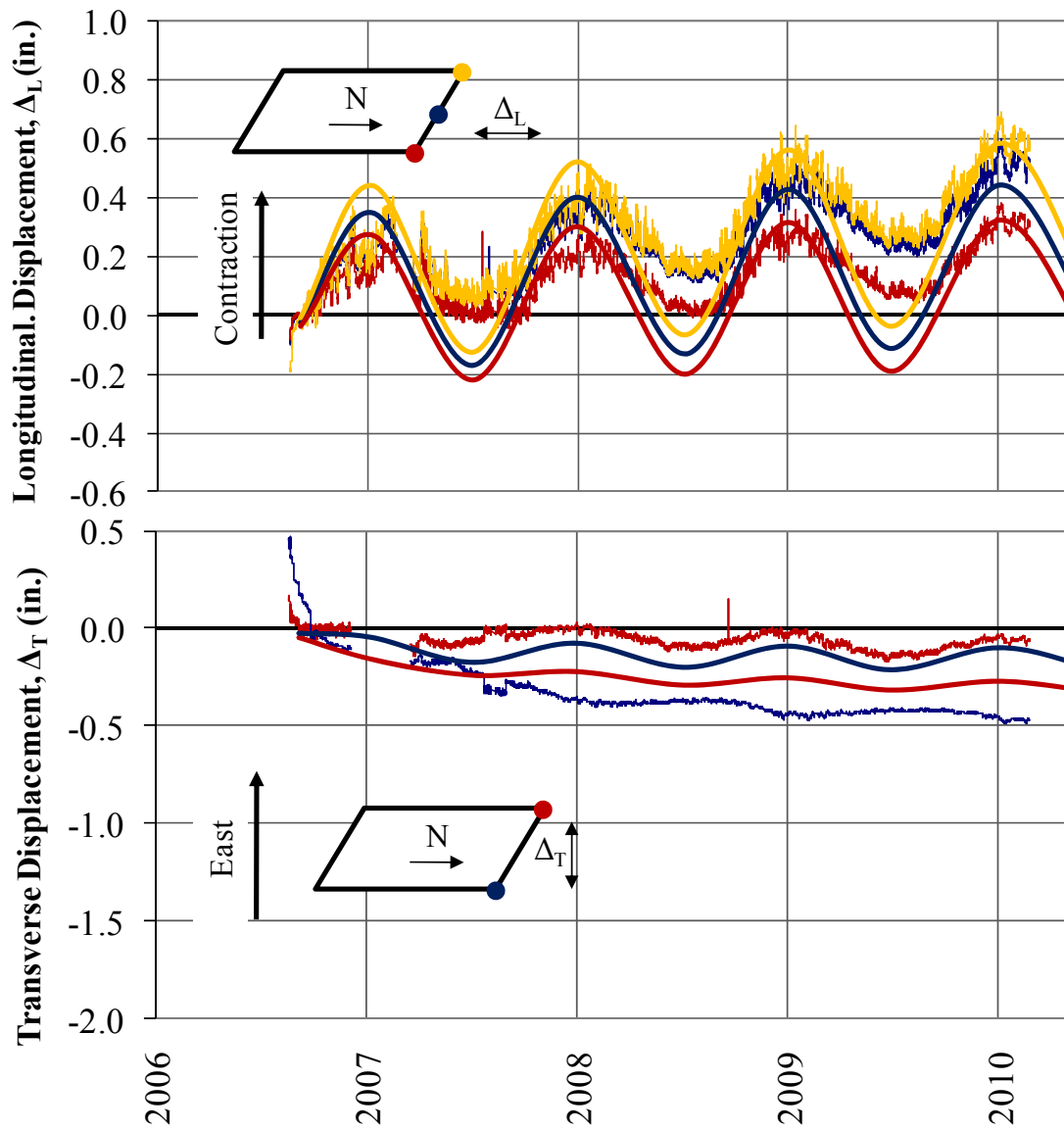
Figure 3.37: US-231 Case 4 Results
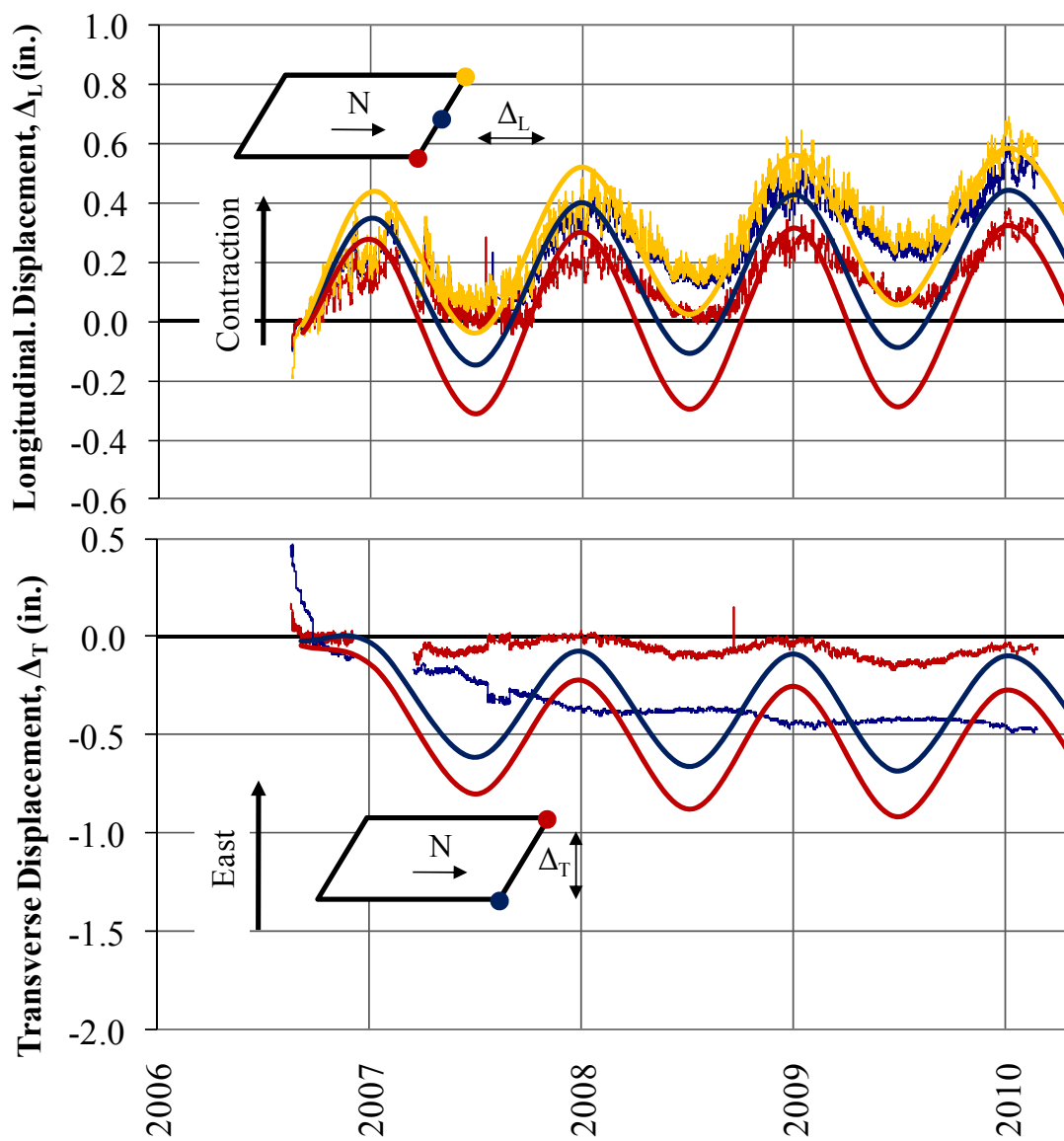
Figure 3.38: US-231 Case 5 Results
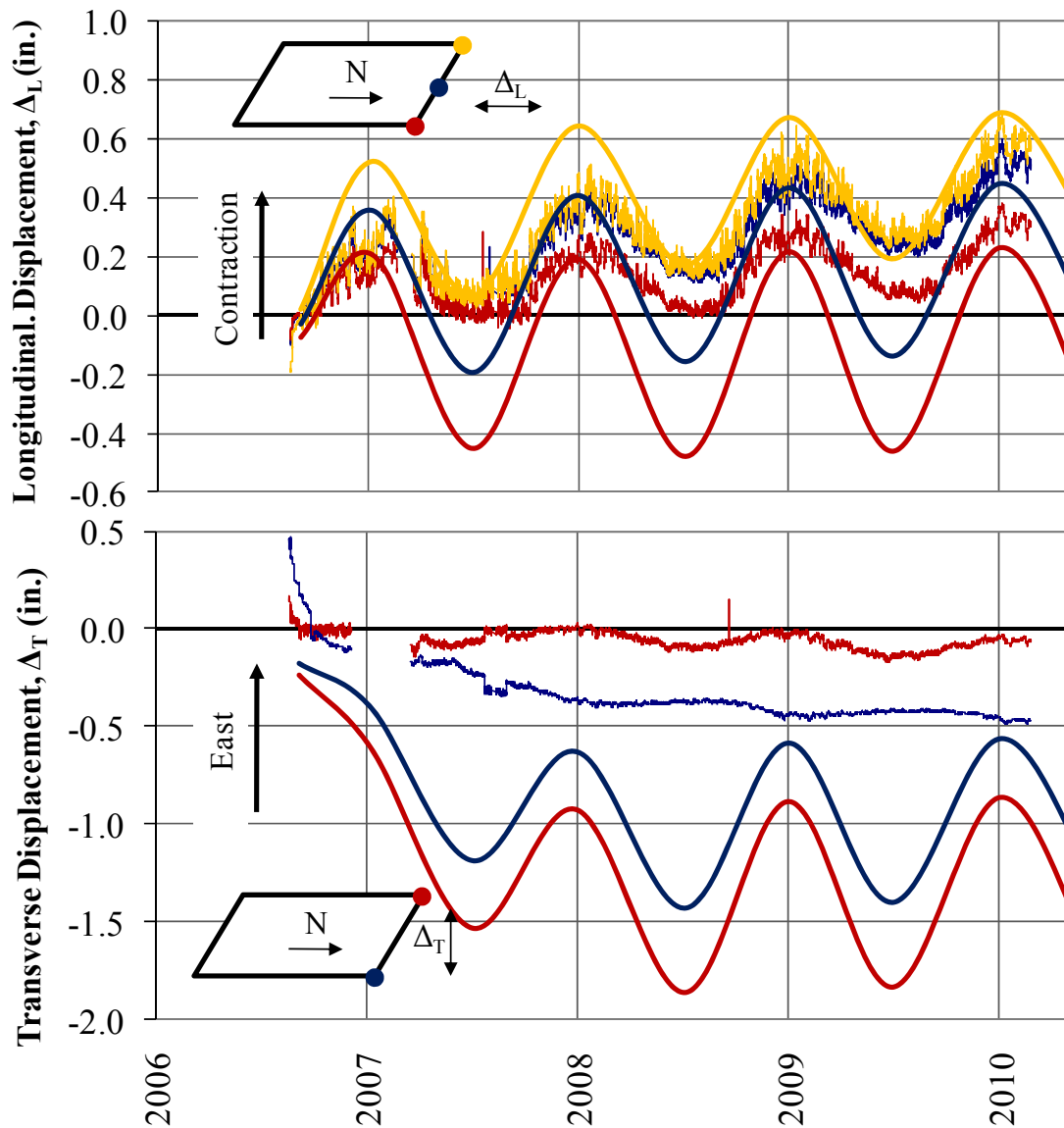
Figure 3.39: US-231 Case 6 Results

While Case 6 accurately calculated the measured movement of SR18, Case 6 performed poorly for US-231. Specifically, the transverse movement is extremely over exaggerated and the acute and obtuse corners appear switched. It is clear, based on comparison of Case 4 and Case 5, that a larger passive earth pressure stiffness results in increased cyclic amplitude. In addition, the removal of the pile springs over the entire height of the piles causes significant transverse

displacement. Because Case 6 did not perform adequately for US-231, an additional analysis case was executed (Case 7).

For Case 7, it was determined to mimic Case 3 but remove all pile springs. However, rather than using the full pile length, it was determined to fix the pile at 20 ft below the abutment. Previous research has shown that piles in integral abutment bridges have an inflection point between 5 and 10 ft below the abutment (Chovichien 2004). This length varies based on soil and pile stiffness. At a distance twice the inflection point, the pile can be assumed as fixed. Because SR-18 and US-231 have the same pile section (CFT14x0.312) and the calculation of the deflected pile shape for SR-18 best matched with no pile springs and a fixed connection at the base (Figure 3.33), it was determined to use the same length of pile for US-231. The results for Case 7 are shown in Figure 3.40.

In addition to the findings for analysis Case 1 through Case 6, the following findings were made regarding Case 7:

- It is apparent that the geometry, pile configuration, and lateral earth pressure each have an effect on transverse movement. The geometry and pile configuration control the average magnitude of transverse displacement, and the lateral earth pressure stiffness controls the magnitude of the annual cycles.

- Removing the pile springs and abutment springs provide the best calculation for movement of the abutment. The behavior of the piles can adequately be modeled as a cantilever pile at the location of twice the inflection point while neglecting the soil around the pile. Representing the pile-soil interaction as a cantilever agrees well with the equivalent column method described by Abendroth et al. (1989). In addition, this results in extremely simplified modeling techniques for designers.

- As with previous analysis results, the calculation of transverse displacement is greater for the acute corner as opposed to the obtuse corner for the field investigation. In fact, the calculation for the transverse displacement of the acute corner matches that of the measured field transverse displacement of the obtuse corner. It is unclear why this occurs. However, one possibility may be due to the wiring error as discussed in Section 2.4.3.1. Regardless, the analytical model calculates the worst longitudinal and transverse displacement to occur at the acute corner. As a worst case scenario, this would be conservative.
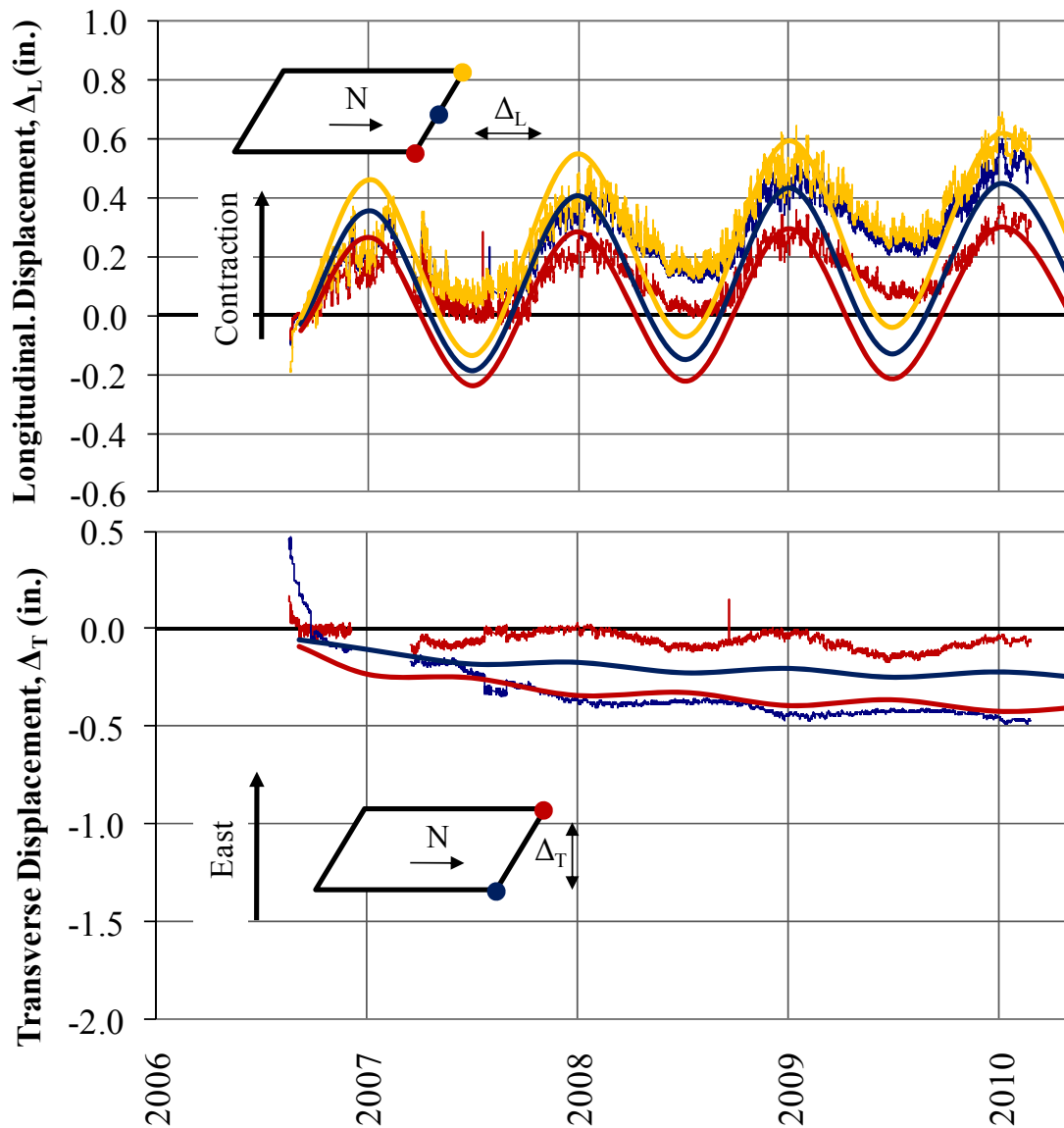
Figure 3.40: US-231 Case 7 Results

3.6. CONCLUSIONS

Based on the findings from the analysis of the field results, several conclusions can be made regarding general modeling of integral abutment structures:

1. There are two primary phenomenons that control the behavior of integral bridges, thermal response of the entire superstructure and shrinkage of the concrete deck.

2. Average ambient temperature is appropriate for determining the demand strain due to temperature differentials. For Indiana, an average maximum temperature range of 70 °F is considered appropriate.

3. Shrinkage strain, as opposed to buildup of lateral earth pressure, is the apparent cause of the ratcheting phenomenon. The model that best predicts the rate of shrinkage for the long term behavior of the monitored structures is the European shrinkage model, CEB MC90 (ACI 209 2008).

4. When determining the effect of the abutment backfill, the maximum lateral earth pressure is not as significant as the stiffness of the material. Therefore, a simple lateral earth pressure theory can be used, as long as the stiffness can be reasonably estimated.

5. The stiffness method developed by Coduto (2001) results in backfill material that is too soft. The stiffness method by Duncan and Mokwa (2001) is shown to predict values that are very high. Further research is required to determine adequate stiffness models for modeling backfill in integral abutment bridges.

6. For structures with zero skew:

   - A two dimensional model is sufficient for calculating the demand lateral displacement on the supporting piles.

   - The demand displacement of the piles is longitudinal and a function of temperature, concrete deck shrinkage, and to some degree the soil surrounding the piles. The abutment soil does not have an impact on the maximum longitudinal displacement.

   - The soil surrounding the pile can be ignored if the piles are represented by an equivalent cantilever with a length of twice the point of inflection.

7. For structures with skew:

   - A three dimensional model is required to calculate the demand lateral displacement on the supporting piles.

   - The maximum demand displacement will occur for the pile closest to the acute corner of the structure.

   - The demand displacement of the piles is longitudinal and transverse.

   - The longitudinal displacement is a function of temperature, concrete deck shrinkage, and to some degree the soil surrounding the piles. The abutment soil does not have an impact on the maximum longitudinal displacement.

- The transverse displacement is a function of bridge geometry and the soil surrounding the piles and abutments. The geometry and pile orientation control the average transverse displacement. The abutment soil affects the amplitude of the annual transverse displacement cycle. The stiffer the soil behind the abutment, the larger the annual displacement cycle.

- Similar to the zero skew structure, it is adequate to model the structure by ignoring soil surrounding the pile and modeling as an equivalent column. This method was shown to produce the most accurate calculations.

CHAPTER 4. EXPERIMENTAL INVESTIGATION

4.1. INTRODUCTION

Various tests have been conducted to determine the lateral deformation capacity of standard pile sections used in integral abutment bridges (Talbott 2008, Chovichien 2004, Griemann 1984). However, accurate recommendations for the demand imposed on the piles do not exist. It is clear that integral abutment bridges cycle through expansion and contraction phases throughout their life-cycle. The supporting single row of piles must accommodate this lateral displacement while maintaining their axial load capacity. Traditionally, a simplified method is used to determine the lateral demand based on unrestrained thermal expansion and contraction of the deck.

$$\Delta L = \alpha(\Delta T)\frac{L}{2} \tag{4.1}$$

where:

ΔL = temperature induced change in bridge length, in.

α = coefficient of thermal expansion, 1/°F

ΔT = change in temperature, °F

L = total length of structure, in.

As can be seen, this demand displacement is dependant only on the length of the structure and an assumed maximum temperature differential. Length limitations have been developed to ensure that the standard pile sections used in integral construction are capable of maintaining their axial integrity while accommodating the assumed lateral demand of Equation (4.1) without consideration of skew. For that reason, skew limitations are commonly imposed. While this method is intuitive, as well as extremely simple, for defining the maximum length of integral abutment bridges with low skews, this method is not correct for structures with high skew angles.

Prior to this study, one study has been conducted for integral abutment bridges with high skew. However, that study did not adequately monitor transverse movements. While this study has investigated a 33 degree skewed structure, it was observed some differences in behavior from that predicted by the analytical model occurred. To provide additional information on the effects of high skew angles on integral abutment structures, a quarter scale integral abutment bridge with a skew angle of 45 degrees was constructed and tested at the Bowen Laboratory at Purdue University. Due to the nature of laboratory testing, improved control on displacement measurements could be provided to eliminate any measurement errors that may have been responsible for variations in structural behavior experienced by the field structure. In addition, it was possible to construct a highly skewed structure without waiting for one to be constructed in the field.

4.2. Specimen Design

Because the typical lateral pile displacements for an integral abutment bridge are a small fraction of the total structure length, it was advantageous to construct a large scale model to accentuate the behavior of the abutment. Therefore, it was determined to construct a quarter-scale, single-span structure. The structure was scaled to be an approximate quarter-scale representation of the SR-18 structure and was built with a 28'-4.5" length and 45 degree skew. The superstructure consisted of a 4 in. deck supported by three girders each 10" x 12". A 3 ft tall abutment was supported by five 6 in. outer-diameter concrete filled tubes (CFT 6x0.25"). A plan view of the model structure is shown in Figure 4.1, and an elevation view is shown in Figure 4.2.

A gap, as shown in Figure 4.1 and Figure 4.2, was formed into the superstructure at midspan. Because the driver of the behavior of integral abutment bridges is annual temperature differentials and shrinkage, the gap allowed for simulation of internal strains. Using a loading system, an entire life-cycle of the structure could be represented in a single day. As will be discussed later, a set of transfer beams served to provide continuity of the deck, resist shear forces, and allow for longitudinal expansion and contraction of the superstructure.
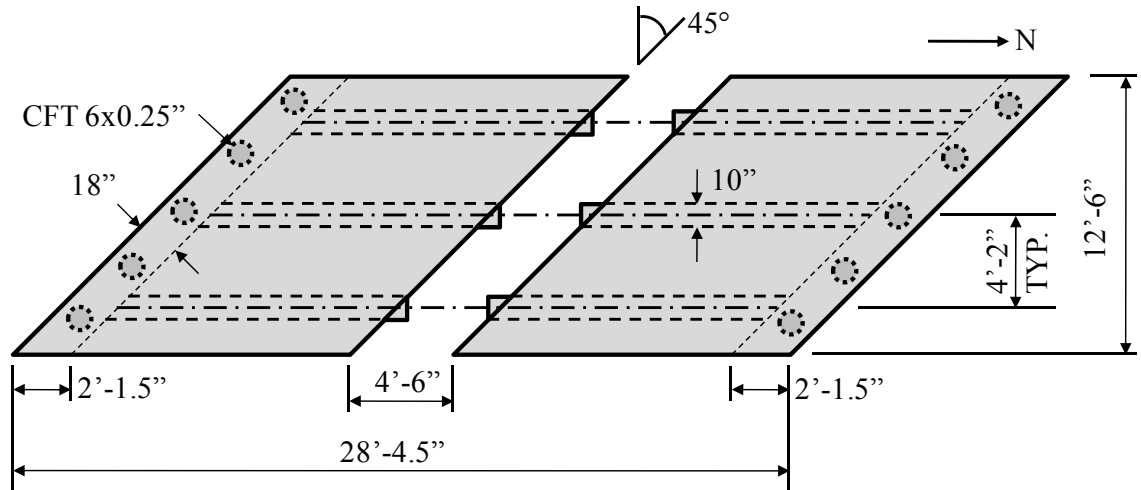
Figure 4.1: Plan View of Quarter-Scale Integral Abutment Experimental Model
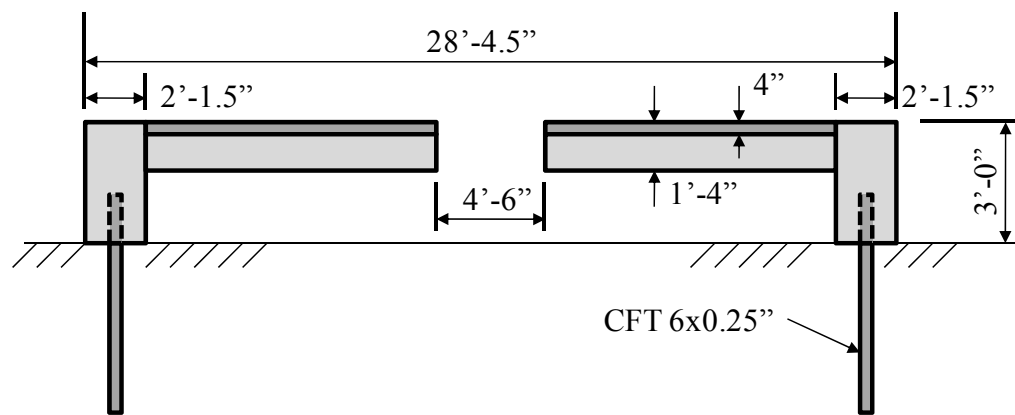
Figure 4.2: Elevation View of Quarter-Scale Integral Abutment Experimental Model

4.3. CONSTRUCTION MATERIALS

4.3.1. CONCRETE

The quarter-scaled integral abutment bridge was constructed using a concrete mix provided by Irving Materials Inc. (IMI), a local ready-mix concrete supplier. Because the structure was cast during the winter months, a 6 bag mix was used for the concrete in the structure. To facilitate casting, both super-plasticizer and a non-chloride accelerant were added to

the mixture. The structure was cast with two separate batches of the same concrete mix design, one for each half of the structure. Both ends of the structure contained a maximum aggregate size of ¾ in., while the water cement ratio was 0.36 for the north end of the structure and 0.37 for the south end. The slumps for the north and south mixes were 6" and 8", respectively. The mix proportions are shown in Table 4.1.

In addition to the concrete in the superstructure and abutments, the supporting piles were filled with concrete. The concrete used in the concrete filled tubes was specified to be an INDOT Class B mix. The mix included a maximum ¾" aggregate size and a water cement ratio of 0.47. The concrete used in the piles had a slump of 4 in. The specific mix proportions for the concrete used in the piles are shown in Table 4.2.

Table 4.1: Batch Weights – Abutments and Superstructure

Material"	Quantity	
	North Abutment	South Abutment
#8 Gravel (¾")	1800 pcy	1800 pcy
Sand #23	1340 pcy	1340 pcy
Cement (Type 1)	564 pcy	564 pcy
Air	1.4 ozcy	1.4 ozcy
Water	200 pcy	210 pcy
Super-plasticizer	39.5 ozcy	39.5 ozcy
Non-Chloride Accelerant	100 ozcy	100 ozcy

Table 4.2: Batch Weights – CFT Concrete

Material	Quantity
#8 Gravel (¾")	1850 pcy
Sand #23	1416 pcy
Cement (Type 1)	470 pcy
Air	2.4 ozcy
Water	220 pcy
Water Reducer	9.4 ozcy

Compressive tests were performed for all of the concrete used in the experimental program. A set of tests were conducted for both the north and south ends of the structure as well as the concrete in the piles. The compressive tests were conducted following ASTM-C39 using a 600-kip Forney. The test specimens were 6" x 12" cylinders. The casting dates for each of the

concrete mixes are shown in Table 4.3. The strength-gain curves for the concrete in the structure and piles are shown in Figure 4.3 and Figure 4.4, respectively. The series of compressive tests consisted of strengths at 3, 7, 14, 28 days as well as the testing date. The structure was tested on March 3, 2010. The compressive strengths for the concrete at the time of testing is to be taken as 6000 psi for the bridge and 5000 psi for the piles.

Table 4.3: Casting Dates

Description	Date
Concrete in CFT 6x0.25"	10/20/2009
North Half of Bridge	12/17/2009
South Half of Bridge	12/17/2009
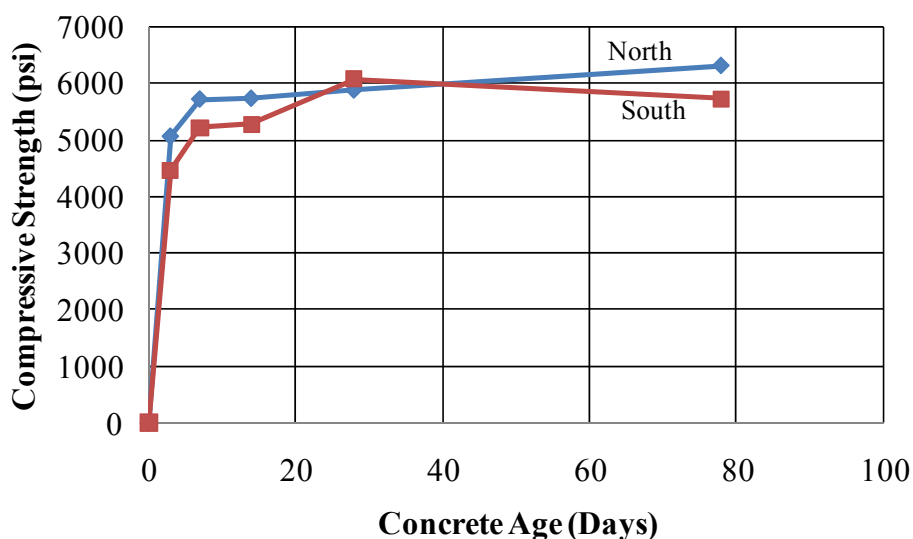
Figure 4.3: Abutment Concrete Compressive Strength
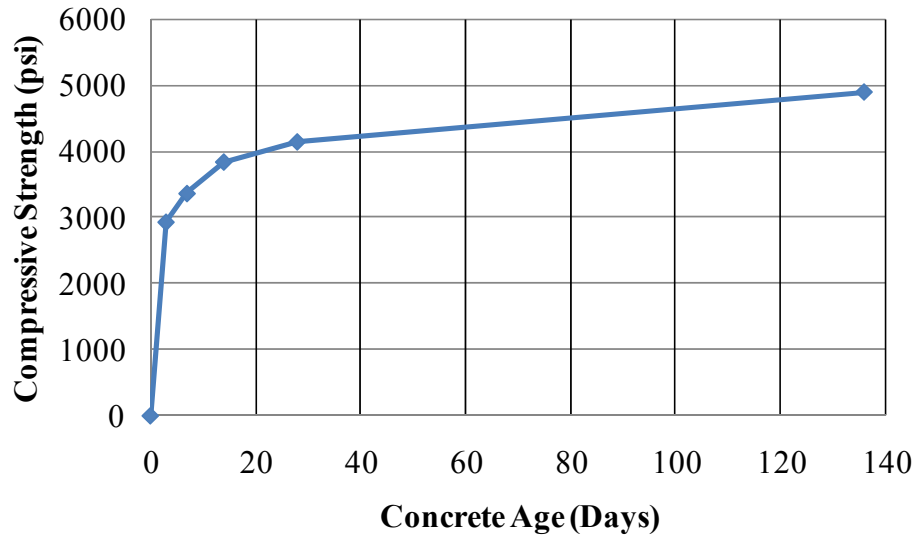
Figure 4.4: Pile Concrete Compressive Strength

To determine the modulus of elasticity of the concrete used in the experimental investigation, the recommendation of ACI 318 (2008) was used (Equation 4.2). The calculated modulus of elasticity for the concrete in both the structure and piles are shown below.

$$E_c = 57\sqrt{f_c^{'}} \tag{4.2}$$

where:

E_c = modulus of elasticity of concrete, ksi

$f_c^{'}$ = concrete compressive strength, psi

For the structure: $E_c = 57\sqrt{6000}ksi = 4415ksi$

For the piles: $E_c = 57\sqrt{5000}ksi = 4031ksi$

4.3.2. REINFORCING STEEL

ASTM Grade 60, #4, #5, and #6 reinforcing bars were used in the concrete deck and the concrete abutment. Because the lateral deflection of the supporting piles was the primary focus of the investigation, material tests were not performed.

4.3.3. STEEL PILES

The steel pipe piles used to support each abutment were 6x0.25" round sections in 21 ft lengths. The specified material was ASTM A500B, and the nominal properties are provided in Table 4.4 in addition to transformed section properties determined following the methods provided in Section 3.2.2. Five piles were used to support each abutment with one additional pile used for a lateral pile test. Each pile was driven to a depth of 18 ft or until refusal. The piles were then cut to length, and the remaining material (Figure 4.5) was used to create three testing coupons (Figure 4.6). The coupons were taken from outside of the visibly yielded portion to obtain virgin material properties. A T/O 120 kip Super L Tension-Compression Extensometer was used to perform tensile tests according to ASTM E8 and ASTM A370.

The dimensions of the coupons cut from the round section are shown in Figure 4.7. The specimen had a total length of 8 in. The thickness of the coupons was nominally ¼". The ends of each coupon were flattened to allow for accurate gripping of the specimen according to the standard specification, but the rest of the coupon retained the curvature of the original pipe.   The actual material dimensions along with the yield and ultimate strength of each specimen are shown in Table 4.5 and Table 4.6, respectively. It should be noted that the material from the sections did not display a clear yield, and therefore, the 0.2% offset yield strength was determined and used for subsequent analysis. The initial segment of the stress-strain curves for the three specimens is shown in Figure 4.8. The average yield stress for the specimen was determined to be 52 ksi.

Table 4.4: Pile Cross Sectional Properties

Outer Diameter (in.)	6
Inner Diameter (in.)	5.5
Wall Thickness (in.)	0.25
Composite Effective Area (in.^{2})	7.80
Composite Effective Moment of Inertia (in.^{4})	24.9

Figure 4.5: Remaining Material from Which Tension Coupons Were Cut
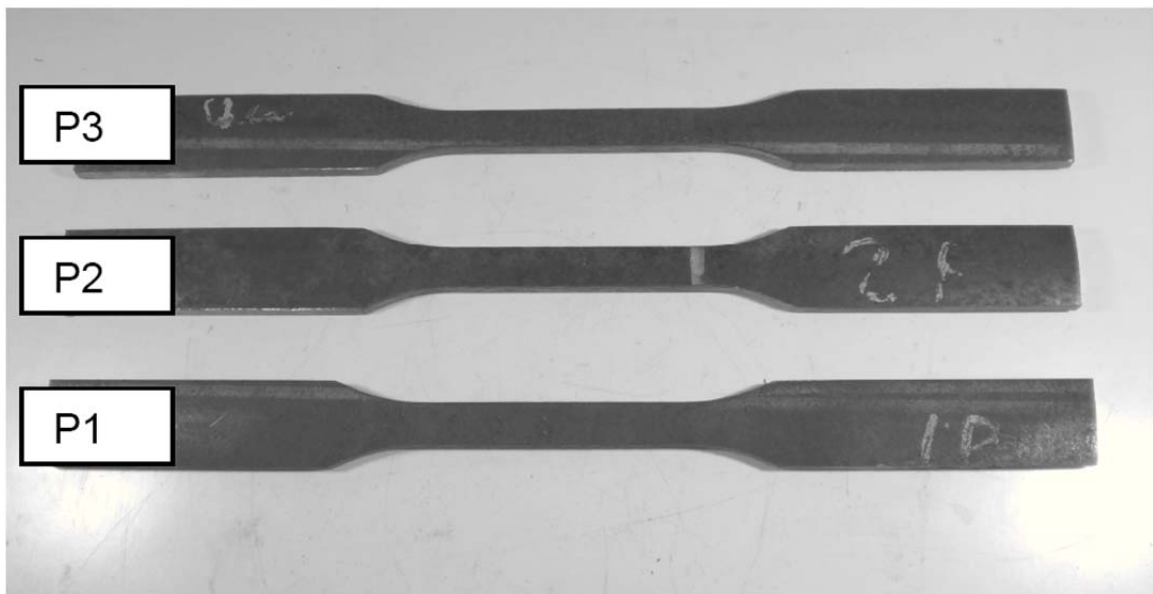
Figure 4.6 Set of Material Coupons
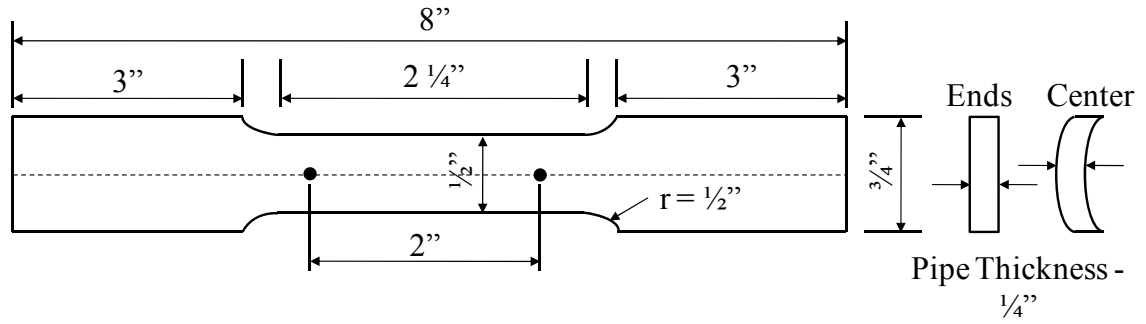
Figure 4.7 Dimensions of Tension Specimen

Table 4.5: Tension Coupon Dimensions

ID	Item	Width (in.)	Thickness (in.)	Area (in.^{2})
P1	6" O.D. Pipe	0.500	0.235	0.1175
P2	6" O.D. Pipe	0.498	0.234	0.1165
P3	6" O.D. Pipe	0.520	0.235	0.1222

Table 4.6: Tension Coupon Results

ID	Yield Load (lbf)	Yield Stress (psi)	Ultimate Load (lbf)	Ultimate Stress (psi)	Elongation in. / in. (%)	Reduction in Area (%)	Hardness (RB)
P1	6078	51728	7839	66715	33.7	59.2	84
P2	6029	51751	7831	67219	36.4	36.4	84
P3	6518	53339	7927	64869	34.6	59.3	84
AVG	6208	52273	7866	66268	34.9	51.6	84
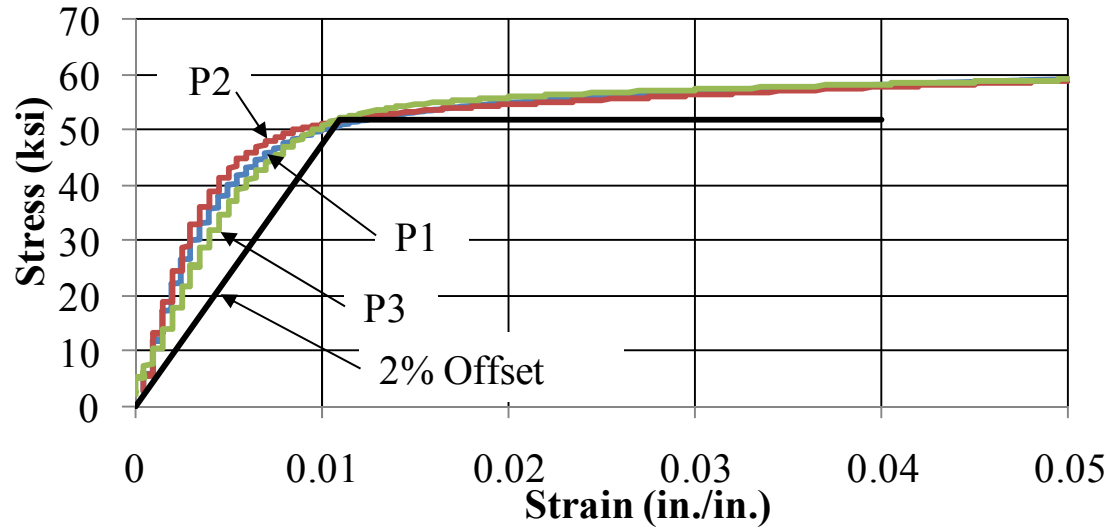
Figure 4.8: Initial Stress-Strain Relationship of Test Coupons

4.3.4. PILE SOIL-STRUCTURE INTERACTION

To determine the lateral stiffness of the soil surrounding the piles, a single lateral pile test was conducted. In close proximity to the quarter-scale integral abutment bridge, a 6" outer-diameter round section with a 0.25" wall thickness was driven to an approximate depth of 18 ft. A 1 in. steel pipe was inserted in the center of the pile to allow for the use of a down-hole displacement gage, and then the pipe pile was filled with 5000 psi concrete. At a distance of 30 in. above the existing ground surface, a pile cap (8"x8"x8") was cast at the top of the pile and clamped with 2" steel plates to provide for a flat, two-way loading surface (Figure 4.9). The soil profile obtained from the soils report (Appendix D) for the Bowen Laboratory, is shown in Table 4.7.

Figure 4.9: Single Pile for Lateral Pile Test

Table 4.7: Soil Profile for Lateral Pile Test

Depth of Soil Layer (ft)		N	Description of Layer
From	To		
0	1	8	Brown Clayey Silt Topsoil
1	16	30	Brown Silty Sandy Clay with a trace of Sand, Gravel, and Cobbles (Fill)
16	17	44	Brown Silty Clay with a trace of Sand and Gravel
17	20	23	Gray Silt
20	22	50+	Gray Silty Clay

A two-way hydraulic cylinder was used to apply lateral loading in both tension and compression to the top of the pile. The hydraulic cylinder had a stroke of 12 in., a bore hole diameter of 3.25 in., and a rod diameter of 1.38 in. The cylinder was connected to the single pile

and support block by the use of two clevises to provide a pin-ended condition for the pile (Figure 4.10). Loading was controlled by the use of a single 10,000 psi hand pump.
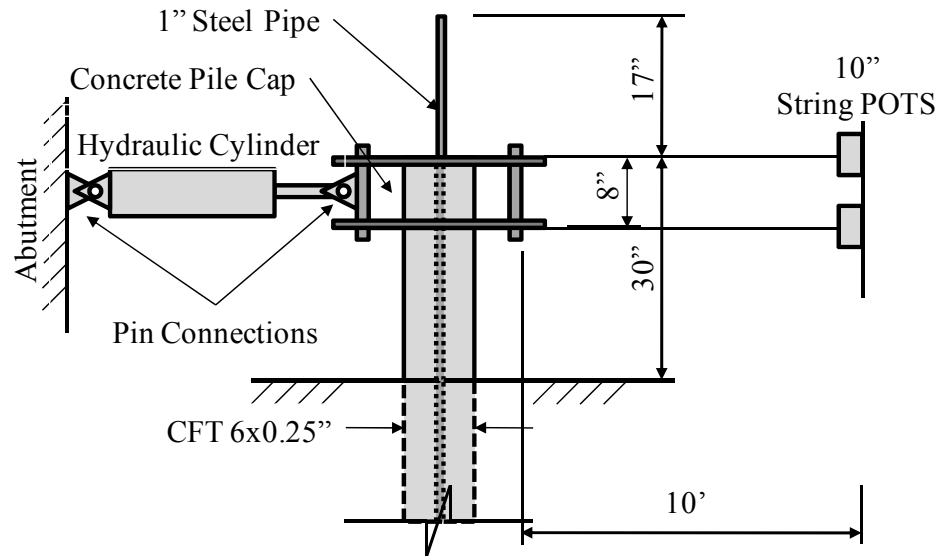
Figure 4.10: Lateral Pile Test Setup

To monitor the loading of the system, one 5000 psi pressure transducer (Omegadyne Inc. Model Number: PX409-5.0KG10V) was placed on each side of the hydraulic pathway of the two-way cylinder. Lateral displacements at the top of the pile were measured by the use of two 10 in. string potentiometers (UniMeasure Model Number: PA-10-DS). One potentiometer was placed at the top of the pile cap and the second potentiometer was located at the bottom of the pile cap (Figure 4.10). The two potentiometers were used to measure both the lateral displacement as well as the rotation at the top of the pile. To measure the pile deflected shape along the depth of the pile, two methods were implemented. Strain gages were installed along the length of the pile at 3 ft increments (Figure 4.11). Three strain gages were installed at each level; two perpendicular to the axis of bending to determine curvature, and one parallel to the axis of bending to ensure no out-of-plane bending occurred (Figure 4.12). The second method involved the use of a down-hole array (Measurand Model: SAAF). The down-hole array consists of a series of rigid segments separated by joints containing 3-axis MEMS (Microelectromechanical Systems) gravity sensors. Using geometry, the array produces a complete 3-D shape of the segments as a whole. When the array is lowered down the 1 in. pipe in the center of the test pile, a 3-D shape of the pile

is outputted. A reference shape of the pile is stored, and relative displacements can be measured in any direction. The array also provides the ability to confirm the lateral displacement and rotation information collected by the potentiometers.
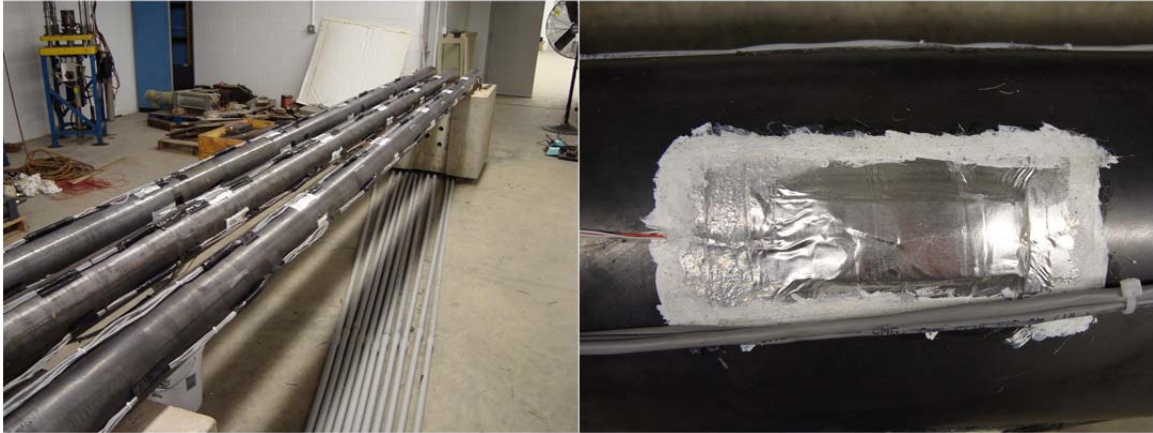
Figure 4.11: Strain Gages Along the Length of the Pile
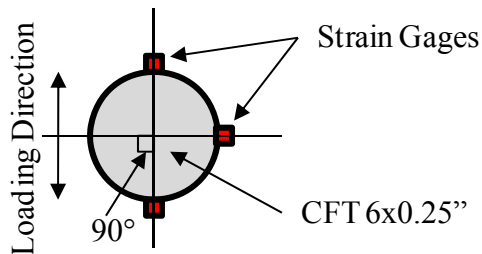
Figure 4.12: Cross-Section of Strain Gage Location

The lateral pile test was conducted by pushing and pulling the pile using 0.25 in. increments. One cycle was completed at each magnitude starting at 0.25 in. up to 1.5 in. However, the cycle for 1.25 in was skipped. Upon reaching the cycle of 1.5 in., it was planned to conduct several cycles at $\pm$ 1.5 in. However, the second half of the first cycle at 1.5 in. cracked the support block, and the test had to be discontinued (Figure 4.13). The data collected up to that point was of good quality and assumed to be directly applicable to the large scale test. Therefore, the test was not repeated.

Figure 4.13: Lateral Pile Test Cracked Support Block

4.3.4.1. LATERAL PILE TEST RESULTS

To understand the behavior of the single laterally loaded pile, a low cycle lateral displacement test was conducted. The general behavior of the lateral pile subjected to the aforementioned test program is discussed. The subsequent load-displacement curves are shown in Figure 4.14 through Figure 4.18. In addition, deflected shapes of the pile, as produced by the down-hole array, at different lateral displacement levels are shown in Figure 4.19. Regarding the strain gage readings along the depth of the pile, over 50% of the gages were damaged during pile driving. Therefore, the results are solely based on the down-hole array.

In general, the response of the substructure pile-soil system was nonlinear (Figure 4.14 through Figure 4.18). Characteristically, the response consisted of two separate key stiffnesses. Initially as the pile deflected into undisturbed soil, a lateral stiffness was measured to be approximately 7 kip/in. This stiffness was approximately the same for the first cycle of a larger deflection. Upon subsequent cycles, an initial lower stiffness (5 kip/in.) was measured as the pile displaced through soil that had previously been disturbed. Each time the pile was cycled, this initial lower stiffness was measured. It is apparent that after a primary cycle, the pile behavior follows a steady state hysteretic behavior.

Regarding the deflected shape of the pile, the down-hole array shows that the pile tends to deflect about a point 7 ft below the top of the pile and 5 ft below the existing surface (Figure 4.19). Below this depth, essentially no deflection was measured, therefore, the pile deflected as a cantilever with a depth of fixity of 7 ft. Symmetrical behavior was observed considering both loading directions.
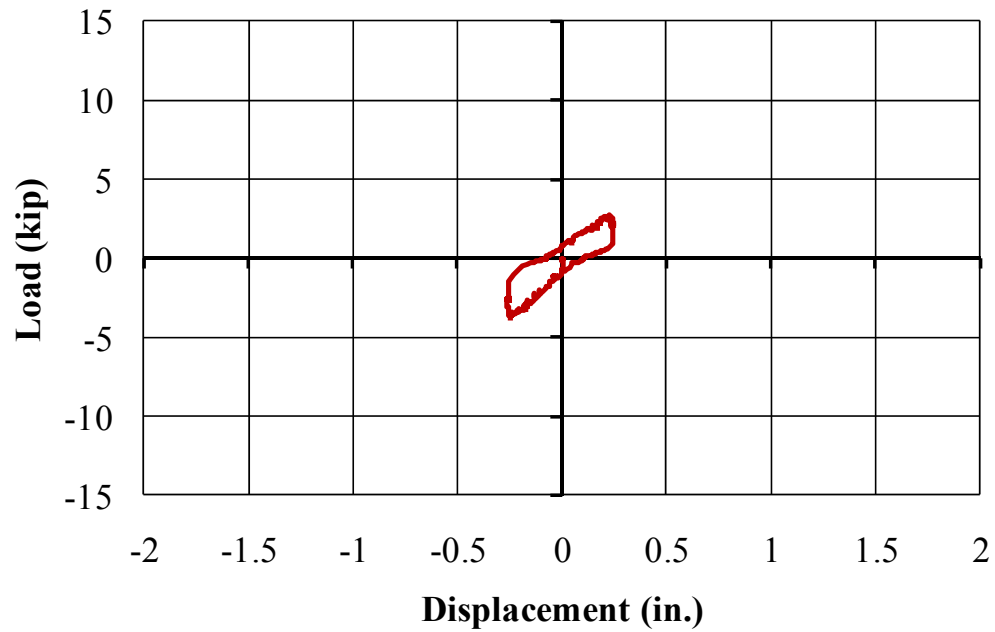
Figure 4.14: Pile Load-Deflection Response (±0.25 in.)
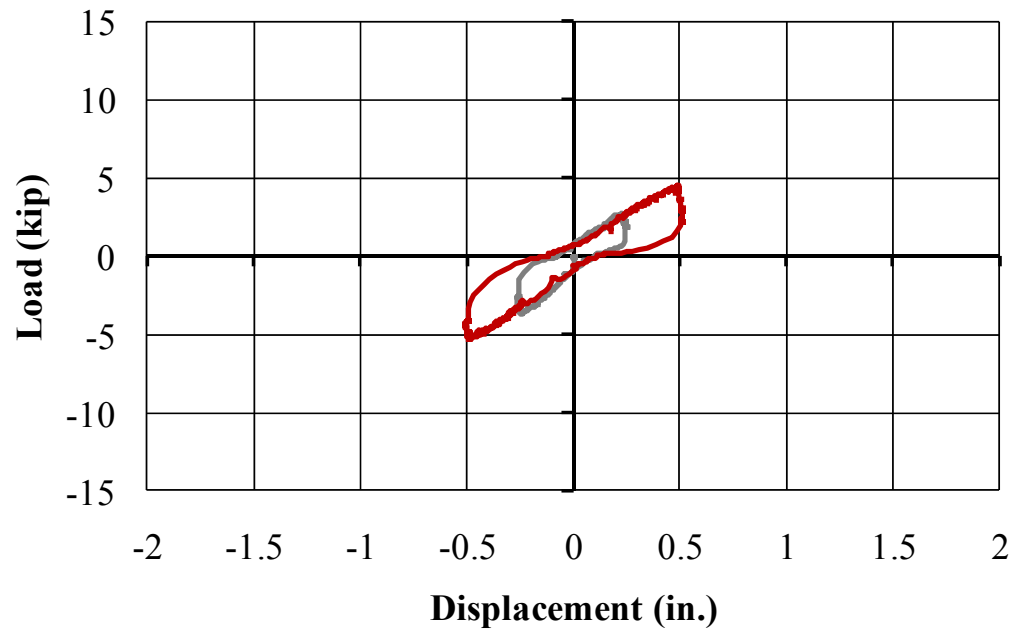
Figure 4.15: Pile Load-Deflection Response (±0.50 in.)
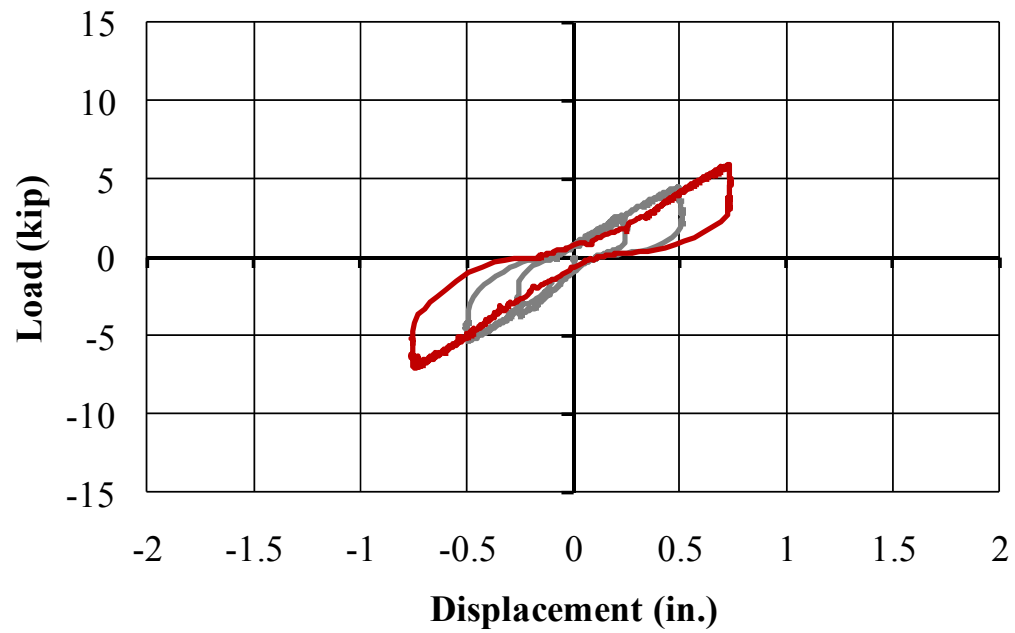
Figure 4.16: Pile Load-Displacement Response (±0.75 in.)
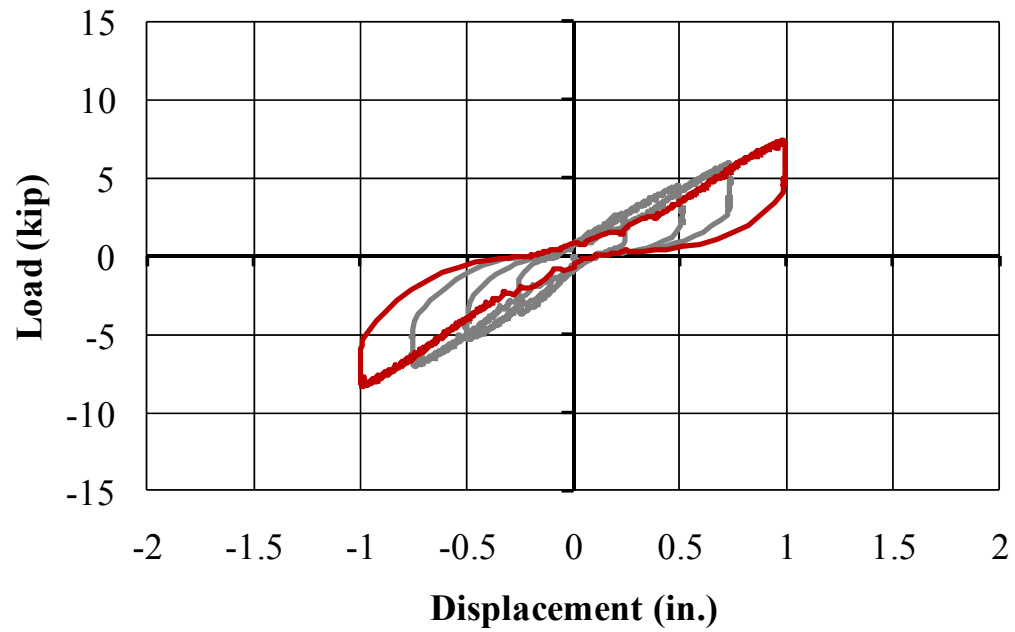
Figure 4.17: Pile Load-Displacement Response (±1.00 in.)
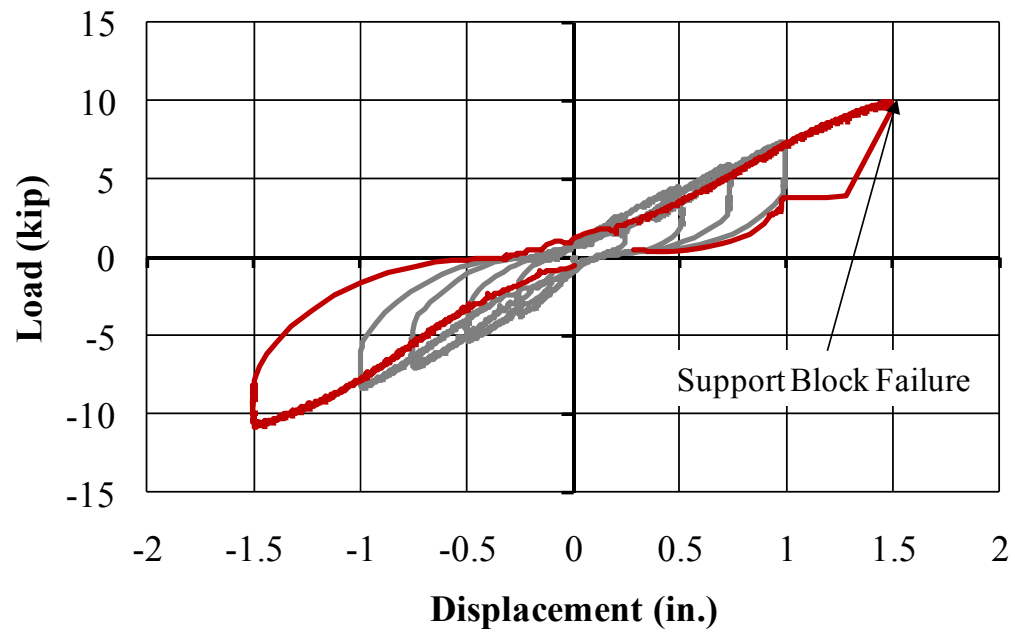
Figure 4.18: Pile Load-Deflection Response (±1.50 in.)
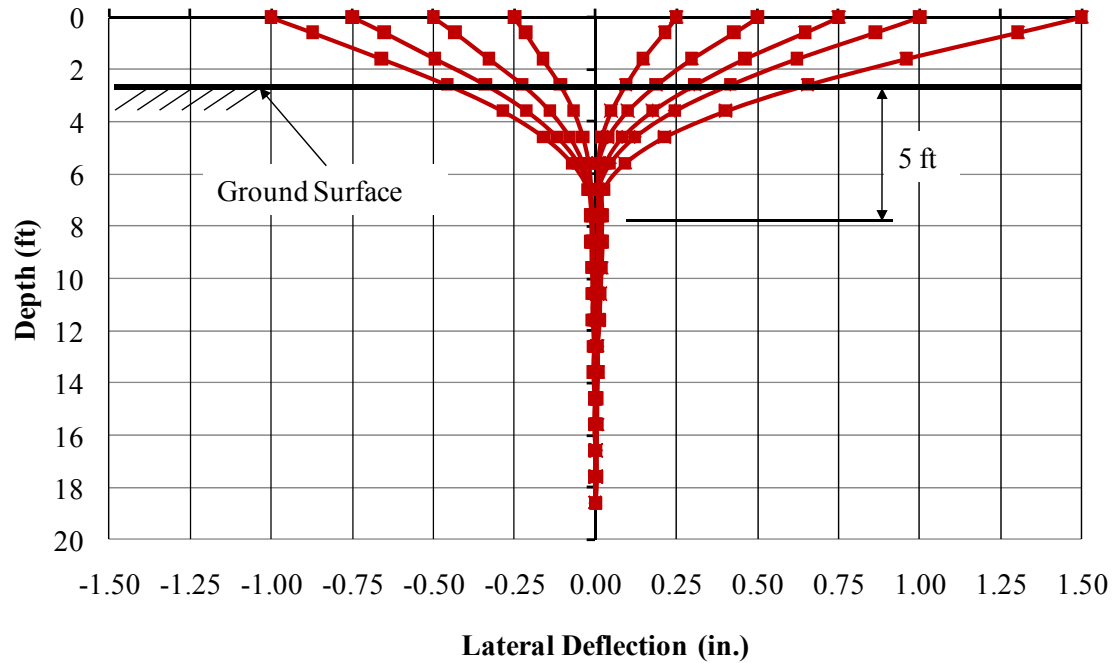
Figure 4.19: Pile Deflected Shape

4.3.4.2. EVALUATION LATERAL PILE TEST RESULTS

To adequately understand the behavior of the pile-soil system, the collected test results were used to calibrate an analytical model. The analytical model consisted of a single frame element developed to represent the pile using the transformed pile section described in Section 4.3.3. The surrounding soil was represented by soil springs following the methods describe in Section 3.3.1. A schematic of the analytical model is shown in Figure 4.20.
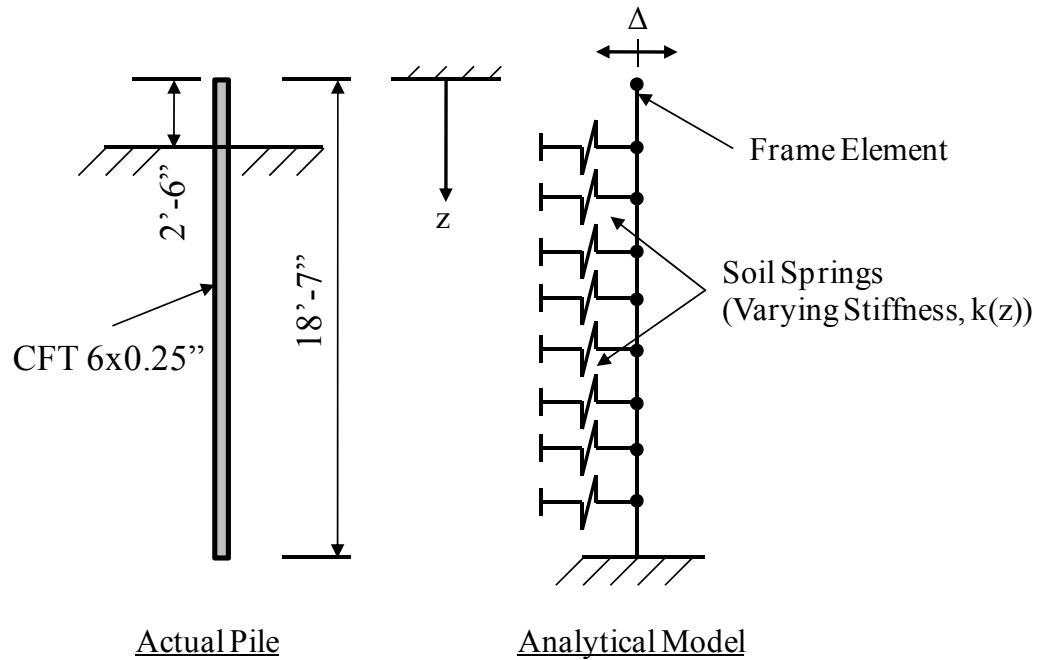
Figure 4.20: Modeling Schematic of Lateral Pile Test

Three separate soil conditions were used to determine equivalent springs for the pile test. According to the soils report, the subsurface consisted of mostly clay. Therefore, springs were calculated for soft, stiff, and very stiff clays. Because the existing site consisted of a dense compacted fill material, the unit weight of the material was assumed to be 130 pcf regardless of the stiffness. The undrained shear strength for the material was assumed to be 750 pcf, 1500 pcf, and 3000 pcf for the soft, stiff, and very stiff clay, respectively. Springs were developed at 1 ft increments along the depth of the pile for the three soil conditions, and the stiffnesses are given in Table 4.8.

Table 4.8: Soil Spring Stiffnesses for Lateral Pile Model

Depth Below Pile Top (ft)	Spring Stiffness (k/in.)		
	Soft Clay	Stiff Clay	Very Stiff Clay
0	0	0	0
1	0	0	0
2	0	0	0
2.5 (Ground Level)	0	0	0
3	1.9	7.5	37.5
4	4.5	17.7	88.0
5	5.6	22.5	112.5
6	5.6	22.5	112.5
7	5.6	22.5	112.5
8	5.6	22.5	112.5
9	5.6	22.5	112.5
10	5.6	22.5	112.5
11	5.6	22.5	112.5
12	5.6	22.5	112.5
13	5.6	22.5	112.5
14	5.6	22.5	112.5
15	5.6	22.5	112.5
16	5.6	22.5	112.5
17	5.6	22.5	112.5
18	5.6	22.5	112.5
18.58	5.6	22.5	112.5

The analytical model of the pile-soil system was subjected to a series of lateral displacements at the top of the pile that correspond to the lateral pile test (0.25, 0.5, 0.75, 1.0, and 1.5 in.). Because the behavior of the pile was equivalent in both directions, only one direction was investigated with the analytical model. For a given lateral displacement, the model computed the necessary lateral force, as well as the deflected shape of the pile. Figure 4.21 through Figure 4.23 show the computed deflected shapes for the three different soil conditions. The results from the model are superimposed over the measured deflected shapes from the down-hole array. The deflected shapes are only shown to a depth of 10 ft, because the displacement is essentially zero beyond 10 ft. Table 4.9 shows the comparison of the forces required to achieve the lateral deflection at the top of the pile for the three analytical models and the experimental model.
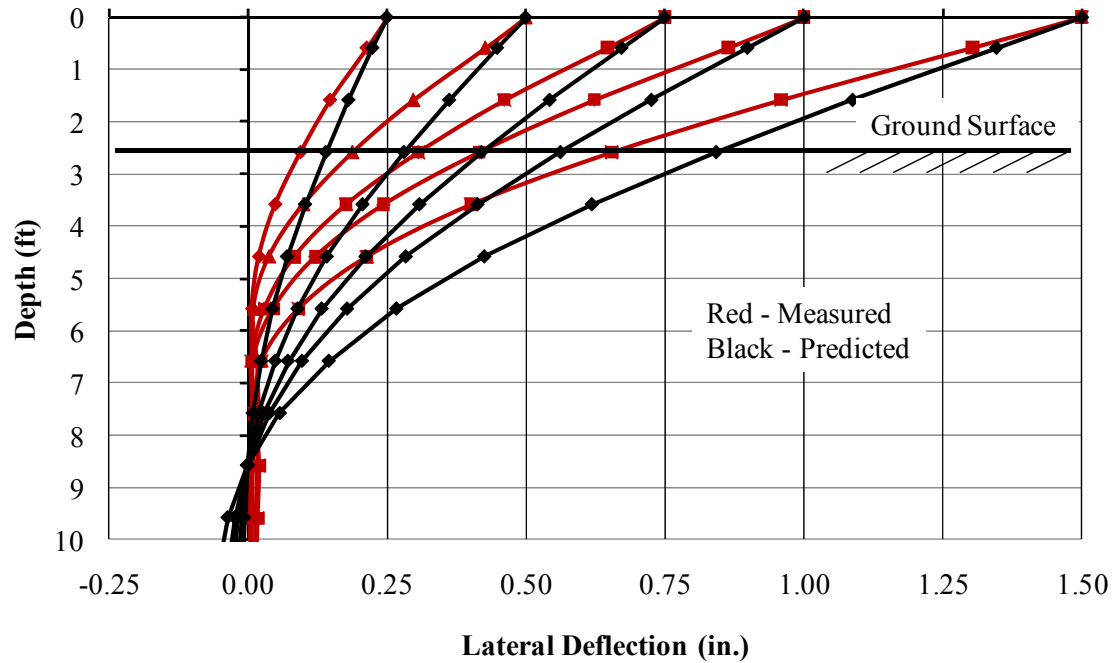
Figure 4.21: Predicted vs. Measured Pile Deflected Shape (Soft Clay)
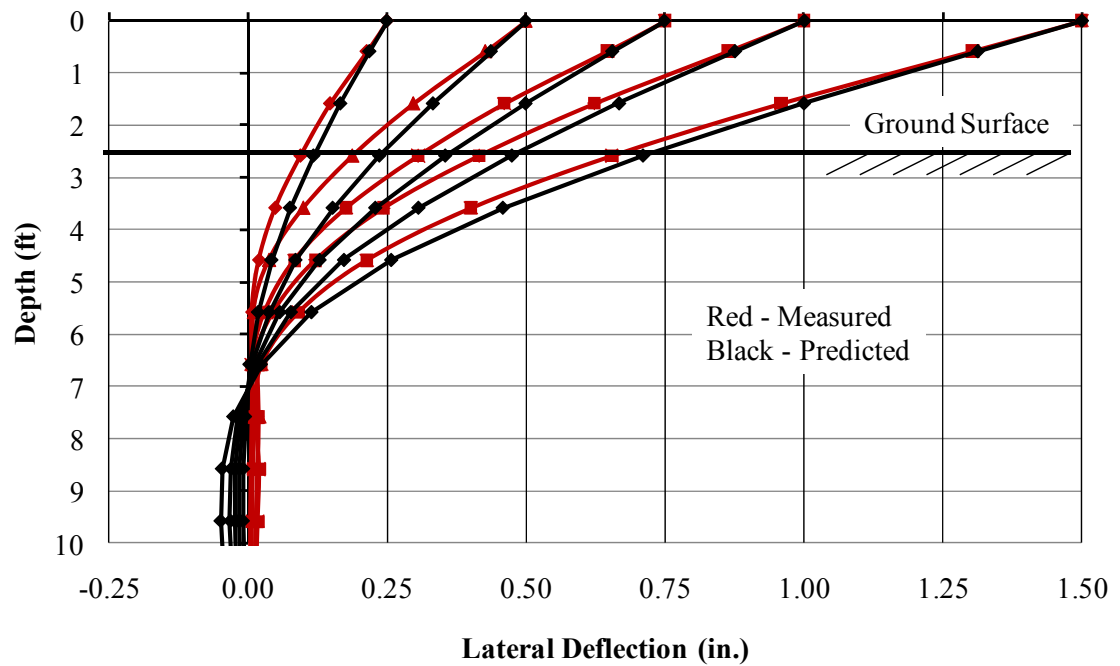
Figure 4.22: Predicted vs. Measured Pile Deflected Shape (Stiff Clay)
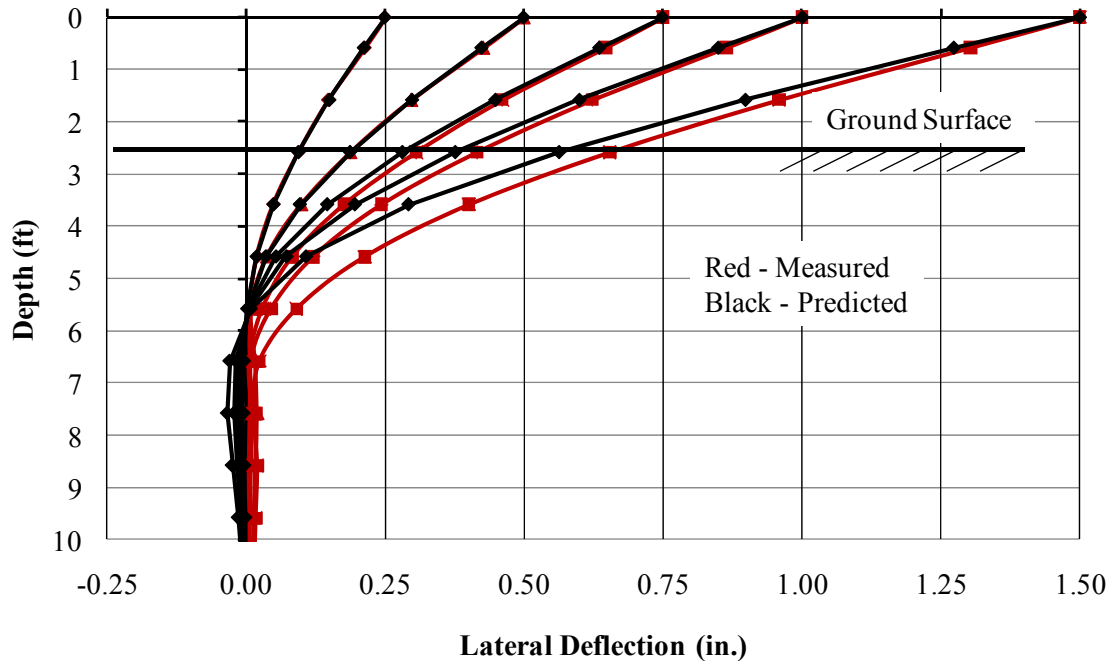
Figure 4.23: Predicted vs. Measured Pile Deflected Shape (Very Stiff Clay)

Table 4.9: Lateral Load for Single Pile

Displacement (in.)	Lateral Load (kip)			
	Analytical			Experimental
	Soft	Stiff	Very Stiff	
0.25	0.5	1.0	1.7	2.3
0.50	1.1	2.0	3.4	4.2
0.75	1.7	3.0	5.1	5.6
1.00	2.3	3.9	6.7	7.0
1.50	3.4	5.9	10.1	10.0

When compared to the lateral pile test, the displacement and load results of the analytical indicate that the model for the very stiff clay represents the overall system fairly well. The predicted deflected shapes of the pile in the very stiff clay are very close to the measured results of the lateral pile test for all lateral deflections except at the larger displacements (especially 1.5 in.). The stiff clay provides an improved deflected shape estimation at the larger displacements. Perhaps at larger displacements, a reduced stiffness is appropriate. Considering the lateral load; however, the very stiff clay provides the best matches for all displacement levels. The

discrepancies between the analytical model and the experimental test can be most likely explained by the fact that the soil was assumed to be uniform in the model, while the soil is not uniform. The soil was also assumed to behave linear elastic, while soil rarely behaves in that manner. However, with these simplifications, the results of the analytical model are very close to that of reality for these displacement ranges. Therefore, the modeling techniques and spring values derived in this section, specifically the very stiff clay, will be used in modeling the full scale test structure.

4.4. SPECIMEN CONSTRUCTION

4.4.1. PILES

Steel piles were used to support the abutment and superstructure for the quarter-scale integral abutment bridge. The piles are a 6" O.D. round section with 0.25 in. wall thickness and were 21 ft in length (Figure 4.24). Each pile had a cap installed at the base for driving (Figure 4.25). To drive the piles, 6 ft starter holes were augured (Figure 4.26). A Movak excavator with a vibratory attachment was used to drive the piles to a depth of 18 ft or until refusal (Figure 4.27). The piles were oriented to follow the determined 45 degree skew angle of the abutment. The final layout of the piles is shown in Figure 4.28. After the piles were in place, they were each cut to height, and a 1 in. steel pipe was inserted into the center of the pile to allow for the use of the down-hole array. The piles were then filled with Class B concrete (5000 psi actual). The actual length of each pile after driving and cutting varied, and the actual lengths are shown displayed in Figure 4.29.

Figure 4.24: Piles (6 in. O.D. Round Section)

Pile Caps

Figure 4.25: Pile Driving Caps

Figure 4.26: Drilling 6 ft. Starter Hole for Pile

Figure 4.27: Driving Piles with Movac Vibrator

Figure 4.28: Abutment Piles after Driving

Pile	Depth, z (ft)
N1	17.92
N2	19.67
N3	19.75
N4	19.71
N5	19.42
S1	19.25
S2	19.50
S3	19.54
S4	19.33
S5	18.79
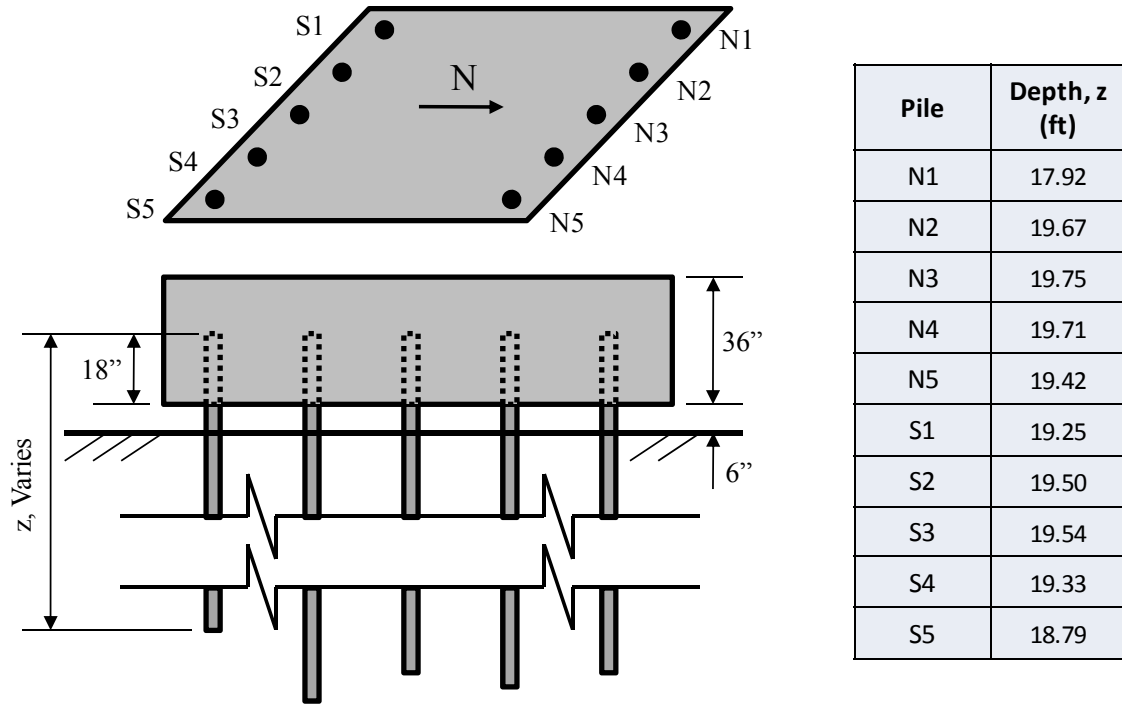
Figure 4.29: Actual Depth of Bridge Piles

4.4.2. ABUTMENT

The two abutments for the quarter-scale integral abutment bridge were designed to ensure that the shear forces from the lateral loading could be accommodated. Each abutment was 12'-6" wide and constructed with a skew of 45 degrees. The abutments were cast 6" above the existing ground. A plan view of an abutment is shown in Figure 4.30, and a cross-section is shown in Figure 4.31. A cage of #5 bars in both directions was provided to accommodate the expected shear and bending forces. Each abutment was supported by five piles (CFT 6x0.25") each with a 1 in. steel pipe that extended through the top of the abutment. Formwork for each abutment, shown in Figure 4.32, was equipped with whales to maintain dimensional tolerances. A view of the reinforcement placed in the abutment is shown in Figure 4.33 and Figure 4.34. The abutment was cast continuously with the deck using a 6 bag mix which achieved 6000 psi (Section 4.3.1).
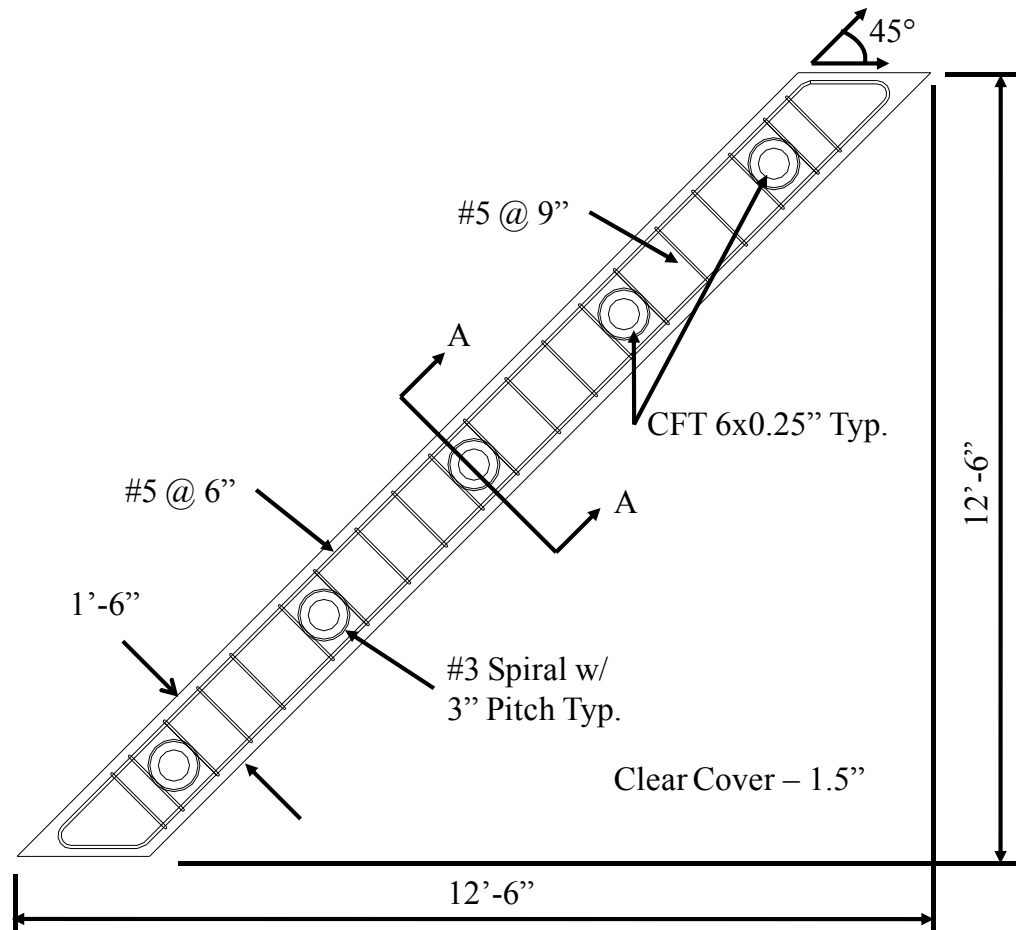
Figure 4.30: Plan View of Abutment
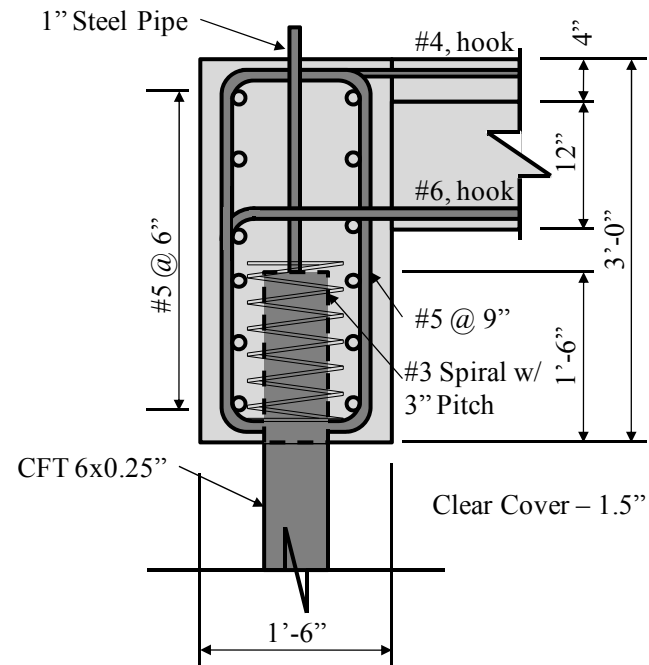
Figure 4.31: Abutment Cross-Section (Section A-A)

Figure 4.32: Abutment Formwork

Figure 4.33: Reinforcement Cage for Abutment

Figure 4.34: Close-up of Abutment Reinforcement

4.4.3. SUPERSTRUCTURE

The superstructure for the quarter-scale integral abutment bridge consisted of a 4 in. concrete deck supported by three 10 in. x 12 in. beams (W x H). A plan view and cross-section of the superstructure are shown in Figure 4.35. The deck was cast with a mat of #4 bars, and the girders contained three #6 bars each for flexure. Shear in the beams was resisted using #3 stirrups spaced at 6 in. The longitudinal bars in the deck and the girder continued into the abutment and were hooked on the backside. The formwork and reinforcement for the superstructure is shown in Figure 4.36. To allow for the ability to expand and contract the superstructure for the simulation of seasonal strains, a gap was cast at midspan of the superstructure (Figure 4.37). The superstructure was cast continuously with the abutments with a 6 bag mix which achieved 6000 psi (Section 4.3.1).
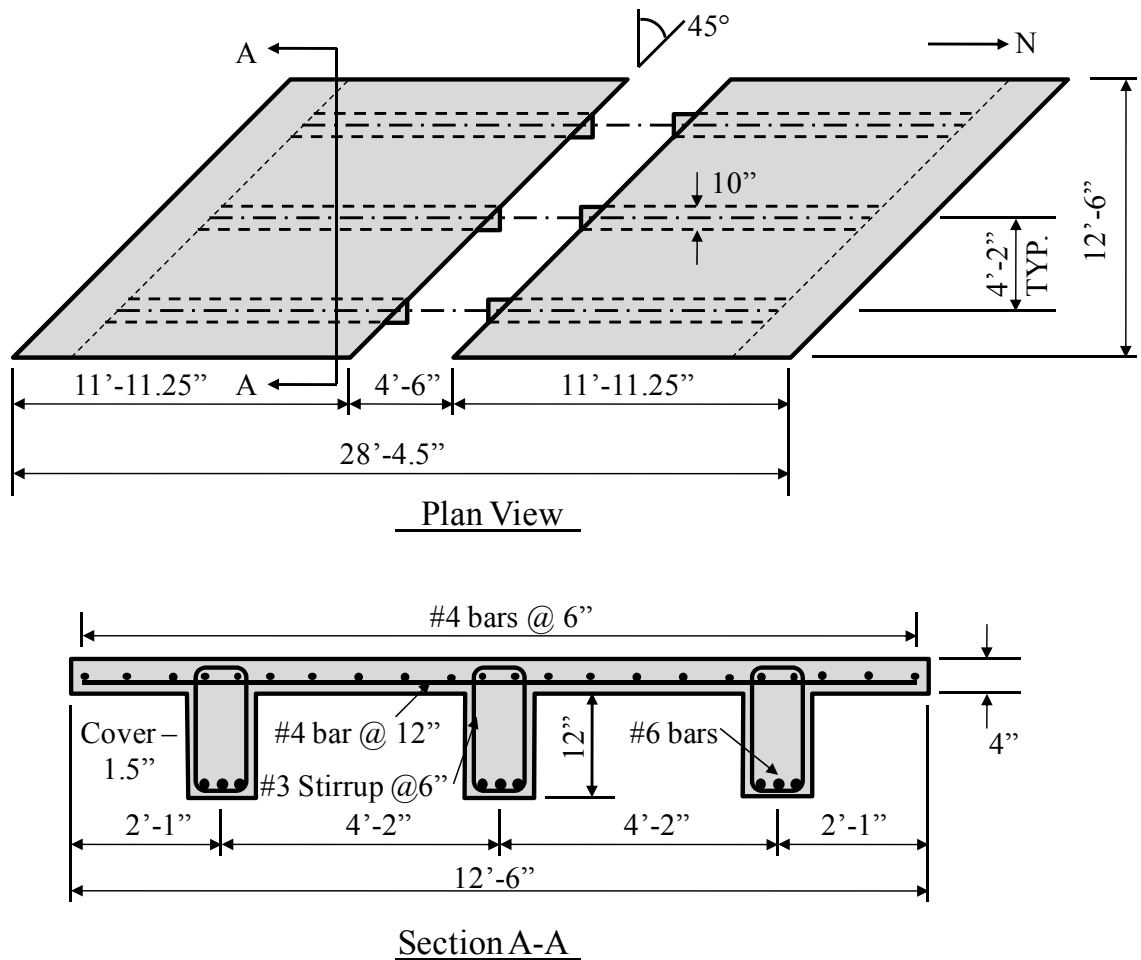
Figure 4.35: Superstructure Details

Figure 4.36: Superstructure Formwork and Reinforcement

Figure 4.37: Formwork for Gap in Superstructure

4.4.4. TRANSFER BEAM

A gap was cast into the superstructure at midspan so that the structure could be expanded and contracted to artificially simulate seasonal movements. However, the gap in the structure created a discontinuity. Transfer beams were designed and attached to the structure to provided flexural and shear continuity while allowing the structure to move longitudinally. Three W14x68 beams were used as the transfer beams (Figure 4.38); one over each concrete girder. This specific section was selected because the flexural stiffness of the steel section and the concrete superstructure is similar. The steel beams were fabricated with long slotted holes in the top and bottom flange on one end and standard holes on the other (Figure 4.39). The end with the slotted holes was coated with Teflon on the top flange surfaces. The beams were clamped to the concrete structure by the use of ¾" all-thread rods and ½" bearing plates. The bearing plates that contacted the steel beam's Teflon surface were also coated with Teflon.

While carrying the gravity loads, the steel beam allows the two halves of the bridge to expand and contract along the axis of the slotted holes by means of sliding on the two Teflon surfaces. Ideally, the resistance is minimal. The transfer beams also serve to keep each half of the concrete structure from sliding out of plane to one another. An elevation view of the system is shown in Figure 4.40. The slotted and fixed ends are shown in Figure 4.41.

Figure 4.38: Transfer Beams

Teflon Coating
(36"x10")
Top and Bottom of Section

Slotted Hole
Standard Dia. for 3/4" Bolt
Top and Bottom Flange

Standard Hole for
3/4" Bolt
Typ.

3.0"

10.0"

3.0"

3.5"

2'-6.0"

3 Spa. @ 6"

3.5"

3'

8'-8.0"

Teflon Coating
(36"x10")
Top and Bottom of
Section

3.0"

1'-2.0"

3.50"

3.50"

10.0"

W14x68
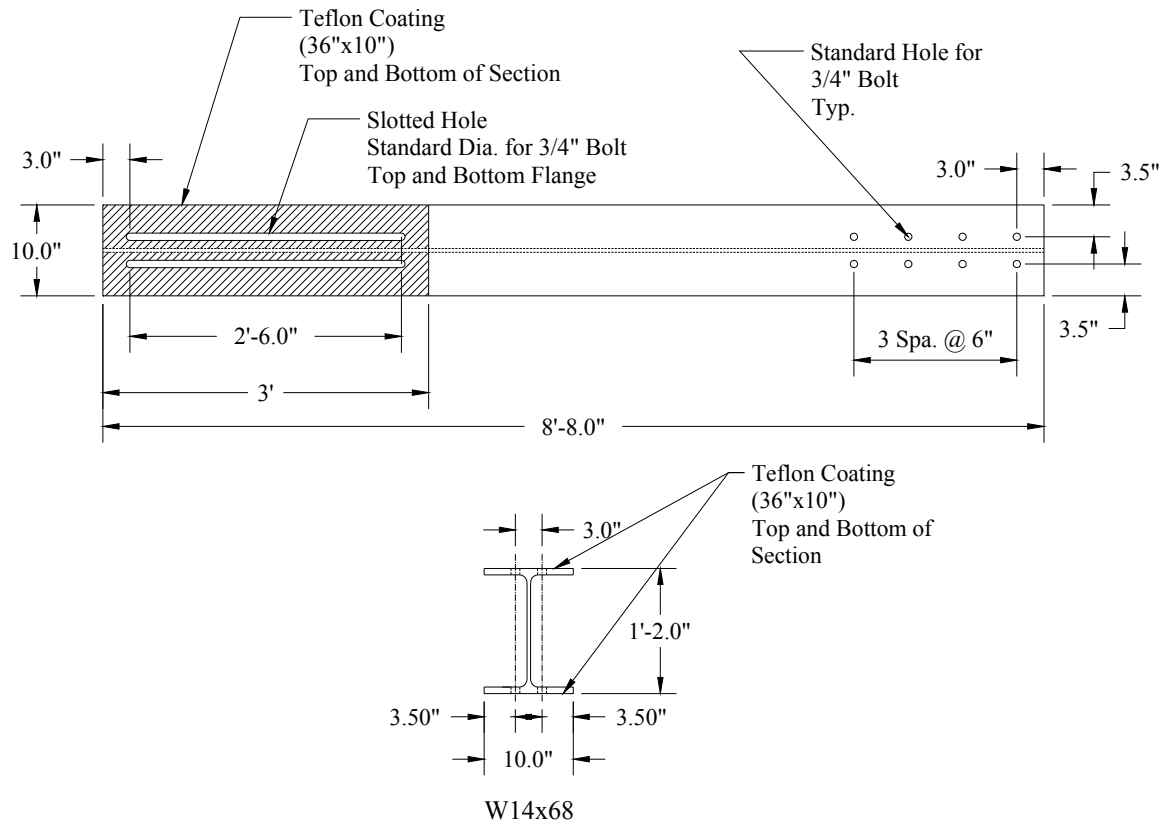
Figure 4.39: Transfer Beam Details

½" Bearing Plates

Teflon Surface

Standard Holes

Slotted Hole

W14x68

Deck

Deck

Loading

16"

Girder

Girder

¾" All thread
Bars

4'-6"

GAP
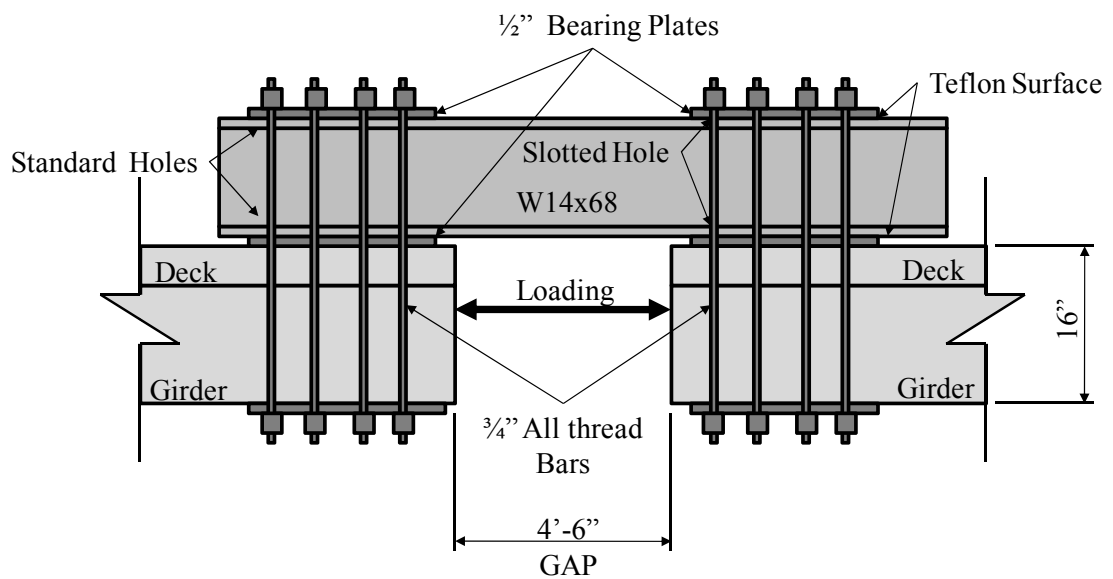
Figure 4.40 Elevation Schematic of Transfer Beam

Slotted End   Fixed End
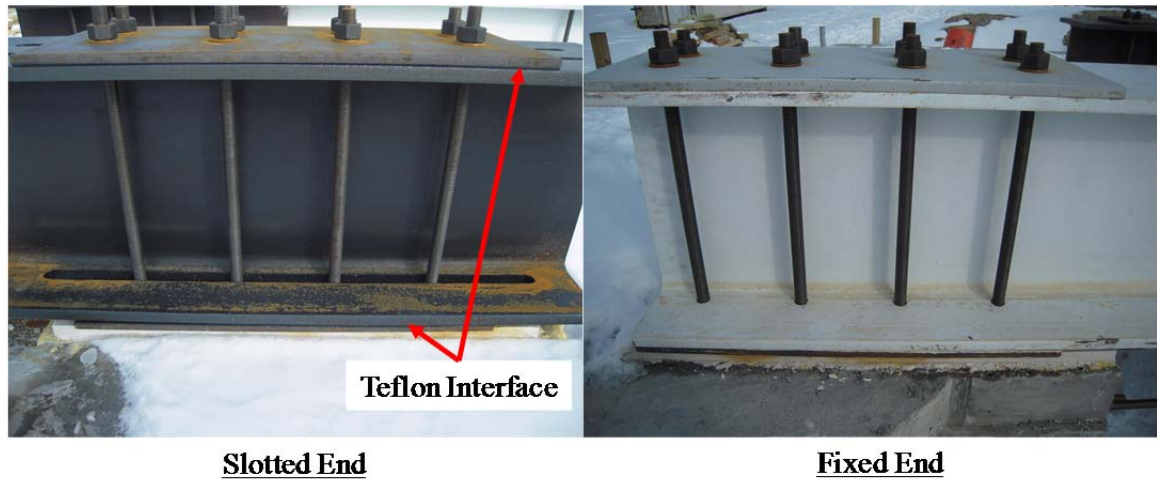
Figure 4.41: Transfer Beam Ends

4.4.5. LOADING SYSTEM

Seasonal expansion and contraction of the superstructure was simulated by three hydraulic cylinders at midspan of the structure. A two-way cylinder with a 6 in. bore diameter and a 2.5 in. rod diameter was installed at the centroid of each girder (Figure 4.42). Each end of the cylinder was connected to the structure by the use of a clevis to provide a pin-ended connection. The clevises were connected to the deck by attaching to #4 bars embedded into the concrete and developed into the beam. Each cylinder was controlled using a separate 10,000 psi hand pump.

Figure 4.42: Two-Way Hydraulic Cylinder

4.4.6. CASTING AND CURING

Concrete casting for the quarter-scale bridge was completed on December 17th, 2009. The casting was conducted in two stages: one for each half of the structure. Because of cold weather, the concrete was covered with insulated blankets shortly after placement, and a salamander heater was placed beneath the superstructure to maintain the concrete's temperature above freezing. The concrete was continually covered and cured for seven days, and then the formwork was stripped. Test cylinders were cured separately for the first 24 hours underneath thermal blankets and then moved beneath the superstructure into the heated tent to provide a similar curing and temperature history.

4.5. INSTRUMENTATION

To monitor the response of the quarter-scale integral abutment bridge, string potentiometers, pressure transducers, strain gages, and a down-hole array were used. The description and implementation of the various instruments are given in the following sections.

4.5.1. DISPLACEMENT

String Potentiometers (UniMeasure Model PA-10-DS and PA-25-DS) were used to measure the movement of the gap and both abutments. To monitor movements at each abutment, 10 in. potentiometers were used while 25 in. potentiometers were used to measure the gap displacements. The abutments were highly instrumented to measure displacement and rotation in three directions. Figure 4.43 shows the location of the 18 potentiometers used. It should be noted that locations with two numbers have two gages, and the lower number is located at the base of the abutment.
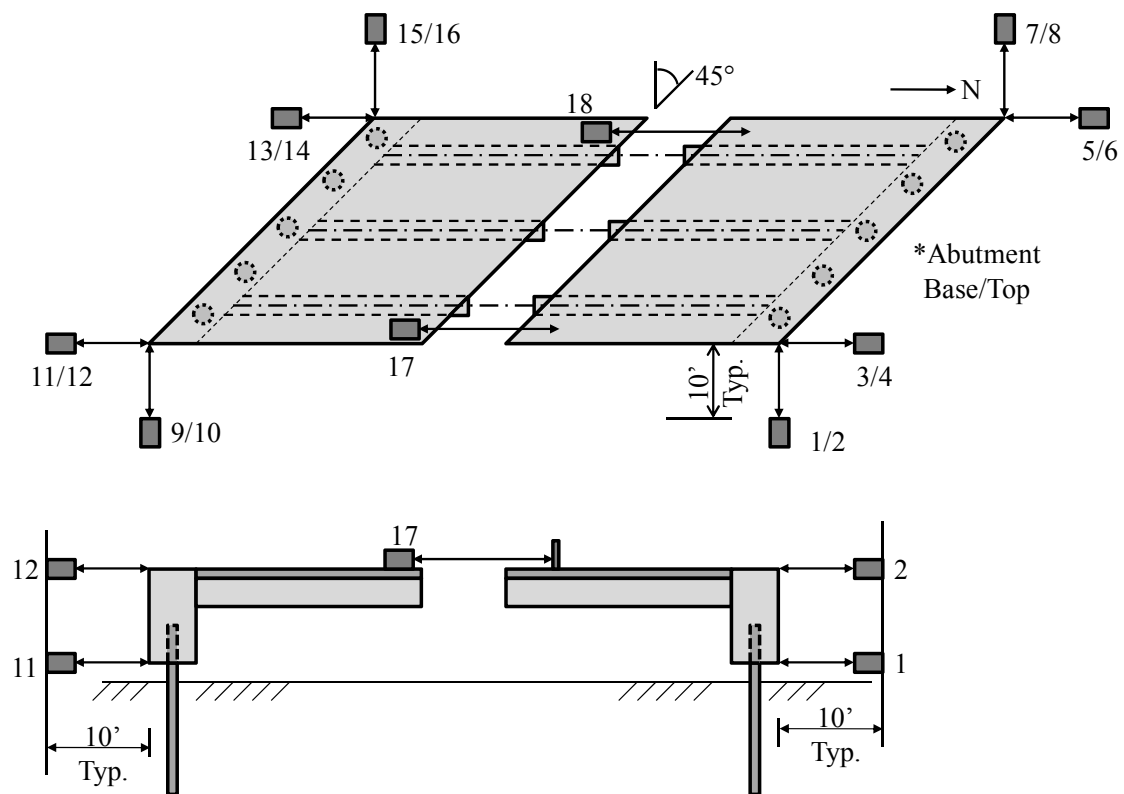
Figure 4.43: String Potentiometer Locations

4.5.2. LOAD

To monitor loading of the system, one 5000 psi pressure transducer (Omegadyne Inc. Model Number: PX409-5.0KG10V) was placed on each side of the hydraulic pathway of the

three two-way cylinders. The gages were factory calibrated and verified to accurately measure load by testing the hydraulic cylinders in a 600 kip Forney.

4.5.3. STRAIN GAGES

Strain gages were installed in the superstructure and along the length of two selected piles. The strain gages were obtained from Vishay Micro-Measurements. The strain gages were 350 ohm weldable strain gages (Vishay Model LWK-06-W250B-350) and were installed along the length of the east and west piles of the south abutment prior to being driven. Four strain gages were installed orthogonal to one another at 3 ft increments over the depth of the pile (Figure 4.44). The top strain gages were installed after the piles were driven at the base of the abutment. These strain gages were designed to determine the curvature of the piles and the corresponding deflected shape. During pile driving, over half of the strain gages along the length of the piles were damaged. Therefore, the strain gage readings were not used in analysis.
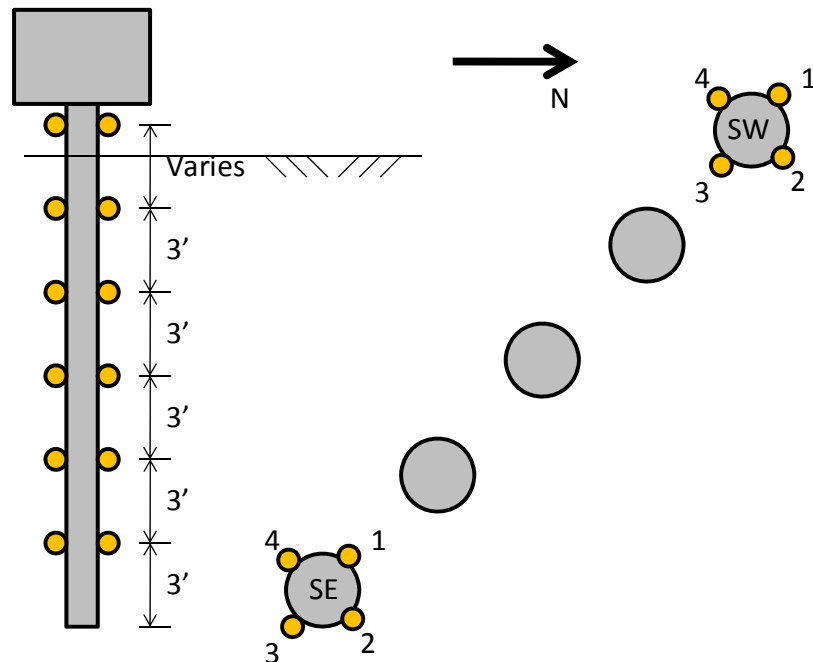
Figure 4.44: Locations of Pile Strain Gages in South Abutment

4.5.4. SAA ROPE

A down-hole array (Measurand Model: SAAF) was used to monitor the deflected shape of the piles supporting the abutment. The down-hole array consists of a series of rigid segments separated by joints containing 3-axis MEMS (Microelectromechanical Systems) gravity sensors. Using geometry, the array produces a complete 3-D shape of the segments as a whole. When the array is lowered down the 1 in. steel pipe in the center of the test pile, a 3-D shape of the pile is provided. A reference shape of the pile is stored, and relative displacements can be measured in any direction.   A single array was used, therefore each reading of deflected shape for each corresponding pile required the rope to be lowered and raised for each pile.   The array also provides the ability to confirm the lateral displacement and rotation information collected by the potentiometers.

4.5.5. TEST PROCEDURE

The test program for the quarter-scale integral abutment bridge used the following procedure:

1. All gages were zeroed.

2. Initial readings were taken for each pile using the down-hole array to determine the original positions.

3. The gap was loaded by the three hydraulic cylinders ensuring that the change in length at the gap was constant across the width of the bridge (different magnitude of load at each cylinder). The first stage was an expansion of 0.5 in.

4. While the gap was maintained at the desired deflection, a measurement of the deflected shape was taken for each pile using the down-hole array.

5. The load was released, and the first contraction phase was conducted (-0.5 in.). In the same way as during the expansion phase, the deflection of the gap was forced to be constant across the width of the structure.

6. While the gap was maintained at the desired deflection, a measurement of the deflected shape was taken for each pile using the down-hole array.

7. Steps 3 through 7 were repeated for the following gap deflections: ±1.0 in., ±1.5 in., and ±2.0 in.

4.5.5.1. TEST PROBLEM

During the second half of the final phase (-2.0 in.) a failure one of the hydraulic hand pumps occurred. The pump was unable to build pressure of the system. However, the contraction of the gap was near 2 in. Therefore, the test was not repeated.

4.6. RESULTS

4.6.1. ABUTMENT DISPLACEMENT

To develop an understanding of how a skewed abutment behaves when subjected to longitudinal forces, the abutment's deflections were monitored. The test was controlled by the displacement of the gap. Figure 4.45 shows the displacement of the gap over the duration of the test for both the east and west ends. Also shown is the average gap displacement. Because the gap displacements were approximately the same, the average gap displacement will be used for all future analysis. Using the average displacement, Figure 4.46 shows the load-deflection response for the gap for the entire testing program. The load shown is the average load measured by the two exterior hydraulic cylinders.
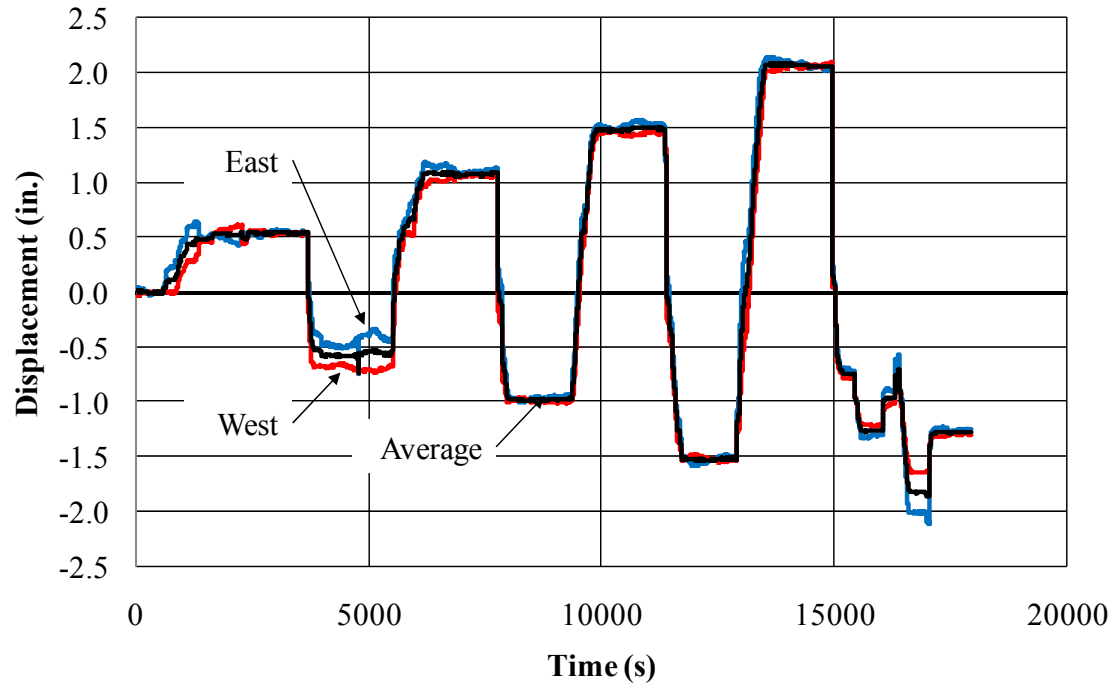
Figure 4.45: Gap Displacements
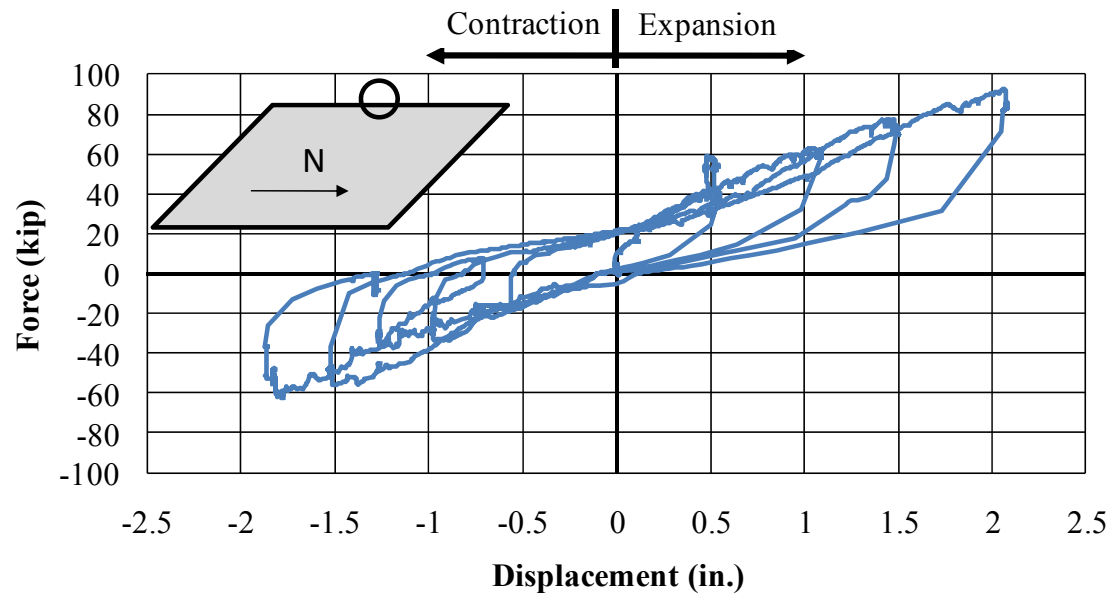
Figure 4.46: Load-Deflection Response at Gap

To monitor the behavior of the abutment, measurements were taken at each corner for longitudinal and transverse displacements of both the north and south abutments. Figure 4.47 through Figure 4.62 show the load-displacement responses for each position. In addition, the positive direction of the displacement measurements is noted in each figure. For figures that are crossed-out, the data are considered as erroneous.
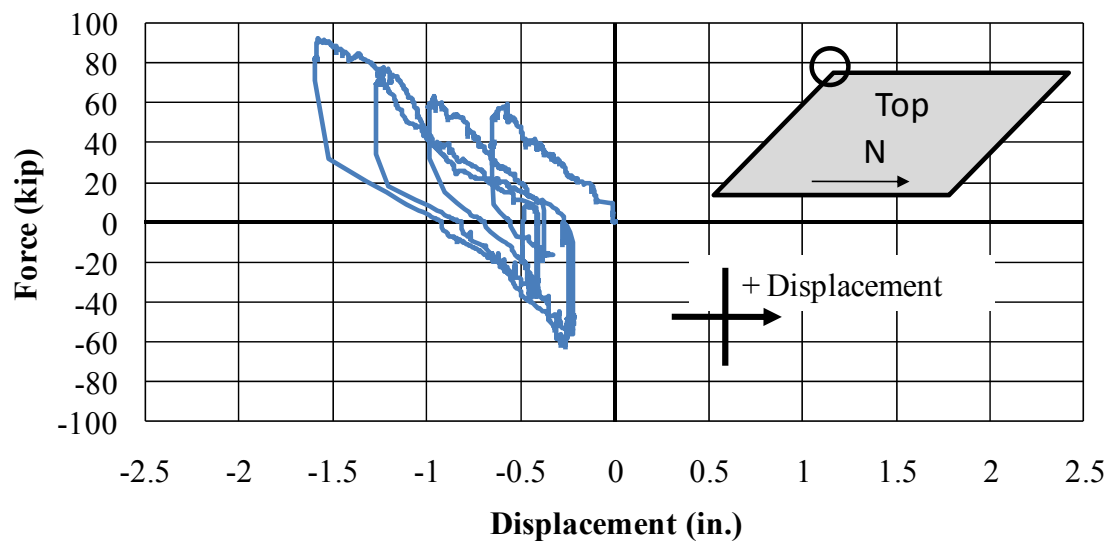
Figure 4.47: Longitudinal Load-Deflection Response – SW, Top
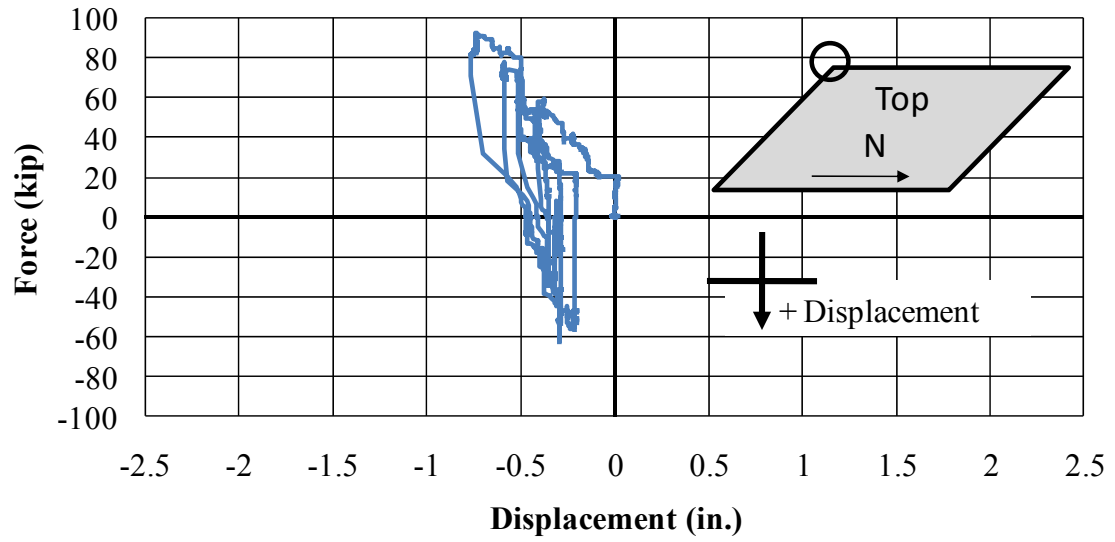
Figure 4.48: Lateral Load-Deflection Response – SW, Top
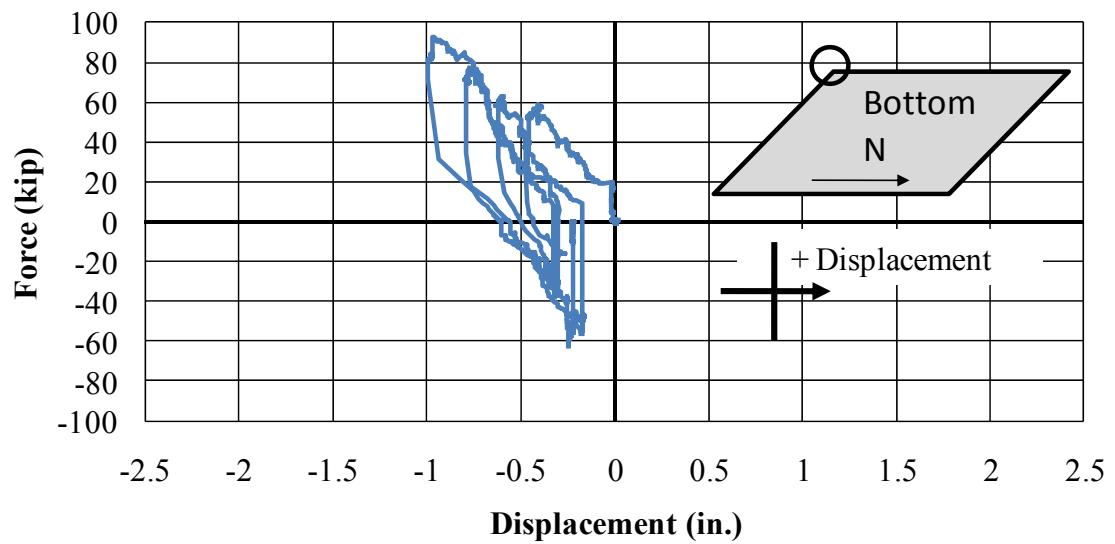
Figure 4.49: Longitudinal Load-Deflection Response – SW, Bottom
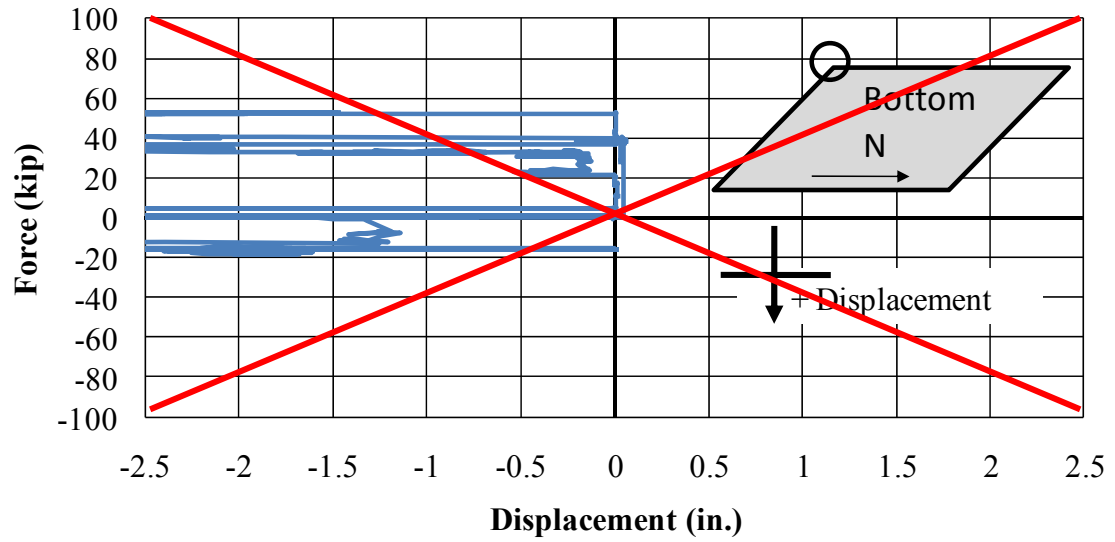
Figure 4.50: Lateral Load-Deflection Response – SW, Bottom
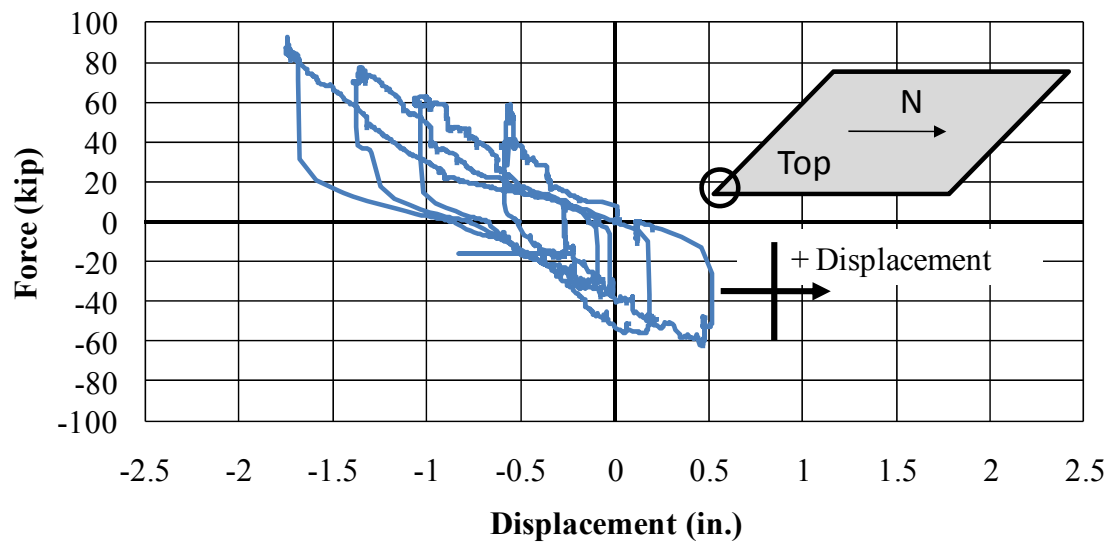
Figure 4.51: Longitudinal Load-Deflection Response – SE, Top
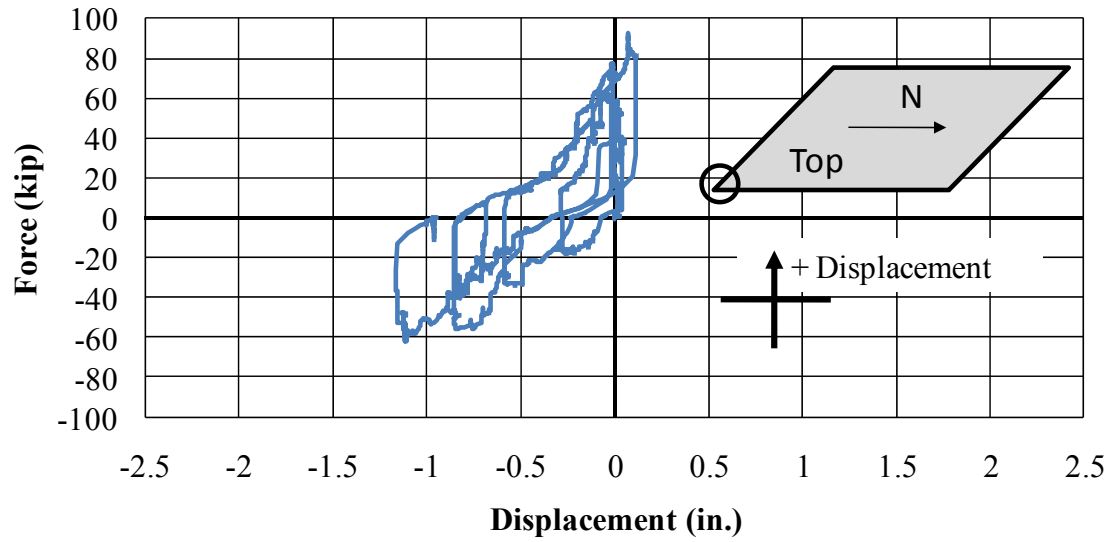
Figure 4.52: Lateral Load-Deflection Response – SE, Top
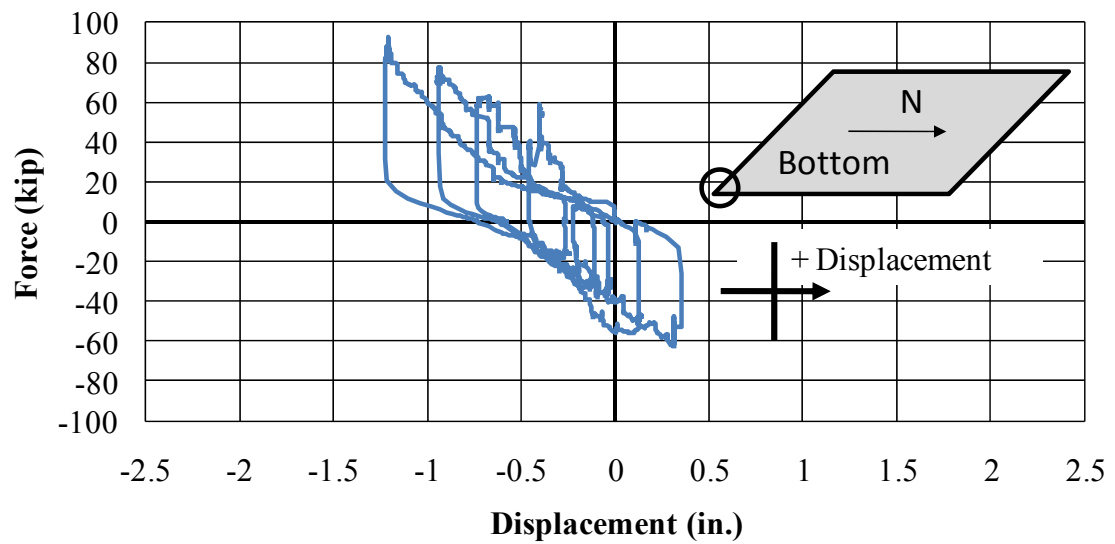
Figure 4.53: Longitudinal Load-Deflection Response – SE, Bottom
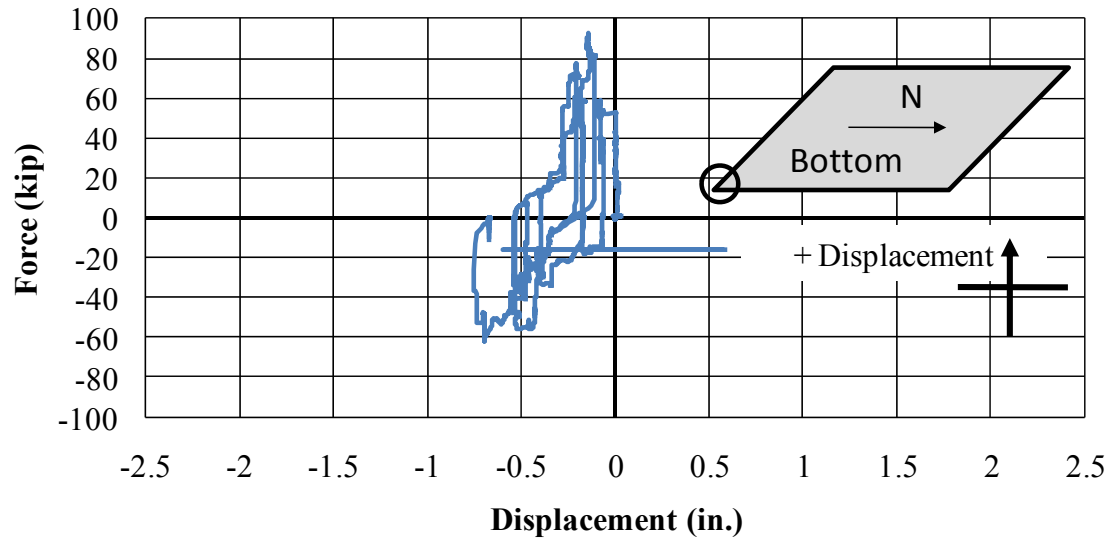
Figure 4.54: Lateral Load-Displacement Response – SE, Bottom
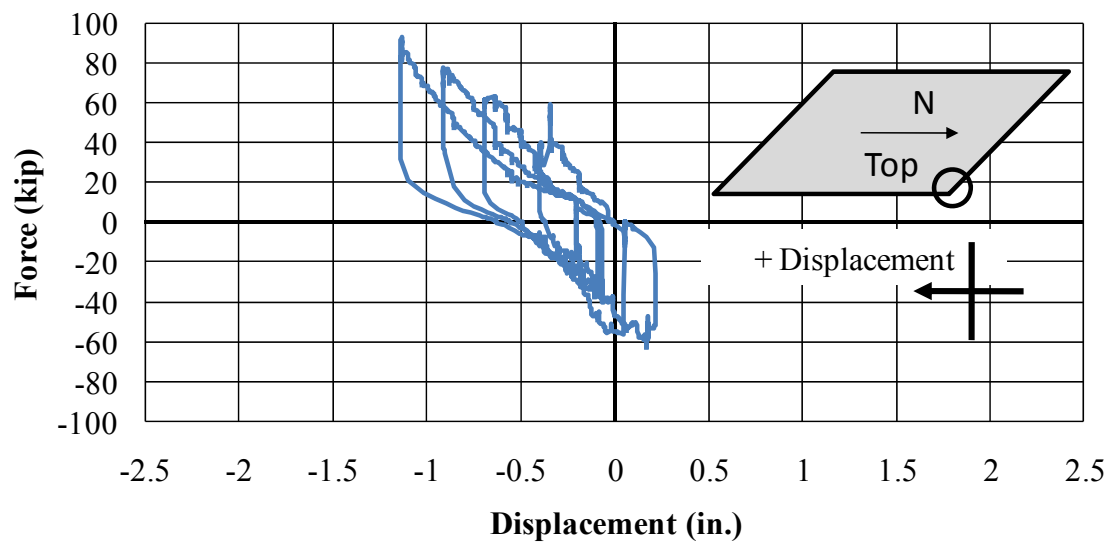
Figure 4.55: Longitudinal Load-Displacement Response – NE, Top
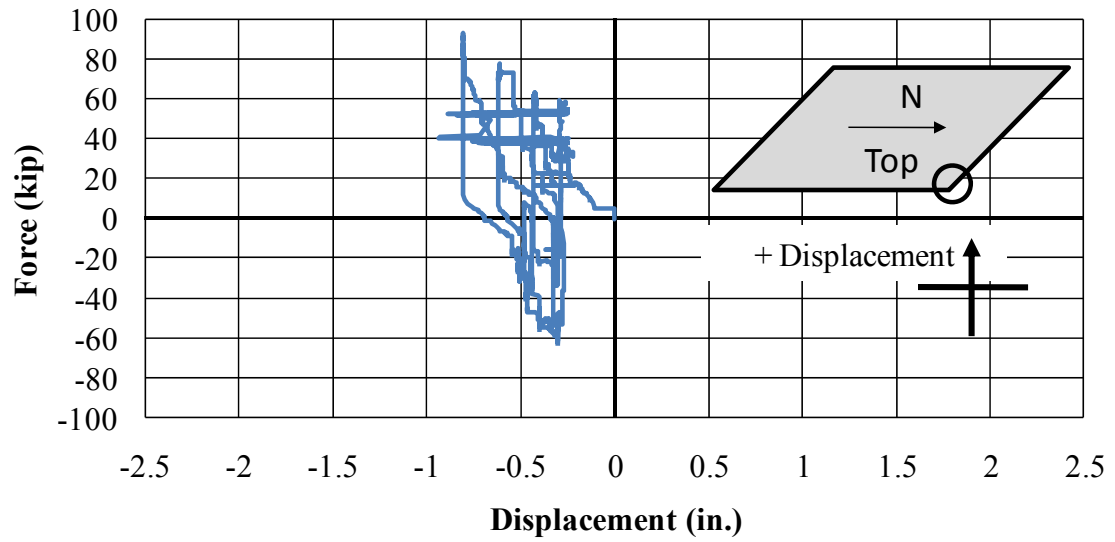
Figure 4.56: Lateral Load-Displacement Response – NE, Top
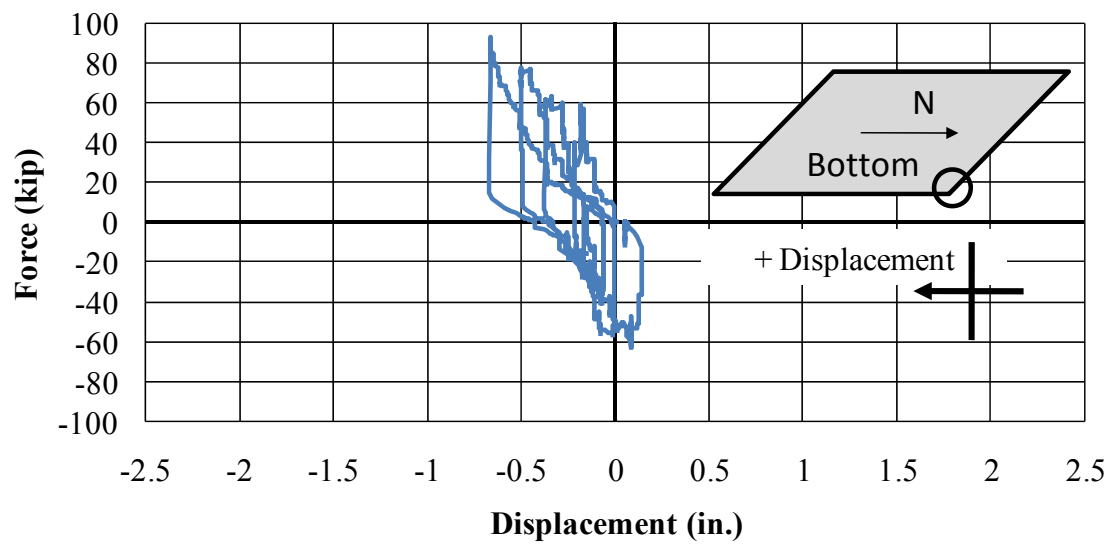
Figure 4.57: Longitudinal Load-Displacement Response – NE, Bottom
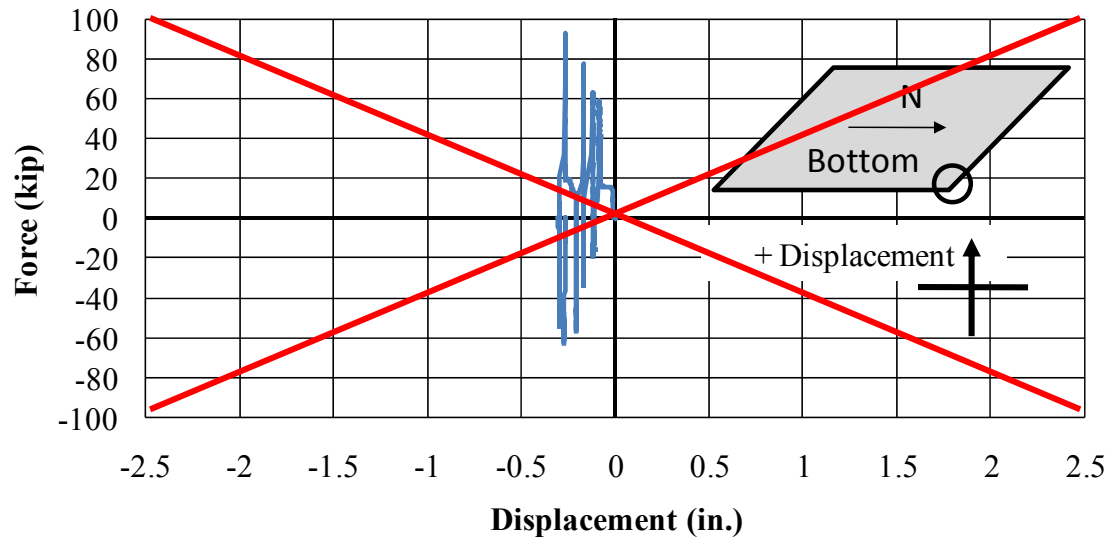
Figure 4.58: Lateral Load-Displacement Response – NE, Bottom
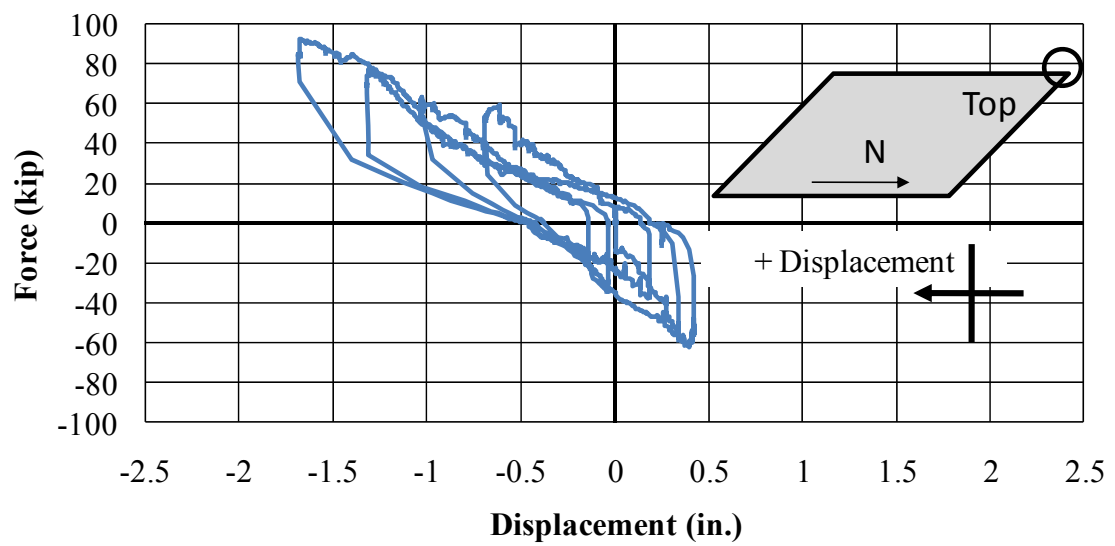
Figure 4.59: Longitudinal Load-Displacement Response – NW, Top
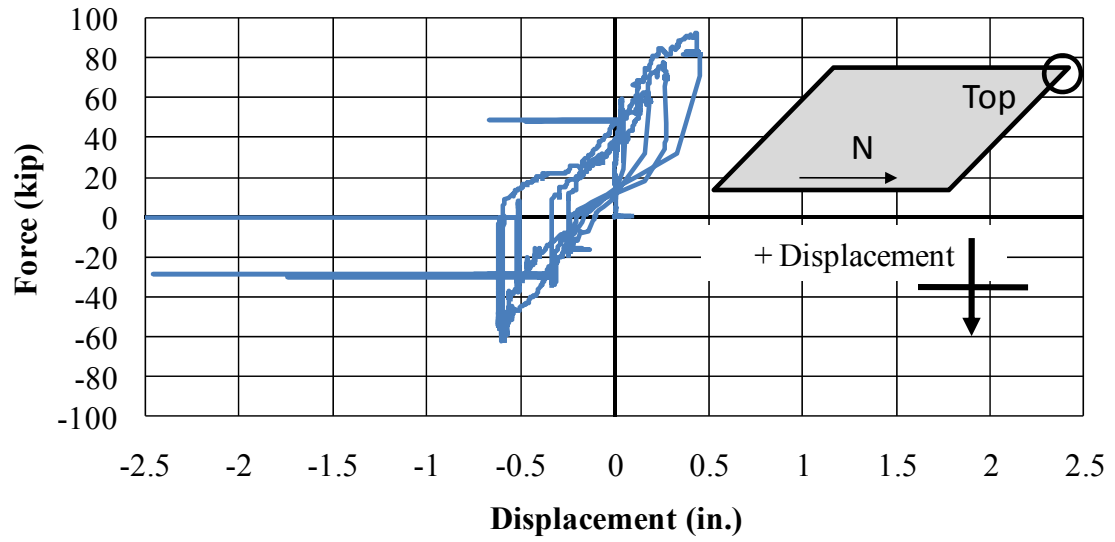
Figure 4.60: Lateral Load-Displacement Response – NW, Top
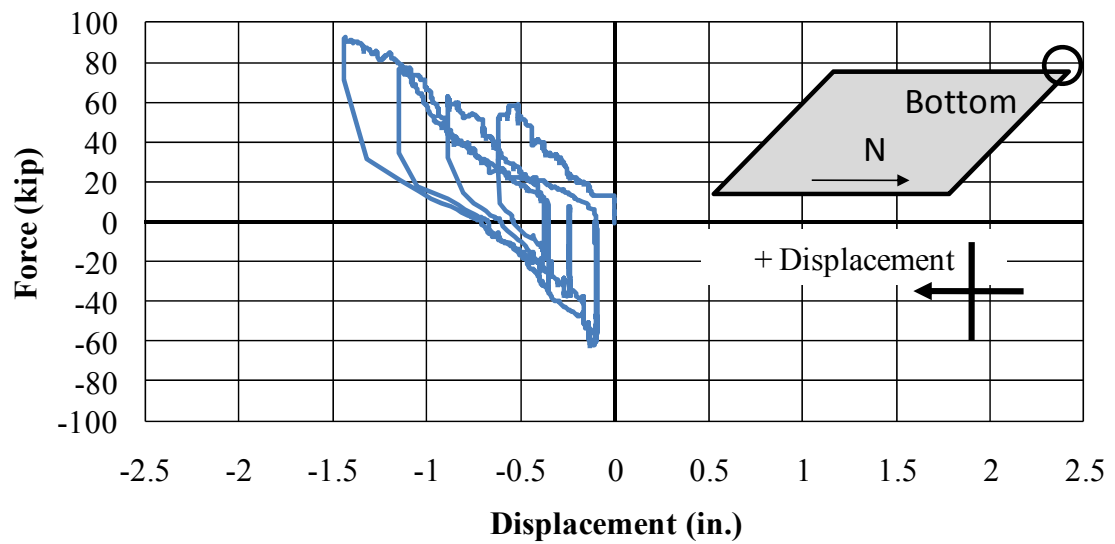
Figure 4.61: Longitudinal Load-Displacement Response – NW, Bottom
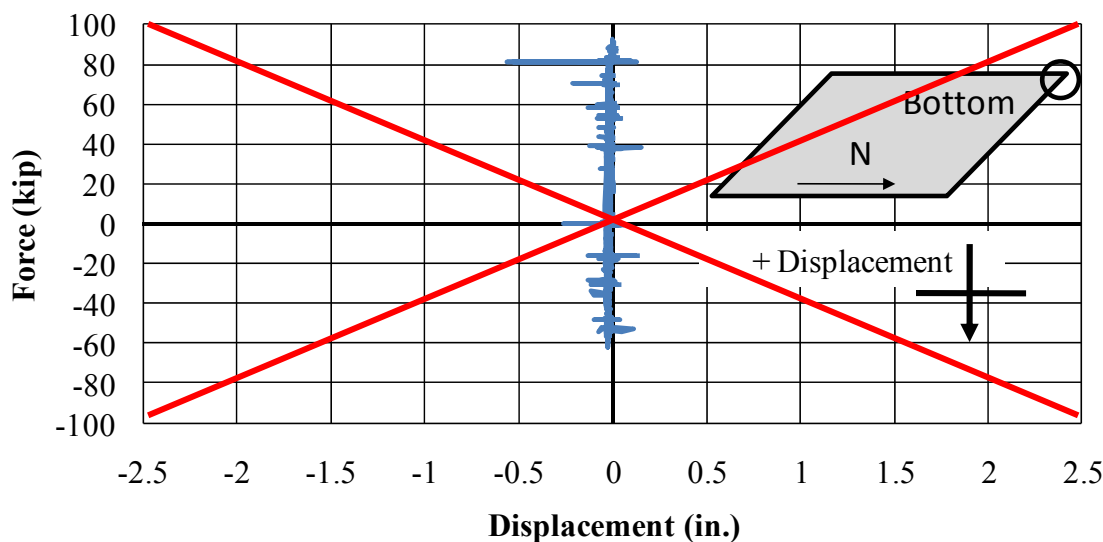
Figure 4.62: Lateral Load-Displacement Response – NW, Bottom

4.6.2. PILE DISPLACEMENT

During the testing program, lateral deflections were monitored for each pile using a down-hole array. For each target displacement, a relative deflected shape was recorded for each pile using the respective original position. For future reference, Figure 4.63 shows the identification scheme used during testing. Figure 4.64 through Figure 4.83 show the recorded lateral displacements for the ten piles in the quarter-scale integral abutment bridge. Longitudinal movement is in the direction of the length of the structure, and lateral movement is in the direction of the width of the structure. For the various deflected shapes shown, the curve label is denoted by a letter followed by a number. The letter is either E for expansion or C for contraction. The number designates the top displacement in tenths of an inch: 05 = 0.5 in., 10 = 1.0 in., 15 = 1.5 in., and 20 = 2.0 in.
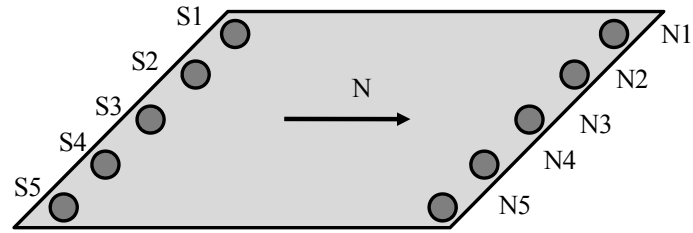
Figure 4.63: Identification Scheme for Scale-Model Piles
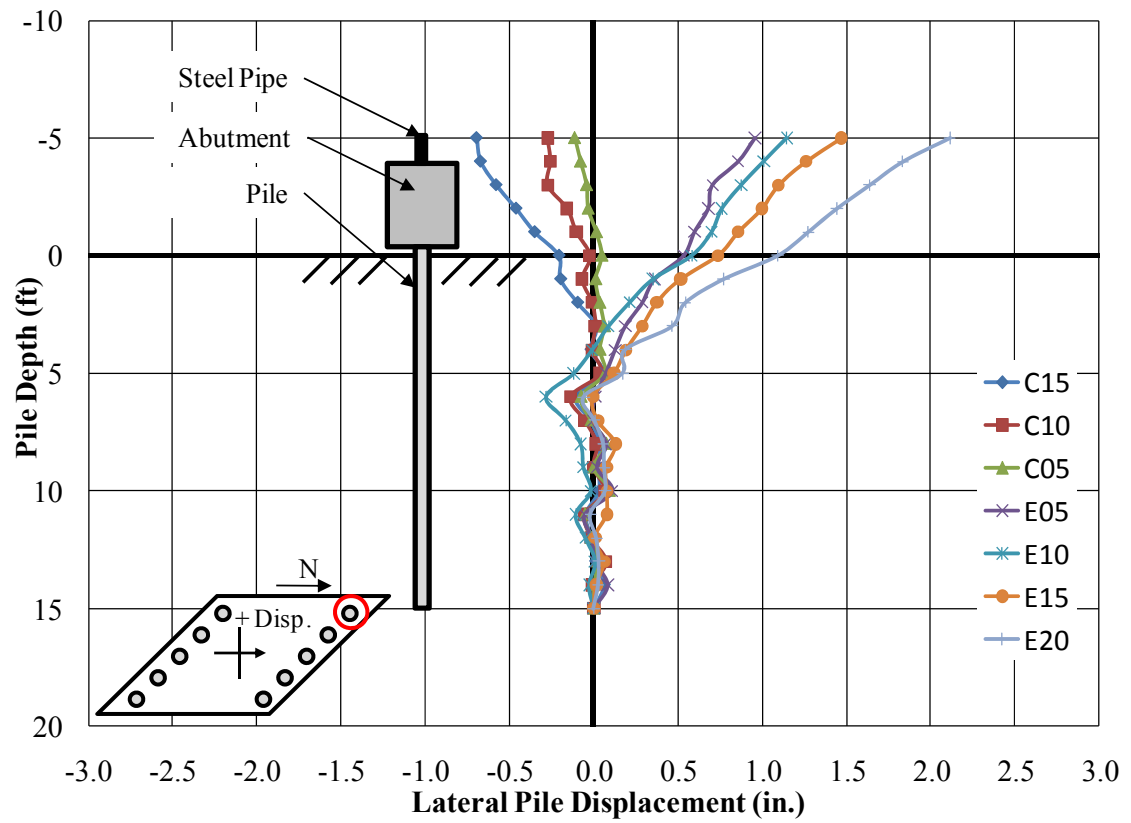
Figure 4.64: Longitudinal Movement of Pile N1
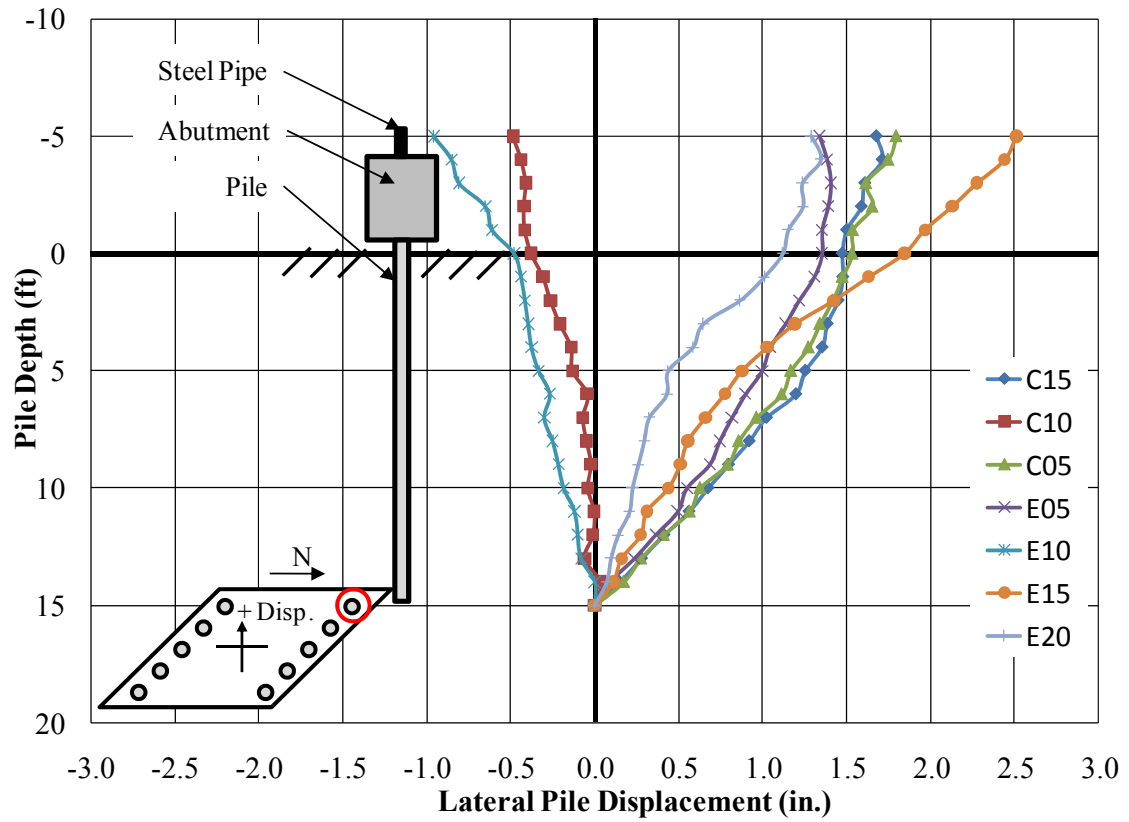
Figure 4.65: Lateral Movement of Pile N1
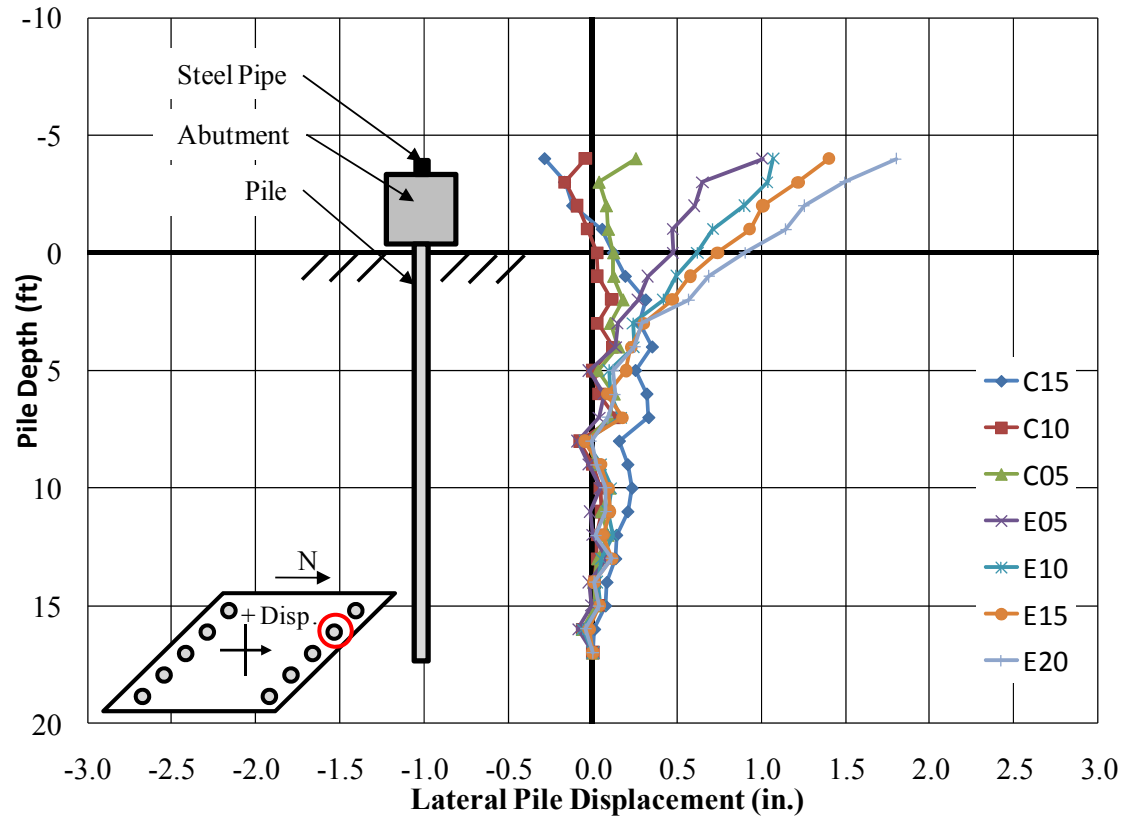
Figure 4.66: Longitudinal Movement of Pile N2
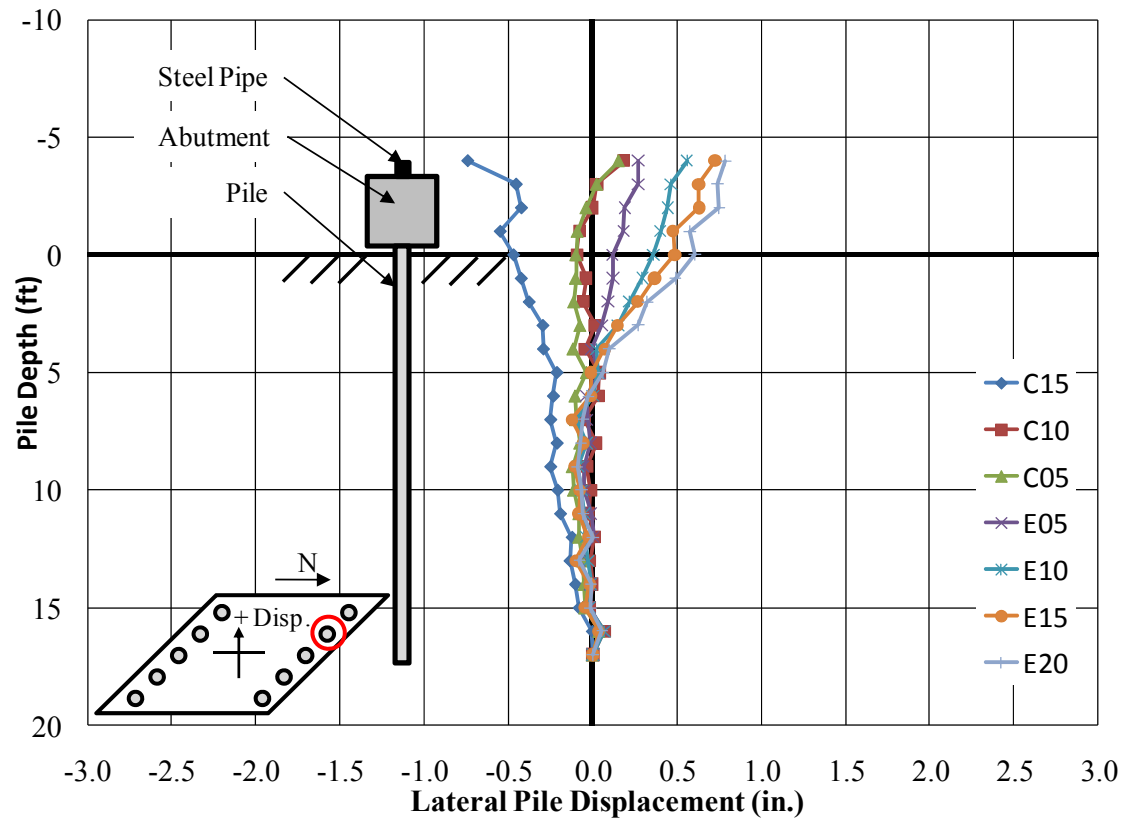
Figure 4.67: Lateral Movement of Pile N2
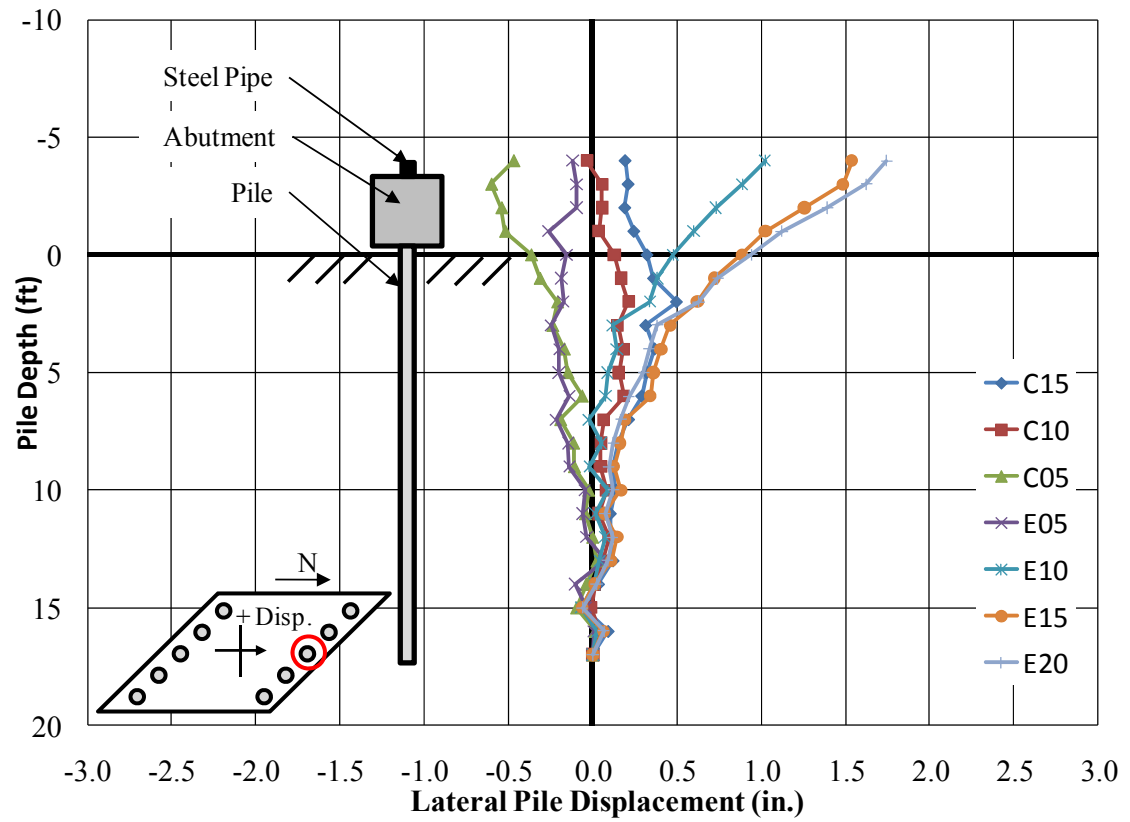
Figure 4.68: Longitudinal Movement of Pile N3
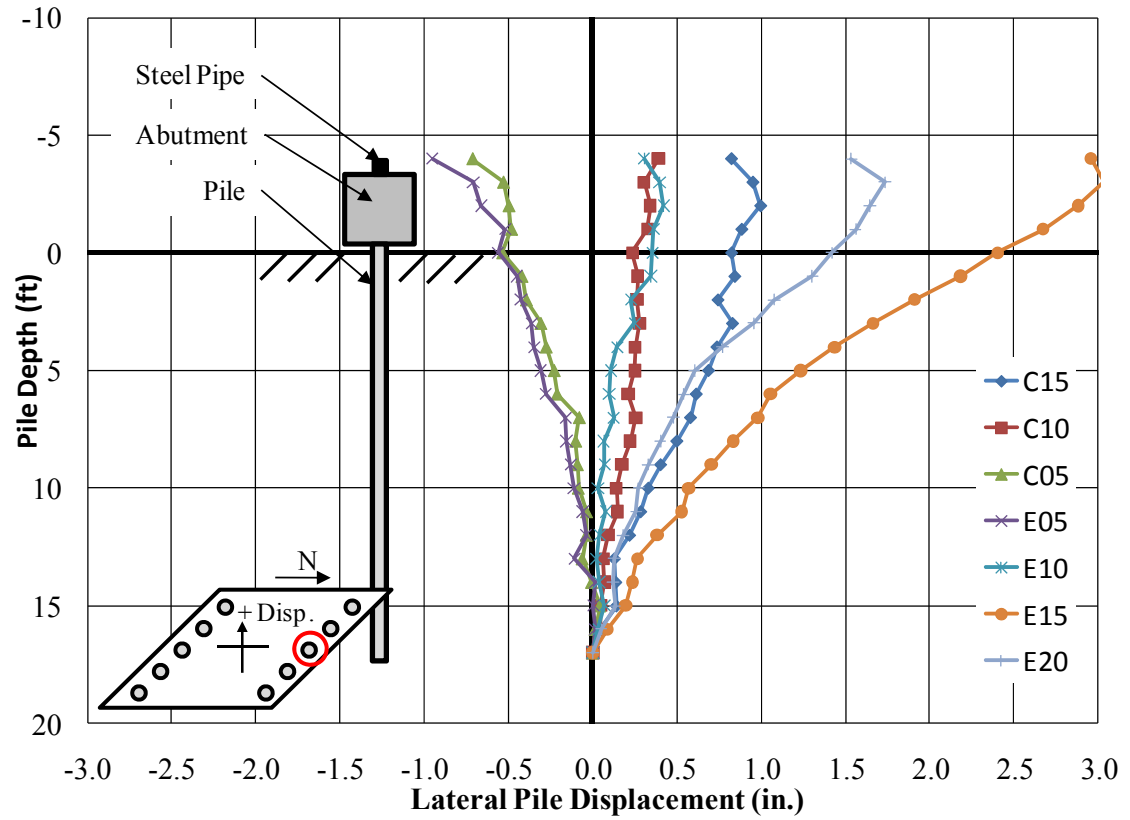
Figure 4.69: Lateral Movement of Pile N3
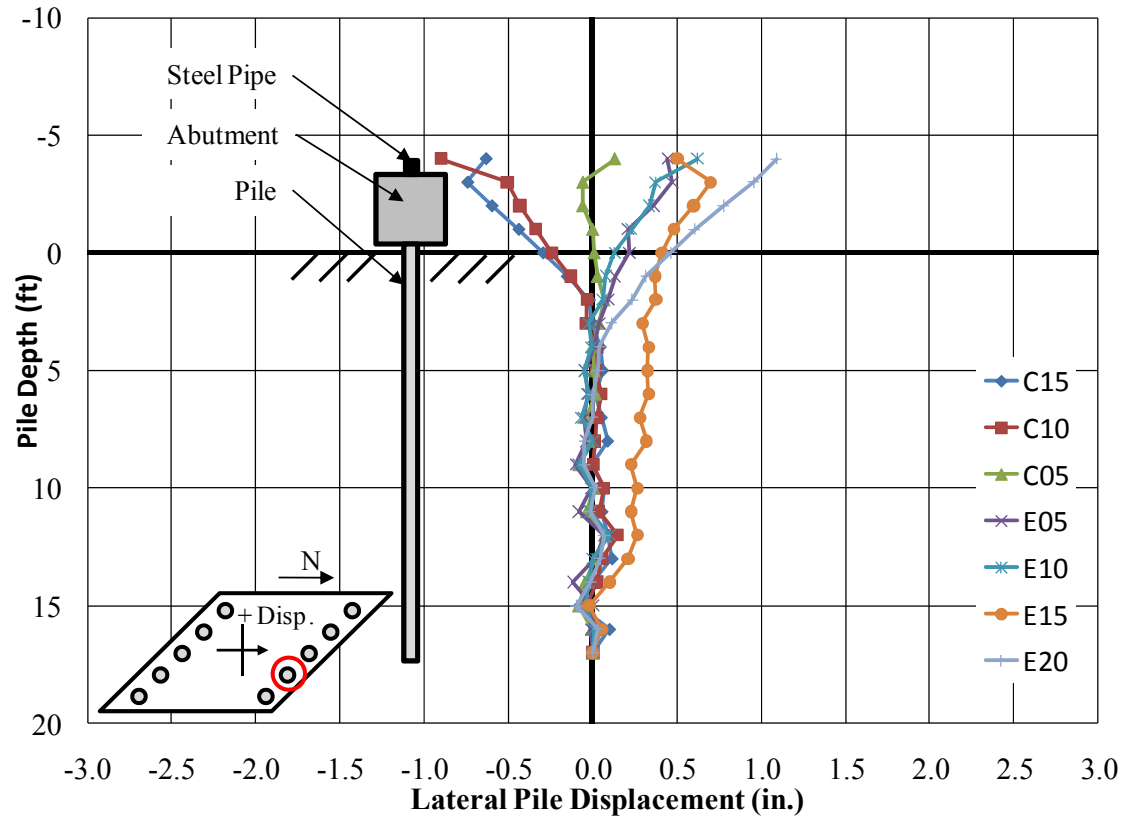
Figure 4.70: Longitudinal Movement of Pile N4
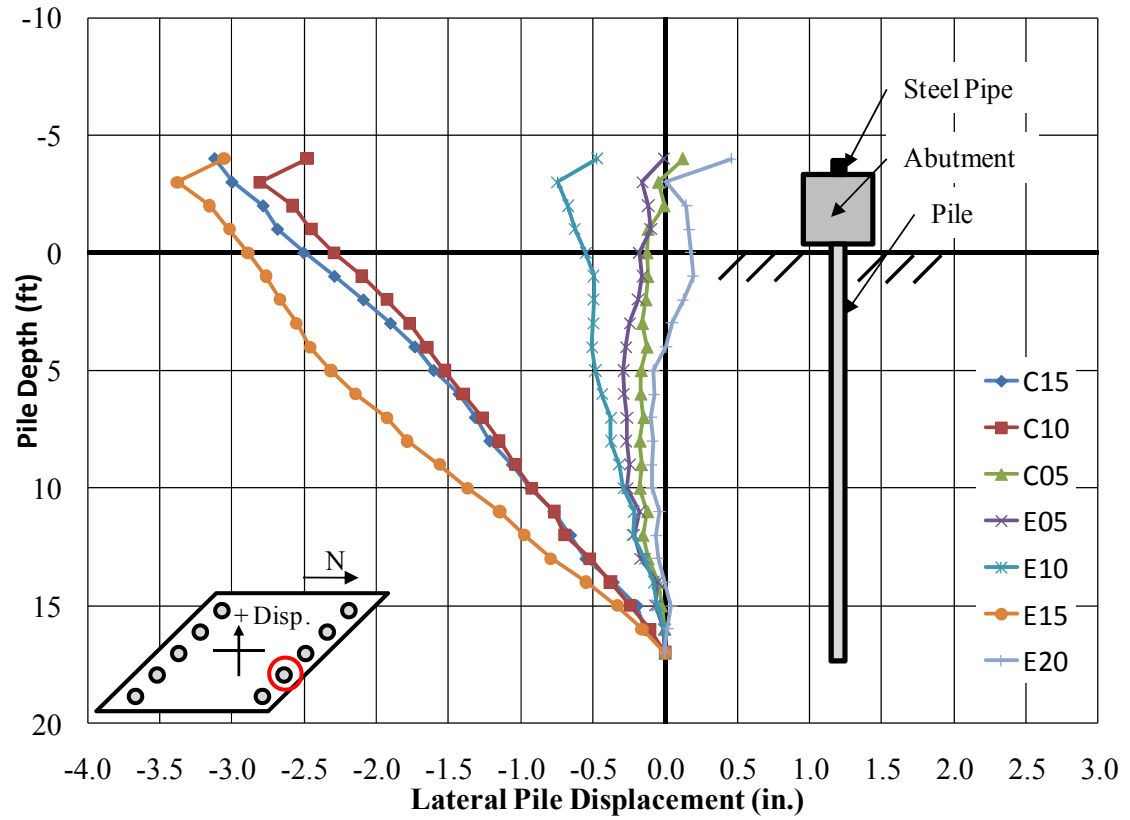
Figure 4.71: Lateral Movement of Pile N4
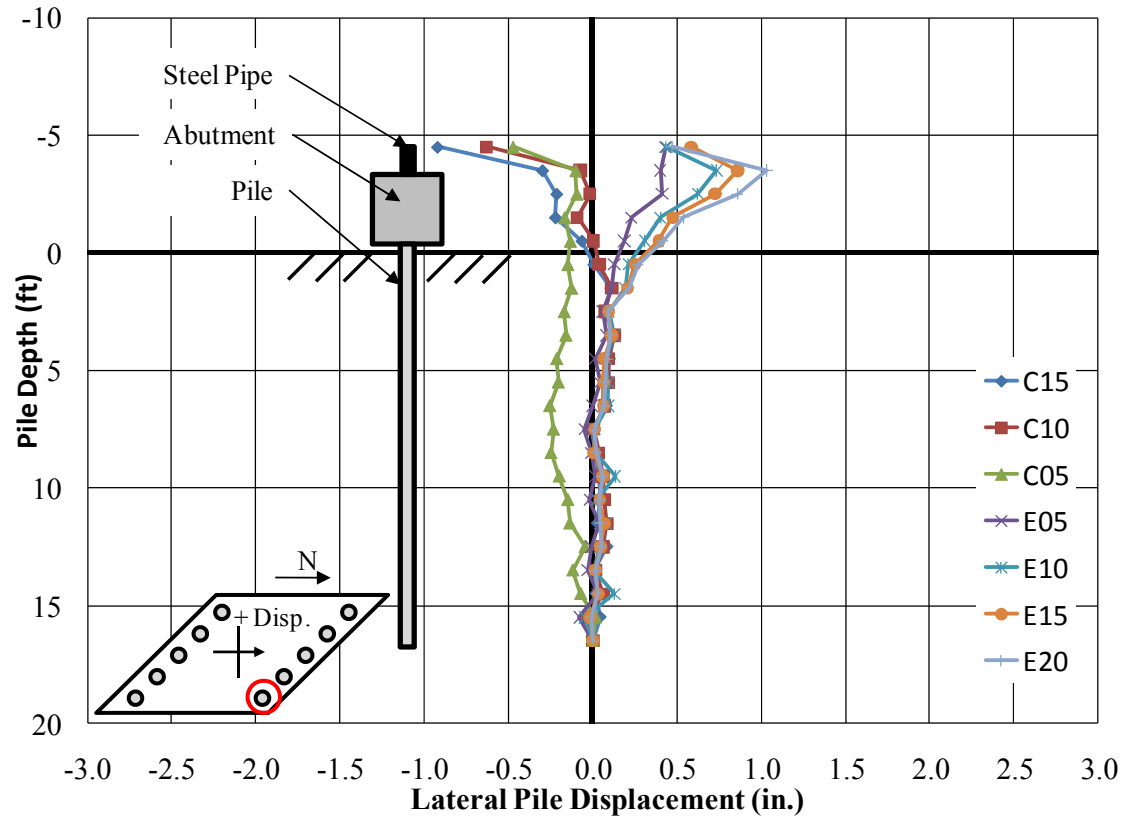
Figure 4.72: Longitudinal Movement of Pile N5
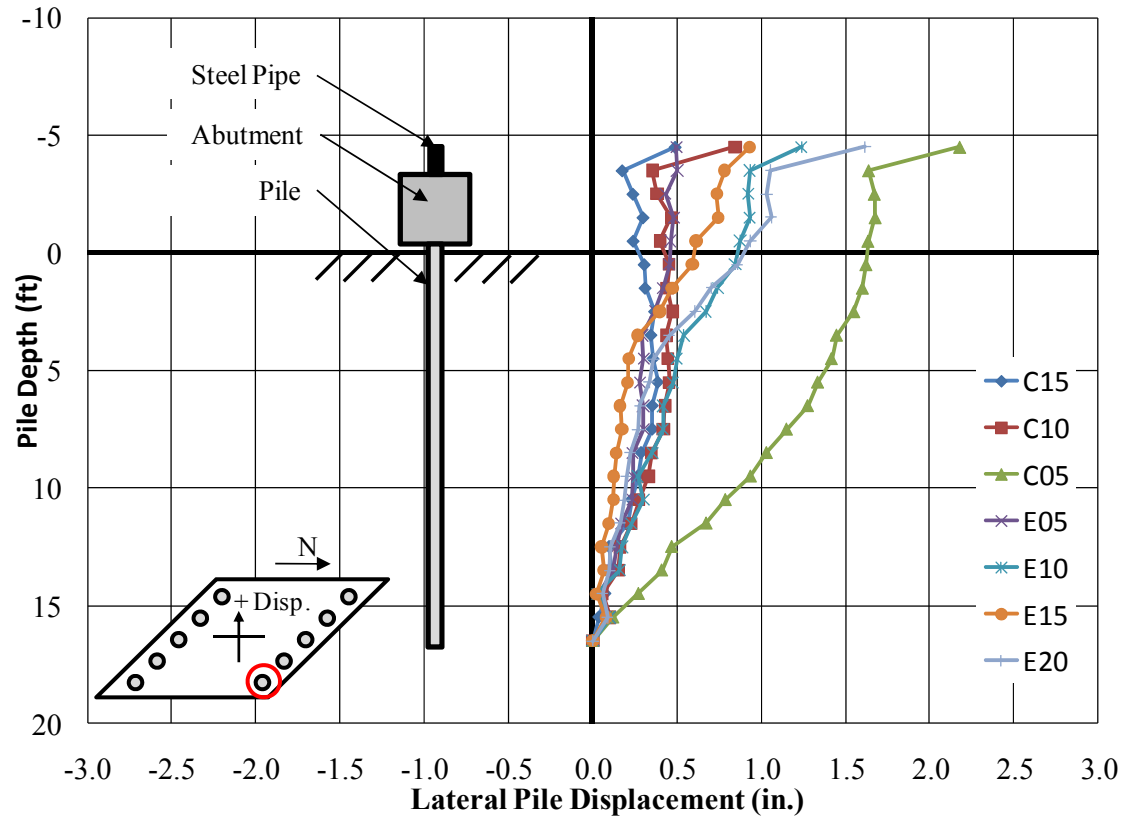
Figure 4.73: Lateral Movement of Pile N5
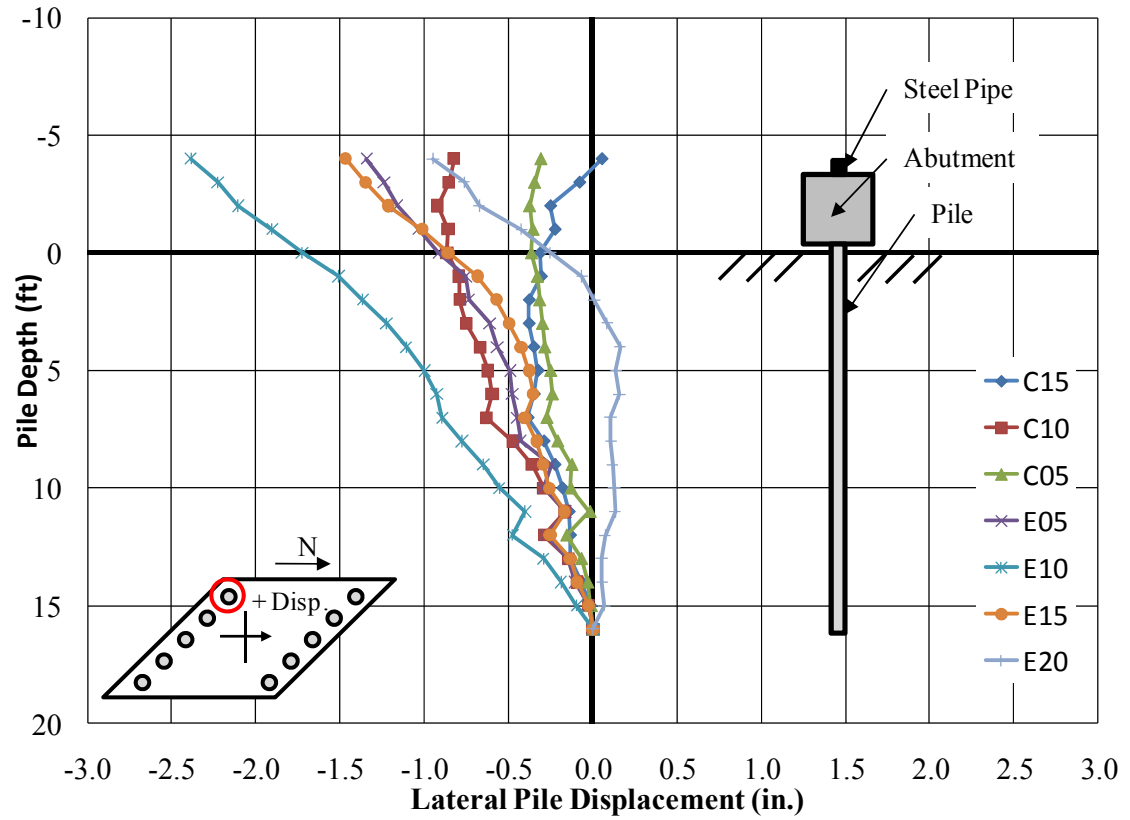
Figure 4.74: Longitudinal Movement of Pile S1
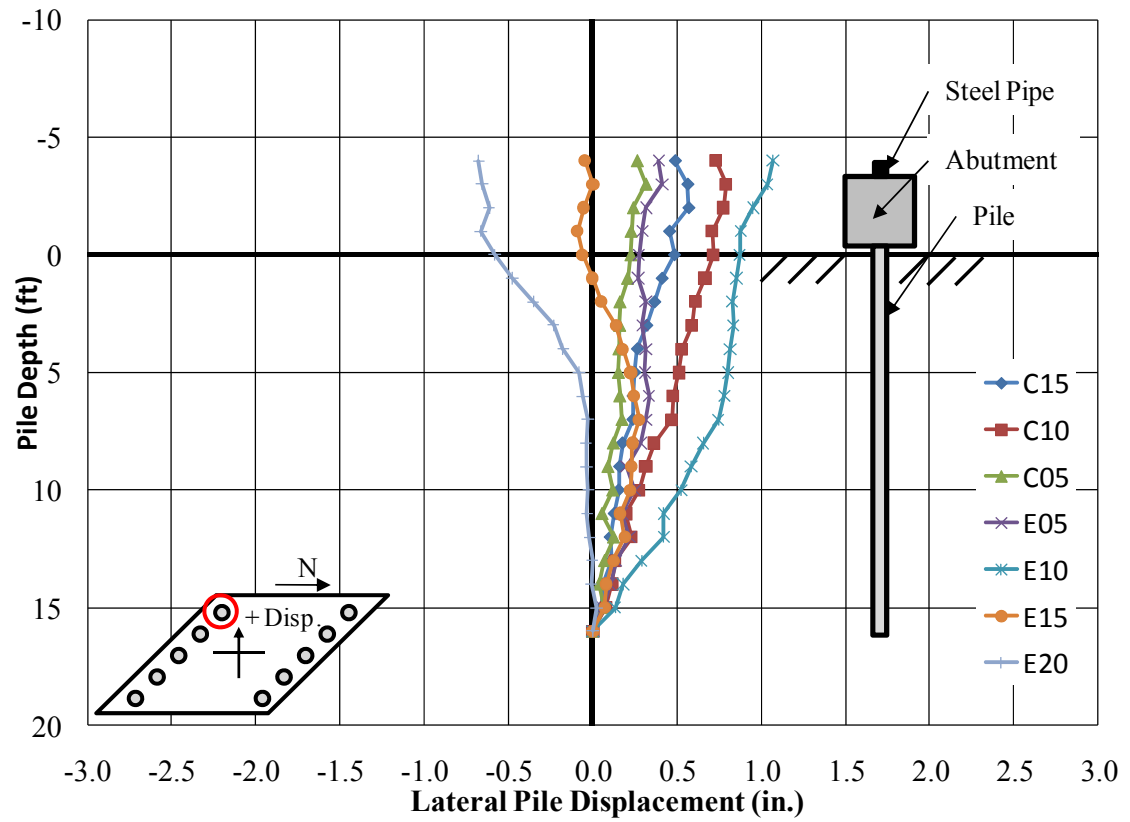
Figure 4.75: Lateral Movement of Pile S1
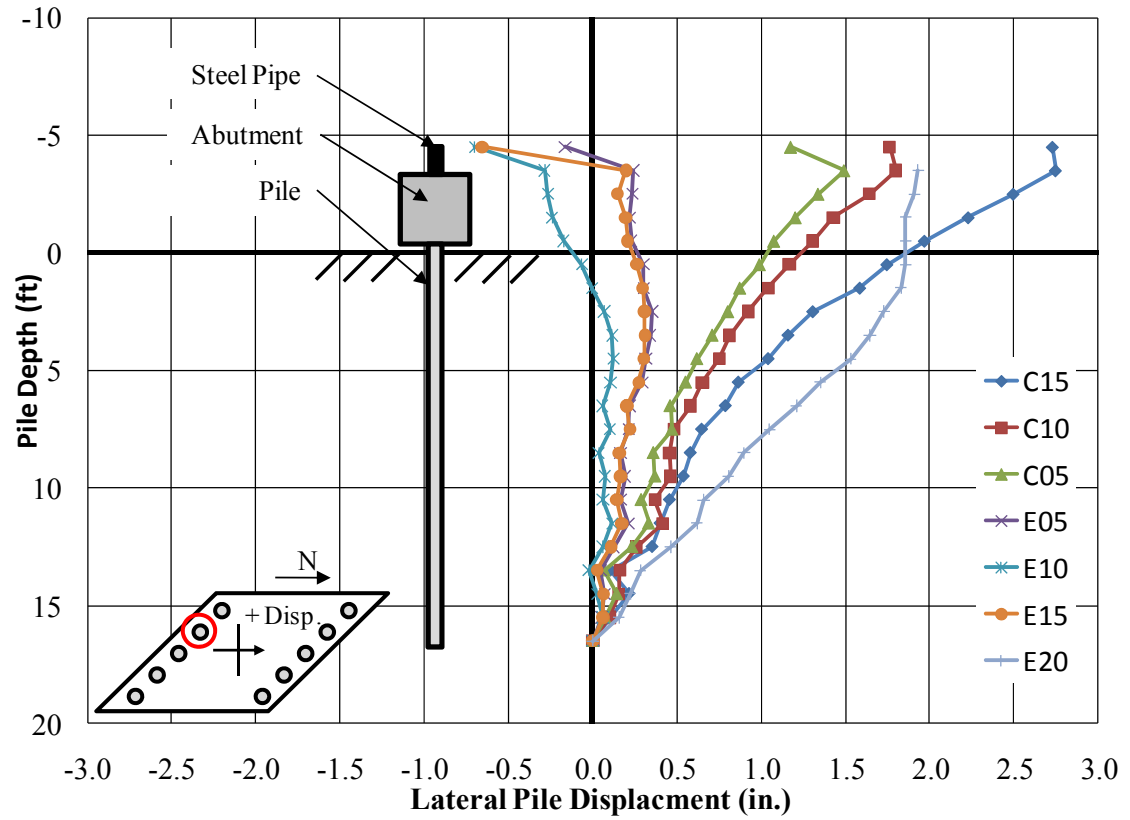
Figure 4.76: Longitudinal Movement of Pile S2
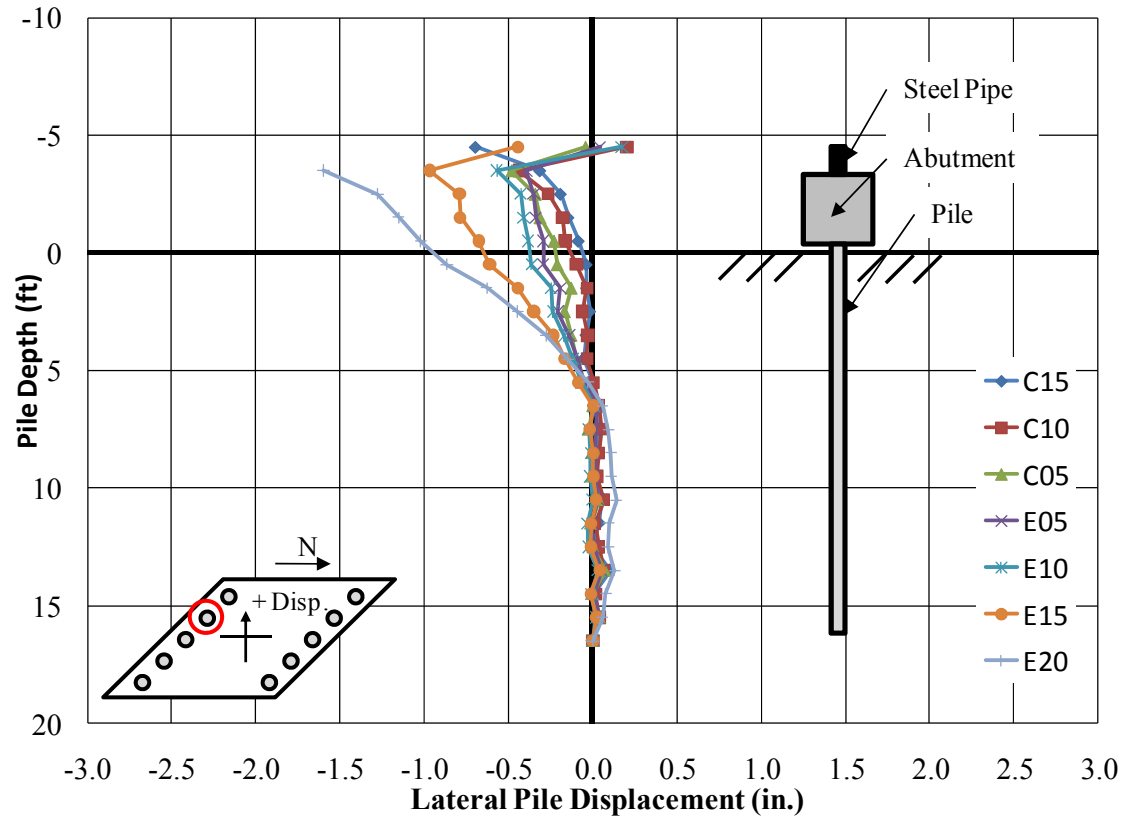
Figure 4.77: Lateral Movement of Pile S2
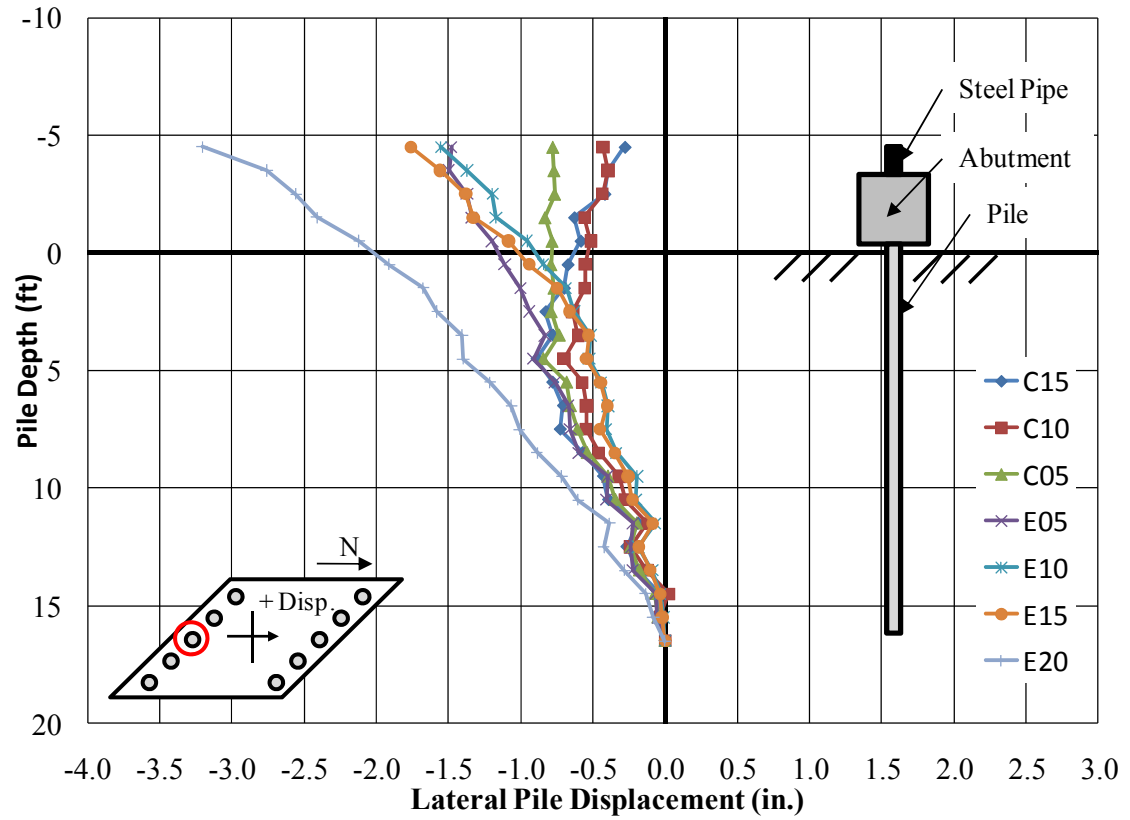
Figure 4.78: Longitudinal Movement of Pile S3
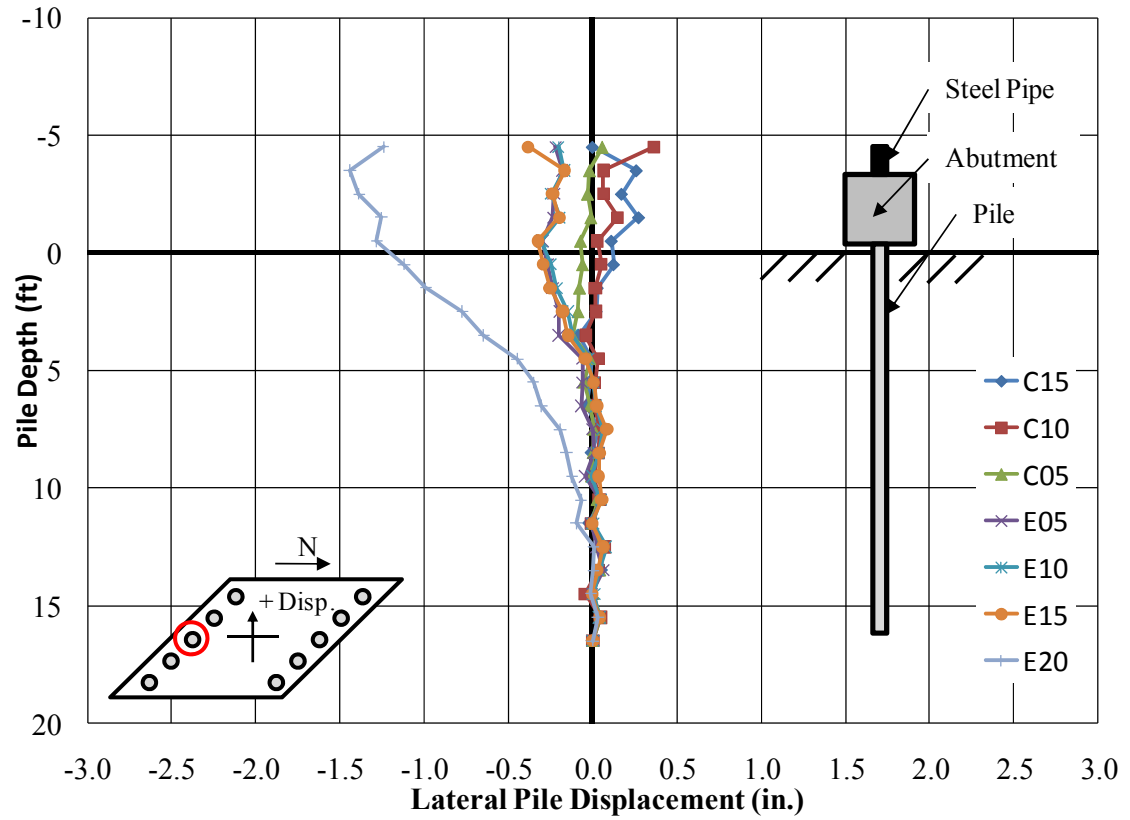
Figure 4.79: Lateral Movement of Pile S3
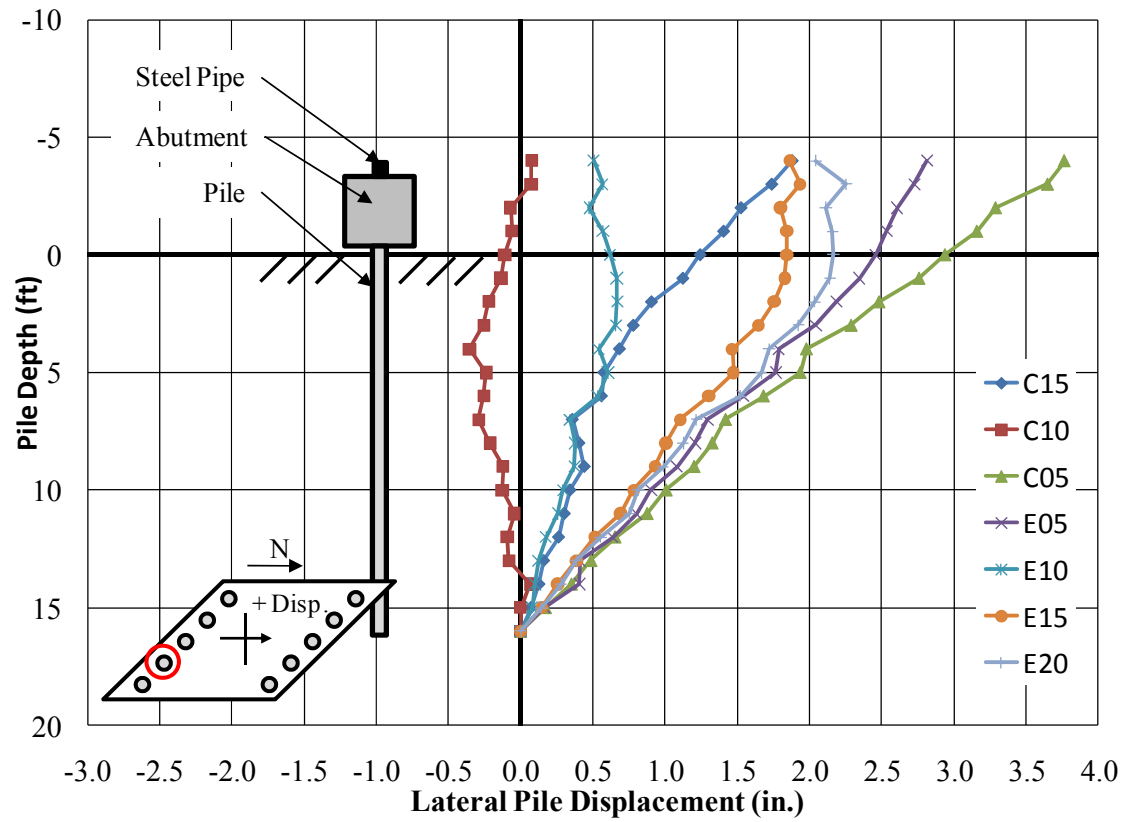
Figure 4.80: Longitudinal Movement of Pile S4
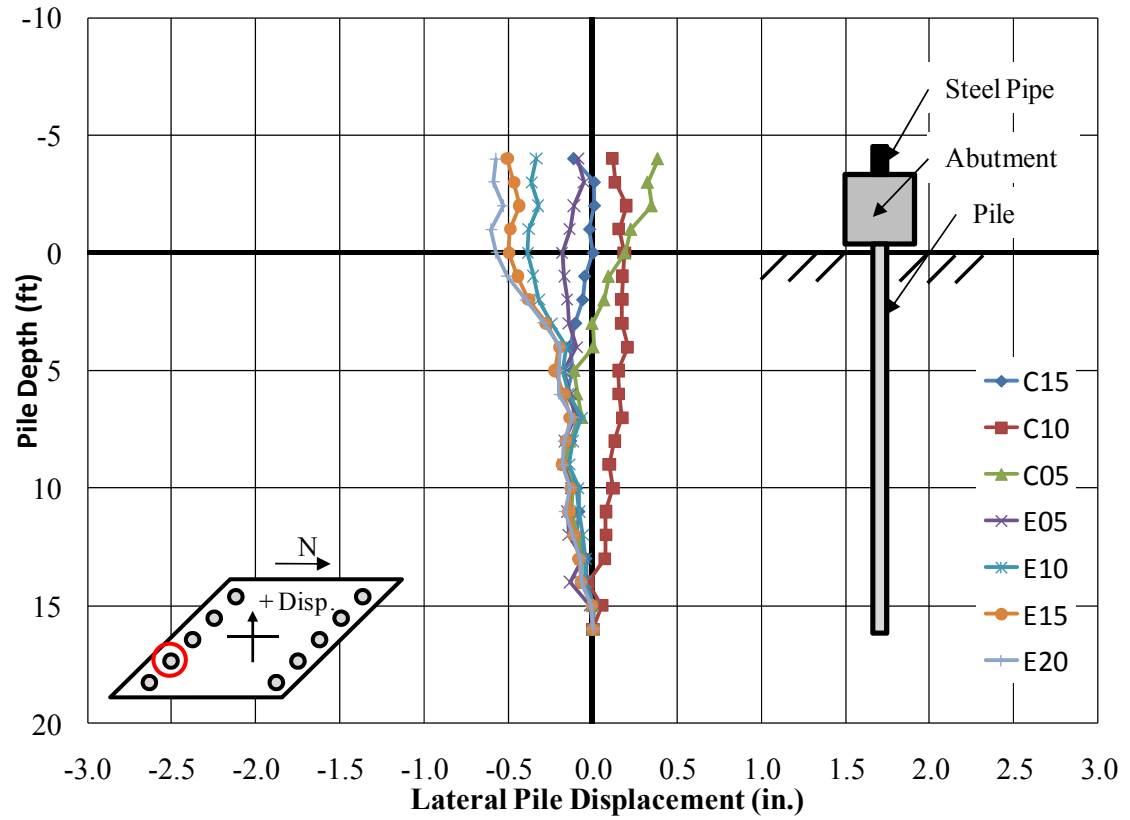
Figure 4.81: Lateral Movement of Pile S4
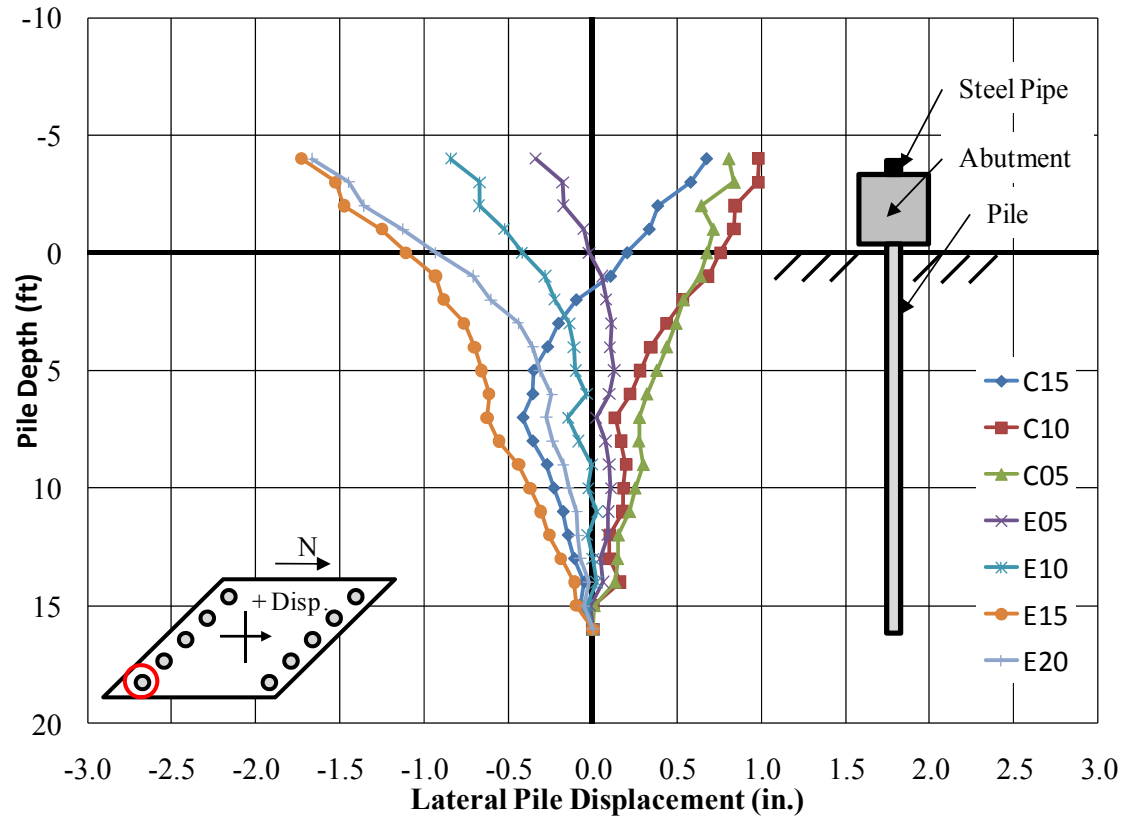
Figure 4.82: Longitudinal Movement of Pile S5
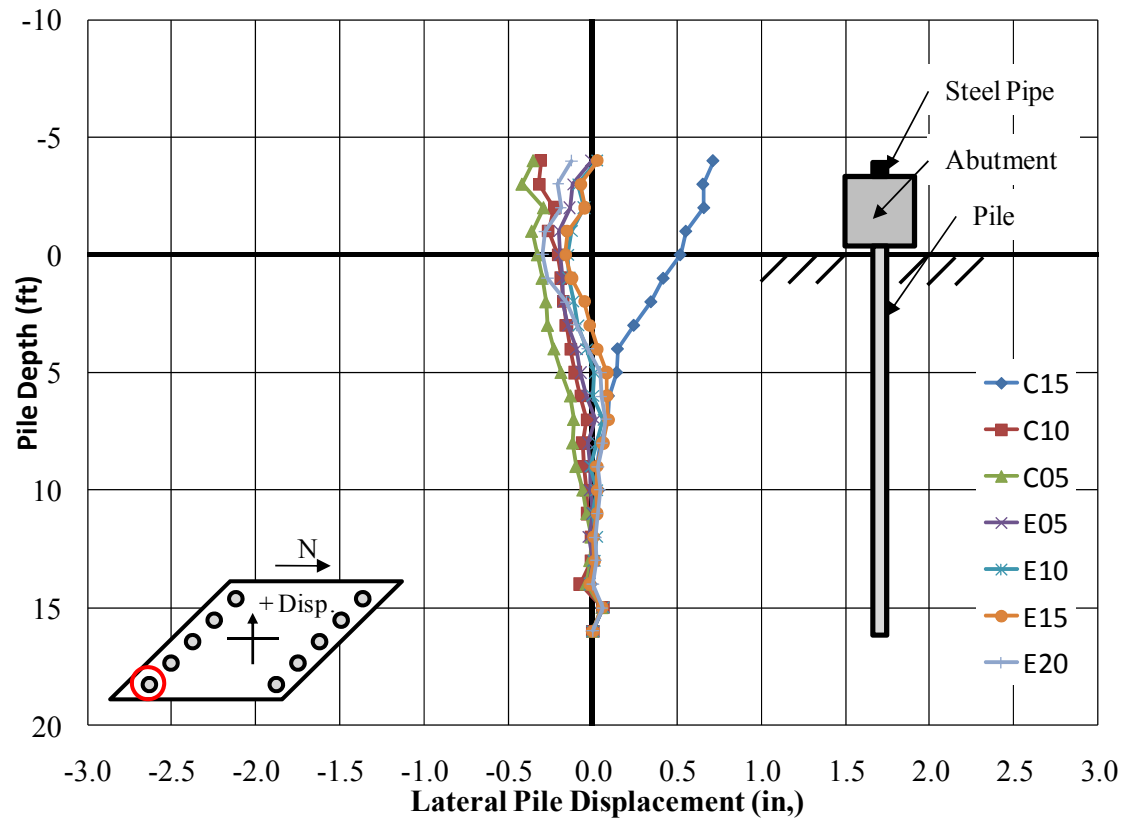
Figure 4.83: Lateral Movement of Pile S5

4.7. EVALUATION OF RESULTS

Based on the experimental results, the behavior corresponding to the displacements of the abutment and piles are discussed. Discussion is also included on the influence of skew on integral abutment bridges.

4.7.1. ABUTMENT MOVEMENT

Upon inspecting the deflection of the two abutments, it is first apparent that a non-linearity occurred for all displacement records early in the testing program. This non-linearity caused the data to be shifted for the duration of the test (Figure 4.84). It is unknown why this shift occurred; however, there are several possible causes for the shift. It is possible that a slip occurred in the gap gages with the connecting string of the string pot. It is also possible that a phenomenon of the transfer beams and/or the skew of the piles caused a movement into an equilibrium position at the beginning of the test. What is known about the shift of the data is that

it occurred only at the beginning of the test. This is shown by plotting the gap deflection versus the various abutment displacements. As an example, the two longitudinal gages at the top of the north abutment are plotted versus the gap displacement (Figure 4.85 and Figure 4.86). If the behavior was perfectly linear elastic, the curve would be a straight line. If the behavior involved some nonlinear movement, the curve would produce a hysteretic loop. However, what is seen is that a shift occurs at the beginning of the test that is not recovered. The remainder of the test shows slight hysteretic behavior. In addition, when a gap displacement of 0.5 in. was applied in the initial cycle, a displacement of approximately 0.5 in. at the abutment was measured. This is not physically possible as a gap displacement of 0.5 in. can only cause a maximum of 0.5 in total displacement which is accommodated at both sides of the bridge. Therefore, the initial shift at the beginning of the test is assumed to be an error of the test setup and not a phenomenon of the structural behavior. This behavior indicates that slip of the string pot string occurred in the initial loading. It appears that once the slack was taken out, future loading was not affected by additional slip. Because of the slip, the test structure was actually subjected to much larger displacements in its first cycle than that indicated by the gap gages.
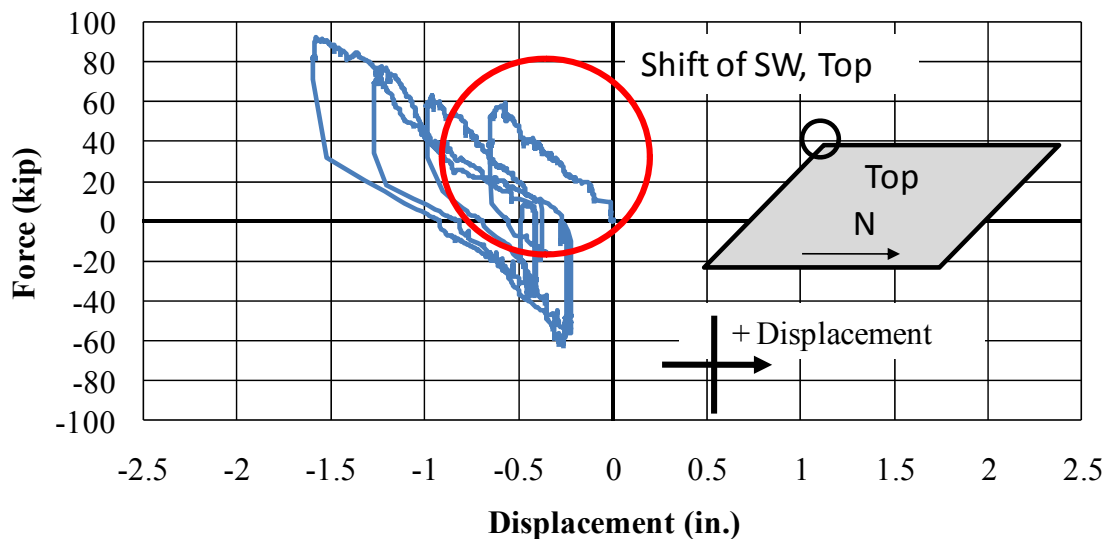
Figure 4.84: Shift in Abutment Displacement Record for SW, Top
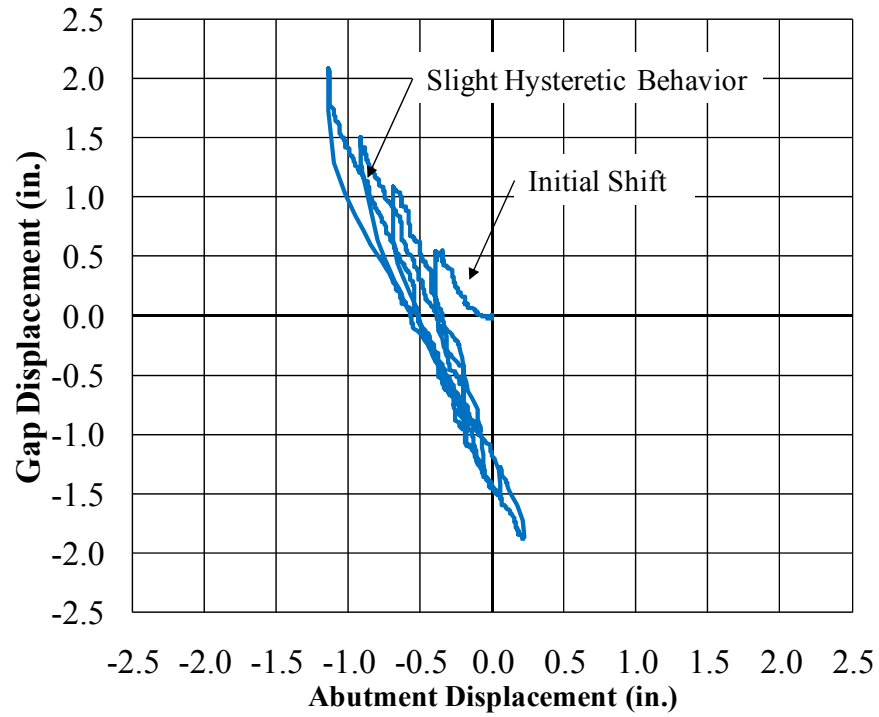
Figure 4.85: Initial Shift of Longitudinal NE, Top
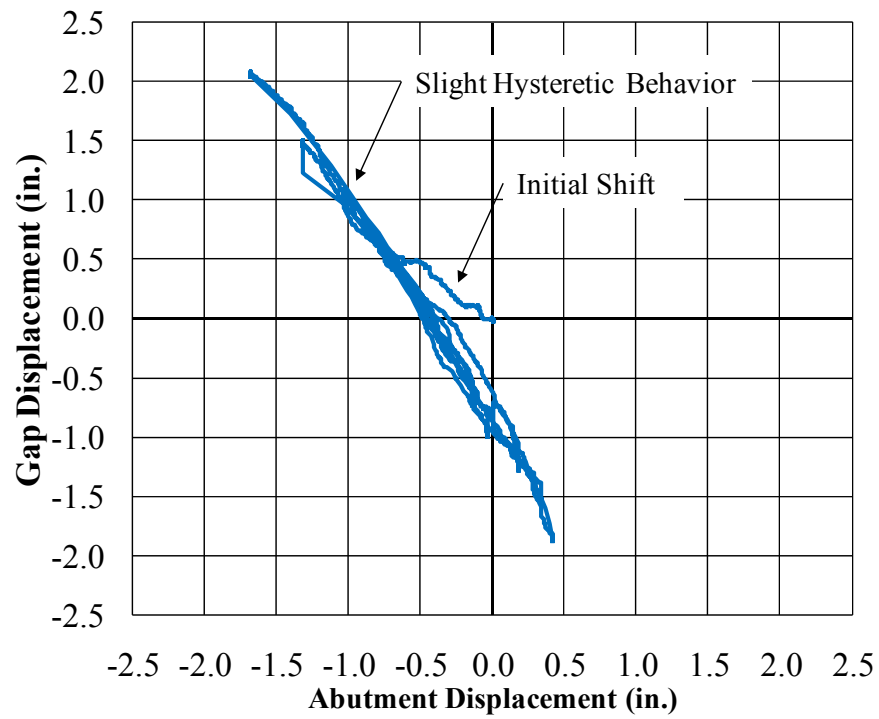
Figure 4.86: Initial Shift of Longitudinal NW, Top

Regarding the movement of the abutments, it can be seen that each half of the structure behaves similar to the other. As with the structures monitored in the field investigation, the acute corners of each abutment displace approximately the same amount. In the same way, the obtuse corners of each abutment move the same. Figure 4.87 through Figure 4.90 show a comparison of longitudinal and lateral displacement for the top displacement gages of respective corners. The envelope of the total movement is shown for each half of the abutment for comparison purposes. As can be seen, the magnitudes and responses are approximately the same for the final cycle which removes the initial offset. The south abutment deflected more for each gage, but only slightly. This is likely due to variations in soil conditions at both ends of the bridge. Due to the similarity of behavior, only the south abutment will be used for further analysis, and all corresponding conclusions will apply to both halves of the structure.
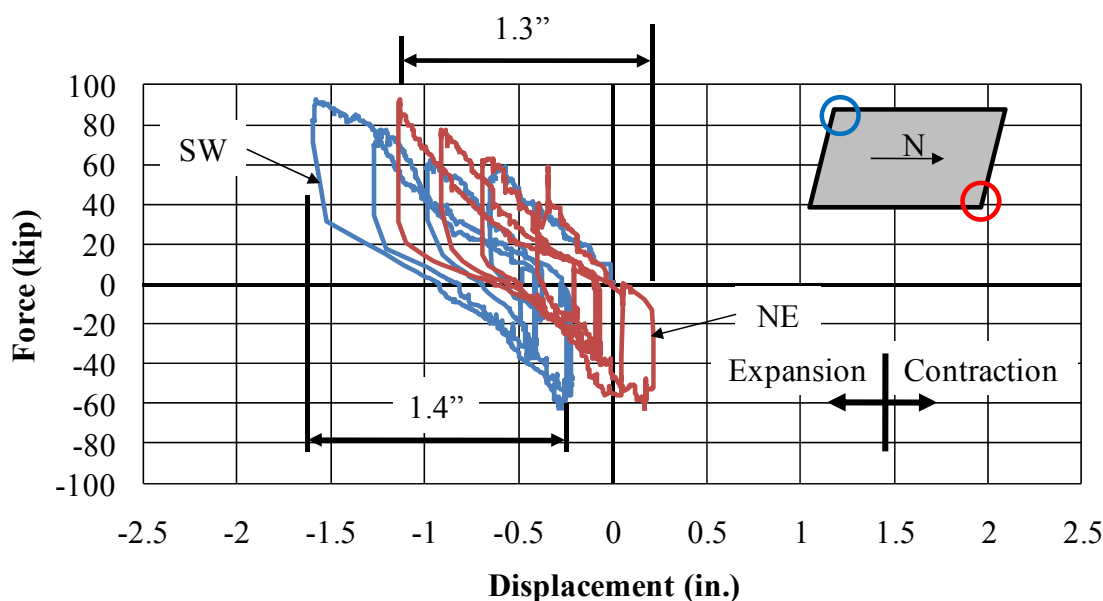
Figure 4.87: Similar Longitudinal Movement of Top Obtuse Corners
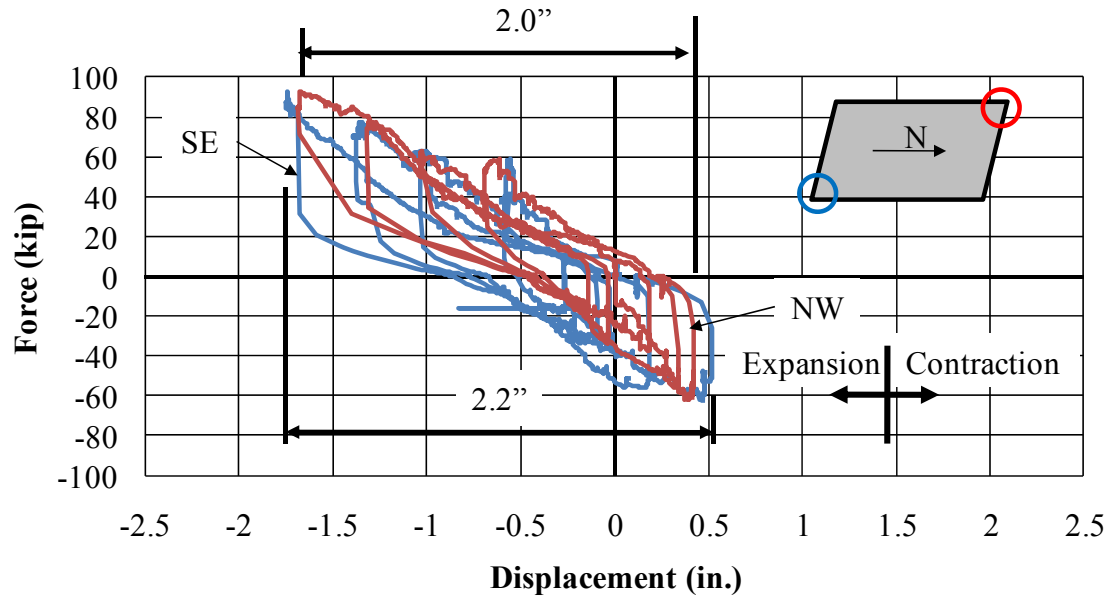
Figure 4.88: Similar Longitudinal Movements of Top Acute Corners
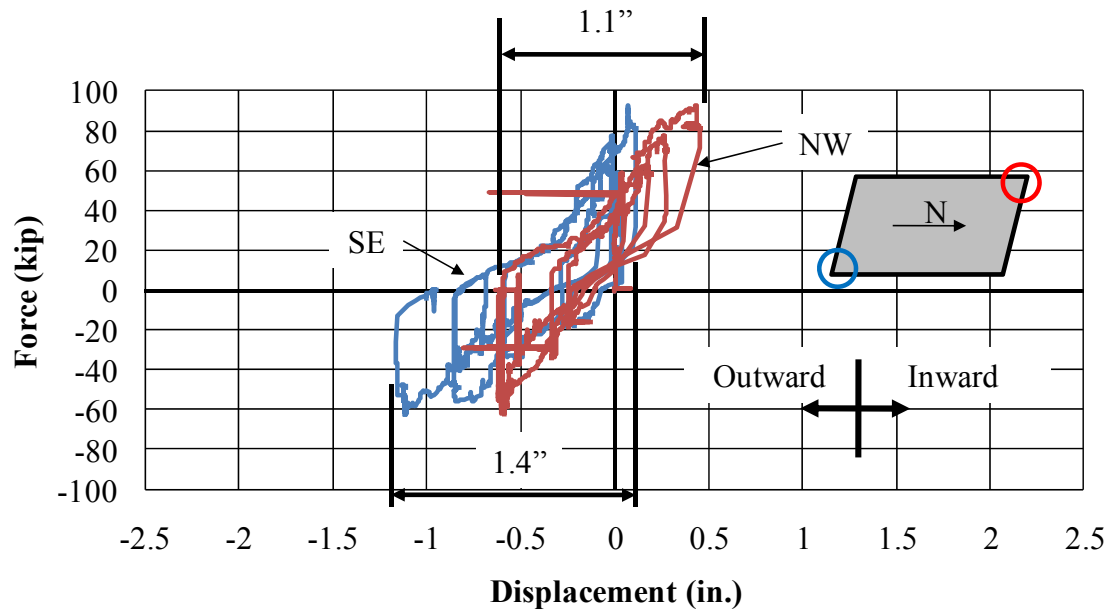
Figure 4.89: Similar Lateral Movements of Top Acute Corners
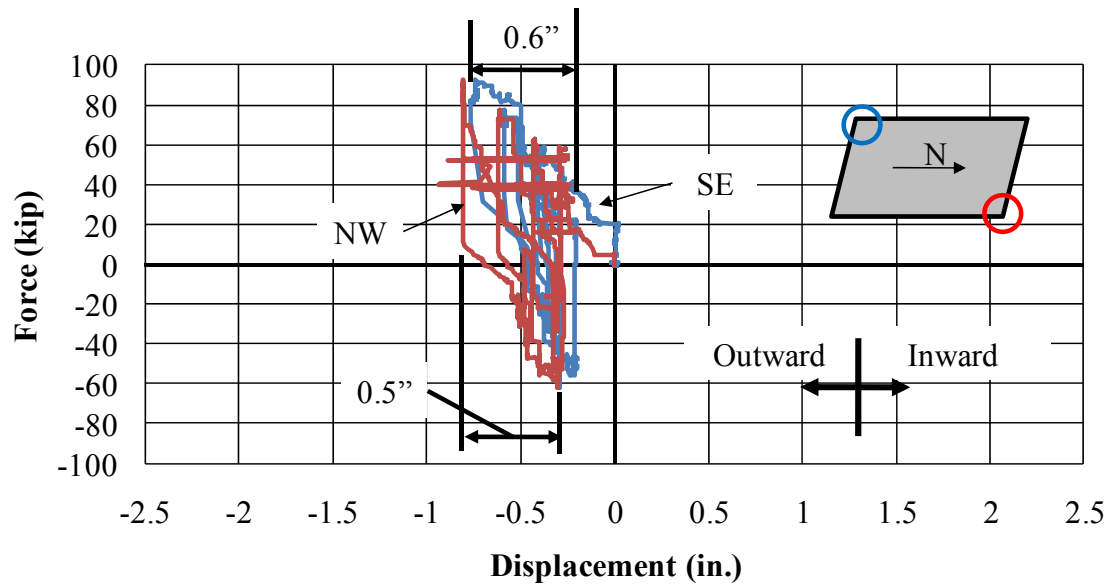
Figure 4.90: Similar Lateral Movements of Top Obtuse Corners

The general behavior of each abutment can also be inferred from the previous figures (Figure 4.87 - Figure 4.90). It is clear that the acute corner deflects significantly more than the obtuse corner for the entire spectrum of loading. This behavior matches that of the behavior of US-231 in the field investigation. Because of this deflection differential, the abutment is rotating in addition to translating (Figure 4.91). Therefore, the greatest lateral displacement demand will occur for the pile at the acute corners.
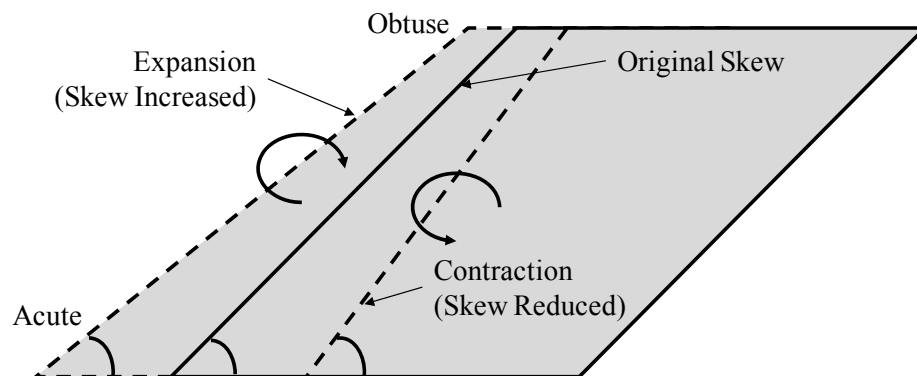
Figure 4.91: Rotation of Skewed Abutment for Expansion and Contraction

In addition to rotating in plan view, the abutment also rotates (tilts) over its height as shown over the duration of the test in Figure 4.92. For periods of expansion, the rotation was at a maximum. During phases of contraction, the rotation of the abutment reduced to nearly zero. The contraction phase shows a rotation of zero because the initial expansion phase, as discussed previously, went too far. It is apparent, due to the fact that the abutment rotates when subjected to lateral displacement, the abutment does not produce a completely fixed condition for the pile head. This is contrary to a common design assumption. However, the rotation is fairly small.
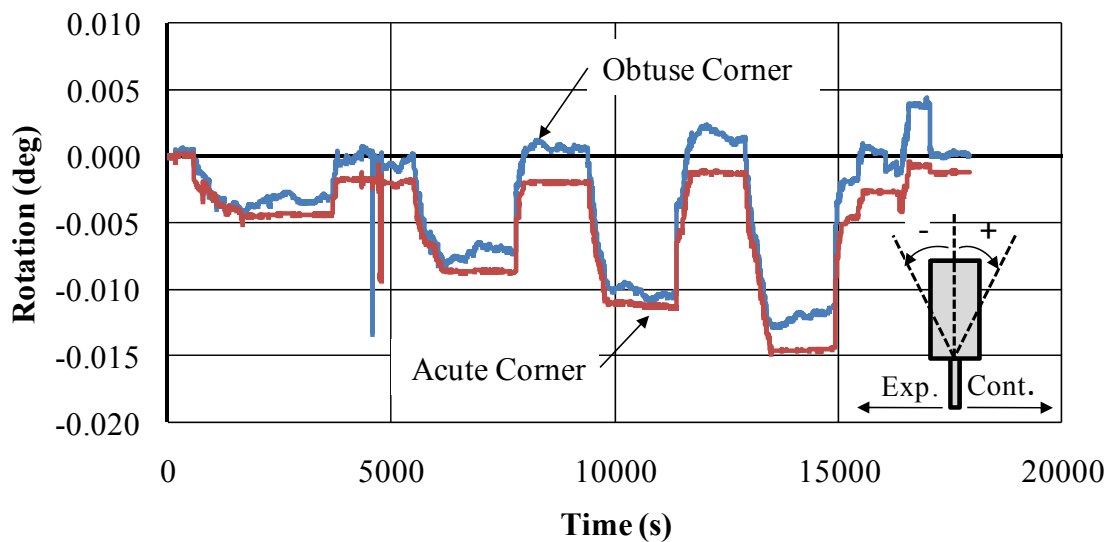
Figure 4.92: Rotation of Abutment

4.7.2. PILE MOVEMENT

The behavior recorded from the quarter-scale integral abutment bridge for the pile deflected shapes is significantly more erratic than that collected from the single lateral pile test. The primary difference in data collection revolved around moving the down-hole array for each reading. Because only one array was used, the array was lowered and raised down each pile of the structure for each consecutive reading, as opposed to remaining in place for the duration of the lateral pile test. Because it is impossible to return the array to it exact original position, errors occurred in the calculation of relative displacements. Some magnitudes of the relative deflected

shapes seem to match that of the displacement gages while others are not close. Two primary behaviors are observed regarding the deflected shapes: a point of fixity occurs approximately 6 ft below the ground surface, and rotation occurs over the height of the abutment. The point of fixity at 6 ft agrees well with the behavior of the single lateral pile test. Although the magnitudes of the deflected shapes may not be accurate, information can be gleaned from the characteristics of the pile deflected shapes.

In many of the deflected shapes (Figure 4.64 through Figure 4.83), there is clear evidence of double curvature in the piles. Even though rotation occurs at the bottom of the abutment, double curvature still occurs in the top 10 ft to 12 ft of the pile. While is it apparent that the pile exhibits double curvature, the standard design assumption of a fixed-fixed case for the piles is not accurate. As can be seen in both the pile deflected shapes (Figure 4.64 through Figure 4.83) and the abutment rotation (Figure 4.92), the abutment does not simply translate, but there is also a component of rotation. Current design methods calculate the demand lateral displacement at the top of the abutment based on thermal expansion as described in Section 1.2. The supporting piles are then designed to accommodate the full displacement demand as a fixed-fixed column. Based on these results, it is observed that current design procedures are conservative.

4.8. ANALYSIS OF RESULTS

To analyze the collected data from the quarter-scale integral abutment bridge, a three-dimensional analytical model was developed following the procedures and guidelines as developed in Chapter 3. It is assumed that if the analytical model can predict the movements of the scaled bridge, the behavior is well understood.

4.8.1. LOADING

To mimic the loading of the experiment, strain values were applied to the girders and deck of the analytical model. Using Equation 4.3, equivalent strains were calculated to represent the demand displacements.

$$\varepsilon = \frac{\Delta L}{L} \tag{4.3}$$

where:

ε = strain, in./in.

L = total length of structure, in.

ΔL = change in length, in. = ±0.5", ±1.0", ±1.5", ±2.0"

4.8.2. RESULTS

To determine the behavior of the analytical model, the displacements of the four corners of each abutment were monitored, similar to that of the experimental test. The displacements at the acute corner of each abutment were the same along with the displacements at each of the obtuse corners. This behavior matches that of the experiment. Figure 4.93 and Figure 4.94 show the calculated movements of the abutments as a function of the demand displacement (gap) for the longitudinal and lateral directions, respectively.
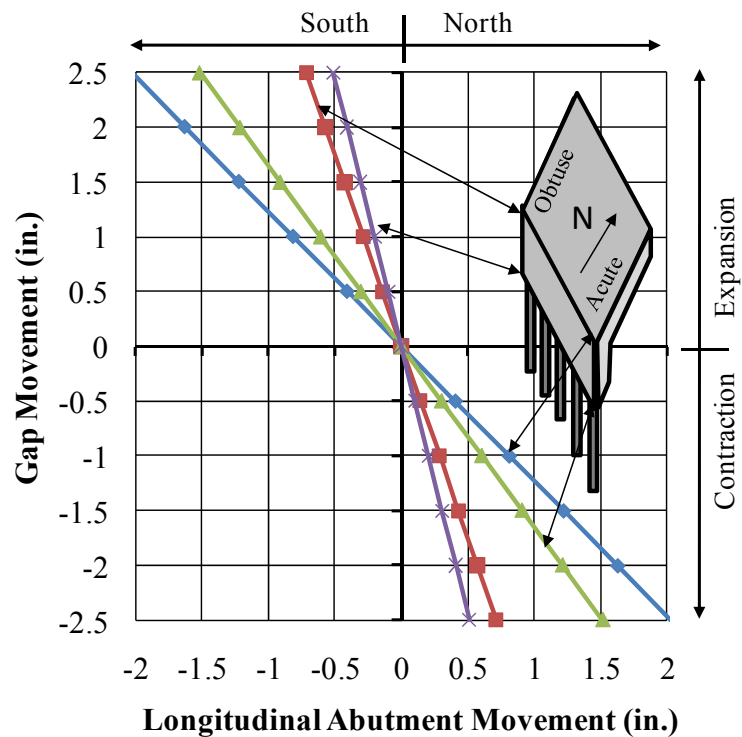
Figure 4.93: Prediction for Longitudinal Displacement of Abutment Corners
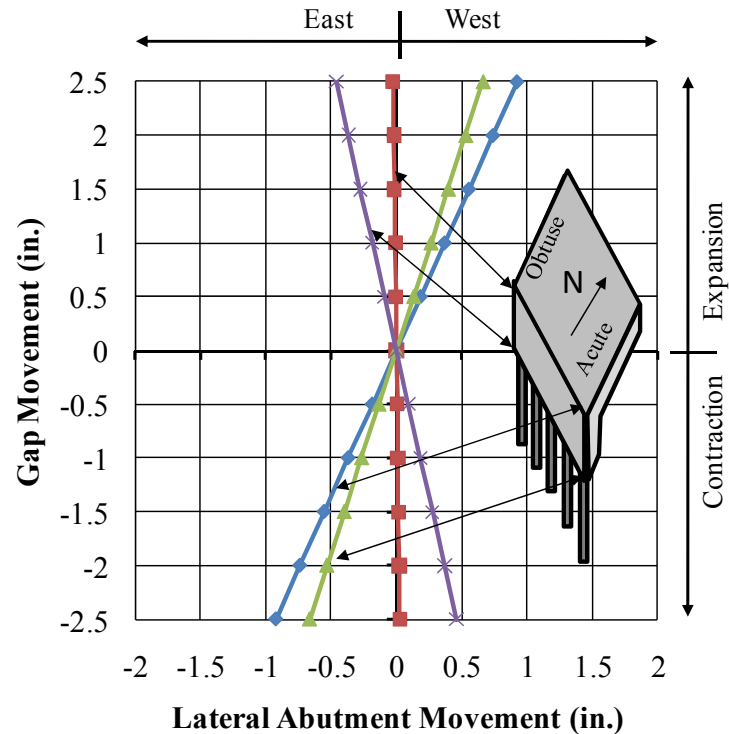
Figure 4.94: Prediction of Lateral Displacement of Abutment Corners

As observed in the test results of the quarter-scale structure, the analytical model calculates that the acute corner displaces much more than the obtuse corner in both the longitudinal and lateral directions. In addition, the analytical model also calculates rotation over the height of the abutment, as is evidenced by the difference in deflection between the top and bottom of the abutment.

To compare the magnitudes of the deflections between the analytical model and the experimental test, an attempt was made to remove the shift in the collected data caused by the initial error from the string pots. Each response curve of the abutment displacement was divided into separate, complete cycles. The relative displacements of each monitored corner was calculated and related to the corresponding demand displacement. Figure 4.95 and Figure 4.96 show two examples of how the adjusted relative displacements were calculated for the final cycle (±2.0 in.) for both top gages of the two acute corners. For example, in Figure 4.95, the recorded displacement value of the gap gage was 2.1 in. (the recording started at zero displacement and continued until 2.1 in. was reached). It is important to note that, during the expansion phase, the load started at 20 kips and increased to 90 kips. To determine the corresponding displacement of

the abutment during the 2.1 in. of displacement at the gap, continuity of the load must be maintained. Therefore, the relative displacement at the abutment corner during the load path from 20 kip to 90 kips is 1.0 in. (this corresponds to the abutment gage recording a displacement of -0.7 in. to -1.7 in.). These adjusted valued were used to compare with the results of the analytical model. Table 4.10 through Table 4.13 show the comparison of the adjusted measured displacements and the calculated displacement from the analytical models. Graphical representation of the comparison of the calculated displacements and the adjusted measured displacement for the south abutment is shown in Figure 4.97 through Figure 4.100.

As can be seen, the calculated values of the analytical model match fairly closely the measured movements of the quarter-scale integral abutment. The model accurately calculates the movements of the obtuse corner. Some of the calculated measurements for the acute corner are slightly off. Generally speaking, the physical model is stiffer than that estimated by the analytical model. Therefore, if the model is in error, it is on the conservative side (more displacement estimated).
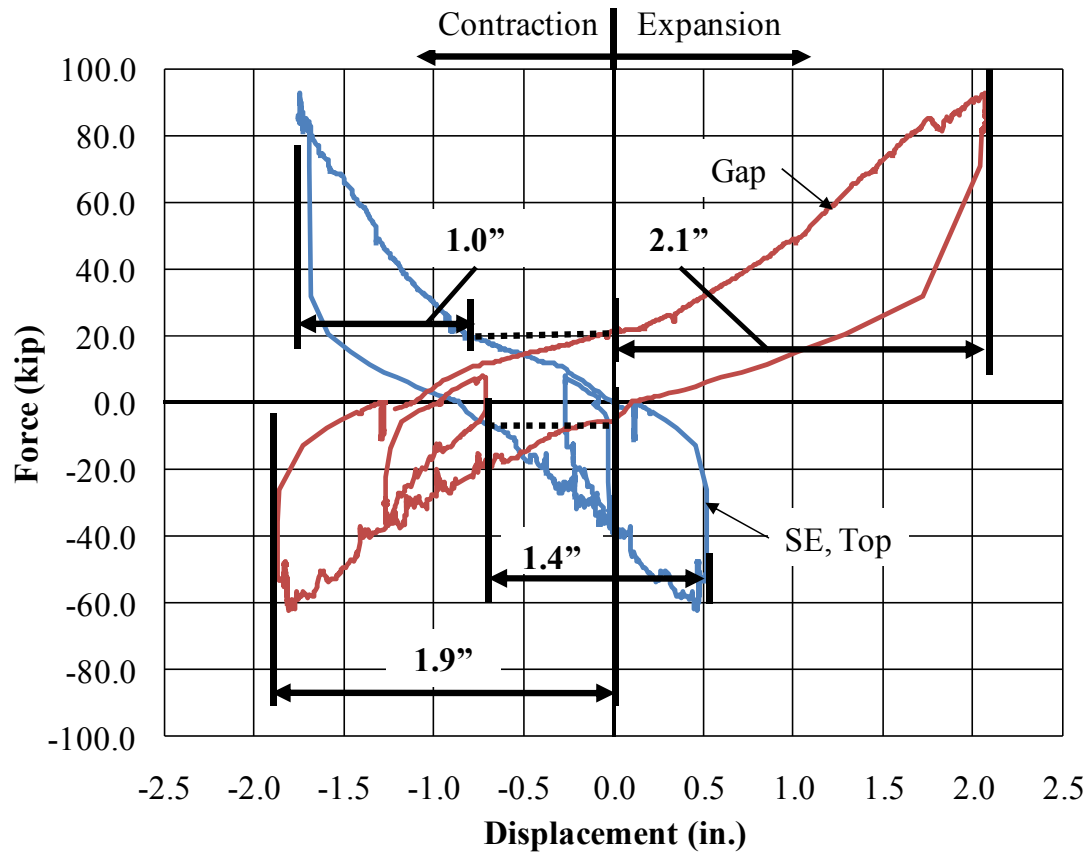
Figure 4.95: Relative Displacement Calculation for Longitudinal Displacement (SE, Top)
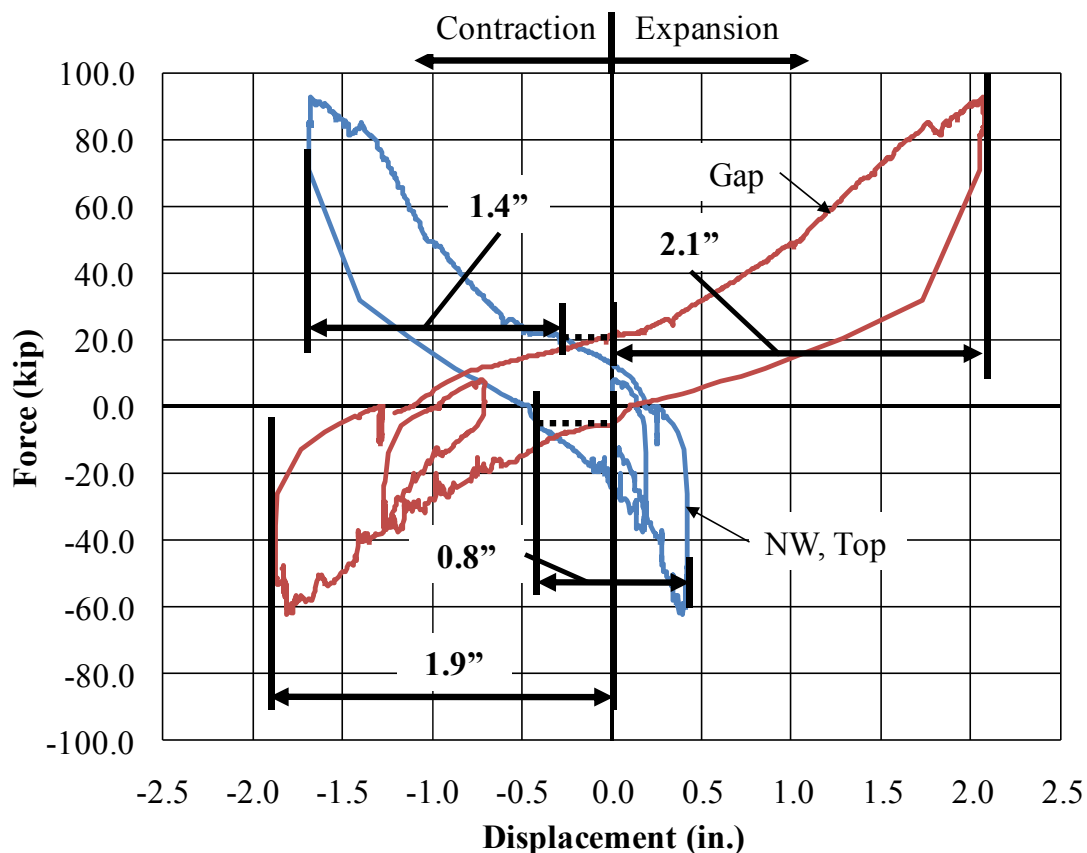
Figure 4.96: Relative Displacement Calculation for Longitudinal Displacement (NW, Top)

Table 4.10: Predicted and Measured Longitudinal Displacements for South Abutment

Control Gap Displacement (in.)	South Abutment Displacements (in.)							
	SE,TOP		SE, BOTTOM		SW, TOP		SW, BOTTOM	
	Measured	Predicted	Measured	Predicted	Measured	Predicted	Measured	Predicted
0.5	-0.6	-0.4	-0.5	-0.3	-0.7	-0.1	-0.5	-0.1
-0.6	0.3	0.5	0.1	0.4	0.1	0.2	0.2	0.1
1.1	-0.5	-0.9	-0.4	-0.7	-0.5	-0.3	-0.2	-0.2
-1.0	0.6	0.8	0.4	0.6	0.3	0.3	0.3	0.2
1.5	-0.7	-1.2	-0.4	-0.9	-0.7	-0.4	-0.3	-0.3
-1.5	1.0	1.2	0.7	0.9	0.6	0.4	0.4	0.3
2.1	-1.0	-1.7	-0.9	-1.3	-0.8	-0.6	-0.4	-0.4
-1.9	1.4	1.5	1.0	1.2	0.4	0.5	0.4	0.4

Table 4.11: Predicted and Measured Longitudinal Displacements for North Abutment

Control Gap Displacement (in.)	North Abutment Displacements (in.)							
	NE,TOP		NE, BOTTOM		NW, TOP		NW, BOTTOM	
	Measured	Predicted	Measured	Predicted	Measured	Predicted	Measured	Predicted
0.5	-0.4	-0.1	-0.2	-0.1	-0.7	-0.4	-0.6	-0.3
-0.6	0.2	0.2	0.1	0.1	0.3	0.5	0.1	0.4
1.1	-0.4	-0.3	-0.2	-0.2	-0.7	-0.9	-0.5	-0.7
-1.0	0.4	0.3	0.2	0.2	0.5	0.8	0.3	0.6
1.5	-0.5	-0.4	-0.3	-0.3	-0.8	-1.2	-0.6	-0.9
-1.5	0.7	0.4	0.4	0.3	0.8	1.2	0.6	0.9
2.1	-0.6	-0.6	-0.3	-0.4	-1.4	-1.7	-1.1	-1.3
-1.9	0.7	0.5	0.4	0.4	0.8	1.5	0.6	1.2

Table 4.12: Predicted and Measured Lateral Displacements for South Abutment

Control Gap Displacement (in.)	South Abutment Displacements (in.)							
	SE,TOP		SE, BOTTOM		SW, TOP		SW, BOTTOM	
	Measured	Predicted	Measured	Predicted	Measured	Predicted	Measured	Predicted
0.5	0.0	0.2	0.0	0.1	-0.4	0.0	-	-0.1
-0.6	-0.3	-0.2	0.2	-0.2	0.1	0.0	-	0.1
1.1	0.2	0.4	0.0	0.3	-0.2	0.0	-	-0.2
-1.0	-0.4	-0.4	-0.2	-0.3	0.0	0.0	-	0.2
1.5	0.4	0.6	0.1	0.4	-0.2	0.0	-	-0.3
-1.5	-0.6	-0.6	-0.3	-0.4	0.3	0.0	-	0.3
2.1	0.4	0.8	0.2	0.6	-0.6	0.0	-	-0.4
-1.9	-0.7	-0.7	-0.4	-0.5	0.2	0.0	-	0.3

Grey area / omitted data represents data that is considered erroneous from experiment.

Table 4.13: Predicted and Measured Lateral Displacements for North Abutment

Control Gap Displacement (in.)	North Abutment Displacements (in.)							
	NE,TOP		NE, BOTTOM		NW, TOP		NW, BOTTOM	
	Measured	Predicted	Measured	Predicted	Measured	Predicted	Measured	Predicted
0.5	-0.3	0.0	-	0.1	0.0	0.2	-	-0.1
-0.6	0.0	0.0	-	-0.2	-0.1	-0.2	-	0.1
1.1	-0.1	0.0	-	0.3	0.4	0.4	-	-0.2
-1.0	0.1	0.0	-	-0.3	-0.1	-0.4	-	0.2
1.5	-0.2	0.0	-	0.4	0.5	0.6	-	-0.3
-1.5	0.3	0.0	-	-0.4	-0.4	-0.6	-	0.3
2.1	-0.2	0.0	-	0.6	0.9	0.8	-	-0.4
-1.9	0.3	0.0	-	-0.5	-0.4	-0.7	-	0.3

Grey area / omitted data represents data that is considered erroneous from experiment.
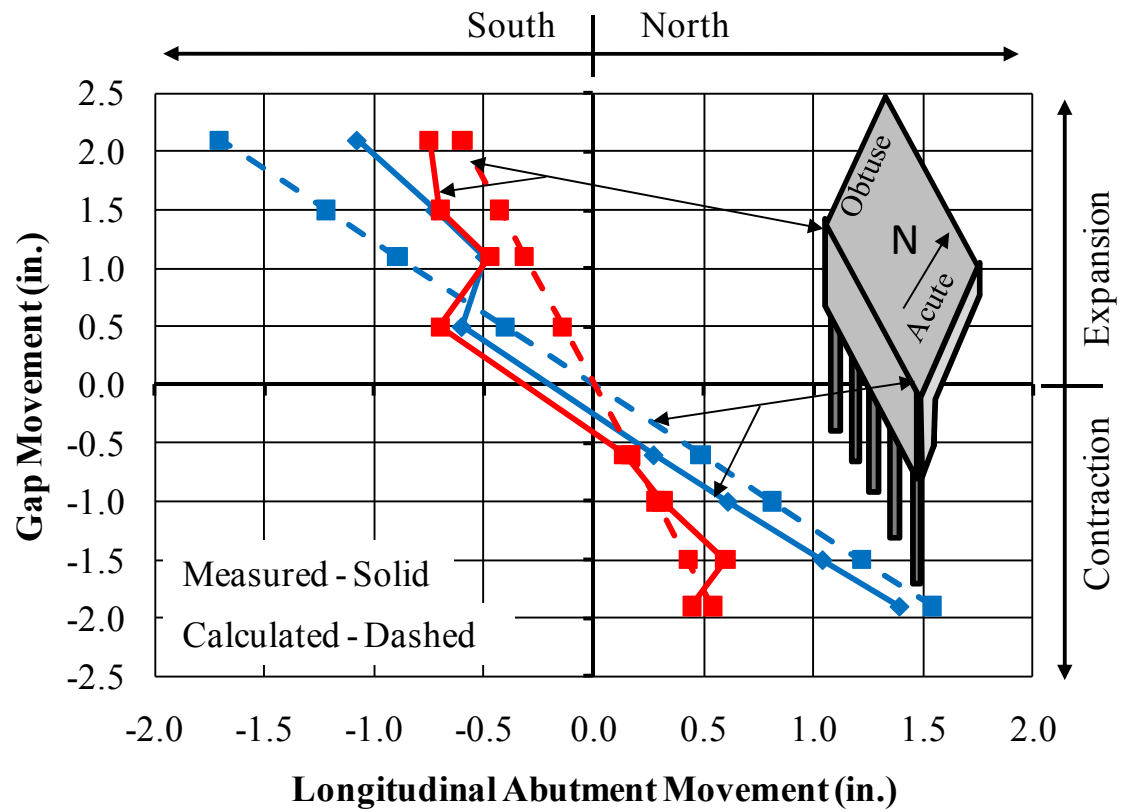
Figure 4.97: Comparison of Calculated Longitudinal Displacement and Adjusted Measured Displacement for Top of South Abutment
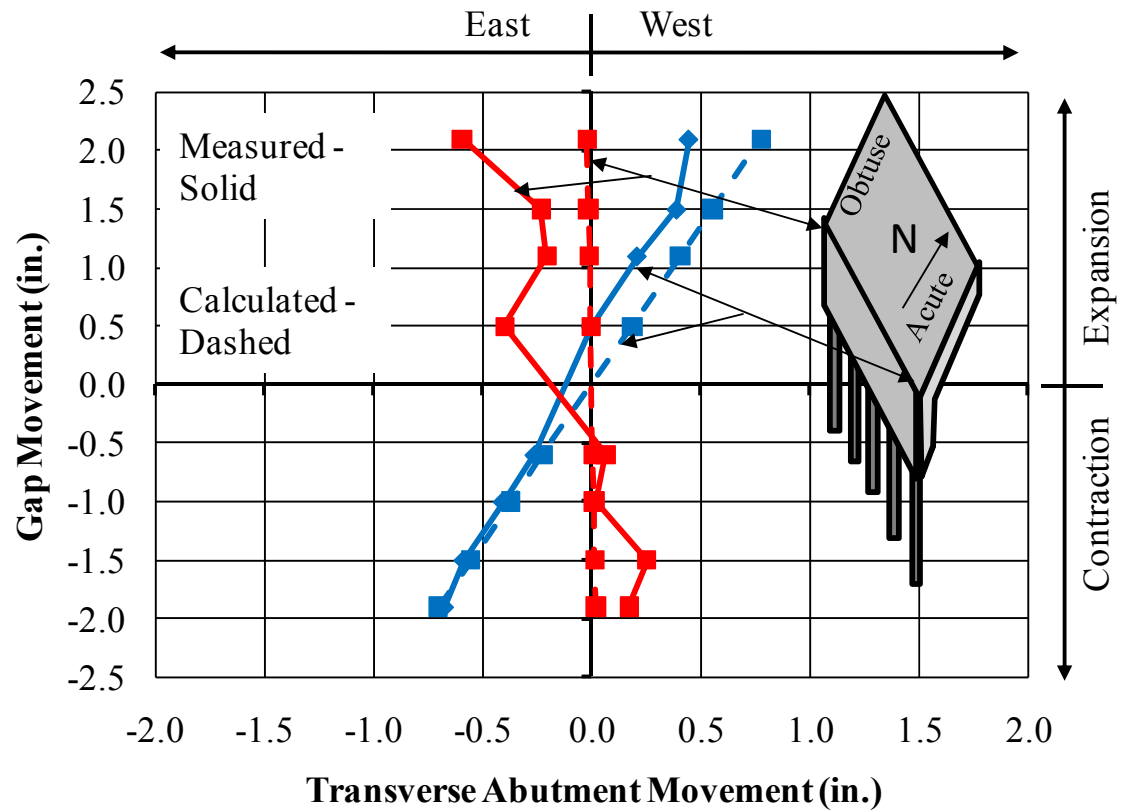
Figure 4.98: Comparison of Calculated Lateral Displacement and Adjusted Measured Displacement for Top of South Abutment
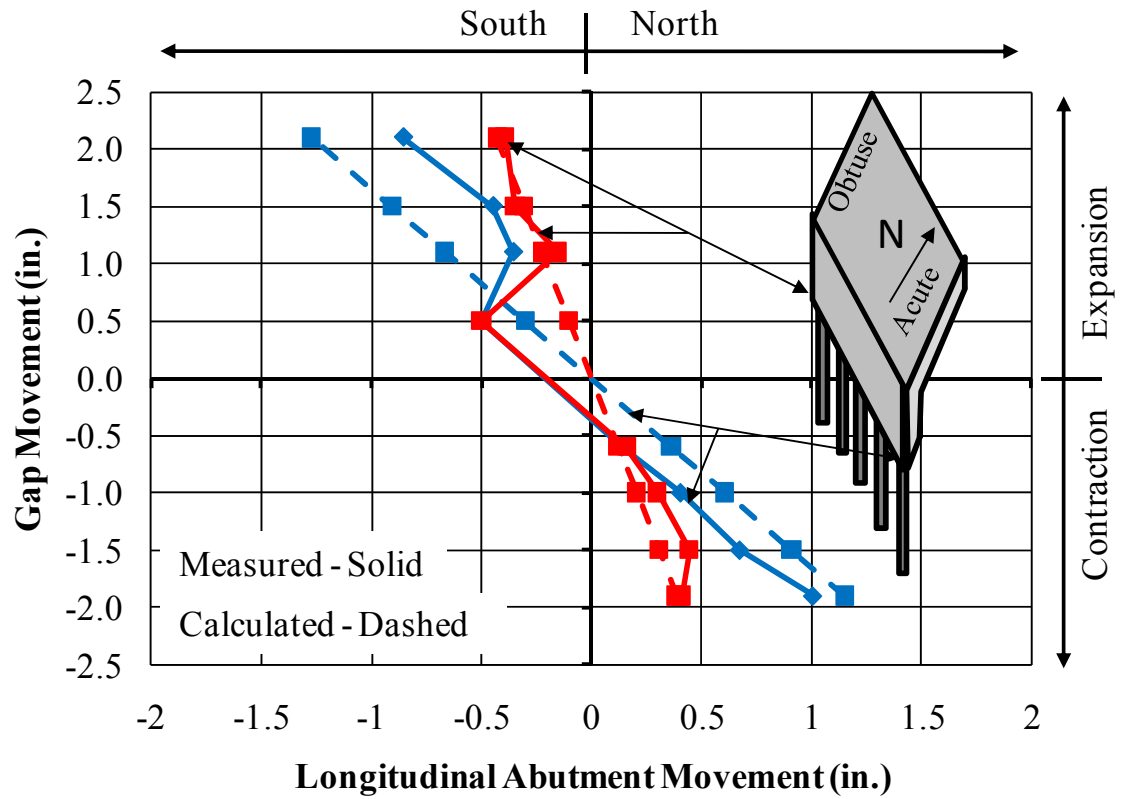
Figure 4.99: Comparison of Calculated Longitudinal Displacement and Adjusted Measured Displacement for Bottom of South Abutment

East   West
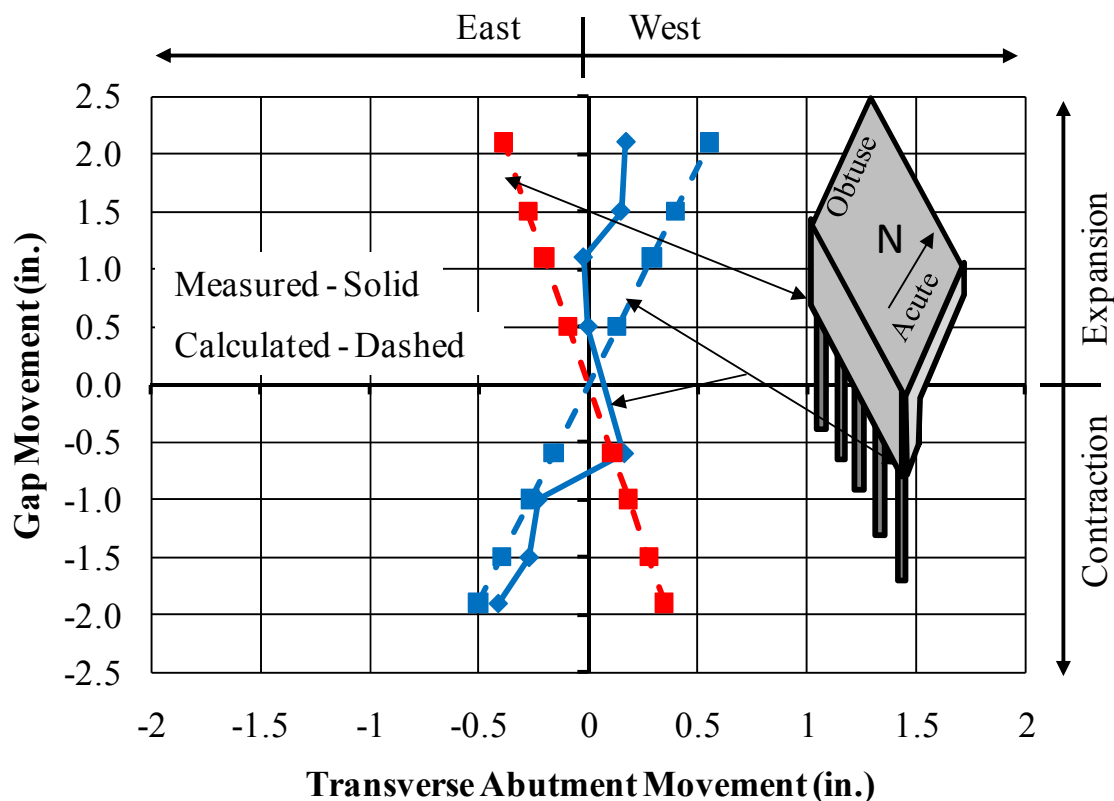
Measured lateral displacement for obtuse corner is omitted and considered erroneous from experiment.

Figure 4.100: Comparison of Calculated Lateral Displacement and Adjusted Measured Displacement for Bottom of South Abutment

Because the quantitative results from the down-hole array have considerable scatter and are potentially incorrect, a direct comparison between the measured deflected shapes and the analytical calculations have not been conducted. However, for completeness, calculated deflected shapes of two piles using the analytical model are shown in Figure 4.101 through Figure 4.104. These specific piles were chosen because they represent the least and greatest demand. The piles are only shown to a depth of 10 ft. Below 10 ft, the displacement is zero. It can be seen that the pile beneath the acute corner of the abutment is subjected to the greatest demand deflection in both the longitudinal and lateral directions. Conversely, the pile beneath the obtuse corner is subjected to the least demand. Therefore, when designing an integral abutment structure with skew, the pile closest to the acute corner will be the controlling pile.
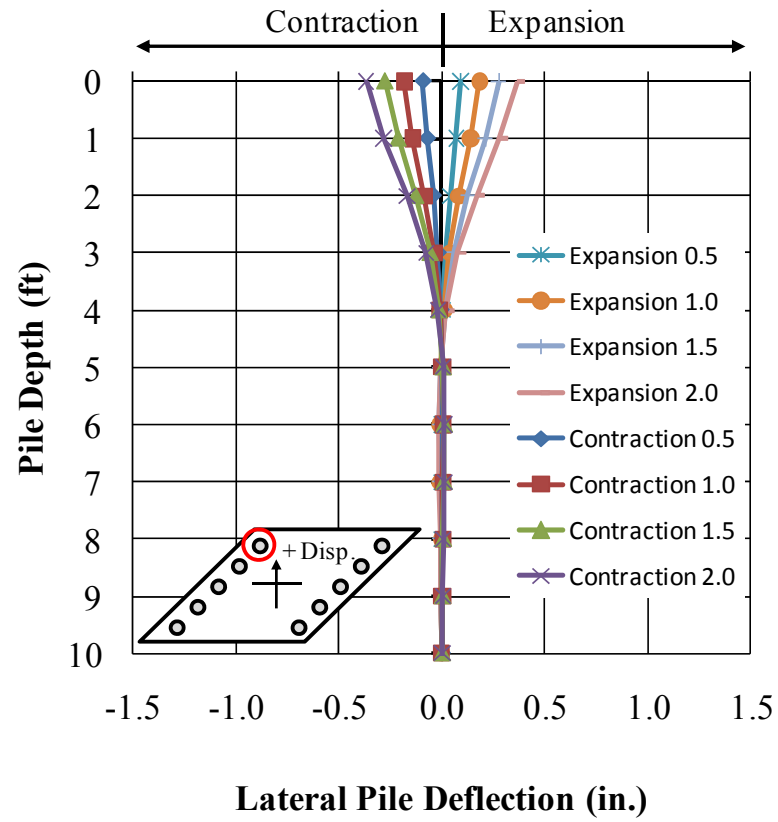
Figure 4.101: Predicted Pile Deflected Shape in Longitudinal Direction for Obtuse Corner
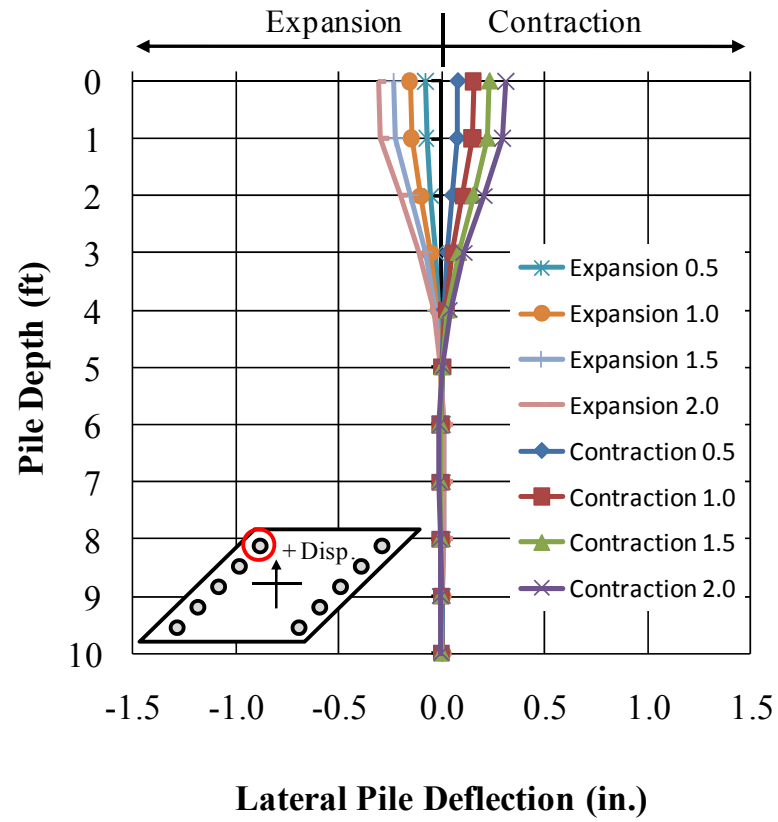
Figure 4.102: Predicted Pile Deflected Shape in Lateral Direction for Obtuse Corner
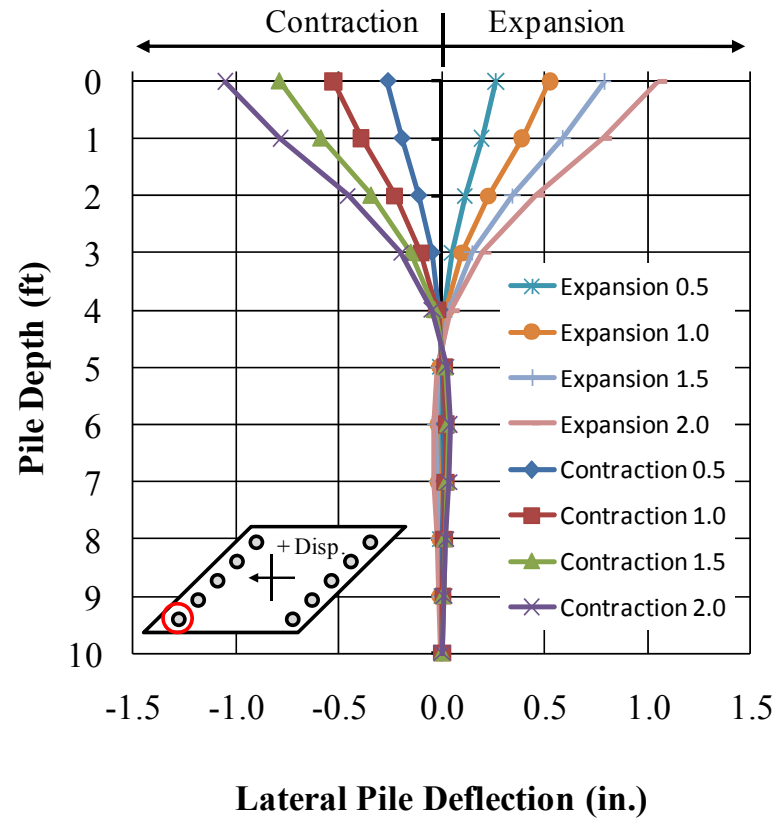
Figure 4.103: Predicted Pile Deflected Shape in Longitudinal Direction for Acute Corner
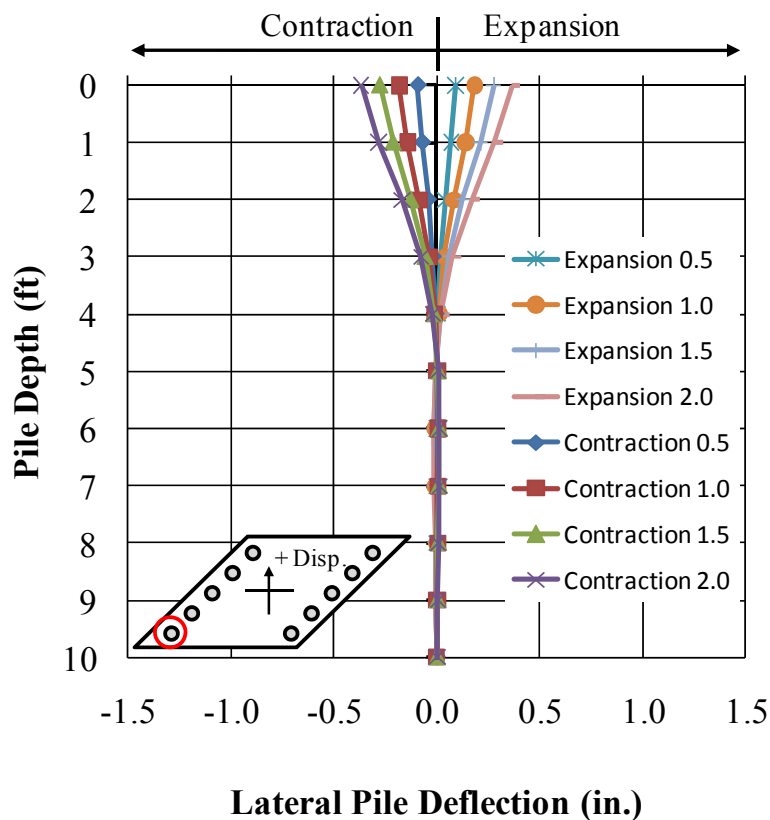
Figure 4.104: Predicted Pile Deflected Shape in Lateral Direction for Acute Corner

As can be seen, the pile deflected shapes are very similar to many of the deflected shapes measured using the down-hole array (Figure 4.64 - Figure 4.83). There is obviously some double curvature that occurs in the pile. However, the abutment does not provide fixity from rotation especially in the longitudinal direction of the structure. In the lateral direction, on the other hand, the abutment-pile connection is much more rotationally rigid. This behavior is also evident in the measured curves. The analytical models also predict that, due to the very stiff clay, the pile will have a point of fixity approximately 5-6 ft below the surface. This agrees reasonably well with the measured response.

4.9. CONCLUSIONS FROM EXPERIMENTAL INVESTIGATION

Understanding the effect that skew has on the behavior of integral abutment bridges is vital to developing rational design guidelines. The experimental investigation presented in this chapter revealed many characteristics about the behavior of these types of structures. The following conclusions were made:

Pile Behavior:

- When using a down-hole array to monitor the deflected shape of a pile, it is necessary to leave the array in the pile throughout the test duration. Removing and replacing the array in the pile introduces a great deal of error and uncertainty in measurements.

- Piles in integral abutment bridges behave somewhere between a fixed-pined and a fixed-fixed condition.

- The analytical model used to represent lateral pile behavior provides a good representation of actual field behavior.

- As shown by a single lateral pile test, the methods developed by Griemann et al. (1984) to determine lateral springs to represent soil stiffness are reasonably accurate.

- The controlling lateral pile deflection will always be the acute corner. Both longitudinal and lateral demand displacements are largest for the acute corner pile.

Structural Behavior:

- In addition to longitudinal translation (along the length of the structure), the abutments of integral abutment bridges rotate in plan-view. The acute corner of the abutment displaces much more that the obtuse corner for both expansion and contraction of the deck.

- Rotation of the abutment also occurs over the height of the abutment. The top of the abutment displaces more than the bottom. This behavior was also observed considering rotations measured at the top of the pile and over the height of the abutment.

Analytical Modeling:

- An initial transverse shift of the entire structure was not noticed in either the experimental test or the analytical model of the structure. The initial behavior was different from that of US-231 where an initial transverse shift was measured. As discussed in Chapter 3, it was assumed that the initial shift may be a measurement error and not a physical

behavior. The results of this test support that the initial shift of US-231 is most likely measurement error.

- The results of the analytical model closely matched that of the experimental program.
- The modeling procedure develop in Chapter 3 provides a realistic representation of the behavior of integral abutment bridges (skewed and non-skewed). This modeling approach should be applicable to integral abutment structures in general.

CHAPTER 5. ANALYTICAL INVESTIGATION

5.1. INTRODUCTION

Integral construction is the option of choice when constructing highway bridges. However, the applicability of these structures is limited by current DOT geometric limitations. The limiting factor for these structures is based on the demand imposed on the supporting piles in the abutments and their capacity to sustain the demand lateral displacements. Because data is limited on the behavior of integral structures outside of the current geometric limitations, an analytical investigation was conducted. The analytical investigation involves a parametric analysis of various characteristics of integral abutment bridges. Analytical models were developed using the calibrated methods described in Chapter 3 and Chapter 4. A series of models was developed to highlight a specific characteristic of the behavior of integral abutment bridges. Using the composite view provided by each series of models, the overall behavior of these structures can be understood. Understanding how these structures behave provides the potential for extended applicability.

5.2. PARAMETRIC STUDY

To develop an understanding for how various characteristics affect the behavior of integral abutment structures, a range of analytical models were developed as a part of a parametric study. The primary focus of the investigation is the effect of length and skew on the structure and how they control the demand on the supporting abutment piles. In addition to the effects of length and skew, secondary variables including temperature, span length, shrinkage models, soil stiffness, pile sections, and pile orientation were investigated. Because it was shown that the abutment backfill soil does not have a significant effect on the deflection demand of the supporting piles, the abutment soil was not included as part of the parametric analysis. Table 5.1 shows a matrix for the variables included in the parametric analysis. The variables are described in further detail in the sections below. For illustration purposes, an arbitrary construction date of

September 2000 is chosen and continued for a 10 year period. The analysis, however, is valid for any 10 year period.

Table 5.1: Parametric Analysis

Primary Variables					
Length (ft)	200	400	600	800	1000
Skew (degrees)	0	15	30	45	60
Secondary Variables					
	Default	**Alternate**			
Span Length (ft)	100	50	200		
Positive Temperature Differential (°F)	25	70	90		
Negative Temperature Differential (°F)	-45	-70	-90		
Shrinkage Model	CEB MC90	ACI 209	GL2000		
Pile Sections	CFT 14x0.312	HP14x117 / HP10x42	HP14x89 / CFT 14x0.203	HP12x84	HP12x53
Pile Orientation	N/A	Weak Axis	Strong Axis	Weak With Skew	Strong With Skew
Soil Stiffness	Loose Sand	Dense Sand	Soft Clay	Very Stiff Clay	No Soil

5.2.1. LENGTH

The lateral deflection of the supporting pile is the primary controlling factor for the limiting length of these structures. As described in previous chapters, the length of the structure is directly proportional to the demand on the pile. This behavior has been well understood for many years; however, only temperature has been included as a driving force. The effect of the length of the structure is investigated here with the addition of shrinkage strains applied to the superstructure. With the additional driving force, the following lengths of integral abutment bridges are investigated: 200, 400, 600, 800, and 1000 ft.

5.2.2. SKEW

In addition to the length of the structure, questions have been raised about the effects of skew on the behavior of integral abutment bridges. It is believed and has been shown in previous chapters, that the skew of the structure causes out-of-plane movements and rotation of the abutment. Therefore, the longitudinal displacement (a function of length) of the bridge as caused by temperature and shrinkage is only a component of the lateral demand on the pile. To determine the effect of the skew of a structure on the lateral demand of the piles, the following skew angles are investigated: 0, 15, 30, 45, and 60°. Each skew is investigated for each length of structure outlined in the previous section. For the various models, it is assumed that the direction of the skew angle has no differing effect on the behavior of the structure. Therefore, for this parametric analysis, structures that include skew are skewed to the right (Figure 5.1).
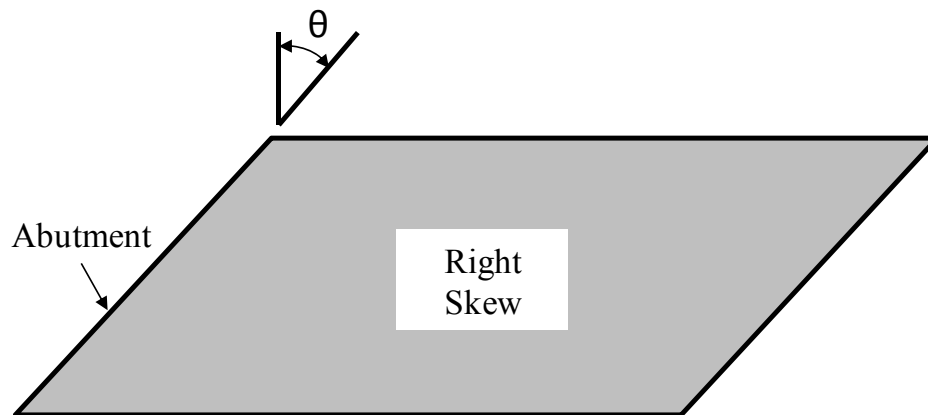
Figure 5.1: Direction of Skew for Parametric Analysis

5.2.3. SPAN LENGTH

The following span lengths are investigated to determine the effect of the stiffness of the superstructure on the rotation of the abutment and corresponding lateral demand on the piles: 50, 100, and 200 ft. The various span lengths are investigated on a structure having a total length of 400 ft considering the various skew angles. While it is typical to have shorter first interior spans to balance moments, the spans are set equal for ease of modeling.

5.2.4. TEMPERATURE

Three major temperature values are critical for understanding the behavior of integral abutment structures: initial construction temperature, maximum annual temperature, and minimum annual temperature. While the magnitudes of these various temperature stages are not important, the differences between the values control the thermal demand. Maximum expansion will be controlled by the difference between the initial construction temperature and the maximum annual temperature. The maximum contraction, on the other hand, will be controlled difference between the initial construction temperature and the minimum annual temperature. A geographical area will have approximately the same annual maximum and minimum temperatures. However, dependant on the time of year the structure is cast, the reference temperature can have a significant impact on the demand on the structure and the supporting piles. In Indiana, the annual daily average temperatures range from a high of 89 °F to a low of 16 °F (Famighetti 1997). So that the effect of thermal demand can be understood, several temperature differentials throughout that range are investigated. For use in analysis, the annual temperature differentials are converted to equivalent strains according to Equation 5.1.

$$\varepsilon_t = \Delta T \cdot \alpha \tag{5.1}$$

where:

ε_t = temperature strain, in./in.

ΔT = change in temperature, °F

α = coefficient of thermal expansion, 1/°F

       $= 5.5 \cdot 10^{-6} \; \dfrac{1}{°F}$

Table 5.2 show the various temperature cases used in the various analyses and the converted temperature strains applied to each structure. For temperature Case A, a scenario is developed to represent a series of analysis. It is assumed that a structure was built in September 2000 (Initial Temperature = 65 °F) and monitored for 10 years. The maximum and minimum temperature values for this structure were 90 °F and 20 °F, respectively. These temperatures were chosen because they are close to the daily average temperature of Indiana (World Almanac 1998) and they match well with the measured temperatures from the field investigation. Additional cases were considered to evaluate effects if the construction temperature was the same as the average minimum or maximum (Case B and C), as well as for a larger temperature range

(Case D and E).   Table 5.3 shows a succession of temperature strains (Case A) applied to a single structure over a period of 10 years for a staged analysis. Only Case A is shown because the other temperature cases are not used in a staged analysis. For all analyses, the temperature strain is applied to the entire superstructure, both the concrete deck and the concrete girders.

Table 5.2: Temperature Loading Cases

Temperature Case		Case A	Case B	Case C	Case D	Case E
Positive Differential	Temperature	25 °F	70 °F	0 °F	90 °F	0 °F
	Strain	137.5 με	385 με	0 με	495 με	0 με
Negative Differential	Temperature	-45 °F	0 °F	-70 °F	0 °F	-90 °F
	Strain	-247.5 με	0 με	-385 με	0 με	-495 με

Table 5.3: Strain Values for Temperature Differentials

Date	Equivalent Strains (με) Case A
Sep-00	0
Jan-01	-248
Jul-01	385
Jan-02	-385
Jul-02	385
Jan-03	-385
Jul-03	385
Jan-04	-385
Jul-04	385
Jan-05	-385
Jul-05	385
Jan-06	-385
Jul-06	385
Jan-07	-385
Jul-07	385
Jan-08	-385
Jul-08	385
Jan-09	-385
Jul-09	385
Jan-10	-385
Jul-10	385

5.2.5. SHRINKAGE MODEL

      As indicated by the analysis in Chapter 3, the net-inward movement of abutments is explained by the influence of shrinkage of the concrete in the bridge deck. Several shrinkage models are presented by ACI 209 (2008), and it was shown in that the CEB MC90 model best represents the in-service behavior. However, to have a complete understanding of the effect of variable shrinkage rates and magnitudes, several shrinkage models are investigated to illustrate their respective effects on the lateral demand of the abutment piles. The three shrinkage models that are investigated include the CEB MC90, ACI 209R-92, and GL2000 as outlined in the ACI 209 report. These specific models were chosen because CEB MC90 predicts the least amount of total shrinkage with the slowest rate, the GL2000 model predicts the most amount of shrinkage, and the ACI 209R-92 model predicts the fastest rate of shrinkage. Therefore, the shrinkage effect on the behavior of the structure should be bounded. A plot of the three shrinkage prediction models for a superstructure containing the properties of the reference structure are shown in Figure 5.2. It is assumed that the structure contains the same materials, geometry, and environmental conditions as that of SR-18 from Chapter 2. For the analytical models in the parametric analysis, the shrinkage strains are applied (in cases when they are applied) to only the concrete deck consistent with the modeling recommendations from Chapter 2. Table 5.4 shows the strain values applied to the deck for the relevant analyses over the ten year period.
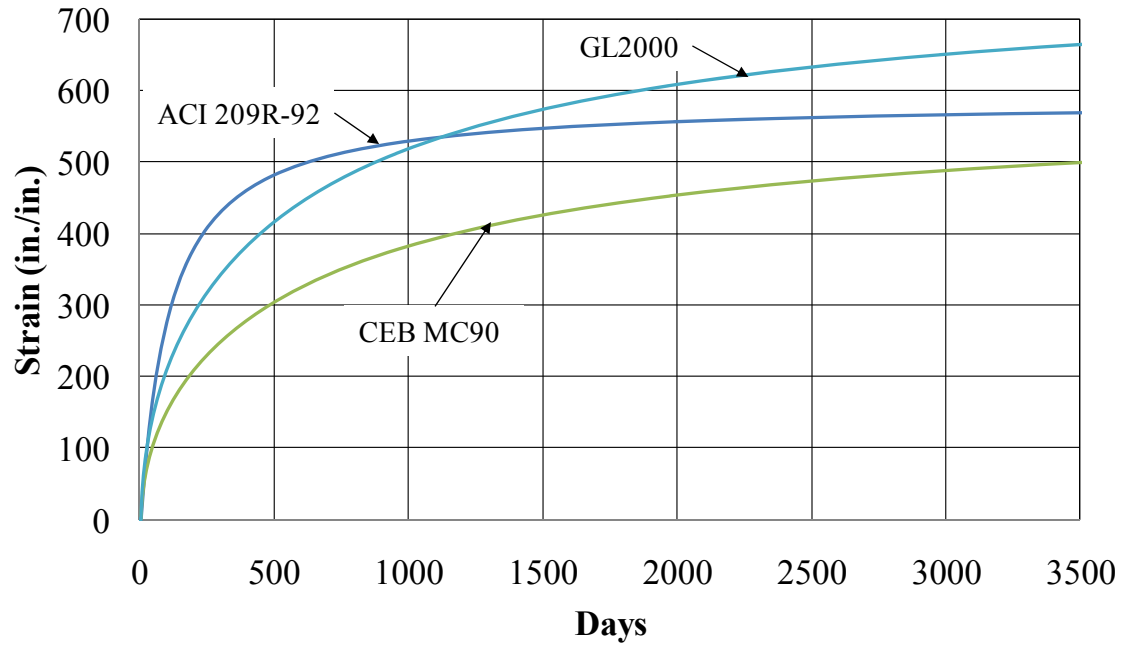
Figure 5.2: Shrinkage Models for Reference Structure

Table 5.4: Strain Values for Three Prediction Models

Date	Shrinkage (µε)		
	ACI 209R-92	**GL2000**	**CEB MC90**
Sept-00	0	0	0
Jan-01	303	228	164
Jul-01	430	342	248
Jan-02	479	412	301
Jul-02	504	459	337
Jan-03	520	495	365
Jul-03	531	523	386
Jan-04	539	546	404
Jul-04	544	564	419
Jan-05	549	580	431
Jul-05	552	594	442
Jan-06	556	606	452
Jul-06	558	616	460
Jan-07	560	625	467
Jul-07	562	633	473
Jan-08	564	640	479
Jul-08	565	646	485
Jan-09	566	652	489
Jul-09	567	657	494
Jan-10	568	662	498
Jul-10	569	667	501

5.2.6. PILE SECTIONS

According to the INDOT design manual (2010), only steel H-piles and steel pipe-piles are permitted for use in integral abutment bridges. Seven sections were chosen to investigate the effect of the pile section on the behavior of integral abutment bridges. Table 5.5 provides the properties of the steel H-piles, while Table 5.6 lists the section properties, as well as transformed section properties of the steel pipe-piles filled with 4000 psi concrete. All piles are assumed to be 40 ft in length. These specific sections were chosen because they are typical sections used by INDOT. In addition, these sections were included as part of separate studies to determine lateral pile capacity (Chovichien 2004, Talbott 2008).

Table 5.5: Section Properties for H-Piles

Pile Type	Area, A_g (in.^{2})	Primary Moment of Inertia, I_{11} (in.^{4})	Secondary Moment of Inertia, I_{22} (in.^{4})	Effective Width, B	
				Strong Axis Bending (in.)	Weak Axis Bending (in.)
HP10x42	12.4	210	71.7	10.1	9.7
HP12x53	15.5	393	127	12.0	11.8
HP12x84	24.6	650	213	12.3	12.3
HP14x89	26.1	904	326	14.7	13.8
HP14x117	34.4	1220	443	14.9	14.2

Table 5.6: Section Properties for Steel Pipe-Piles

Pile Type	CFT14x0.203"	CFT14x0.312"
Outer Diameter, O.D. (in.)	14	14
Wall Thickness, t_{wall} (in.)	0.203	0.312
Effective Area (in.^{2})*	26.7	30.7
Effective Moment of Inertia (in.^{4})*	415	507

*Based on transformed section considering 4000 psi concrete

5.2.7. PILE ORIENTATION

The INDOT Design Manual (2010) requires that the piles supporting integral abutment bridges be oriented with the weak axis perpendicular to the centerline of the structure to minimize flexural forces. This recommendation, however, is not consistent across other DOT's. Obviously, steel pipe-piles are not affected by this requirement since the section is symmetric. However, the various steel H-piles will exhibit different behavior based on their respective orientation. To develop an understanding of how the orientation of steel H-piles affects the behavior of integral abutment bridges, several orientations are investigated:

- Oriented weak axis perpendicular to centerline of structure (Figure 5.3(A)).
- Oriented strong axis perpendicular to centerline of structure (Figure 5.3(B)).
- Oriented weak axis to centerline of abutment (Figure 5.3(C)).
- Oriented strong axis to centerline of abutment (Figure 5.3(D)).
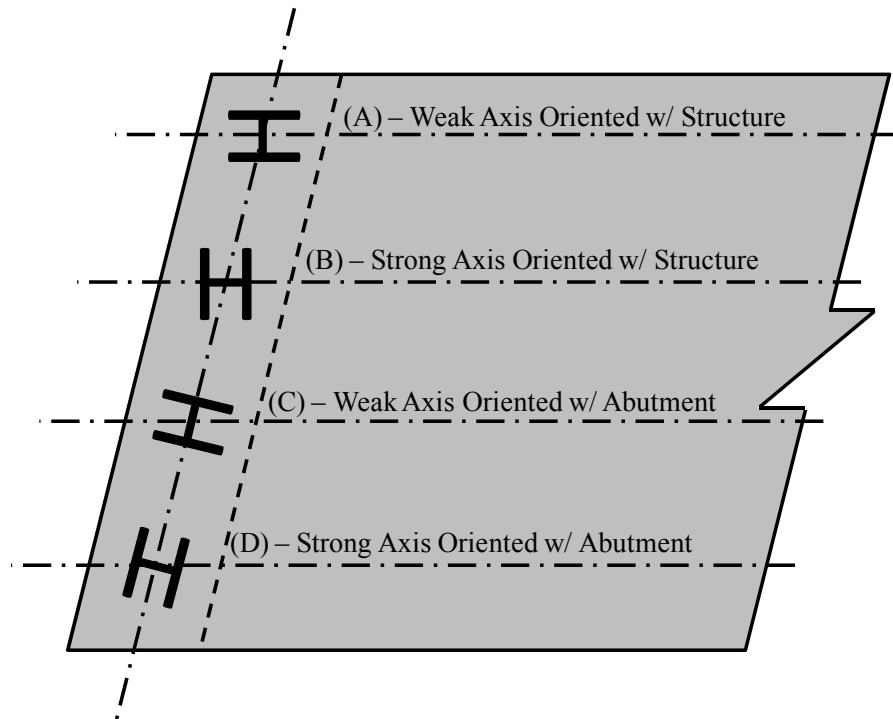
Figure 5.3: Pile Orientation

5.2.8. SOIL STIFFNESS

To evaluate the effect of the stiffness of the soil surrounding the piles, a variety of soil properties are investigated. To capture the range of soil-structure interaction effects, both sand and clay are investigated. The stiffness of the sand and clay ranged from very stiff/dense to zero stiffness. This range allows for bounding the effects of soil on integral abutment structures. To represent the soil stiffness for the piles, springs are developed based on the methods provided in Section 3.3.1. Table 5.7 shows the properties for the various soils used in the parametric study. In addition to the soils presented, an analysis for a case with no soil surrounding the piles is included.

Table 5.7: Soil Properties for Parametric Analysis

Soil Type	Unit Weight, γ (pcf)	Undrained Shear Strength, c_u (psf)	Internal Friction Angle, φ (degrees)
Soft Clay	120	750	-
Very Stiff Clay	130	3000	-
Loose Sand	120	-	30
Dense Sand	135	-	35

The calculated stiffnesses for springs along the depth of 40 ft piles spaced at 2 ft intervals representing the various soils are shown in Table 5.8 through Table 5.10 based on the respective pile section. Because the stiffness of springs representing sand are independent of the effective width of the pile, two sets of springs are provided for all the pile sections: one for loose sand and one for dense sand. However, the stiffness of the springs representing clay are dependent upon the effective width of the pile section. Therefore, there are different stiffness values for each section, as well as, each section orientation. For this investigation, the water table was assumed to be deep and, therefore, have no impact on the lateral stiffness.

Table 5.8: Lateral Pile Spring Stiffness for Sand

Depth of Pile (ft)	Lateral Spring Stiffness for all Pile Sections (kip/in.)	
	Loose Sand	Dense Sand
0	0.0	0.0
2	0.5	4.2
4	1.0	8.3
6	1.5	12.5
8	2.0	16.7
10	2.5	20.8
12	3.0	25.0
14	3.5	29.2
16	4.0	33.3
18	4.4	37.5
20	4.9	41.7
22	5.4	45.8
24	5.9	50.0
26	6.4	54.2
28	6.9	58.3
30	7.4	62.5
32	7.9	66.7
34	8.4	70.8
36	8.9	75.0
38	9.4	79.2
40	9.9	83.3

Table 5.9: Lateral Pile Spring Stiffness for Soft Clay

Depth of Pile (ft)	Lateral Stiffness (k/in.)									
	HP10x42		HP12x53		HP12x84		HP14x89 + CFT 14***		HP14x117	
	SA*	WA**	SA*	WA**	SA*	WA**	SA*	WA**	SA*	WA**
0	0.6	0.6	0.6	0.6	0.6	0.6	0.6	0.6	0.6	0.6
2	0.9	0.9	0.9	0.9	0.9	0.9	0.9	0.9	0.9	0.9
4	1.3	1.3	1.2	1.2	1.2	1.2	1.1	1.1	1.1	1.1
6	1.6	1.6	1.5	1.5	1.4	1.4	1.3	1.4	1.3	1.4
8	1.9	1.9	1.7	1.7	1.7	1.7	1.6	1.6	1.6	1.6
10	1.9	1.9	1.9	1.9	1.9	1.9	1.8	1.9	1.8	1.8
12	1.9	1.9	1.9	1.9	1.9	1.9	1.9	1.9	1.9	1.9
14	1.9	1.9	1.9	1.9	1.9	1.9	1.9	1.9	1.9	1.9
16	1.9	1.9	1.9	1.9	1.9	1.9	1.9	1.9	1.9	1.9
18	1.9	1.9	1.9	1.9	1.9	1.9	1.9	1.9	1.9	1.9
20	1.9	1.9	1.9	1.9	1.9	1.9	1.9	1.9	1.9	1.9
22	1.9	1.9	1.9	1.9	1.9	1.9	1.9	1.9	1.9	1.9
24	1.9	1.9	1.9	1.9	1.9	1.9	1.9	1.9	1.9	1.9
26	1.9	1.9	1.9	1.9	1.9	1.9	1.9	1.9	1.9	1.9
28	1.9	1.9	1.9	1.9	1.9	1.9	1.9	1.9	1.9	1.9
30	1.9	1.9	1.9	1.9	1.9	1.9	1.9	1.9	1.9	1.9
32	1.9	1.9	1.9	1.9	1.9	1.9	1.9	1.9	1.9	1.9
34	1.9	1.9	1.9	1.9	1.9	1.9	1.9	1.9	1.9	1.9
36	1.9	1.9	1.9	1.9	1.9	1.9	1.9	1.9	1.9	1.9
38	1.9	1.9	1.9	1.9	1.9	1.9	1.9	1.9	1.9	1.9
40	1.9	1.9	1.9	1.9	1.9	1.9	1.9	1.9	1.9	1.9

*SA – Strong Axis Bending
**WA – Weak Axis Bending
*** The weak axis for the HP14x89 section has the same effective width as both CFT14 sections.
Therefore the spring stiffnesses reported for the WA are applicable to the CFT14 sections.

Table 5.10: Lateral Pile Spring Stiffness for Very Stiff Clay

Depth of Pile (ft)	Lateral Stiffness (k/in.)									
	HP10x42		HP12x53		HP12x84		HP14x89 + CFT14***		HP14x117	
	SA*	WA**	SA*	WA**	SA*	WA**	SA*	WA**	SA*	WA**
0	6.3	6.3	6.3	6.3	6.3	6.3	6.3	6.3	6.3	6.3
2	16.3	16.7	14.8	14.9	14.6	14.6	13.2	13.7	13.1	13.5
4	18.8	18.8	18.8	18.8	18.8	18.8	18.8	18.8	18.8	18.8
6	18.8	18.8	18.8	18.8	18.8	18.8	18.8	18.8	18.8	18.8
8	18.8	18.8	18.8	18.8	18.8	18.8	18.8	18.8	18.8	18.8
10	18.8	18.8	18.8	18.8	18.8	18.8	18.8	18.8	18.8	18.8
12	18.8	18.8	18.8	18.8	18.8	18.8	18.8	18.8	18.8	18.8
14	18.8	18.8	18.8	18.8	18.8	18.8	18.8	18.8	18.8	18.8
16	18.8	18.8	18.8	18.8	18.8	18.8	18.8	18.8	18.8	18.8
18	18.8	18.8	18.8	18.8	18.8	18.8	18.8	18.8	18.8	18.8
20	18.8	18.8	18.8	18.8	18.8	18.8	18.8	18.8	18.8	18.8
22	18.8	18.8	18.8	18.8	18.8	18.8	18.8	18.8	18.8	18.8
24	18.8	18.8	18.8	18.8	18.8	18.8	18.8	18.8	18.8	18.8
26	18.8	18.8	18.8	18.8	18.8	18.8	18.8	18.8	18.8	18.8
28	18.8	18.8	18.8	18.8	18.8	18.8	18.8	18.8	18.8	18.8
30	18.8	18.8	18.8	18.8	18.8	18.8	18.8	18.8	18.8	18.8
32	18.8	18.8	18.8	18.8	18.8	18.8	18.8	18.8	18.8	18.8
34	18.8	18.8	18.8	18.8	18.8	18.8	18.8	18.8	18.8	18.8
36	18.8	18.8	18.8	18.8	18.8	18.8	18.8	18.8	18.8	18.8
38	18.8	18.8	18.8	18.8	18.8	18.8	18.8	18.8	18.8	18.8
40	18.8	18.8	18.8	18.8	18.8	18.8	18.8	18.8	18.8	18.8

*SA – Strong Axis Bending
**WA – Weak Axis Bending
*** The weak axis for the HP14x89 section has the same effective width as both CFT14 sections. Therefore the spring stiffnesses reported for the WA are applicable to the CFT14 sections.

5.2.9. ANALYTICAL MODEL

For the parametric study, a reference structure was developed. The structure is based on many of the details from the SR-18 structure discussed in Chapter 2. The reference structure is a 400 ft bridge with four equal 100 ft spans and no skew. An elevation is shown in Figure 5.4, a plan view is shown in Figure 5.5, and a cross-section of the girder is shown in Figure 5.6.

The superstructure consists of five 60 in. Indiana Bulb Tee Beams spaced at 10'-2" and supporting an 8 in. concrete deck. Table 5.11 shows the properties of the girders. The superstructure is 48 ft in width. Supporting the superstructure, the abutment is 9'-0.5" tall and 3'-

3" thick (Figure 5.7). Each abutment is supported by ten 40 ft piles (CFT14x0.312"). The piles are surrounded by loose sand with a unit weight of 125 pcf and a friction angle of 30 deg.
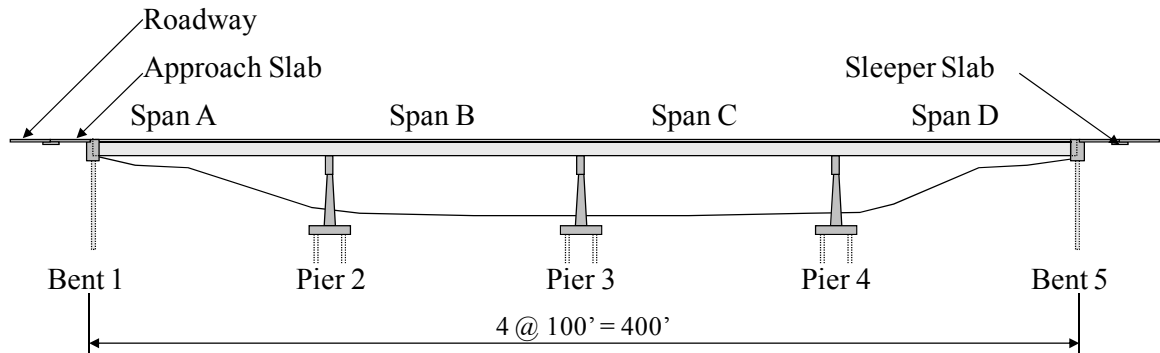
Figure 5.4: Elevation of Reference Structure
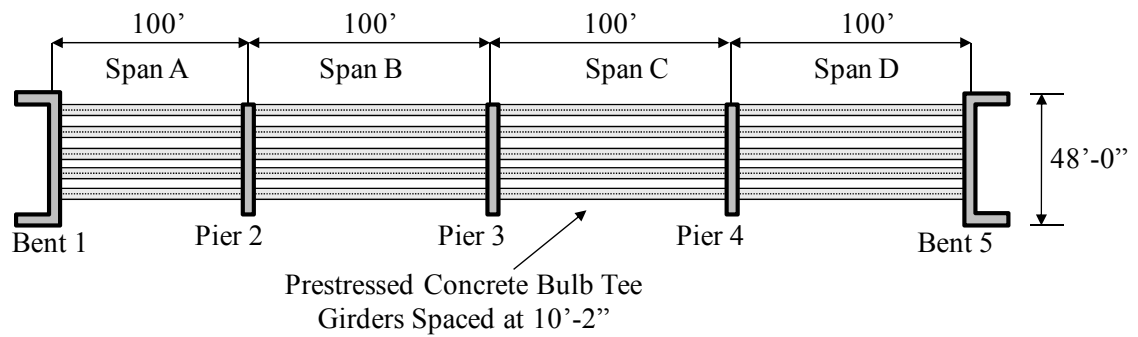
Figure 5.5: Plan View of Reference Structure

Figure 5.6: Girder Cross-section for Reference Structure

Table 5.11: Girder Properties for Reference Structure

Area of Beam, A_g	929.5 in.^{2}
Primary Axis Moment of Inertia, I_{11}	448,036 in.^{4}
Secondary Axis Moment of Inertia, I_{22}	71,156 in.^{4}
Design Concrete Compressive Strength, f_c'	6000 psi
Weight of Beam, w_g	971 plf
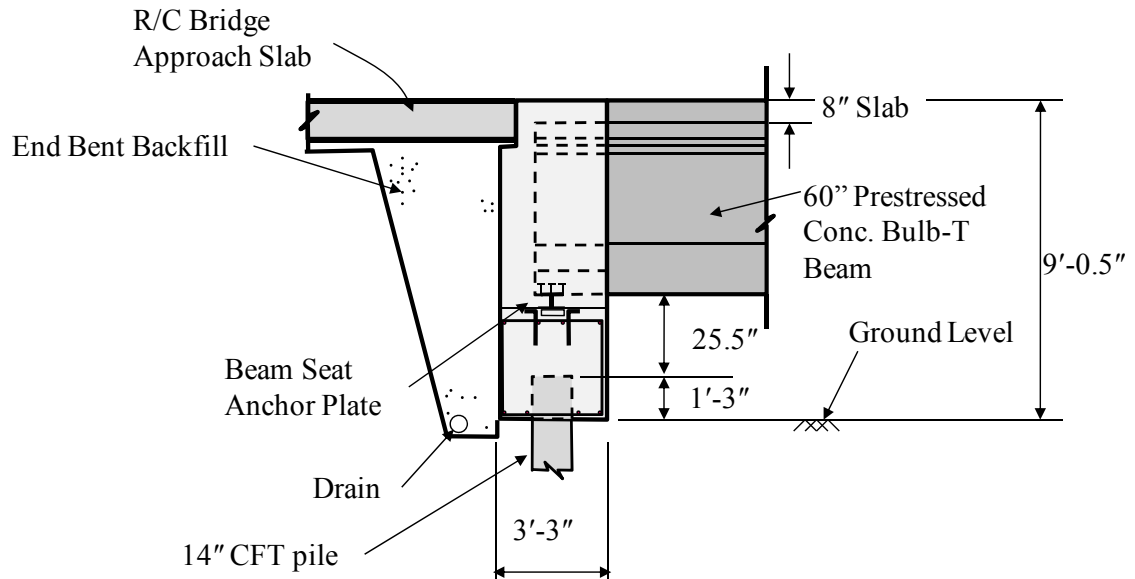
Figure 5.7: Abutment Cross-Section for Reference Structure

The structure is assumed to have been cast in September 2000, and the ambient construction temperature was 65 °F. The annual maximum temperature is 90 °F, while the annual minimum temperature is 20 °F. All materials for the structure are the same as the materials used in the SR-18 structure (Chapter 2). For the various models created for this parametric study, unless otherwise noted, the structure contains the aforementioned properties. Each variable in the parametric analysis was investigated separately to isolate the effect of that specific variable. Finally, each model was analyzed for a period of 10 years to capture the long-term behavior of the structure. The lateral deflection demand of the bottom two corners of a single abutment were used for comparison for all models. The bottom was chosen as it is representative of the demand on the piles.

For the parametric analysis, the primary variables were analyzed for each length and each skew (25 models). For the secondary variables, each skew was investigated, however, only at a bridge length of 400 ft.

5.3. RESULTS

5.3.1. EFFECTS OF LENGTH

      To determine the effects of length, five analytical models were developed for structures with 200, 400, 600, 800, and 1000 ft total lengths. The structures were assumed to have zero skew. Each analytical model was run for a period of 10 years. The strain values for the temperature differentials and CEB MC90 incremental strain are shown in Table 5.3 and Table 5.4, respectively. The calculated deflection of the bottom of the abutment over the life cycle is shown in Figure 5.8. Table 5.12 summarizes the long-term demand deflection of the piles. Because the ratcheting phenomenon is caused by shrinkage, the demand deflection is in the contraction direction. As the length of the structure is increased, the demand on the supporting piles is linearly increased (Figure 5.9). The line is offset from zero due to lateral deflection caused by dead weight.
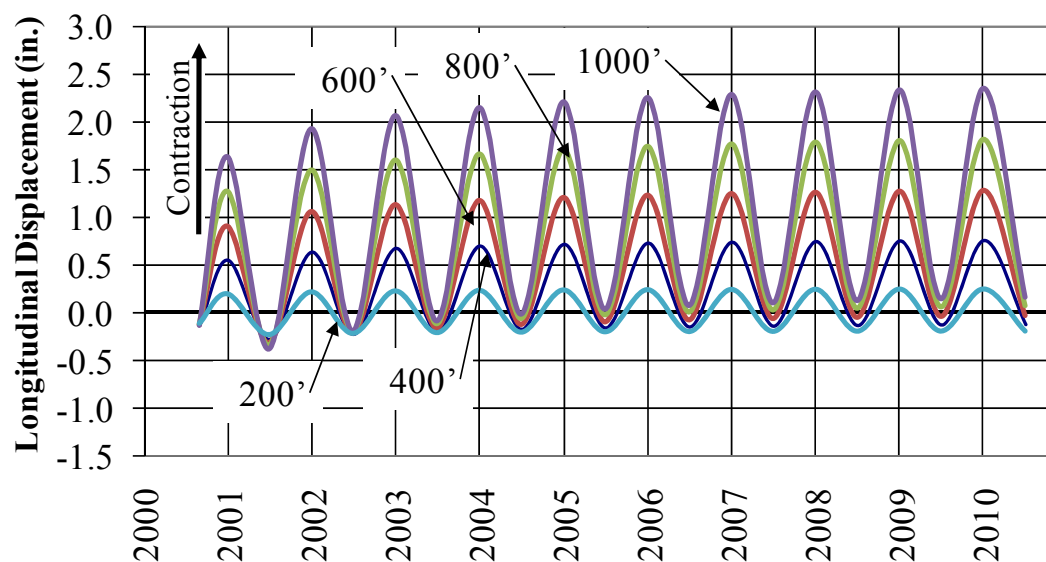
Figure 5.8: Effect of Temperature

Table 5.12: Long-Term Demand Lateral Deflection of Supporting Piles

Length of Structure (ft)	Ultimate Demand Deflection (in.)
200	0.24
400	0.74
600	1.28
800	1.81
1000	2.34
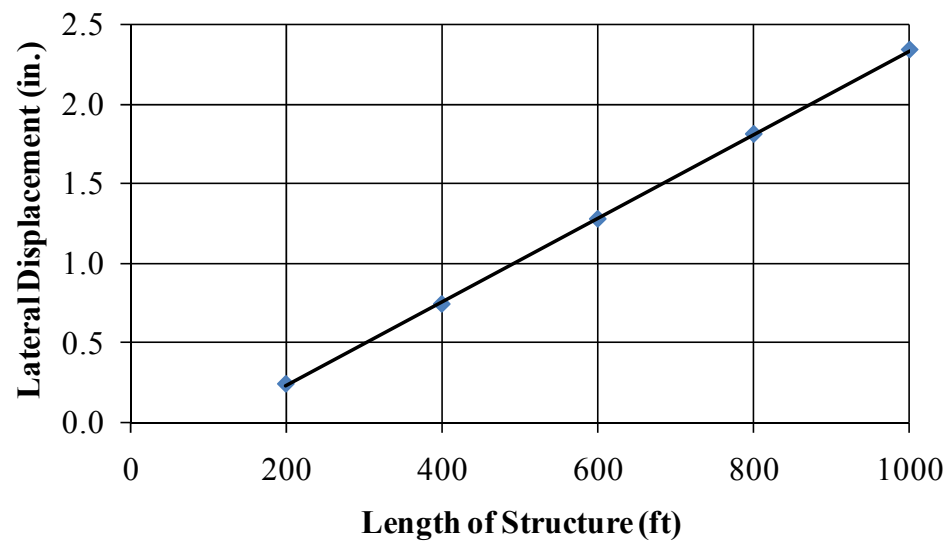
Figure 5.9: Linear Effect of Total Length of Structure

In former studies (Chovichien 2004, Talbott 2008), the demand deflection is determined by calculating a deflection based on unrestrained thermal strains (Equation (5.2)).

$$\Delta = \alpha \cdot \Delta T \cdot \frac{L}{2} \tag{5.2}$$

where:

Δ = demand deflection, in.

α = coefficient of thermal expansion, 1/°F

       $= 5.5 \cdot 10^{-6} \; {}^{1}\!/_{°F}$

ΔT = change in temperature, °F

L = total length of structure, in.

Once this demand was determined, 100% of the demand deflection was used to limit the maximum length of the structure based on the allowable lateral deflection capacity (Chovichien 2004, Talbott 2008). However, it has been shown here that shrinkage, in addition to temperature, has an effect on the lateral demand. Therefore the expression should be:

$$\Delta = \left(\varepsilon_{\Delta T} + \varepsilon_s\right)\frac{L}{2}$$ (5.3)

where:

Δ = demand lateral deflection, in.

$\varepsilon_{\Delta T}$ = thermal strain, in./in.

= $\alpha \cdot \Delta T$

= $5.5 \cdot 10^{-6} \; \frac{1}{{}^\circ F}\left(-45^\circ F\right) = -247.5 \mu\varepsilon$

ε_s = ultimate shrinkage strain, in./in.

= -500 $\mu\varepsilon$

L = total structural length, in.

Using Equation 5.3, estimated demand deflections were calculated for the various structural lengths (Table 5.13). As can be seen, the method over-predicts the deflections calculated by the analytical models. Figure 5.10 shows the relationship between theoretical unrestrained deflection (Equation 5.3) and the analytical procedure. The theoretical values are different by a constant factor. For the specific superstructure cross-section, abutment dimensions, and number of piles, the factor is approximately 0.6 as seen by the equation of the line. This reduction is primarily caused by the piles. Lateral stiffness is provided by the pile, and therefore the actual lateral displacement is less. Also, the piles allow rotation of the abutment to occur such that larger lateral displacements occurs toward the top of the abutment and less occurs at the bottom. The 0.3 in. offset of the line is caused by rotation of the abutment due to deadweight of the structure.

Table 5.13: Comparison of Analytical and Theoretical Demand Displacements

Length of Structure (ft)	Analytical Deflection (in.)	Theoretical Deflection Eq. (5.3) (in.)
200	0.24	0.90
400	0.74	1.79
600	1.28	2.69
800	1.81	3.59
1000	2.34	4.49
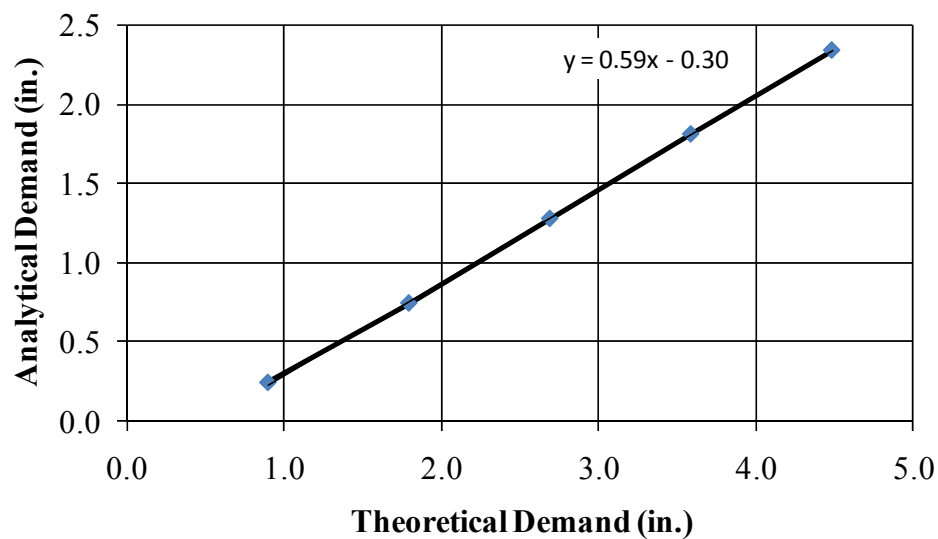
Figure 5.10: Relationship Between Theoretical and Analytical Demands

5.3.2. EFFECTS OF SKEW

To determine the effects of skew, 25 separate analytical models were developed for each length and each skew. The structure was loaded with the temperature strains from Case A (Table 5.3) and the shrinkage strains from CEB MC90 (Table 5.4). Figure 5.11 through Figure 5.20 show the results from the analytical models for both the acute and obtuse corners at the base of the abutment. It should be noted that all figures are plotted to the same scale for comparison purposes.

Table 5.14 and Table 5.15 tabulate the ultimate longitudinal and transverse demand for the acute corner (the controlling corner for pile displacement) for the various lengths and skews. Finally, Table 5.16 provides the total lateral movement of the corner calculated as the square root of the sum of the squares for the two directions. This total movement is the maximum lateral displacement demand for the supporting piles.
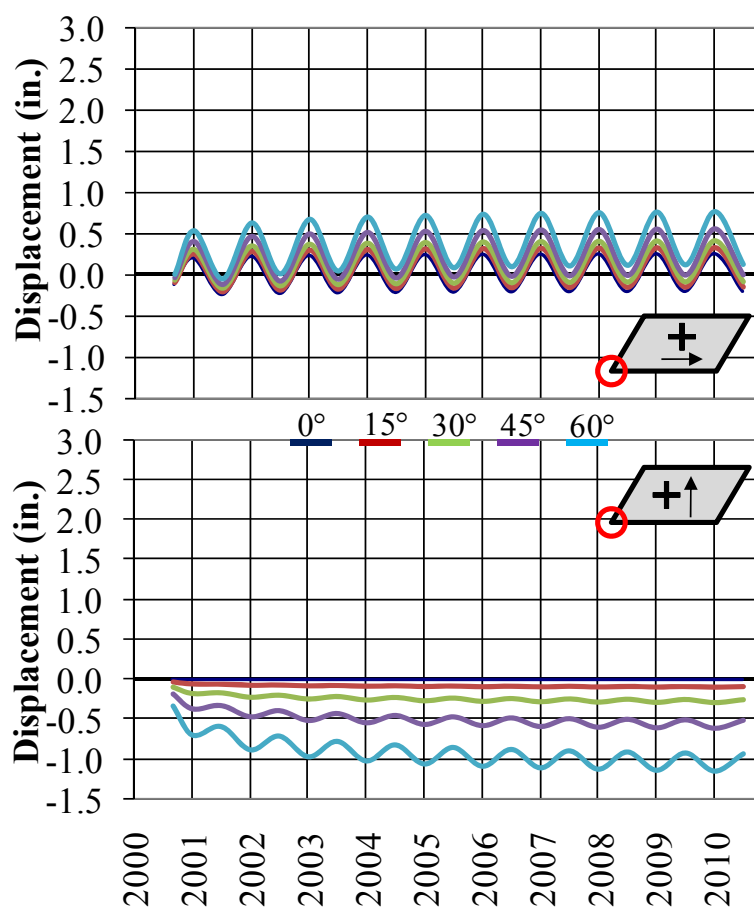
Figure 5.11: Effect of Skew (200 ft – Acute Corner)
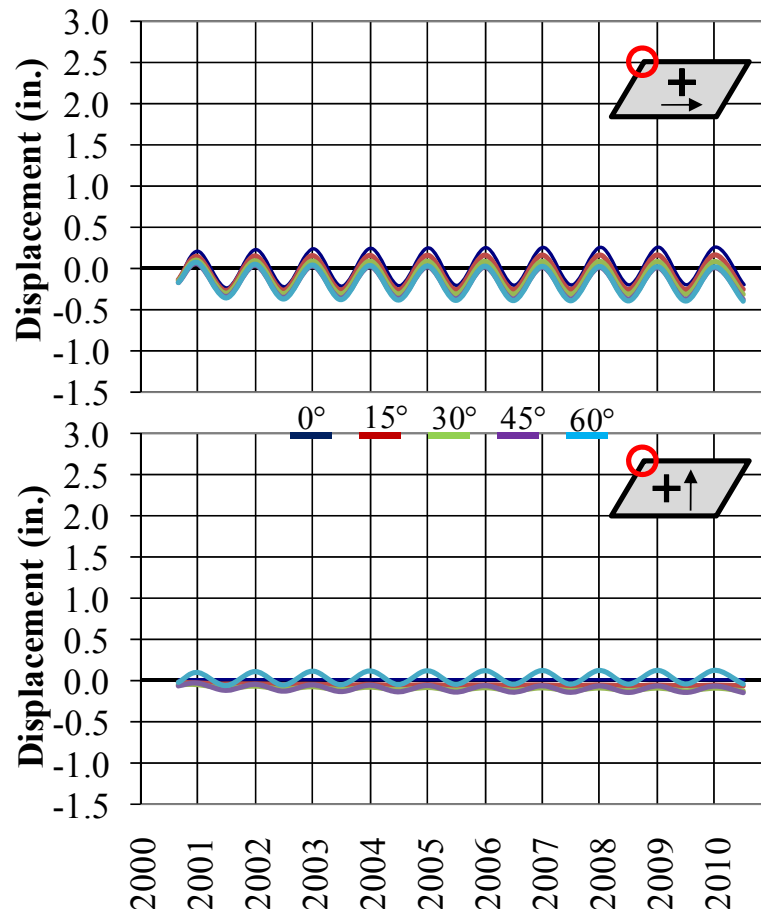
Figure 5.12: Effect of Skew (200 ft – Obtuse Corner)
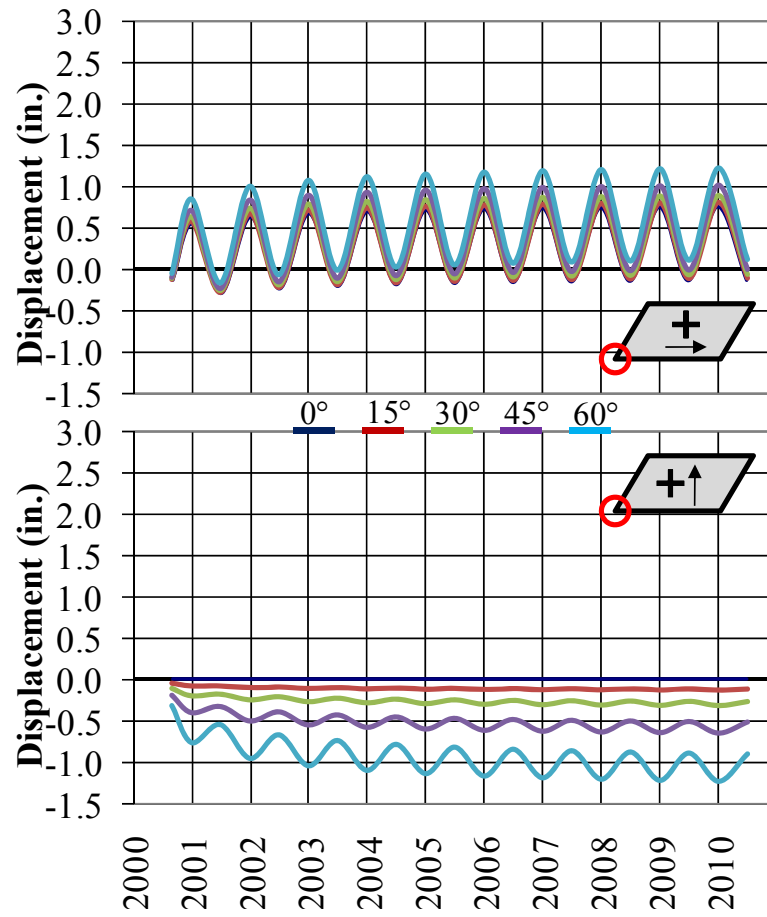
Figure 5.13: Effect of Skew (400 ft – Acute Corner)
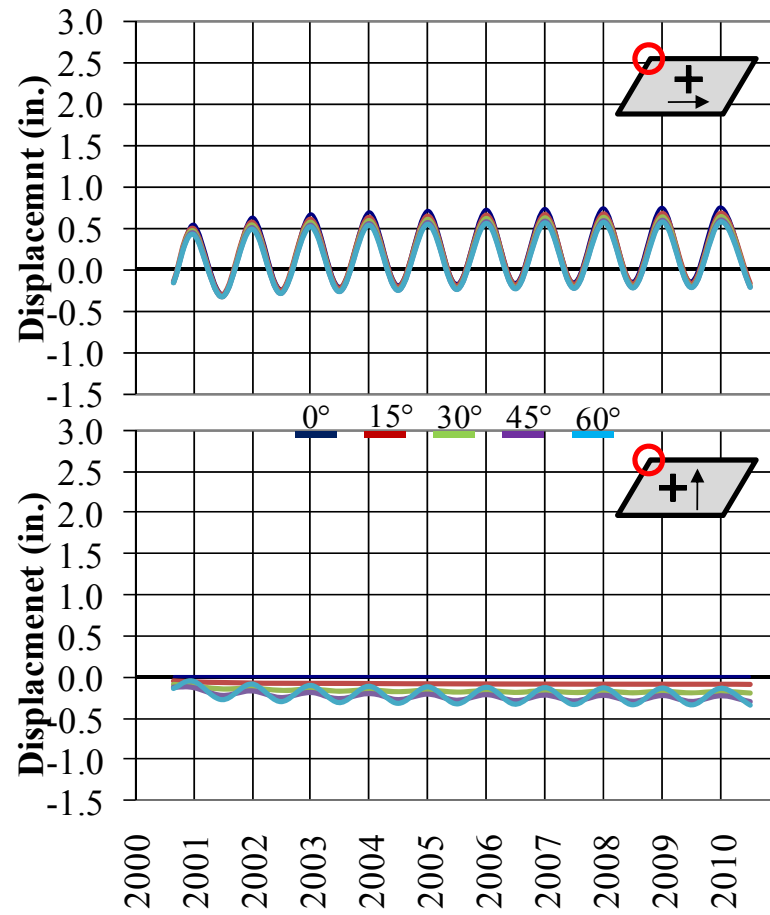
Figure 5.14: Effect of Skew (400 ft – Obtuse Corner)
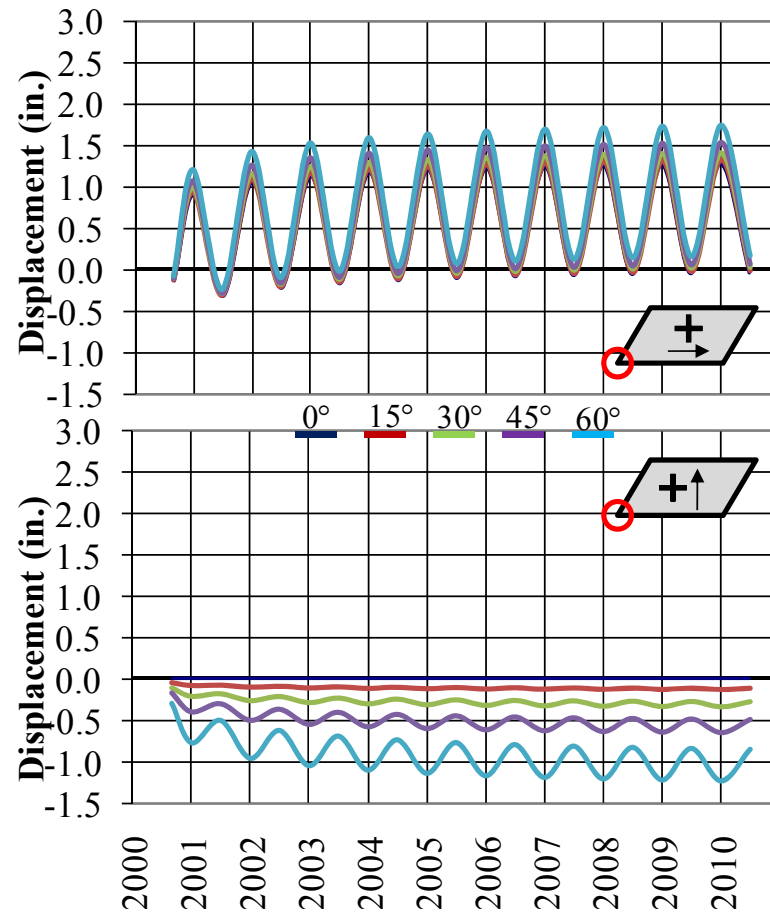
Figure 5.15: Effect of Skew (600 ft – Acute Corner)
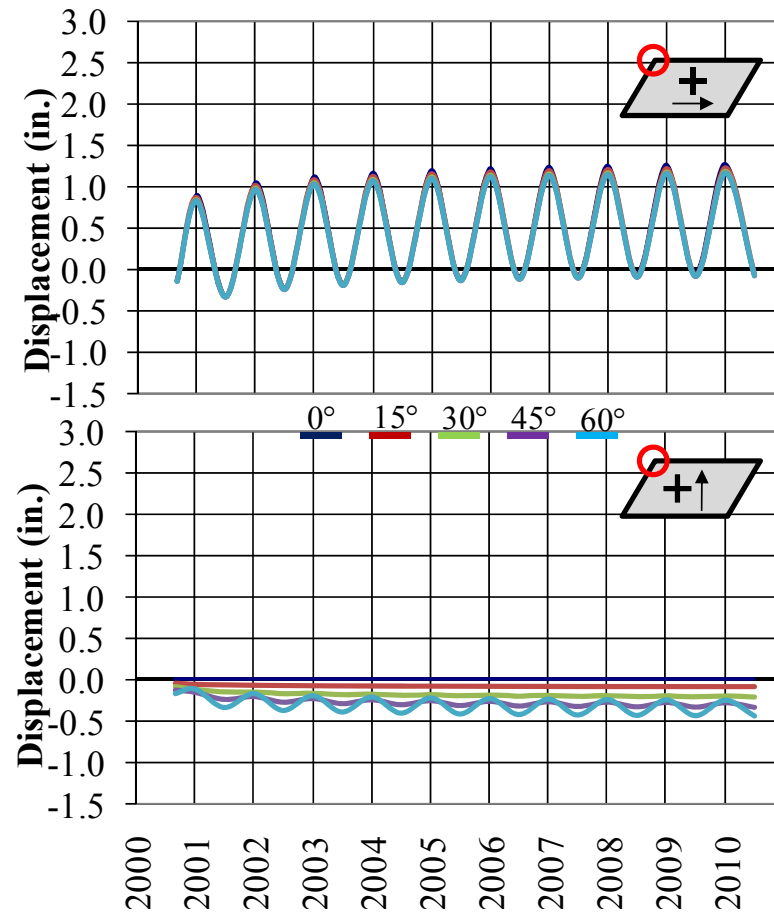
Figure 5.16: Effect of Skew (600 ft – Obtuse Corner)
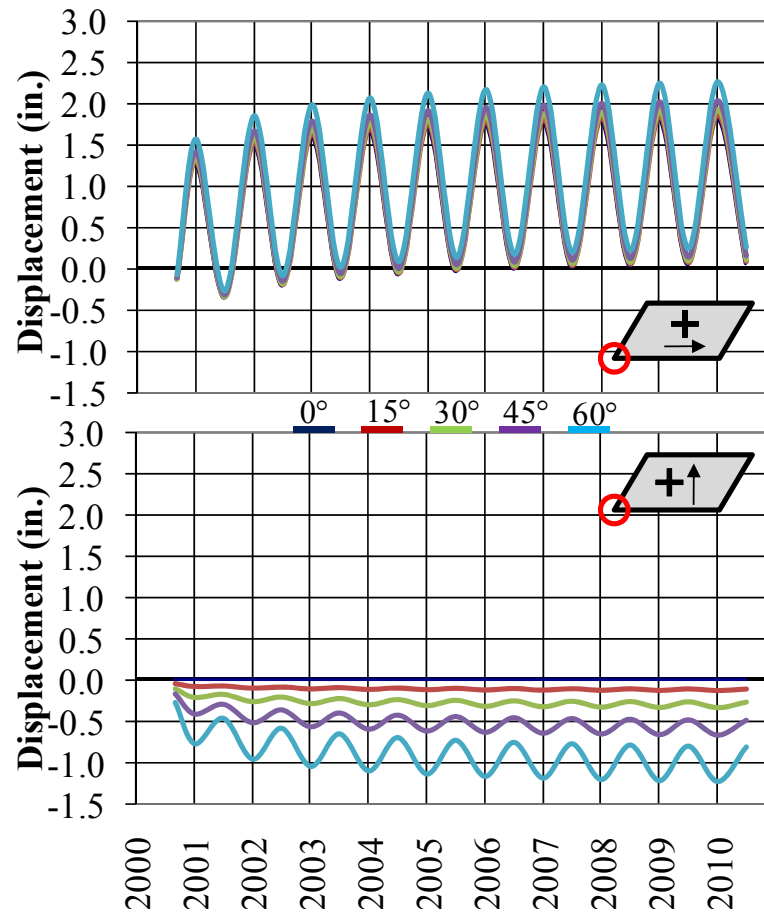
Figure 5.17: Effect of Skew (800 ft – Acute Corner)
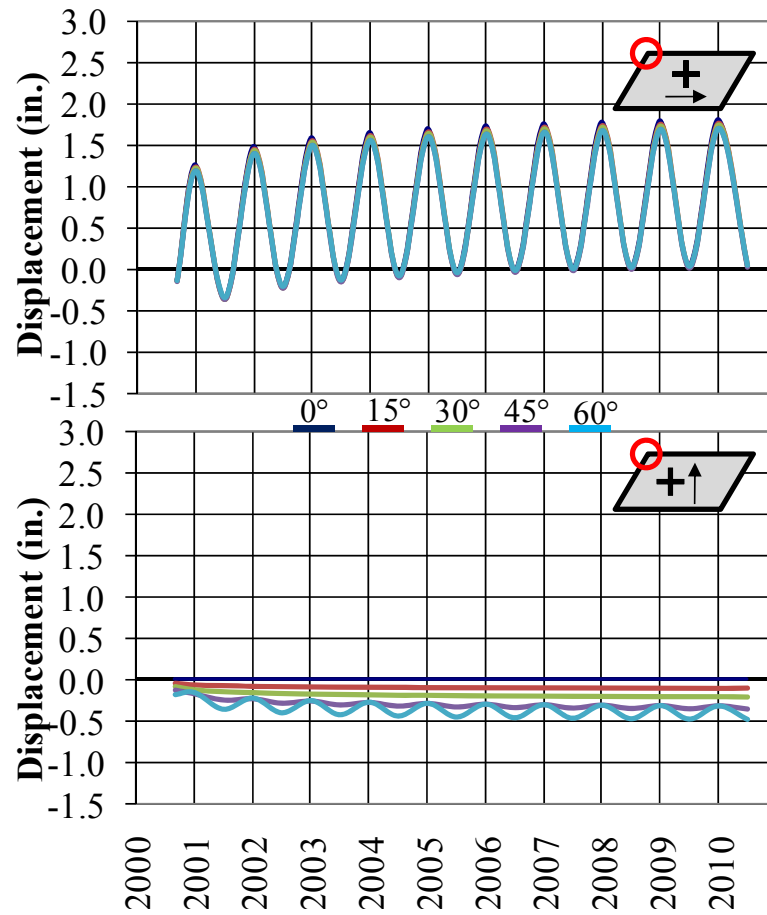
Figure 5.18: Effect of Skew (800 ft – Obtuse Corner)
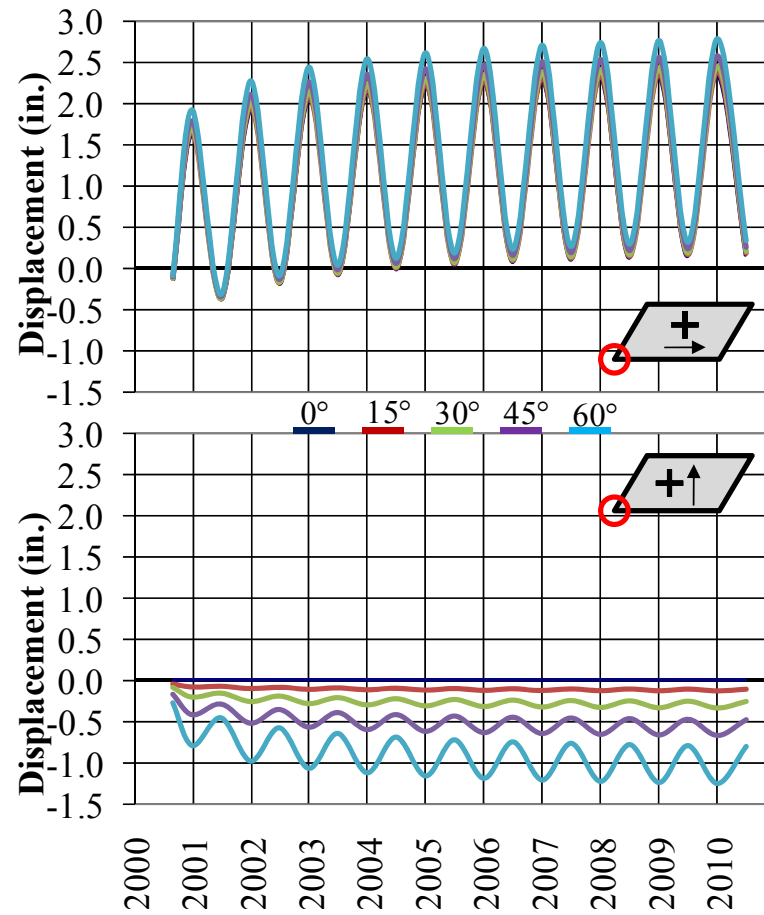
Figure 5.19: Effect of Skew (1000 ft – Acute Corner)
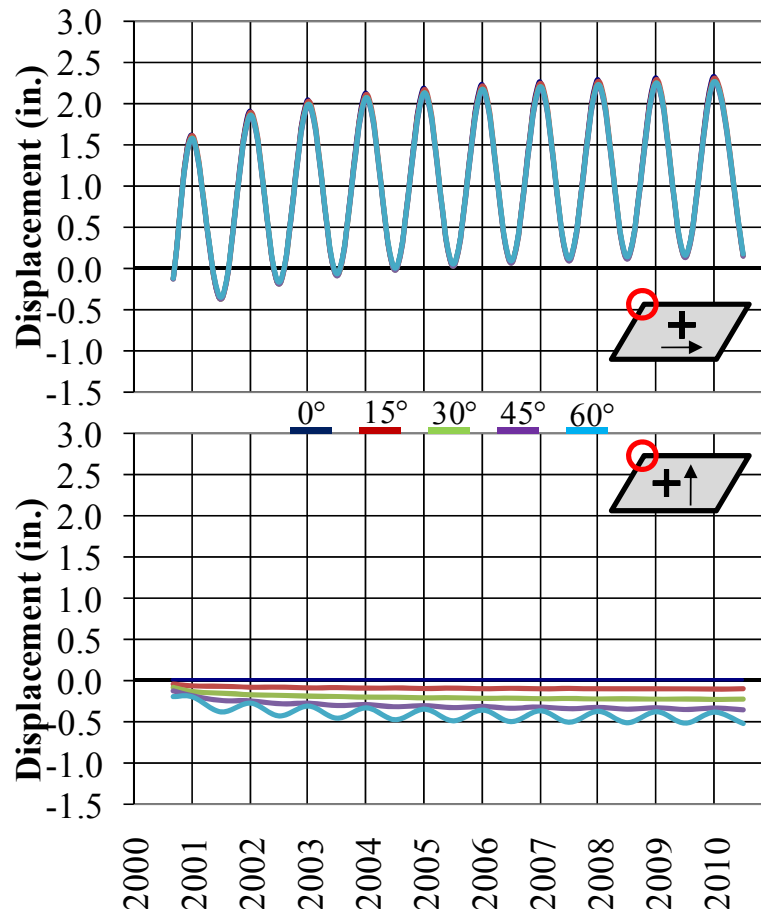
Figure 5.20: Effect of Skew (1000 ft – Obtuse Corner)

Table 5.14: Ultimate Deflection in Longitudinal Direction

Skew Angle	Longitudinal Deflection (in.)				
	Length of Structure (ft)				
	200	400	600	800	1000
0°	0.24	0.74	1.28	1.81	2.34
15°	0.32	0.81	1.33	1.86	2.39
30°	0.41	0.89	1.41	1.93	2.46
45°	0.55	1.02	1.52	2.04	2.57
60°	0.76	1.23	1.74	2.25	2.78

Table 5.15: Ultimate Deflection in Transverse Direction

Skew Angle	Transverse Deflection (in.)				
	Length of Structure (ft)				
	200	400	600	800	1000
0°	0.00	0.00	0.00	0.00	0.00
15°	-0.11	-0.13	-0.13	-0.13	-0.14
30°	-0.30	-0.33	-0.33	-0.34	-0.34
45°	-0.62	-0.65	-0.66	-0.66	-0.68
60°	-1.15	-1.23	-1.23	-1.24	-1.26

Table 5.16: Total Ultimate Deflection

Skew Angle	Total Lateral Deflection (in.)				
	Length of Structure (ft)				
	200	400	600	800	1000
0°	0.24	0.74	1.28	1.81	2.34
15°	0.34	0.82	1.34	1.87	2.39
30°	0.51	0.95	1.45	1.96	2.48
45°	0.83	1.21	1.66	2.15	2.65
60°	1.38	1.74	2.13	2.57	3.05

Using the same method provided in Section 5.3.1 for structures with zero skew, relationships between the theoretical unrestrained demand (Equation 5.3) and the total ultimate deflection calculated by the analysis are developed for skews from 0° to 60° (Figure 5.21). As shown, the relationships for the various skews are nearly linear and have approximately the same slope as the zero skew case. The direct effects of skew, however, are not straightforward from the figure. Therefore, to illustrate the effects, Figure 5.22 and Figure 5.23 show the relationship between the analytical demand and skew for the longitudinal and transverse directions,

respectively. As shown in Figure 5.22, the longitudinal demand is dependent on both length and skew. Conversely, Figure 5.23 shows that the transverse demand is dependent on skew but essentially independent of length. To further evaluate the effects of skew in the longitudinal direction, the difference in longitudinal displacement at a given skew and that at zero skew is plotted (Figure 5.24). As shown, the difference in the longitudinal displacement is essentially independent of length.
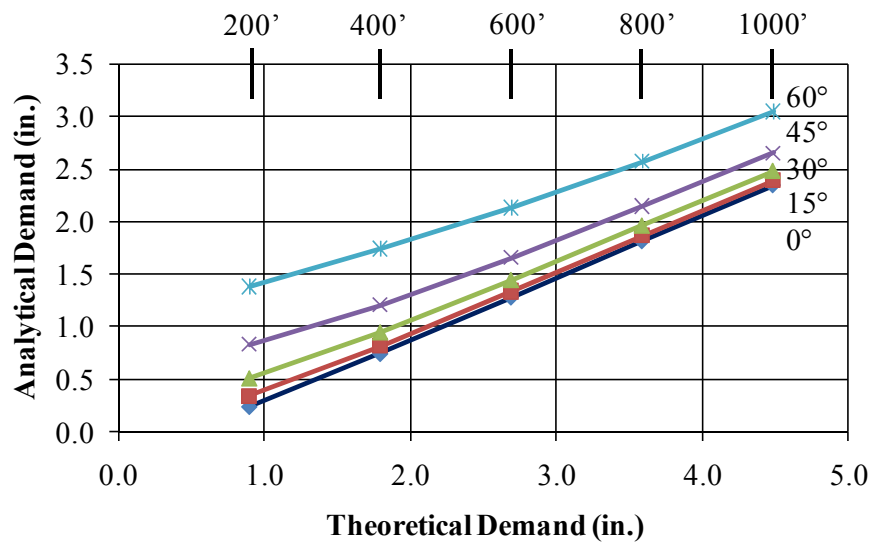
Figure 5.21: Relationship Between Theoretical and Total Ultimate Demand
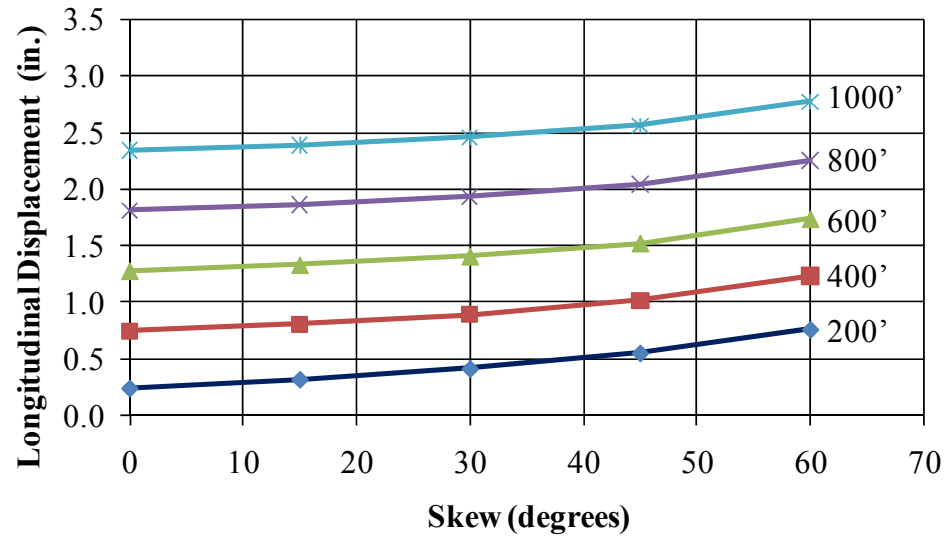
Figure 5.22: Longitudinal Demand as a Function of Skew for Various Lengths
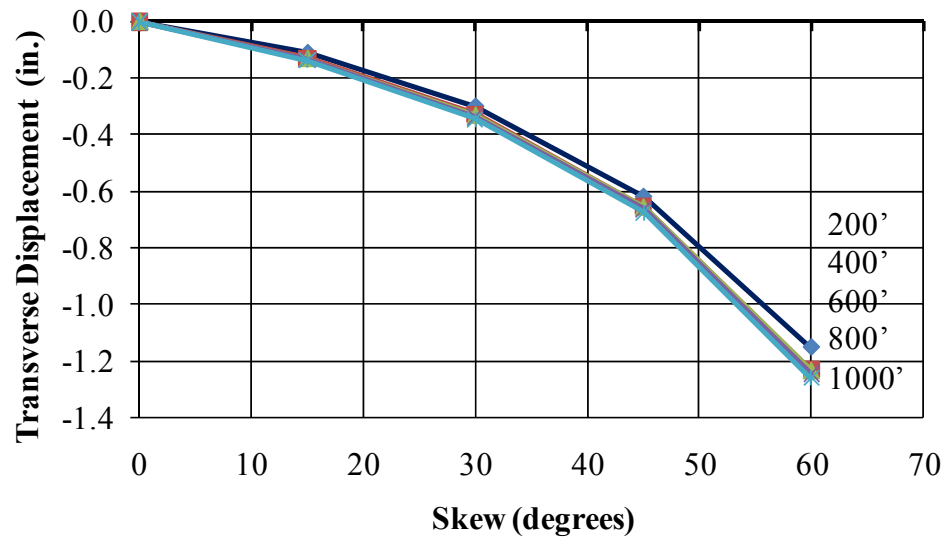
Figure 5.23: Transverse Demand as a Function of Skew for Various Lengths
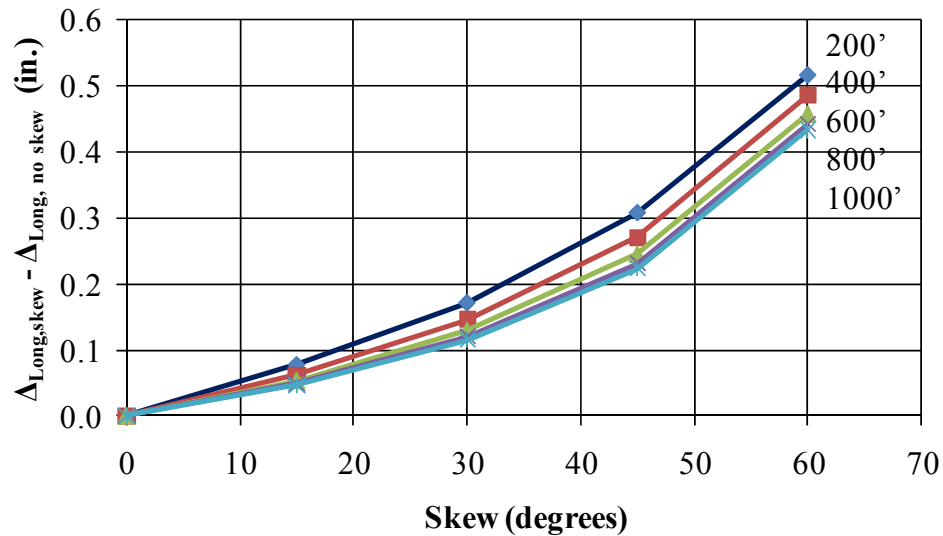
Figure 5.24: Longitudinal Demand As Caused by Skew

It is clear from Figure 5.23 and Figure 5.24 that an increase in skew angle causes an increase in the total lateral demand on supporting piles (both an increase in transverse and longitudinal demand). Two factors are attributed to the increase in demand:

- The skew of the structure causes transverse displacement (Section 3.5.3).
- The skew of the structure causes a rotation of the abutment and thus an increase in the longitudinal demand on the acute corner pile (Section 4.7.1).

However, it is also clear that the increase in demand as caused by skew is minimally affected by an increase/decrease in bridge length. Therefore, the effects of skew can be decoupled from the effects of length. A designer can then use a simplified equation for a zero skew structure and add additional deflection caused by skew to estimate both the longitudinal and transverse displacements.

Two simple bilinear approximations are developed for displacement demand in the longitudinal and transverse directions as a function of skew (Figure 5.25 and Figure 5.26). A designer can, therefore, calculate the ultimate lateral demand for the piles by determining the longitudinal and lateral components and calculating the square root of the sum of the squares. The longitudinal demand is calculated by multiplying the theoretical unrestrained demand

(Equation 5.3) by a 0.6 reduction factor (Figure 5.10) and then adding the corresponding increase in longitudinal displacement as caused by skew (Figure 5.25). The transverse demand is simply determined from Figure 5.26. It is important to note that it is unclear from this analysis alone if the reduction factor or longitudinal and transverse relationships are universal or specific to this structure. Therefore, further analyses will be conducted as part of the secondary variable investigation to provide insight regarding these relationships.
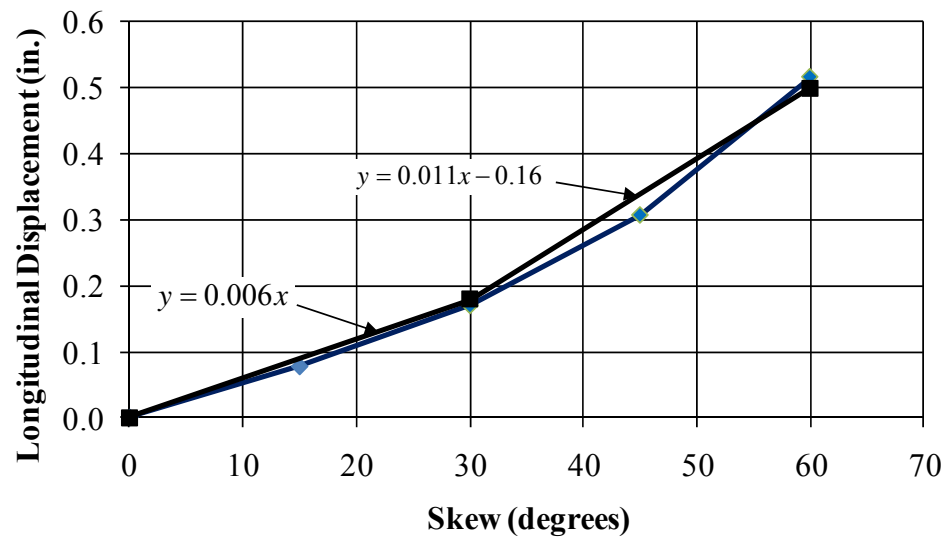
Figure 5.25: Bilinear Approximation of Longitudinal Displacement as a Function of Skew

The chart shows Transverse Displacement (in.) vs Skew (degrees), with curves labeled $y = -0.01x$ and $y = -0.03x + 0.6$.
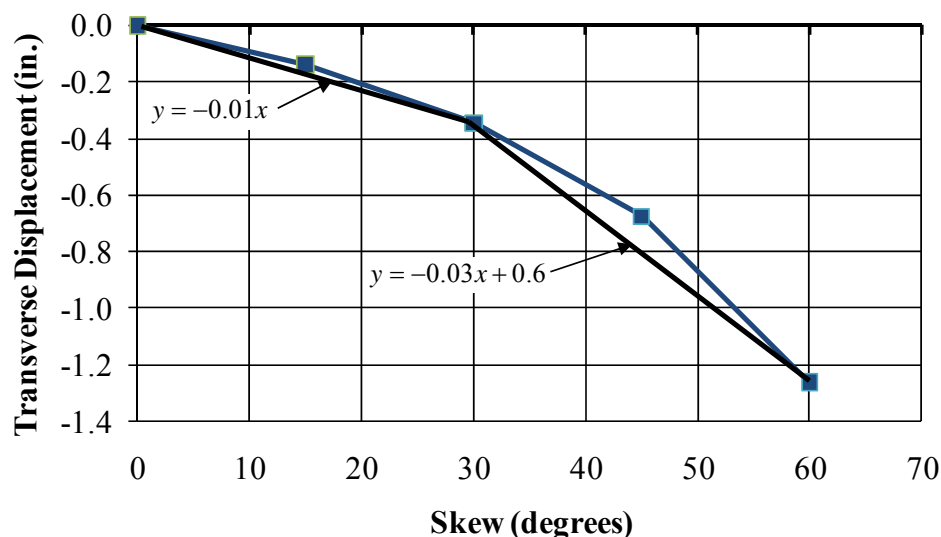
Figure 5.26: Bilinear Approximation of Transverse Displacement as a Function of Skew

5.3.3. EFFECT OF SPAN LENGTH

To understand if the span length has an effect on the demand deflection for supporting piles of integral abutment bridges, three span lengths were investigated for a structure with a total length of 400 ft: 50, 100, and 200 ft. The 100 ft span length serves as a reference length to the previous analysis of length and skew. Each span was analyzed for the five skew values. To represent the intermediate piers, the support conditions were assumed to behave as rollers. Therefore, at these locations the structure was restrained in the z-direction (vertical) and allowed to move for the other degrees of freedom. To load the structure, a single load increment was applied to the superstructure representing the ultimate long-term demand. The girders were loaded with -247.5 με to represent a negative temperature differential of 45 °F. The concrete deck was loaded with -747.5 με to represent the same negative 45 °F temperature differential and 500 με of shrinkage. Because it has been shown that the acute corner is the controlling location for lateral displacement demand, only the results for the acute corner at the base of the abutment are provided. Figure 5.27 and Figure 5.28 show the longitudinal and transverse displacement demands for the various span lengths.
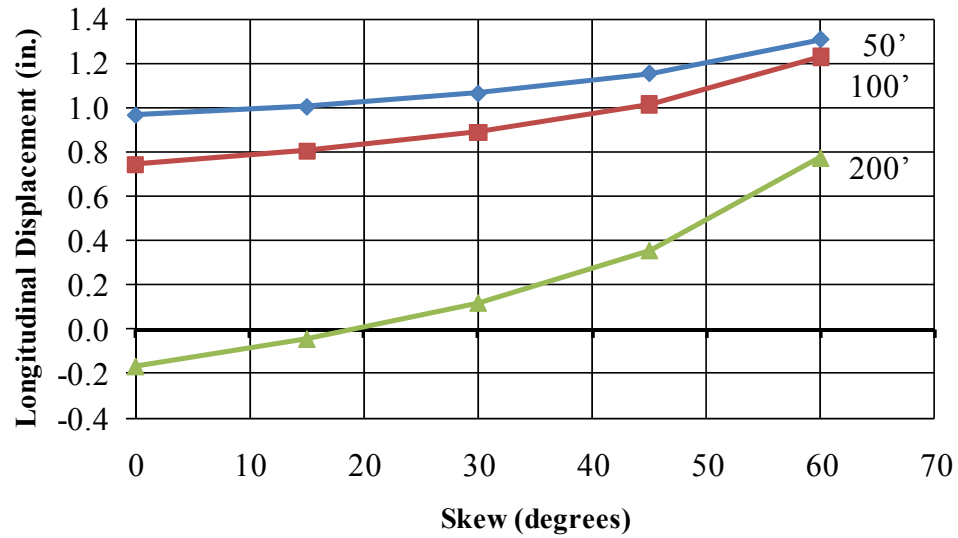
Figure 5.27: Effect of Span Length for Longitudinal Displacement
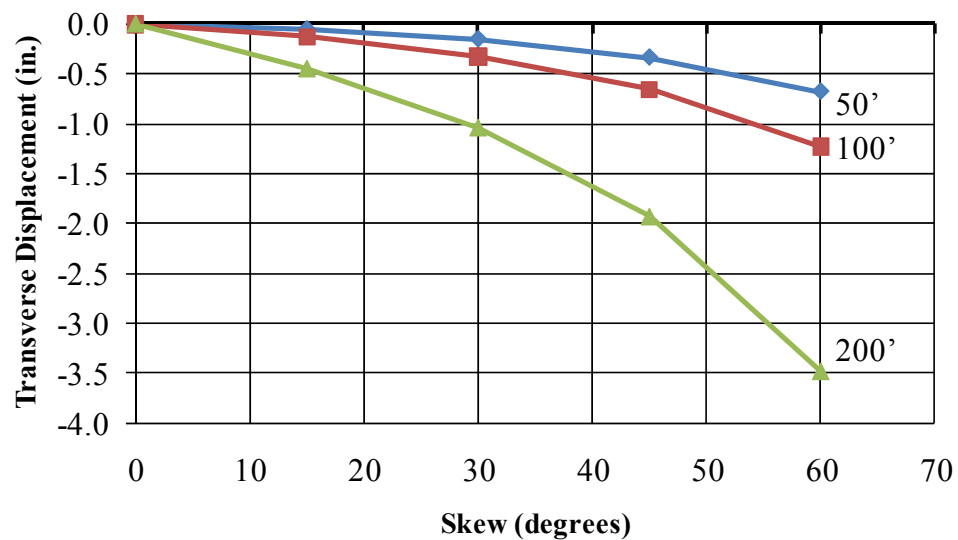
Figure 5.28: Effect of Span Length for Transverse Displacement

As would be expected, as the span length decreases the flexural stiffness of the superstructure increases which reduces the effect of skew in the transverse direction. However, the behavior in the longitudinal direction is not straight forward. For instance, it is not intuitive why the 200 ft span length causes expansion as opposed to the other span length. To illustrate

this behavior, the longitudinal displacement for the top of the abutment is plotted in Figure 5.29. As shown, the 200 ft bridge actually displaces more (contraction) than the shorter span lengths at the top of the abutment in the longitudinal direction. Therefore, as the span length increases, the flexural stiffness of the span is reduced and rotation of the abutment increases. This behavior may be attributed to the fact that the superstructure was not designed for 200' span lengths. For 200 ft spans, deeper girders would be required as the girders used are more typical for 100 ft. In fact, for the 50 ft spans, shallower girders could be used which would increase rotation relative to those presented here. For the lower span lengths, the rotation is greatly reduced and similar displacements are recorded even though the spans are different. In the same way, the transverse displacement at the top of the abutment (Figure 1.1Figure 5.30) is greatly exaggerated for the less stiff 200 ft span. Therefore, it is assumed that this severe rotation of the abutment is a phenomenon of this parametric analysis and the selected superstructure (superstructure constant in all cases). For actual structures built in the field, the superstructure would be stiff enough to minimize rotation.
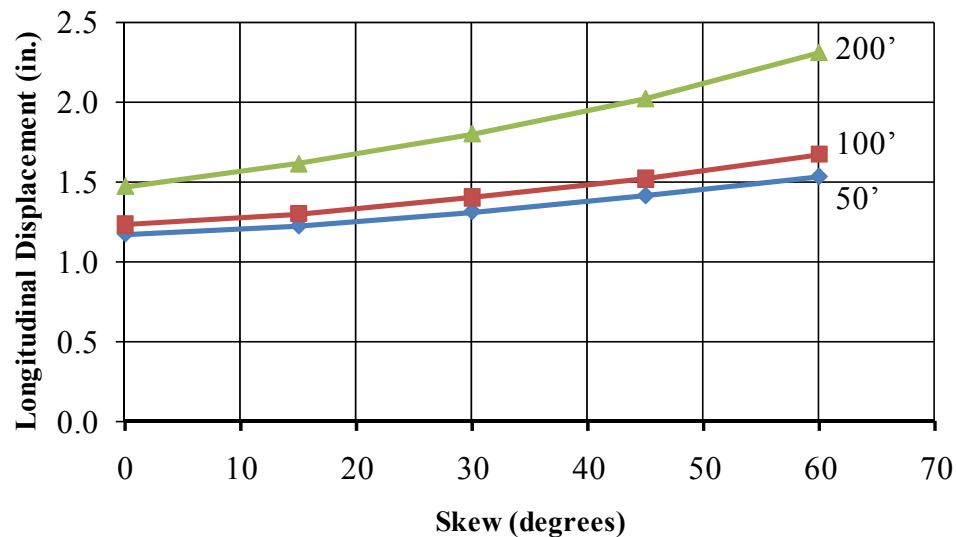
Figure 5.29: Effect of Span Length for Longitudinal Displacement for Top of Abutment
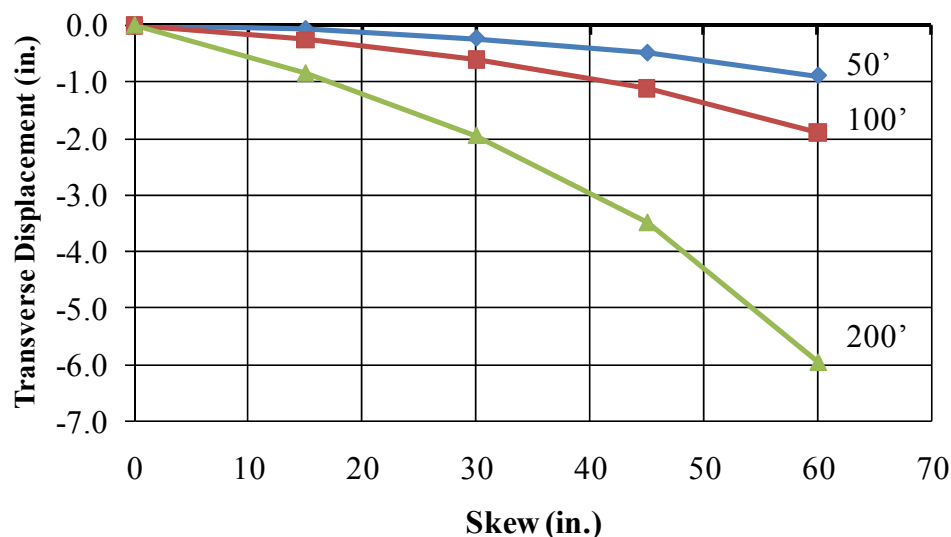
Figure 5.30: Effect of Span Length for Transverse Displacement for Top of Abutment

When comparing Figure 5.27 and Figure 5.28, it is clear that both the calculated longitudinal and transverse deflections are close for the 50 and 100 ft spans. It should also be noticed that the when the displacement components are combined to determine the total lateral demand (Figure 5.31), the calculated values are very similar. Therefore, it can be concluded for the structures with 50 ft and 100 ft spans, the effect of the span length is negligible. The structure with 200 ft spans has a much greater demand for high skews because of the increased abutment rotation allowed by this structure. However, typical spans are in the range of 50-120 ft. Therefore, it is assumed that the span length, within reason, does not have a significant effect on the total demand on the pile and does not impact the reduction factor (Section 5.3.1) or bi-linear approximations for the effect of skew (Section 5.3.2).
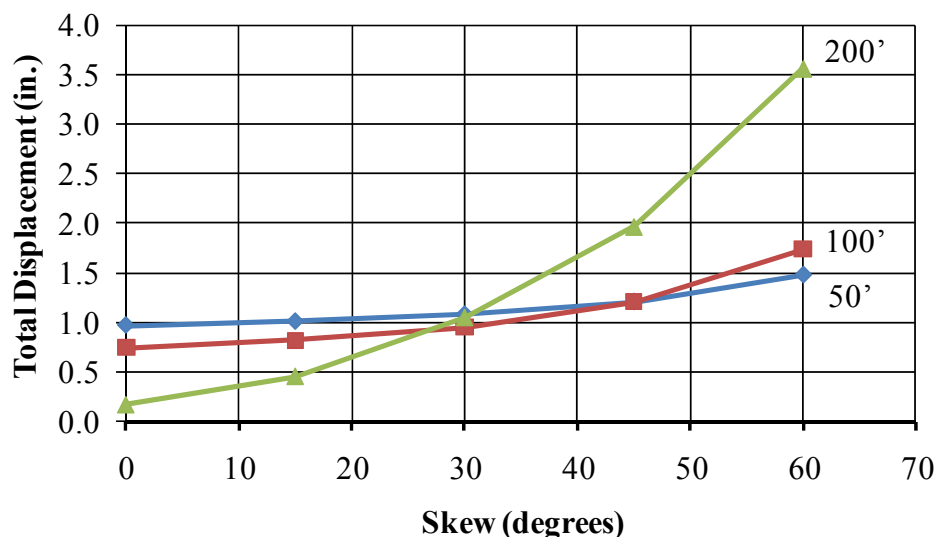
Figure 5.31: Total Demand Deflection for Piles for Various Span Lengths

5.3.4. EFFECT OF TEMPERATURE

The results of the investigation on the effects of various temperature differentials are discussed. For the five skews considered (Table 5.1), a 400 ft structure was subjected to the temperature differentials in Table 5.2, and the deck was subjected to 500 µε of shrinkage. Case A contains two temperature differentials and Case B through Case E each contains one. Therefore six different temperature differentials were investigated. Three values were positive to represent a structure being constructed in cold weather and experiencing thermal expansion. For example, a scenario can be assumed for Case B where a bridge was constructed in the winter with the construction temperature being 20 °F (the average annual lowest temperature). If the average highest annual temperature for the scenario of Case B is 90 °F, then the structure has a positive temperature differential of 70 °F. Therefore, the structure will experience only thermal expansion from the date of construction. In contrast, three values were negative to represent a structure built in hot weather and experiencing thermal contraction. Temperature differentials from -90 °F to +90 °F were chosen to represent a large range of possible temperatures.

Figure 5.32 and Figure 5.33 show the displacement demand for longitudinal and transverse displacements as a function of thermal loading, respectively. It is important to note that the magnitudes of the movement in the contraction direction are higher. This direction (contraction) is the controlling direction due to the effect of shrinkage always acting in that

direction. To design these structures, therefore, it is important to determine the maximum negative temperature differential for the region and use that for design. It is clear that both the longitudinal and transverse demand displacements are affected by temperature.   In the longitudinal direction, an increase in the negative temperature differential results in an increase in demand displacement. The additional demand, as cause by skew, is a result of abutment rotation as previously described (Section 5.3.2). In the transverse direction, it appears that structures with less than 30° skew, there is minimal effect of temperature. For structures with skew, the transverse displacement is primarily caused by shrinkage. The application of shrinkage also explains the calculated displacement with zero temperature differentials.   For different assumptions of ultimate shrinkage, the offset would be different. However, it is assumed that 500$\mu\varepsilon$ is an acceptable number for use in Indiana. For skews greater than 30°, an increase in the negative temperature differential causes an increased demand.

The fact that an increase in thermal loading causes an increase in demand in both the transverse and longitudinal directions is reasonable because the demand imposed on the piles is caused by temperature and shrinkage. However, it is important to determine if the previously developed reduction factor and bilinear approximations are sufficient for all temperature ranges. The simplified method presented in Section 5.3.2 was developed for a -45 °F temperature differential and 500 $\mu\varepsilon$ of shrinkage and is shown to be appropriate for skews up to 60°.   The method is also known to be accurate for zero skewed structures for any temperature loading.
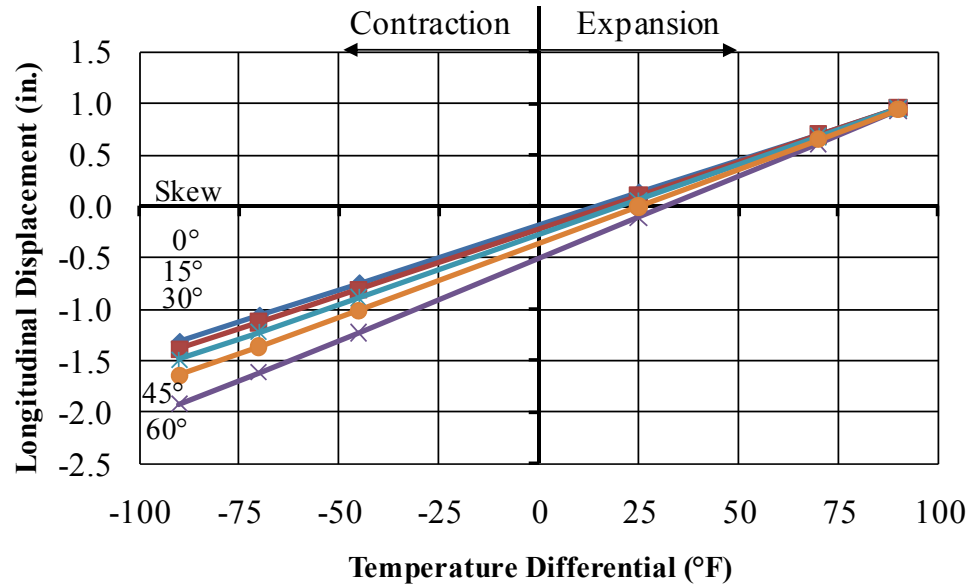
Figure 5.32: Effect of Temperature Differential in Longitudinal Direction
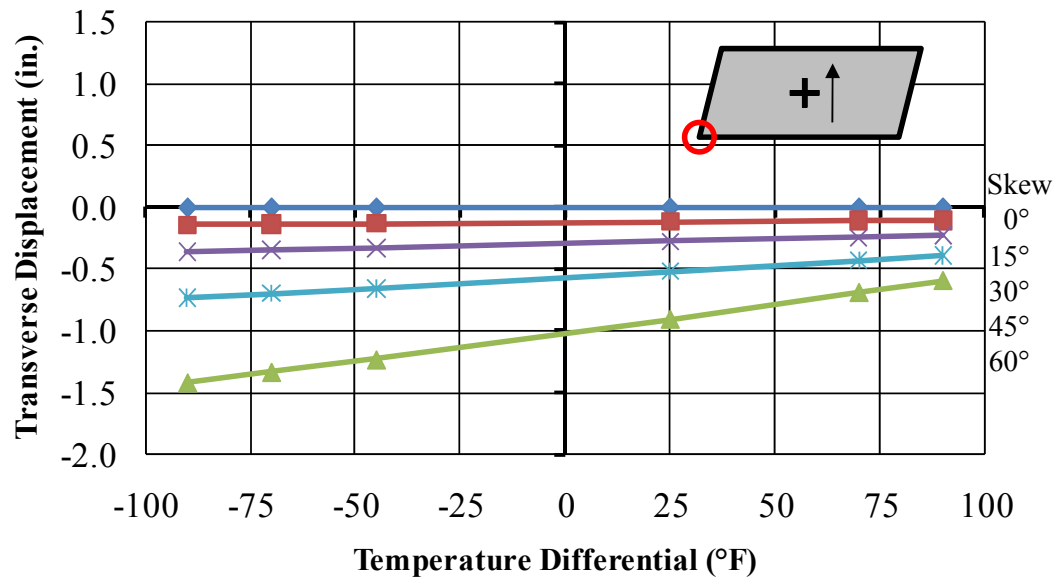
Figure 5.33: Effect of Temperature Differential in Transverse Direction

To determine if the reduction factor and bilinear approximations are sufficient for skewed structures at any temperature differential for both the longitudinal and transverse directions, the differences between the skewed displacement values and the zero skewed displacement values are shown for the -45 °F, -70 °F, and -90 °F temperature differentials (Figure 5.34 and Figure 5.35).

The negative temperature differentials in this range are those that practically will control these structures because the negative temperature differentials work in tandem with shrinkage. As shown, for skews less than 45°, the difference as caused by an increase in thermal demand is negligible for both the longitudinal and transverse displacement demand. For structures with 60° skew the difference becomes slightly larger: approximately 0.1 in. and 0.2 in. between the -45 °F and -90 °F curves for longitudinal and transverse directions, respectively.
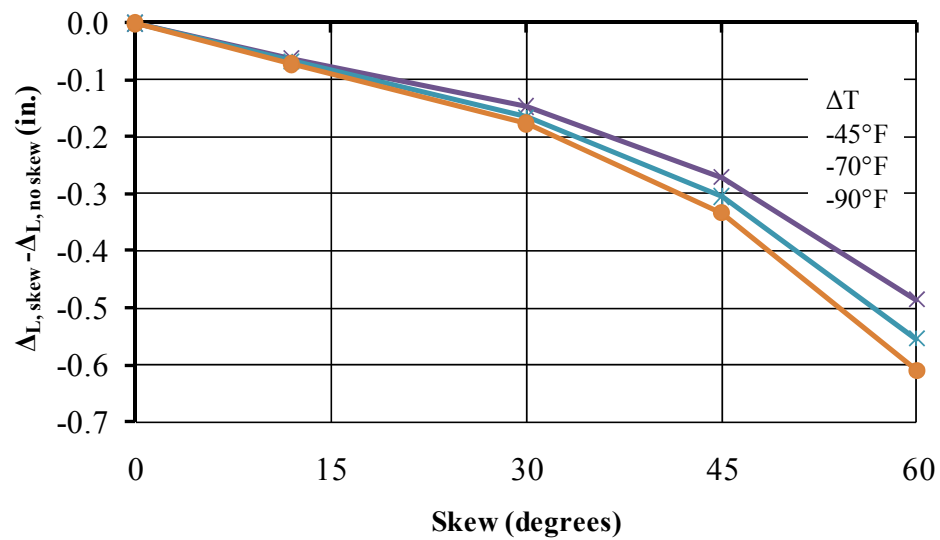
Figure 5.34: Effect of Increase in Negative Temperature Differential on Longitudinal Displacement Demand
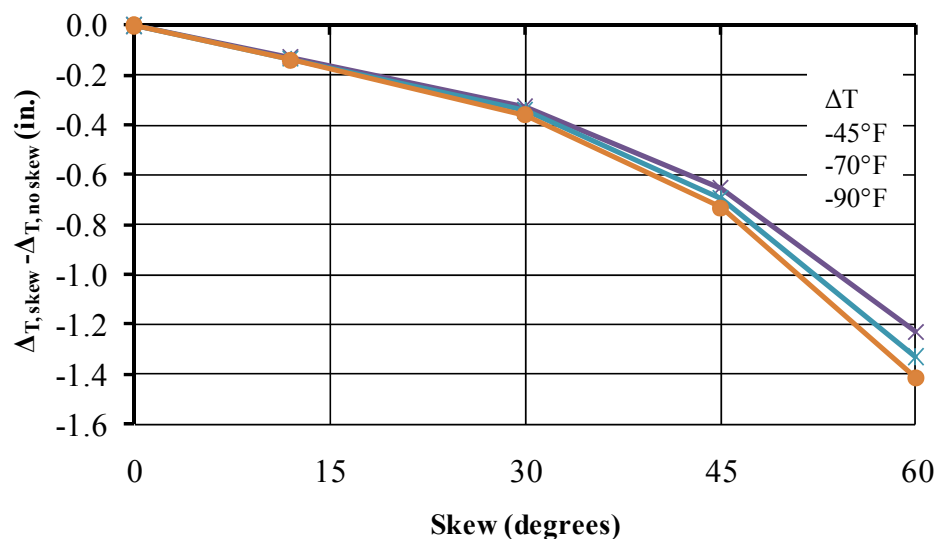
Figure 5.35: Effect of Increase in Negative Temperature Differential on Transverse Displacement Demand

To account for the increase displacement in both the longitudinal and transverse directions for structures with skew and temperature differentials other than -45 °F, additional factors can be added to the simplified calculation procedure.   According to Figure 5.32 and Figure 5.33, the increase in displacement in both the longitudinal and transverse directions is linear for a given skew. To confirm that the linear relationships shown in Figure 5.32 and Figure 5.33 applies to structural lengths other than 400 ft, analytical models were used to calculate the increase in longitudinal and lateral demand for structural lengths of 600, 800, and 1000 ft subjected to temperature differentials of -45°F and -90°F.   The results, shown in Table 5.17 and Table 5.18, reveal that the increase in displacement demand for both the longitudinal and transverse directions as caused by skew is virtually independent of length for a given temperature differential. Therefore, the linear behavior shown in Figure 5.32 and Figure 5.33 can be utilized to determine linear adjustments to the lateral demand of piles for any length of structure.

Table 5.17: Increase in Longitudinal and Transverse Displacement as Caused by Skew for Various Lengths of Structures (-45°F)

Skew (deg)	Total Structural Length (ft)							
	400		600		800		1000	
	$\Delta_{(L,T),skew} - \Delta_{(L,T),no\ skew}$ (in.)							
	Δ_L	Δ_T	Δ_L	Δ_T	Δ_L	Δ_T	Δ_L	Δ_T
0	0.00	0.00	0.00	0.00	0.00	0.00	0.00	0.00
15	-0.06	-0.13	0.05	-0.13	0.05	-0.13	0.05	-0.14
30	-0.15	-0.33	0.13	-0.33	0.12	-0.34	0.12	-0.34
45	-0.27	-0.65	0.24	-0.66	0.23	-0.66	0.22	-0.67
60	-0.49	-1.23	0.46	-1.23	0.44	-1.24	0.43	-1.26

Table 5.18: Increase in Longitudinal and Transverse Displacement as Caused by Skew for Various Lengths of Structures (-90°F)

Skew (deg)	Total Structural Length (ft)							
	400		600		800		1000	
	$\Delta_{(L,T),skew} - \Delta_{(L,T),no\ skew}$ (in.)							
	Δ_L	Δ_T	Δ_L	Δ_T	Δ_L	Δ_T	Δ_L	Δ_T
0	0.00	0.00	0.00	0.00	0.00	0.00	0.00	0.00
15	-0.14	-0.14	0.07	-0.14	0.07	-0.14	0.06	-0.15
30	-0.36	-0.36	0.17	-0.36	0.16	-0.37	0.15	-0.39
45	-0.73	-0.73	0.31	-0.74	0.30	-0.76	0.29	-0.78
60	-1.41	-1.41	0.59	-1.44	0.58	-1.47	0.58	-1.51

To determine an adjustment factor for longitudinal displacement demand to account for temperature differentials other than -45°F, the slope of each curve in Figure 5.32 was determined as a function of skew. This was accomplished by dividing the difference of the calculated longitudinal displacement for a temperature differential of -45°F and the calculated longitudinal displacement for a temperature differential of -70°F by 25°F (the difference between the two temperatures). The calculated slope value was subtracted from the slope of the zero skew line. A bi-linear curve was fit to the results and is shown in Figure 5.36. The same procedure was followed for the transverse direction and the results are shown in Figure 5.37. The bi-linear

curves, therefore, can be used to determine the change in longitudinal and transverse displacement as shown in Equation 5.4 through Equation 5.7 for temperature differentials different from -45°F.
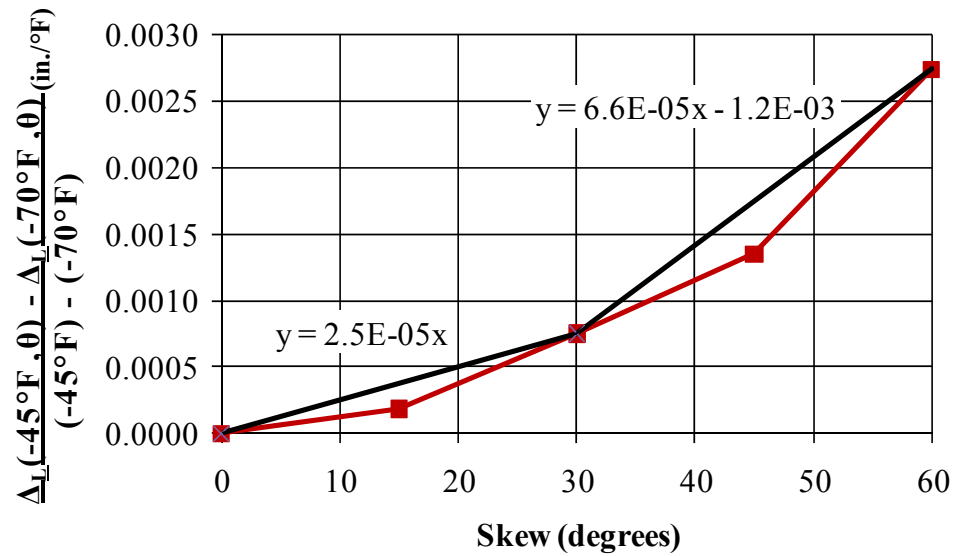
Figure 5.36: Slope of Increased Longitudinal Displacement as a Function of Skew
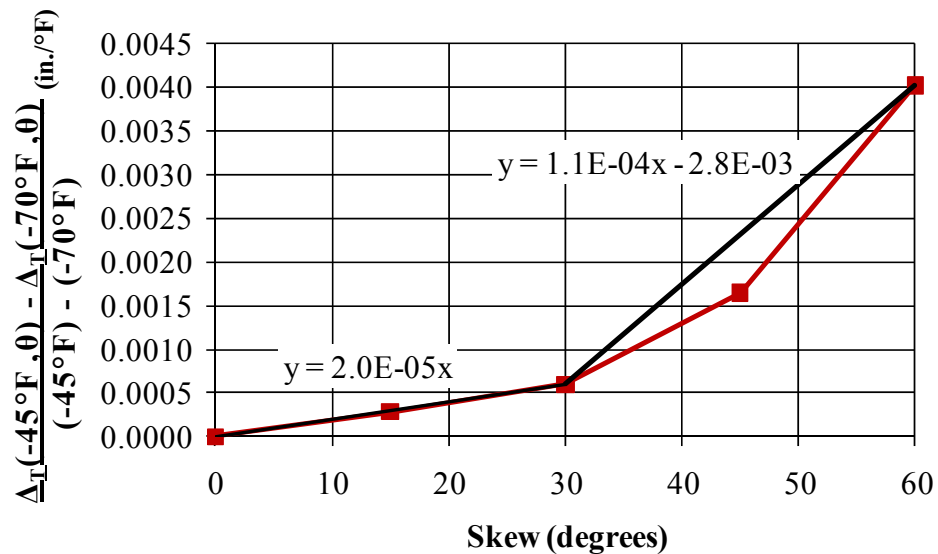
Figure 5.37: Slope of Increased Transverse Displacement as a Function of Skew

Increase in longitudinal displacement due to temperature differential:

For skews $0 \le \theta \le 30°$:

$$\Delta_{L\Delta T} = (2.5 \cdot 10^{-5} \theta)(\Delta T - 45°F) \qquad (5.4)$$

For skews $30 \le \theta \le 60°$:

$$\Delta_{L\Delta T} = (6.6 \cdot 10^{-5} \theta - 1.2 \cdot 10^{-3})(\Delta T - 45°F) \qquad (5.5)$$

where:

$\Delta_{L\Delta T}$ = increase in longitudinal direction due to temperature differential, in.

θ = skew, degrees

ΔT = negative temperature differential as a positive value, °F

Increase in transverse displacement due to temperature differential:

For skews $0 \le \theta \le 30°$:

$$\Delta_{T\Delta T} = (2.0 \cdot 10^{-5} \theta)(\Delta T - 45°F) \qquad (5.6)$$

For skews $30 \le \theta \le 60°$:

$$\Delta_{L\Delta T} = (1.1 \cdot 10^{-4} \theta - 2.8 \cdot 10^{-3})(\Delta T - 45°F) \qquad (5.7)$$

where:

$\Delta_{T\Delta T}$ = increase in longitudinal direction due to temperature differential, in.

θ = skew, degrees

ΔT = negative temperature differential as a positive value, °F

5.3.5. EFFECT OF SHRINKAGE MODELS

The influence of various shrinkage models was investigated. For this analysis, a single 400 ft structure with zero skew was investigated. Temperature strains from Case A were applied to the concrete deck and girders. Three separate shrinkage models were used to determine strains that were applied to the concrete deck. Figure 5.38 show the results of the analytical model over the 10 years period for the CEB MC90, ACI 209, and GL2000 shrinkage models. As can be seen,

the different shrinkage models have minimal effect. The ultimate displacement changes slightly as expected due to changes in the ultimate shrinkage provided by the different models. Also, the time which is required to reach steady state cycling is different depending on which model is used, as the different models predict different rates of shrinkage. On the whole, varying the shrinkage model does not have a significant effect on behavior. The European model (CEB MC90) is considered as the baseline because it was shown to best fit the actual in-service behavior of integral abutment structures (Chapter 3). Therefore, this model will be considered to best represent the long-term behavior of integral abutment bridges.
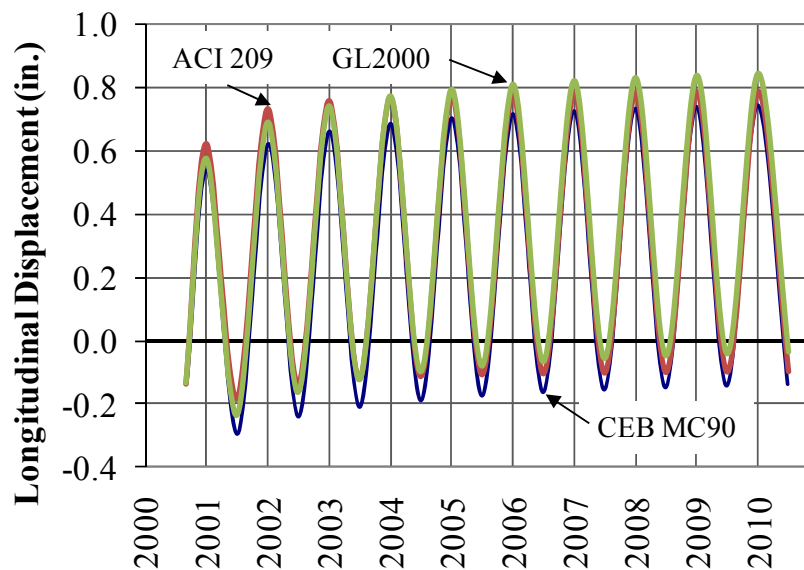
Figure 5.38: Effect of Shrinkage Prediction Models

5.3.6. EFFECT OF PILE SECTION AND ORIENTATION

To evaluate the influence of the pile section and pile orientation, two series of analyses were conducted. The initial analysis consisted of nine separate analyses. Three 400 ft structures with skews equal to 0, 30, and 60° were each analyzed with three different pile sections: default section (CFT14x0.312", I = 507 in.[4]), HP14x117 oriented strong axis (I = 1220 in.[4]), and HP10x42 oriented weak axis (I = 71.1 in.[4]). The two HP sections provide maximum and minimum stiffness values, and the CFT provides comparison with the previous analyses. Figure

5.39 through Figure 5.43 illustrate the results. As can be seen, the demand deflection for each structure is relatively independent of the pile section for all skew angles in both the longitudinal and transverse directions.
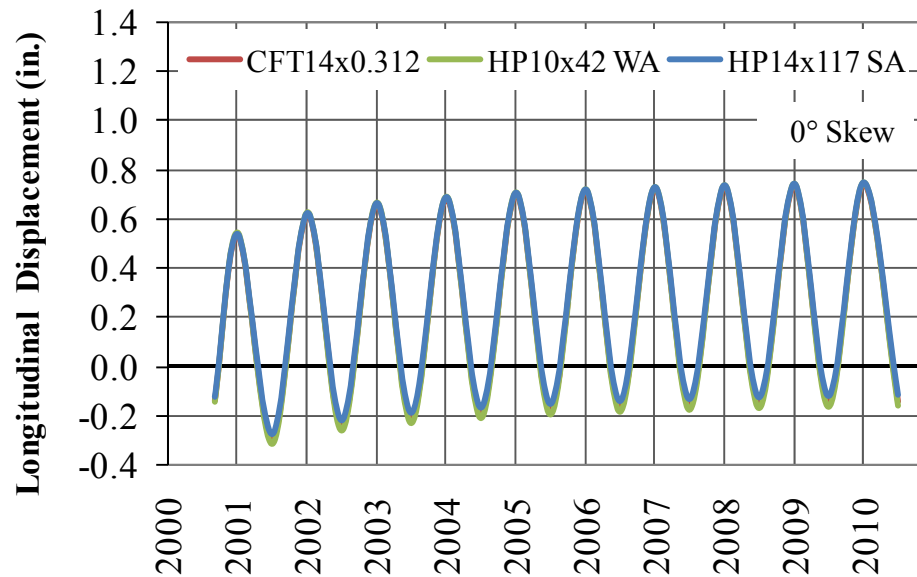
Figure 5.39: Effect of Pile Section for Structures with Zero Skew (Longitudinal Direction)
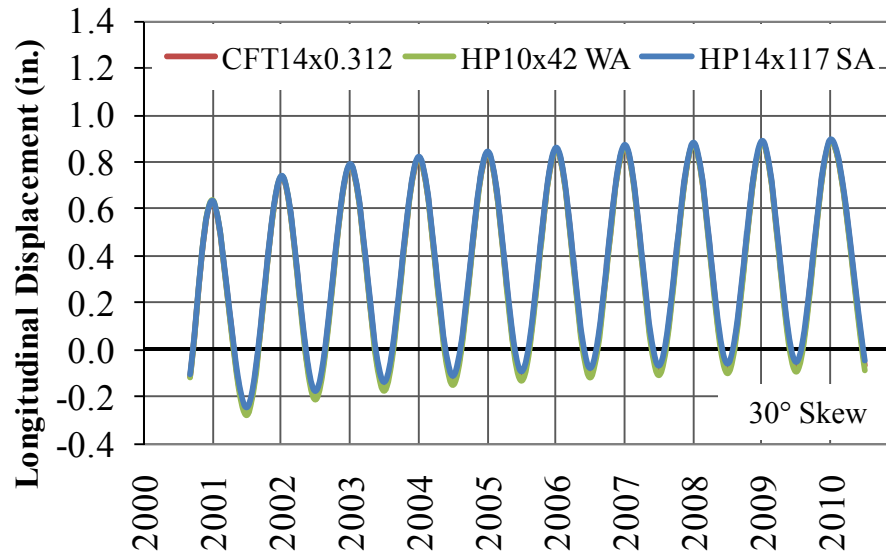
Figure 5.40: Effect of Pile Section for Structures with 30° Skew (Longitudinal Direction)
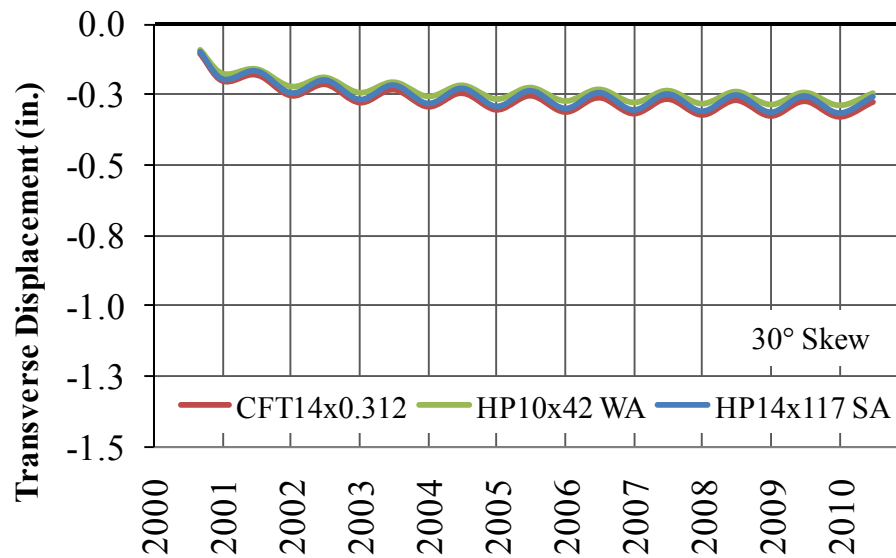
Figure 5.41: Effect of Pile Section for Structures with 30° Skew (Transverse Direction)
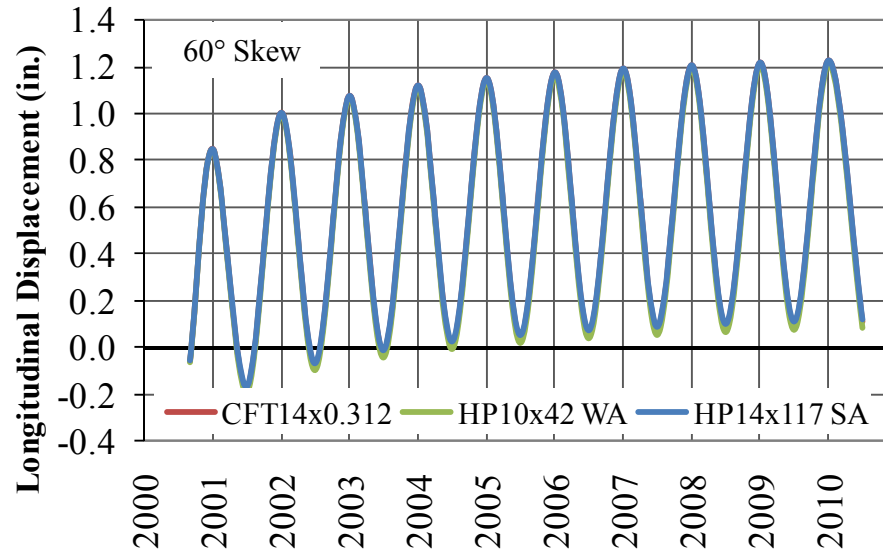
Figure 5.42: Effect of Pile Section for Structures with 60° Skew (Longitudinal Direction)
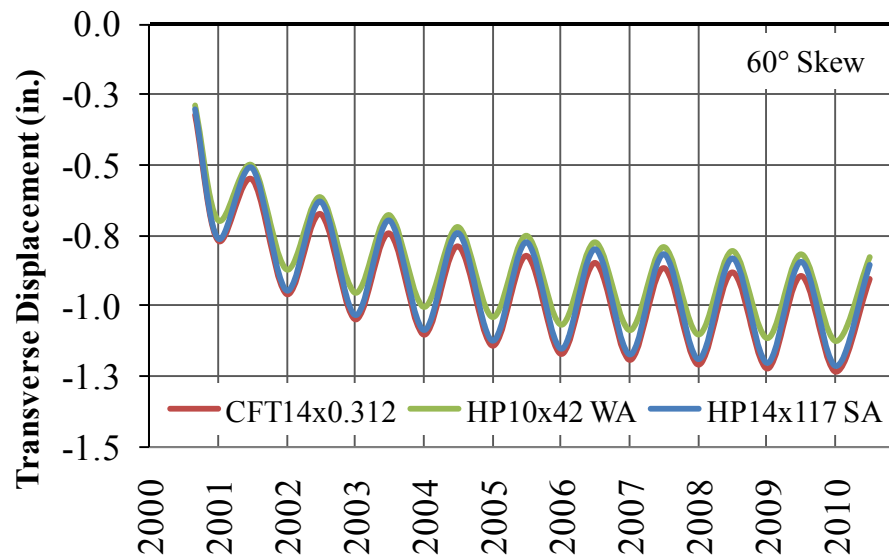
Figure 5.43: Effect of Pile Section for Structures with 60° Skew (Transverse Direction)

To investigate the effect of pile orientation, a single pile (HP14x117, which is also the stiffest) was chosen for two separate skew angles (30° and 60°). For each structure, an analysis was conducted for the pile in four separate orientations as shown in Figure 5.3. The results for

the eight analyses are shown in Figure 5.44 through Figure 5.47. As shown, the longitudinal displacements are independent of the orientation of the piles. However, the out-of-plane (transverse) displacements have some dependence. In general, the ultimate demand displacement at the end of ten years is approximately the same, but the annual amplitude of movement is different. Overall, it appears that the influence of the orientation of the pile is not significant. Therefore, it is advantageous to orient the pile in a manner to incur the least possible stresses, which is weak axis perpendicular to the centerline of the structure. This pile orientation also provides the lowest annual amplitude of response.
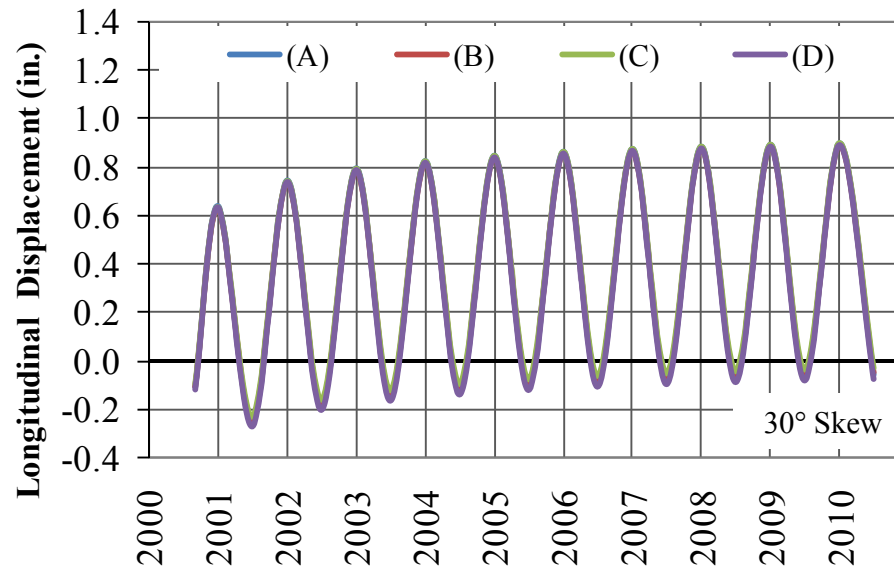
Figure 5.44: Effect of Pile Orientation for Structures with 30° Skew (Longitudinal Direction)
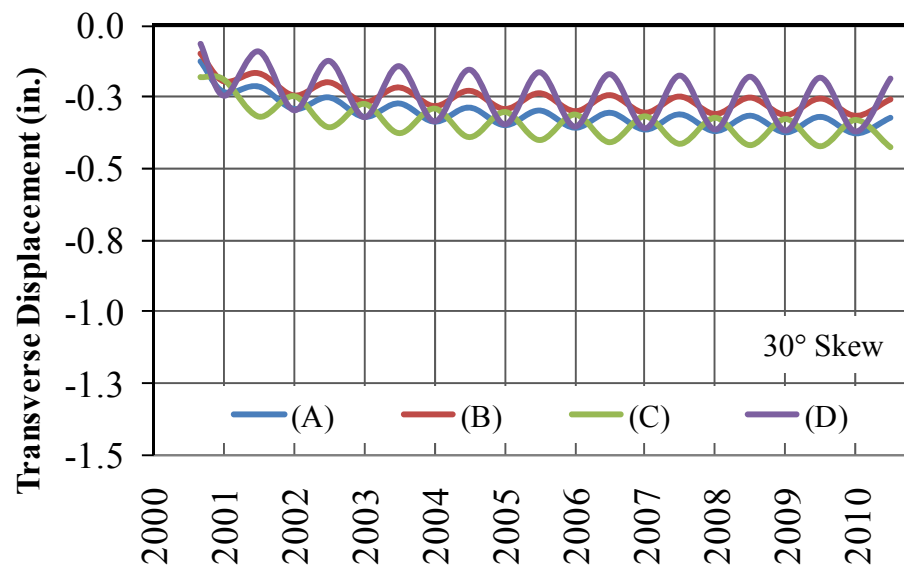
Figure 5.45: Effect of Pile Orientation for Structures with 30° Skew (Transverse Direction)
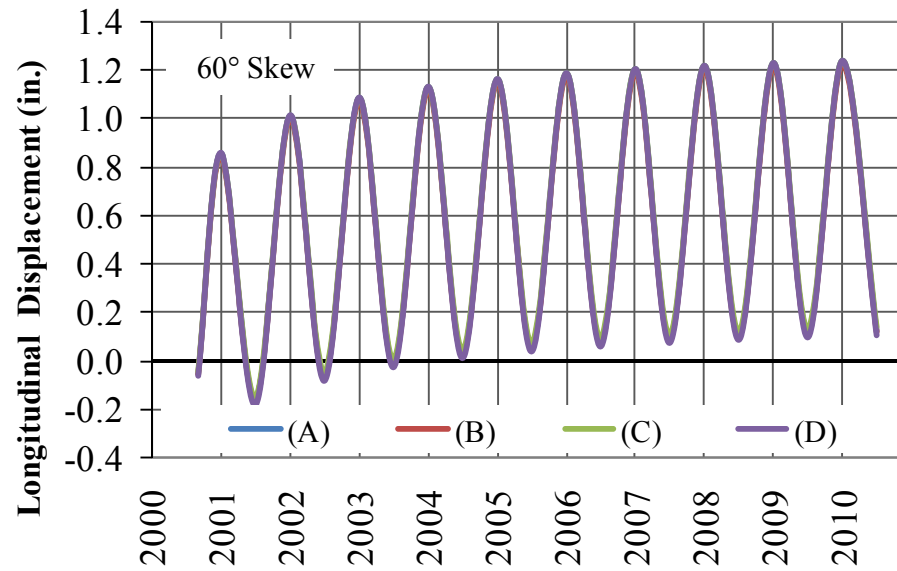
Figure 5.46: Effect of Pile Orientation for Structures with 60° Skew (Longitudinal Direction)
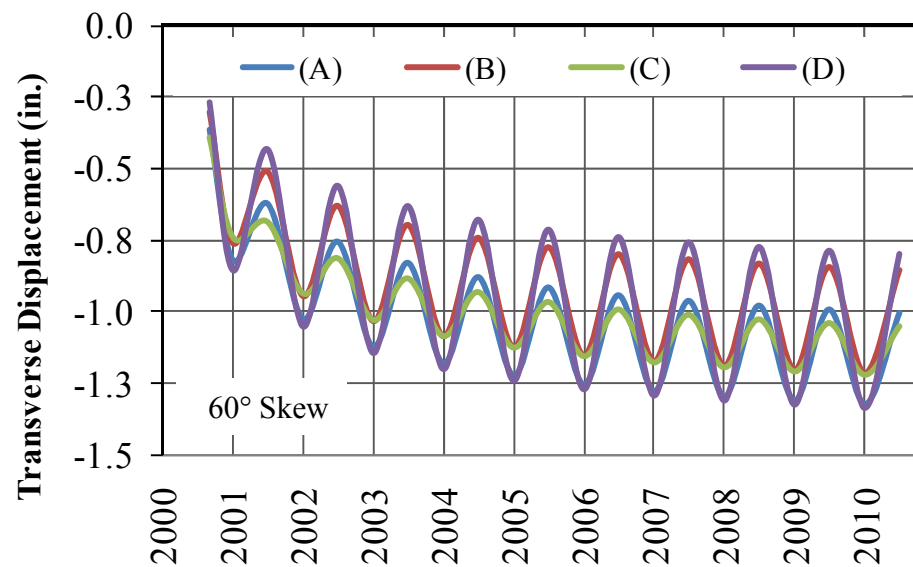
Figure 5.47: Effect of Pile Orientation for Structures with 60° Skew (Transverse Direction)

5.3.7. EFFECT OF SOIL STIFFNESS

A 400 ft structure with zero skew was analyzed for five separate soil conditions (Table 5.7) to determine the effect of soil stiffness for the supporting piles. The soils included constituted a wide range from soft clays to dense sands as well as a case with no soil surrounding the piles with fixity at 40 ft. Figure 5.48 shows the calculated longitudinal displacement for the various soil conditions. As shown, there is minimal difference in the calculated values.

The same soil conditions were also used to analyze a 400 ft structure for both 30 and 60° skews. Besides considering soil springs over the length of the piles, two separate cases were considered. The first provided no springs along the depth of the pile with fixity at 40 ft (No Soil 40'). The second also provided no springs along the depth of the pile, but a point of fixity was provided at 20 ft (No Soil 20') which is consistent with twice the estimated depth of inflection (Chovichien 2004) for soft soil. As shown in Chapter 3, very reasonable analysis results can be obtained by removing the pile springs and providing a fixed condition at twice the depth of inflection.

Figure 5.49 through Figure 5.52 show the calculated longitudinal and transverse displacement. Similar to the zero skew case, there is minimal effect of soil stiffness on the calculated longitudinal displacement. This finding is true for all cases except that of No Soil 40' illustrating that there is need to provide fixity coincident with twice the depth of inflection. The transverse displacement, on the other hand, is shown to be dependent on the soil stiffness. For cases with skew, using no pile springs over the full length of the pile greatly over-estimates the deflection. However, by fixing the pile at twice the depth of inflection, the calculation produces results similar to those provided by the loose sand case. The stiffer the soil, the less transverse displacement occurs. Because the simplified method used to calculate the total lateral demand imposed on the pile is based on loose sand, it considered appropriate to use the reduction factor and the bilinear curves previously illustrated in Section 5.3.2 for all soil stiffnesses.
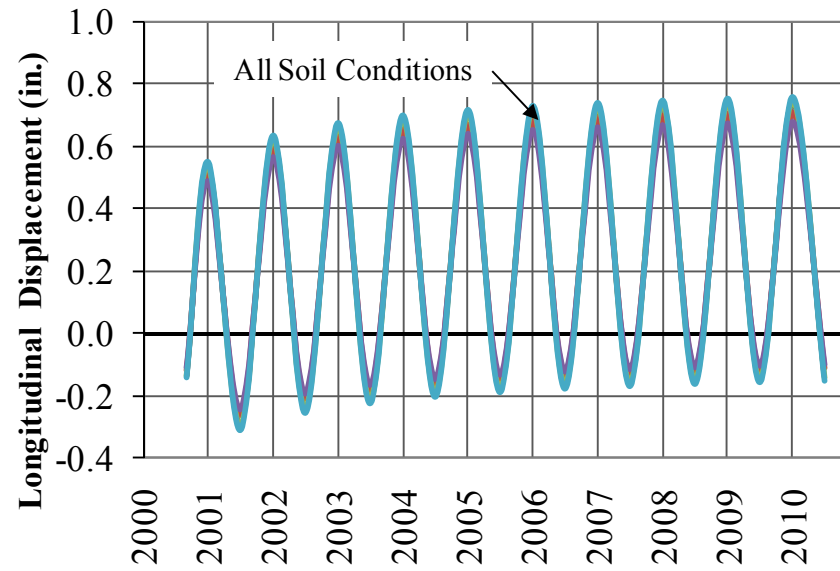
Figure 5.48: Effect of Soil Stiffness on Longitudinal Displacement (Zero Skew)
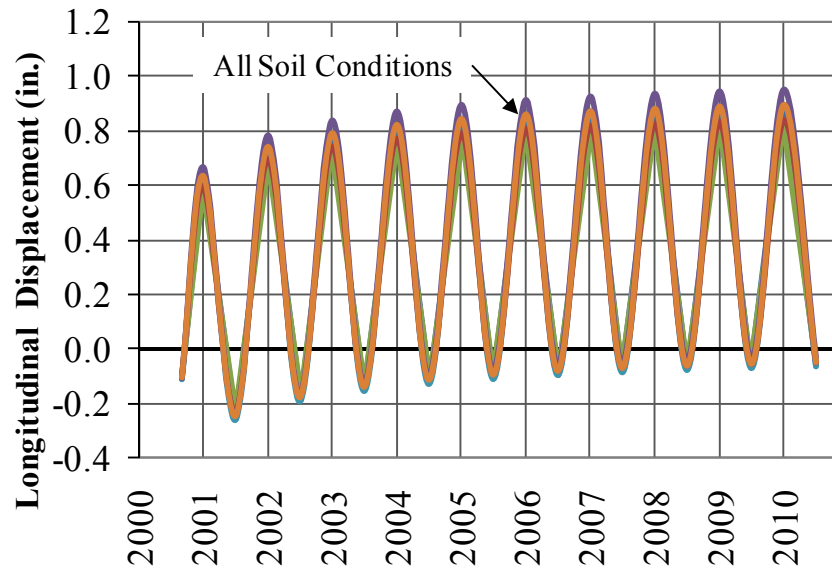
Figure 5.49: Effect of Soil Stiffness on Longitudinal Displacement (30° Skew)
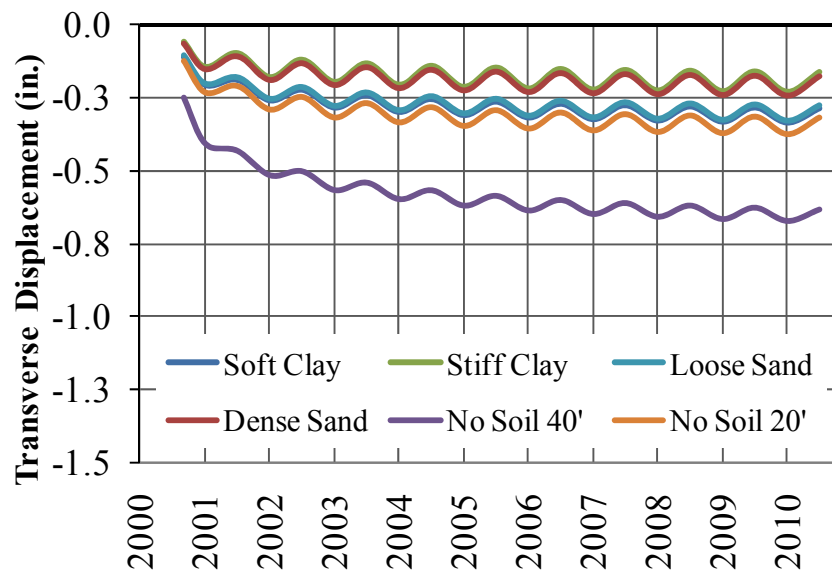
Figure 5.50: Effect of Soil Stiffness on Transverse Displacement (30° Skew)
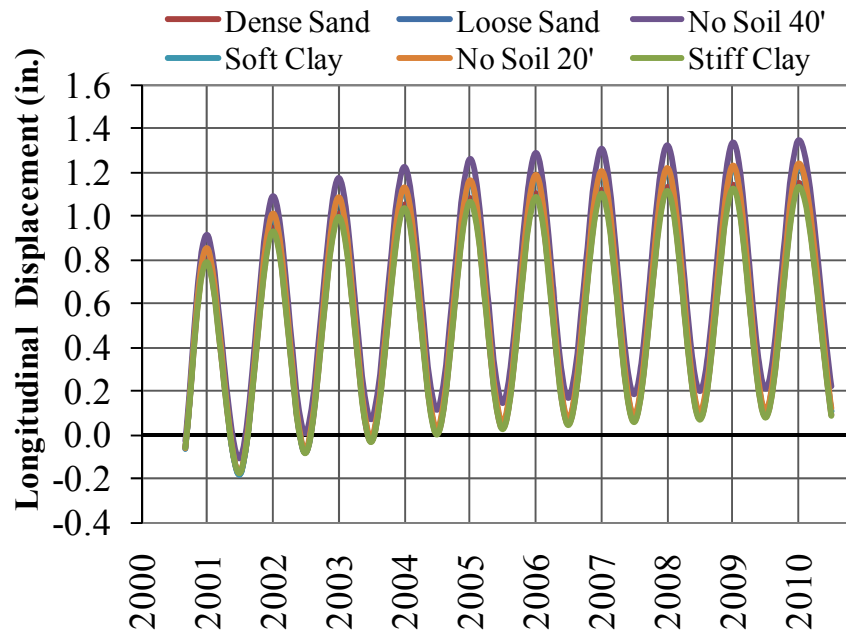
Figure 5.51: Effect of Soil Stiffness on Longitudinal Displacement (60° Skew)
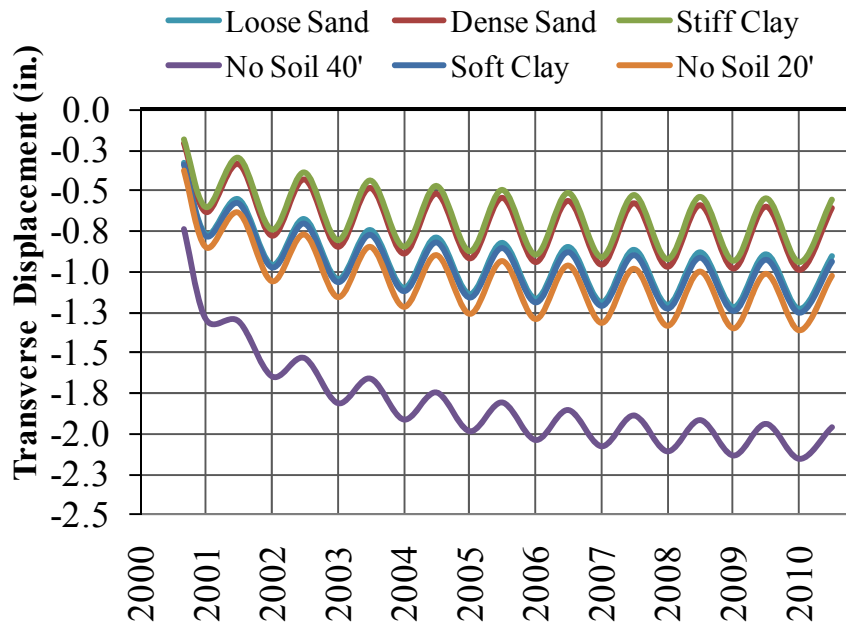
Figure 5.52: Effect of Soil Stiffness on Transverse Displacement (60° Skew)

5.4. CONCLUSIONS OF PARAMETRIC ANALYSIS

To expand the understanding of the long-term behavior of integral abutment bridges, a parametric analysis was conducted to determine the primary variables that control the behavior of these structures. The variables included the structure's total length, skew angle, span length, temperature differentials, shrinkage, pile section, pile orientation, and soil stiffness. The following conclusions for each variable were obtained from this analysis:

Length:

1. Because the controlling load for these structures (temperature and shrinkage) is a function of length, length is one of the primary factors controlling the behavior.

2. As the total structural length increases, the lateral displacement demand for the supporting piles increases.

3. Pile restraint and abutment rotation reduce the amount of lateral displacement imposed on the pile in comparison to the theoretical unrestrained movement (Equation (5.3)). This reduction factor was determined to be approximately 0.6. Therefore, for a zero skew structure, the longitudinal displacement can be estimated by multiplying the theoretical unrestrained movement by the restraint factor.

Skew:

1. Skew of an integral abutment bridge causes rotation of the abutment and transverse movement of the structure. The rotation of the abutment causes an increase in longitudinal displacement for the acute corner pile.

2. For a skewed structure, the total longitudinal deflection can be estimated by multiplying the theoretical unrestrained movement by the restraint factor and adding this value to the longitudinal demand deflection caused by skew.

3. The longitudinal demand caused by skew can be represented by a bilinear expression as shown in Figure 5.25 and given by Equation (5.8) and (5.9).

For skews $0° \leq \theta \leq 30°$:

$$\Delta_L(\theta) = 0.006\theta \tag{5.8}$$

For skews $30° \leq \theta \leq 60°$:

$$\Delta_L(\theta) = 0.011\theta - 0.16 \tag{5.9}$$

where:

$\Delta_L(\theta)$ = longitudinal demand deflection caused by skew, in.

θ = skew, degrees

4. The transverse displacement for a given temperature differential is shown to be essentially independent of the length of the structure.

5. The transverse displacement can be represented by a bilinear expression as shown in Figure 5.26 and given by Equation (5.10) and (5.11).

For skews $0° \leq \theta \leq 30°$:

$$\Delta_T(\theta) = 0.01\theta \tag{5.10}$$

For skews $30° \leq \theta \leq 60°$:

$$\Delta_T(\theta) = 0.03\theta - 0.6 \tag{5.11}$$

where:

$\Delta_T(\theta)$ = transverse demand deflection caused by skew, in.

θ = skew, degrees

6. To account for the demand lateral movement of a pile, both the longitudinal and transverse displacement must be accounted. It is appropriate to combine the components by the square root of the sum of the squares. It is important to note that the bilinear approximations are derived assuming 500 µε of shrinkage which is a good representation of concrete structures. However, if a different magnitude of shrinkage is required, the bilinear curves must be altered.

Span Length:

1. Changing the span length changes the vertical flexural stiffness of the superstructure. As the flexural stiffness is increased, the out-of-plane displacement is reduced. For spans with low flexural stiffness, the behavior of the abutment changes from one where the abutment simply translates to one where the abutment has significant rotation over its height.

2. For the span range and stiffness of typical structures, span length does not control the overall behavior of integral abutment bridges.

Temperature Differential:

1. Temperature differentials cause the structure to expand and contract. This expansion and contraction cause lateral displacement demand on the supporting piles of the abutment.

2. To determine the total lateral displacement demand for a pile supporting an integral abutment bridge, it is necessary to determine the maximum possible negative temperature differential. Contraction of the structure will control behavior because it is additive to the effects of shrinkage.

3. In general, variations in the temperature differential for practical temperature ranges have minimal effect on the restraint reduction factor for longitudinal displacement.

4. Variations in the temperature differential have a minimal effect on the differential longitudinal and transverse displacements as caused by skew. Consequently, the bilinear approximations developed to account for skew are considered accurate for practical temperature ranges.

5. If a designer would like to account for temperature differentials other than -45°F the following increase can be calculated:

Increase in longitudinal displacement due to temperature differential:

For skews $0 \leq \theta \leq 30°$:

$$\Delta_{L\Delta T} = (2.5 \cdot 10^{-5} \theta)(\Delta T - 45°F) \tag{5.4}$$

For skews $30 \leq \theta \leq 60°$:

$$\Delta_{L\Delta T} = (6.6 \cdot 10^{-5} \theta - 1.2 \cdot 10^{-3})(\Delta T - 45°F) \tag{5.5}$$

where:

$\Delta_{L\Delta T}$ = increase in longitudinal direction due to temperature differential, in.

θ = skew, degrees

ΔT = negative temperature differential as a positive value, °F

Increase in transverse displacement due to temperature differential:

For skews $0 \leq \theta \leq 30°$:

$$\Delta_{T\Delta T} = (2.0 \cdot 10^{-5} \theta)(\Delta T - 45°F) \tag{5.6}$$

For skews $30 \leq \theta \leq 60°$:

$$\Delta_{L\Delta T} = (1.1 \cdot 10^{-4} \theta - 2.8 \cdot 10^{-3})(\Delta T - 45°F) \tag{5.7}$$

where:

$\Delta_{T\Delta T}$ = increase in longitudinal direction due to temperature differential, in.

θ = skew, degrees

ΔT = negative temperature differential as a positive value, °F

Shrinkage Model:

1. Shrinkage of the deck causes contraction of the superstructure over its life-cycle. This contraction causes a net inward movement of the abutment for a period of approximately 10 years. This additional inward movement must be accommodated by the piles.

2. Shrinkage, in addition to temperature, must be included to determine the total lateral demand on the piles of integral abutment bridges. Shrinkage strains should be applied only to the deck.

3. Shrinkage does not affect the restraint reduction factor for longitudinal displacement. The magnitude of shrinkage does affect the differential longitudinal and transverse displacements caused by skew. As shrinkage increases, the differential longitudinal and transverse displacement will increase. This analysis assumes an ultimate shrinkage of 500 $\mu\varepsilon$ which is considered realistic and conservative for most concrete structures in Indiana. Consequently, the bilinear approximations developed to account for skew are considered accurate for an ultimate shrinkage of 500 $\mu\varepsilon$. However, if an increased magnitude of shrinkage is required, the bilinear approximations must be modified.

Pile Section and Orientation:

1. Three different pile sections with varying stiffnesses were investigated to bracket the range of piles commonly used in practice. The behavior provided by each section was

essentially identical. Therefore, the pile section was shown to not affect the overall behavior of the structure.

2. The pile orientation does not significantly affect the lateral pile displacement. However, it is important to reduce stresses imposed on the pile. To that end, it is recommended to orient the pile with the weak axis aligned perpendicular to the centerline of the structure.

Soil Stiffness:

- The stiffness of the soil surrounding the pile does not have a significant effect on the longitudinal displacement demand.

- The stiffness of the soil surrounding the pile affects the transverse displacement demand. The softer/looser the pile soil, the more the structure displaces transversely. Conversely, the stiffer the soil, the less it moves transversely. The parametric analysis in this chapter was based on loose sand which provides the least stiffness and is, therefore, a worst case. Consequently, the bilinear approximations developed to account for skew are considered conservative.

- A structure can be adequately modeled by ignoring the pile soil springs and fixing the pile at twice its inflection point. This technique can greatly reduce modeling effort.

In addition to the conclusions determined for the various parameters, several general conclusions were developed from this analysis:

- The lateral demand imposed on the supporting piles is a function of temperature differentials, shrinkage, bridge length, and skew.

- The maximum demand will occur in a structure constructed in the summer on the hottest day. Because the bridge is at its hottest point, only contraction can occur.

- The acute corner of a skewed structure will exhibit the largest deflection demands, and thus displacement at this location will control design of the piles.

- An integral abutment bridge's geometry (length and skew) is limited by the lateral deflection capacity of the supporting abutment piles. The pile must accommodate lateral deformation while maintaining its axial load carrying capacity.

CHAPTER 6. INTEGRAL ABUTMENT BRIDGE DESIGN RECOMMENDATIONS

6.1. INTRODUCTION

There is a desire to increase the range of applicability for integral abutment bridges due to the benefits obtained from this type of construction. Previous studies have served to increase the understanding of integral abutment behavior and their limitations (Talbott 2008, Chovichien 2004, Burke 1993, Greimann et al. 1986). These investigations better defined length limitations, detailing requirements, and the overall general behavior of these structures. However, many questions remained unanswered involving fundamental behaviors, specifically the effects of skew and the long-term displacement demands imposed on the supporting piles. This study serves to provide insight on these characteristic behaviors. Based on the increased understanding provided by this study, design recommendations and guidelines are provided to facilitate the increased use of these structures.

To develop design recommendations, a simplified displacement demand expression was developed based on the results of the parametric analysis in Chapter 5. In addition, research by Chovichien (2004) and Talbott (2008) is reviewed that defines the deformation capacity for typical piles used in integral abutment construction. The displacement demand expressions are coupled with the capacity of typical pile sections, and design curves for maximum length and skew are developed for integral abutment bridges. These design curves allow for the design of integral abutment bridges within defined limits without any special design considerations. Finally, for structures that exceed the recommended length and skew limitations, design recommendations and modeling guidelines are provided to assist engineers in capturing the behavior of these types of structures as this behavior must be considered.

6.2. S<small>IMPLIFIED</small> D<small>ISPLACEMENT</small> D<small>EMAND</small>

Based on the parametric study, it was determined that the primary loading of integral abutment bridges is a result of temperature and shrinkage strains that occur in the superstructure over its life. Length and skew, therefore, are primary factors controlling the movement of these structures. It was also determined that the pile closest to the acute corner of the abutment is subjected to the largest displacement demand. To determine the maximum lateral demand for a pile in an integral abutment bridge, estimated shrinkage and temperature strains are converted to maximum longitudinal and transverse displacement demands at the bottom of the acute corner of the abutment (top of pile) using the results from the parametric analysis. The longitudinal and transverse components can then be combined to determine the total lateral demand displacement.

Longitudinal Displacement:

It was determined from the parametric analysis that the displacement demand of the pile in the longitudinal direction (along the length of the structure) can be determined by multiplying the displacement due to unrestrained thermal and shrinkage strains by a constant reduction factor, as well as adding additional displacement to account for the rotation of the abutment as caused by skew. The displacement is characterized by a bilinear curve given by Equation (6.1) and Equation (6.2). The reduction factor was determined to be approximately 0.6.

For skews $0° \leq \theta \leq 30°$:

$$\Delta_L = F\left(\varepsilon_{\Delta T} + \varepsilon_s\right)\frac{L}{2} + 0.006\theta \qquad (6.1)$$

For skews $30° \leq \theta \leq 60°$:

$$\Delta_L = F\left(\varepsilon_{\Delta T} + \varepsilon_s\right)\frac{L}{2} + \left(0.011\theta - 0.16\right) \qquad (6.2)$$

where:

Δ_L = longitudinal deflection of supporting pile, in.

F = restraint reduction factor

= 0.6

$\varepsilon_{\Delta T}$ = strain due to temperature differential, in./in.

= $\alpha \Delta T$

α = coefficient of thermal expansion, 1/°F

$$= 5.5 \cdot 10^{-6} \; \frac{1}{\text{°F}}$$

ΔT = maximum negative temperature differential (as a positive number), °F

ε_s = shrinkage strain, in./in.

= 500 µε recommended

L = total structural length, in.

θ = skew angle, degrees

Transverse Displacement:

In addition to displacement in the longitudinal direction, the introduction of skew was shown to cause transverse displacement of the structure. This movement is independent of bridge length and is characterized by the bilinear expression given by Equation (6.3) and Equation (6.4).

For skews $0 \le \theta \le 30$:

$$\Delta_T = 0.01\theta \qquad\qquad (6.3)$$

For skews $30 \le \theta \le 60$:

$$\Delta_T = 0.03\theta - 0.6 \qquad\qquad (6.4)$$

where:

Δ_T = transverse deflection of supporting pile, in.

θ = skew angle, degrees

Pile Lateral Displacement:

The total lateral displacement of the pile is provided by both the longitudinal and transverse displacement of the abutment. Therefore, the total displacement can be computed by the square root of the sum of the squares of the transverse and longitudinal displacements as given by Equation (6.5) and Equation (6.6).

For $0 \le \theta \le 30$:

$$\Delta = \sqrt{\left(F\left(\varepsilon_{\Delta T} + \varepsilon_s\right)\frac{L}{2} + 0.006\theta \right)^2 + \left(0.01\theta\right)^2} \qquad (6.5)$$

For $30 \le \theta \le 60$:

$$\Delta = \sqrt{\left(F\left(\varepsilon_{\Delta T} + \varepsilon_s\right)\frac{L}{2} + 0.011\theta - 0.16 \right)^2 + \left(0.03\theta - 0.6\right)^2} \qquad (6.6)$$

where:

Δ = total demand deflection, in.

It should be noted that the equations developed above were based on an assumed temperature differential of 45 °F contraction and 500 με of shrinkage. These assumptions are embedded in the differential displacements caused by skew. As previously discussed in Section 5.3.4, changes in the temperature differential do not cause significant changes to these differential deflections for most common cases. If temperature correction is desired, the recommendations provided in Section 5.3.4 can be used. While changes to the assumed shrinkage strain will cause significant differences in differential deflections, 500 με is considered to be a realistic estimate of the ultimate shrinkage of these bridges.

6.3. PILE DEFORMATION CAPACITY

To define the limiting geometries for integral abutment bridges, the limiting deformation capacity for the piles supporting the abutment must be defined. Chovichien (2004) performed experimental and analytical investigations on typical sections used in integral abutment bridges. A primary focus of his investigation was to evaluate the lateral deformation capacity for the specimens shown in Table 6.1.

Table 6.1: Testing Matrix for Chovichien (2004)

Specimen	Section	Bending Axis			Axial Load Level	
		Weak	Strong	45°	$0.25f_y + 0.40f_c'A_c$	$0.50f_y + 0.40f_c'A_c$
C1	HP8x36	X			X	
C2	HP8x36		X		X	
C3	HP8x36			X	X	
C4	HP8x36	X				X
C5	HP10x42	X			X	
C6	HP12x53	X			X	
C7	CFT8	X*			X	
C8	CFT8	X*				X
C9	CFT10	X*			X	

* CFT sections are round and have only one bending axis.

In this experimental program, the pile abutment connection was clamped to a laboratory strong floor to simulate the case where the abutment does not rotate (worst case scenario). In general, the pile was loaded axially to a stress of $0.25f_y$ which corresponds to the maximum axial stress permitted by INDOT (INDOT Design Manual 2010) and AASHTO (AASHTO LRFD 5th Ed 2010). The pile was then loaded laterally at a point 5 ft away from the abutment, a point representing the assumed inflection point. This procedure inherently represents half the displacement capacity of a pile in the field. The displacement controlled loading continued at 0.25 in. increments until failure.

In a similar manner, Talbott (2008) conducted a similar investigation to supplement the tests conducted by Chovichien (2004). Talbott (2008) tested the pile sections listed in Table 6.2. A schematic of the test setup used by Talbott (2008) is shown in Figure 6.1, and a diagram illustrating the confinement reinforcement for selected tests is shown in Figure 6.2. A comparison of the test setups used by Chovichien (2004) and Talbott (2008) is shown in Figure 6.3. As illustrated, the major difference is the increase in abutment size to eliminate confinement around the embedded portion of the pile.

Table 6.2: Laboratory Test Matrix (Talbott 2008)

Series	Specimen	Section	Embedment Length (in.)		Confining Reinforcement[1]		Hinge Detail
			15	24	A	B	
1	1	HP12x53	X				
	2	HP12x53		X			
	3	HP12x53	X				X
2	4	HP14x89	X				
	5	HP14x89		X			
	6	HP14x89		X	X		
	7	HP14x89		X		X	

(1) – See confinement reinforcement detail (Figure 6.2).
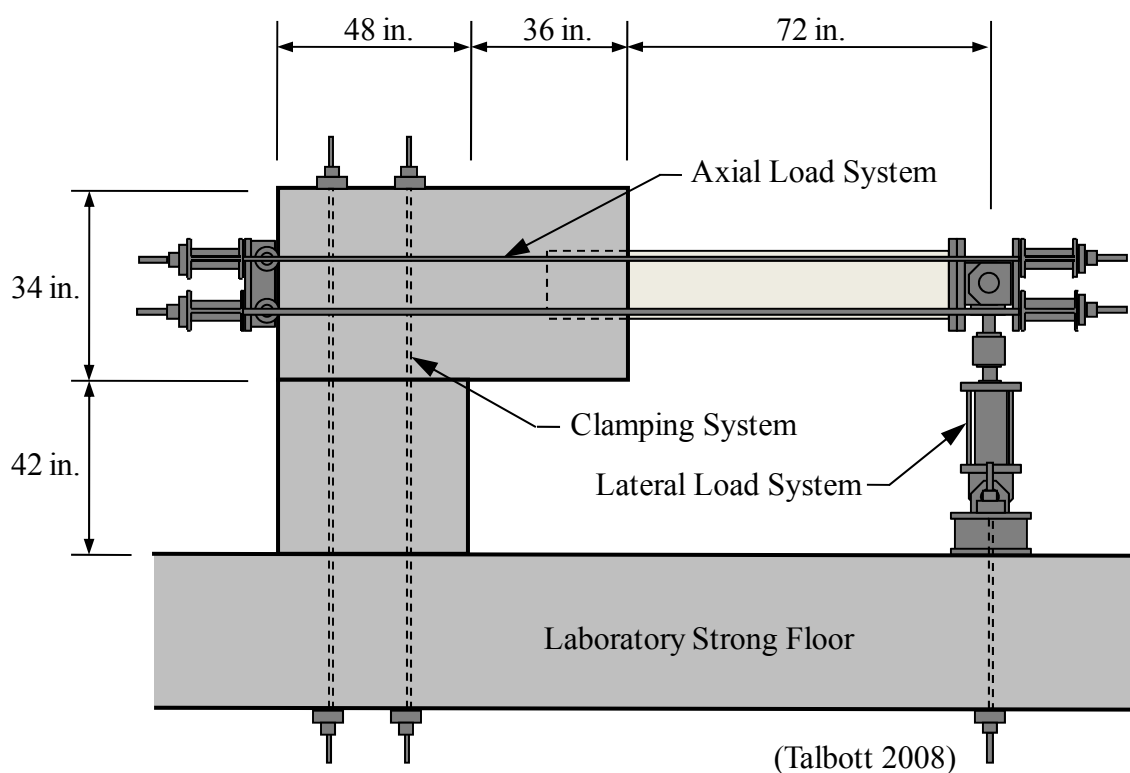
Figure 6.1: Test Setup for Lateral Pile Capacity

Figure 6.2: Confinement Reinforcement Details
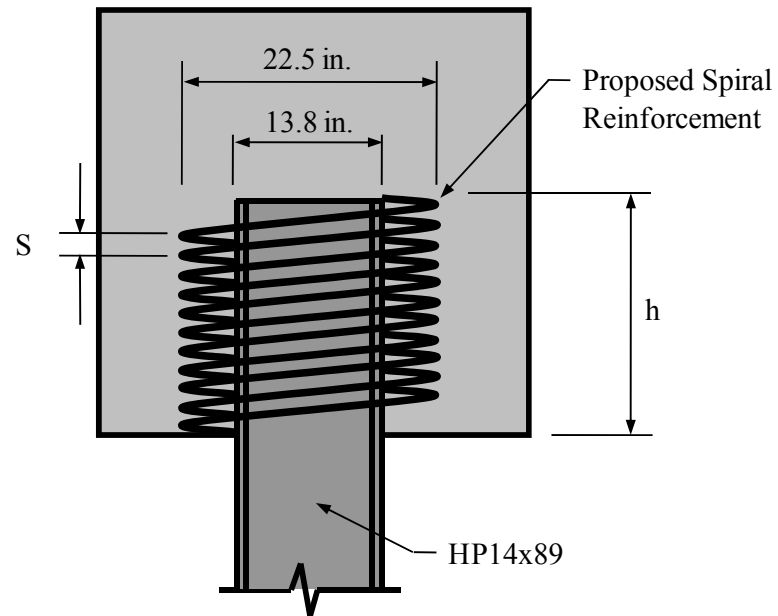
Identifier	Bar Size	Diameter (in.)	Height, h (in.)	Pitch, S (in.)
A	# 4	22.5	24	2.5
B	# 4	22.5	24	1.5

Chovichien

Confined Region

Talbott
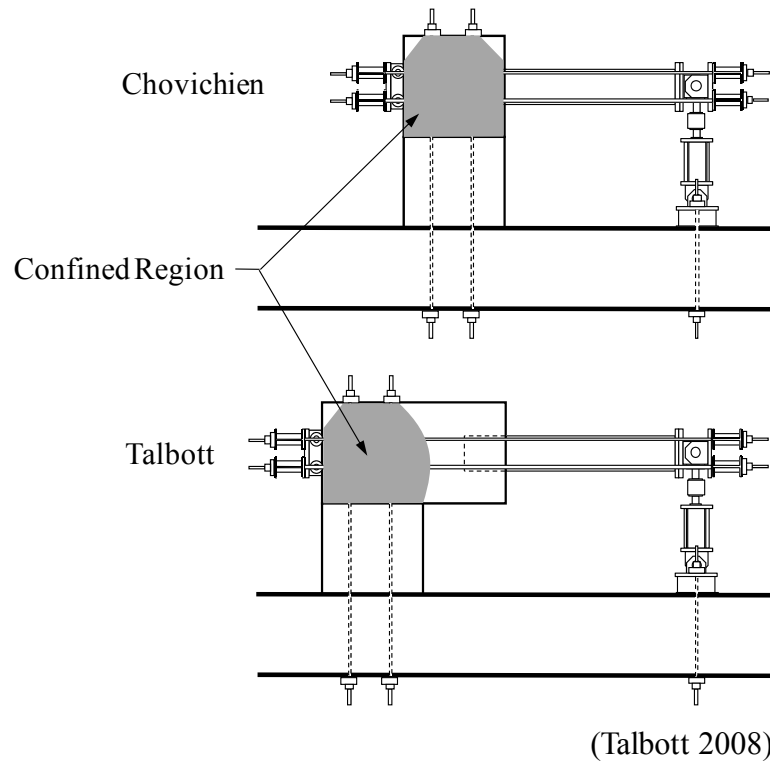
(Talbott 2008)

Figure 6.3: Comparison of Test by Talbott (2008) and Chovichien (2004)

From these experimental programs, the load-deflection response of the pile sections embedded into an integral abutment was evaluated. Talbott (2008) combined the curves from both testing programs. Selected curves for two of the HP sections are shown in Figure 6.4 and Figure 6.5. It is important to note that the laboratory deflections measured correspond to half of the displacement that would be produced in the field.
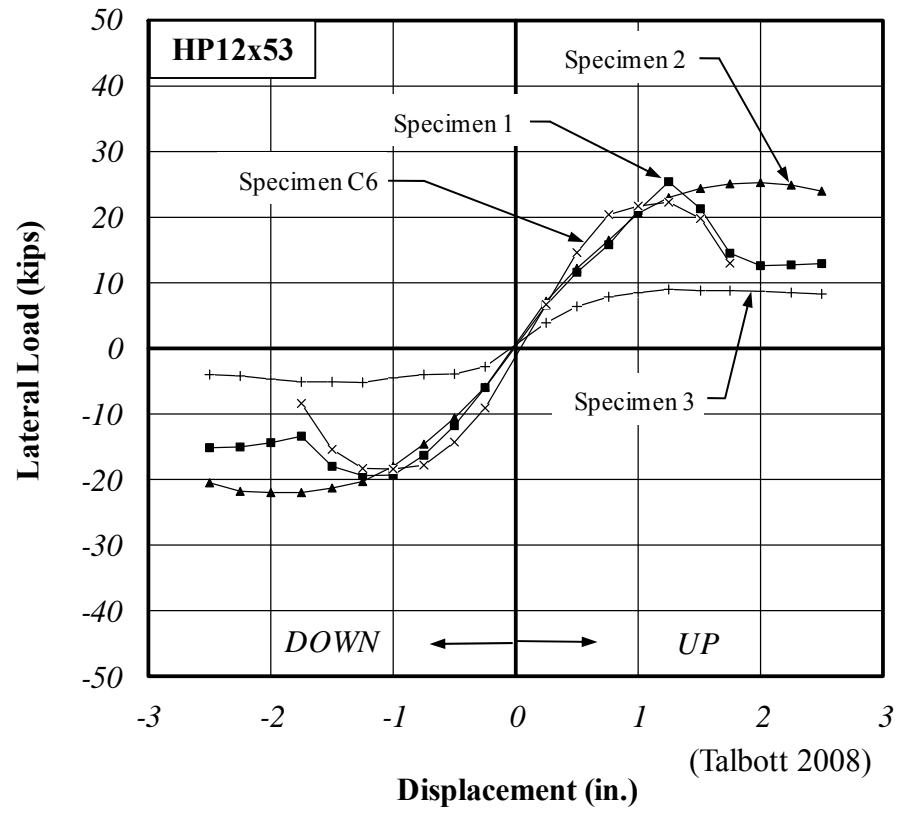
Figure 6.4: Load-Displacement Relationship for HP12x53
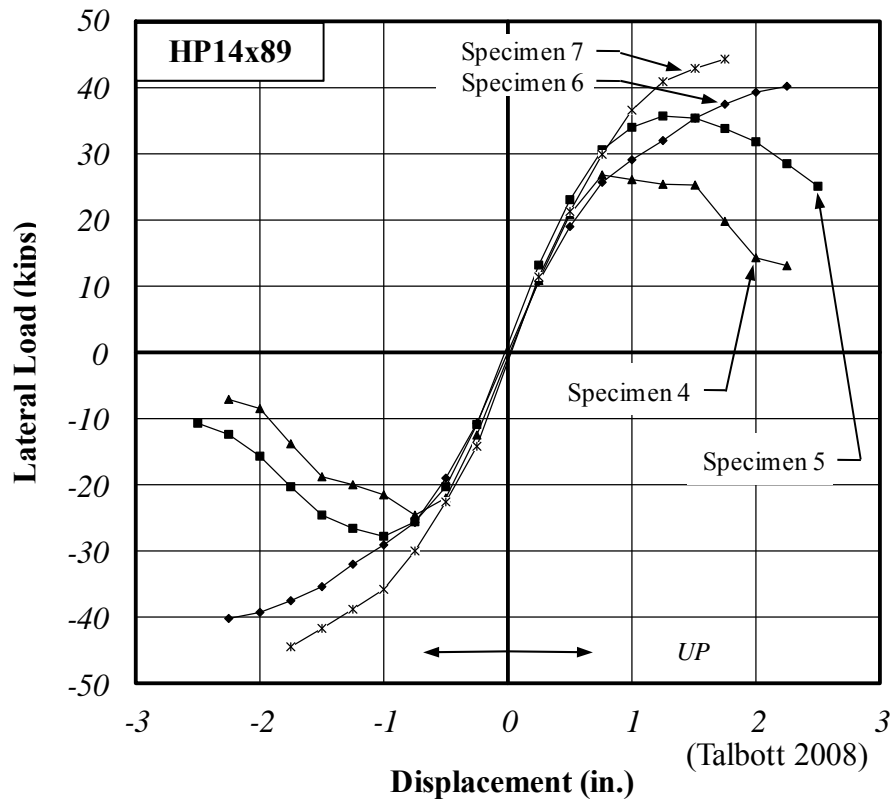
Figure 6.5: Load-Displacement Response Envelope for HP14x89

From the experimental investigations of Talbott (2008) and Chovichien (2004) and the analytical investigations conducted by Chovichien (2004), lateral deformation capacities were defined for a variety of pile sections used in integral abutment structures. First, it was determined that both the HP piles (weak axis bending) and CFT piles could accommodate 2 in. of lateral deformation in the field without suffering a significant loss in the axial load carrying capacity. Talbott (2008) referred to this limit as the zero-damage limit (ZDL).

In addition, Talbott (2008) also defined an acceptable-damage limit (ADL). This limit corresponds to a lateral deformation of 4 in. in the field. Below this amount, the reduction in axial load carrying capacity is less than 5%. This behavior can be ensured with a minimum pile embedment length of 15 in. (preferably 24 in.) and confinement reinforcement provided around the pile-abutment connection. The ADL will only be considered for HP sections because the testing program for Talbott (2008) did not include CFT sections, and the CFT sections in the Chovichien (2004) tests were relatively small sections that experience buckling around 2 in. of lateral field displacement.

6.4. RECOMMENDED DEIGN CURVES FOR BRIDGE LENGTH AND SKEW

Based on the displacement demand equations developed in Section 6.2 and the lateral deformation capacities for piles discussed in Section 6.3, design curves can be developed that provide limitations on the length and skew of integral abutment bridges. Simply, the developed displacement demand equations were set equal to the allowable lateral deflection. For various temperature ranges, maximum allowable length and skew combinations were determined. Structures built within these limitations can use standard integral abutment details (Section 1.4) and do not require any special design considerations regarding pile design. The piles need only be designed for axial load.

To develop the design curves, the amount of long-term shrinkage as well as the maximum negative temperature differential need to be defined. According to ACI 209 (2008), the ultimate shrinkage can range between 400 με and 700 με depending on the prediction model and assumed variables. From the parametric analysis (Chapter 5), it was shown that the European Model (CEB MC90) best predicted the behavior of these structures and a realistic estimate of the ultimate shrinkage is 500 με. Because these structures can be built in any geographic location with a variety of climates, five design curves are provided for the following negative temperature differentials: 25, 50, 75, and 90 °F. For these curves, the equations developed in Section 6.2 were also modified to account for all temperature effects as describe in Section 5.3.4. It is recommended, based on the field monitoring investigation (Chapter 2), that 75 °F is appropriate for representing integral abutment bridges built in Indiana. In addition to temperature and shrinkage, two levels of deformation capacity can be considered as discussed in Section 6.3. Therefore, two sets of design curves are shown, one for the zero-damage limit and another for the acceptable-damage limit. The proposed design curves are shown in Figure 6.6 and Figure 6.7. It is important to note that the two curves are shown with different scales. The solid lines are based on the simplified displacement demand. The dashed lines include the modifications described in Section 5.3.4 that account for all temperature effects. As can be seen, the addition of the temperature effects is negligible for most design cases. Therefore, it is decided that the additional term need not be included in the simplified displacement calculation procedure. To simplify the curves, a bilinear relationship is shown for a negative temperature differential of 75°F (Figure 6.8) which is considered appropriate for Indiana.
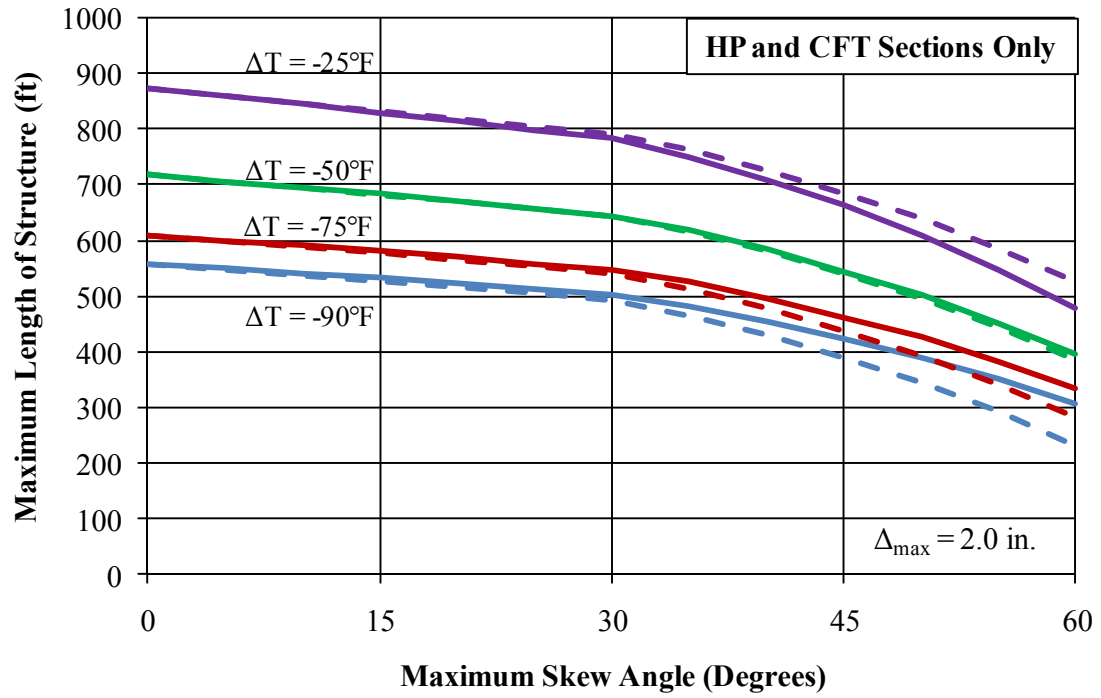
Figure 6.6: Integral Abutment Design Curves for Zero-Damage Limit
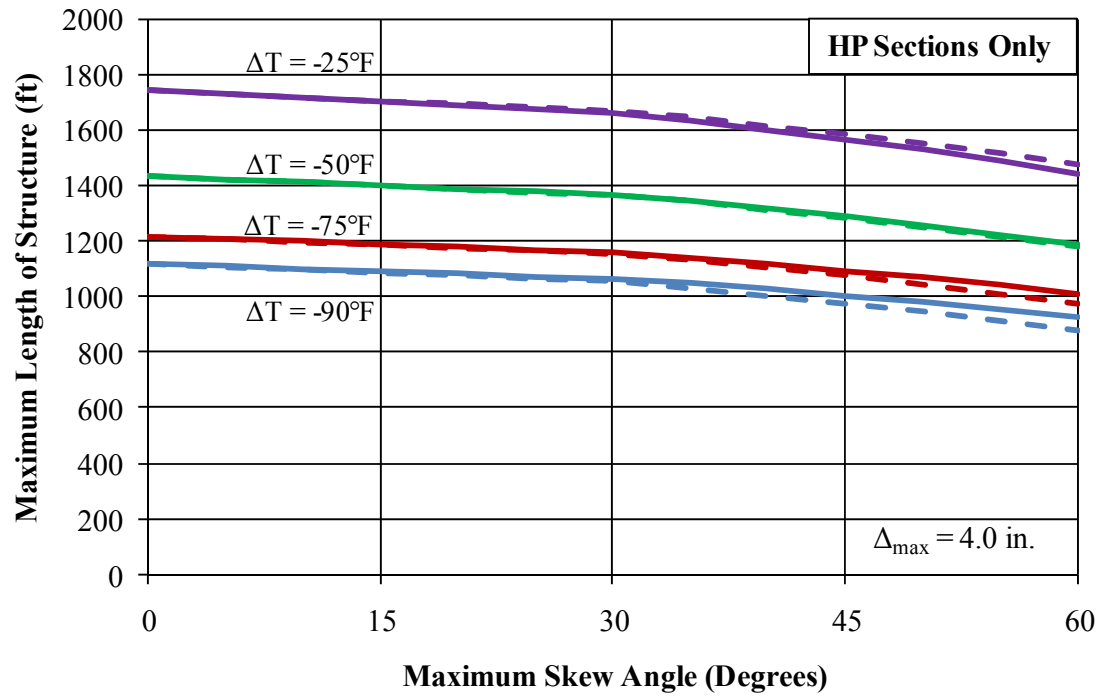
Figure 6.7: Integral Abutment Design Curves for Acceptable-Damage Limit
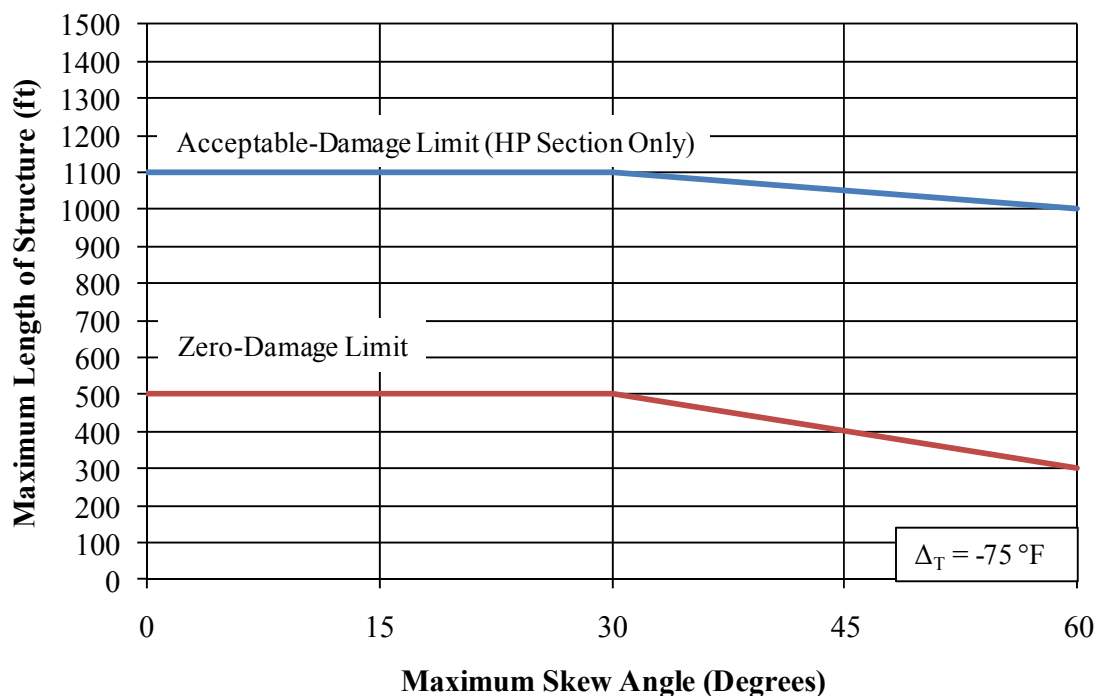
Figure 6.8: Recommended Design Curves for INDOT

6.5. INTEGRAL ABUTMENT MODELING RECOMMENDATIONS AND GUIDELINES

Because integral abutment bridges are the preferred choice for highway structures, there is the potential that the geometry of a proposed bridge will be outside of the limits defined by the design curves. While the simplified design procedure is not appropriate for structures outside these limits, it may be possible to define the specific conditions of an individual structure and to appropriately design the structure as integral. In addition, there may be desire to provide more detailed analysis for structures falling within the design limitations previously presented. Therefore, the following modeling recommendations and guidelines were developed to aid designers in these cases.

Piles:

- The weak link in an integral abutment system is the pile-abutment connection. The pile must be able to maintain its axial load carrying capacity while accommodating the lateral displacement imposed by the structure.

- For structures with skew, the controlling displacements will be associated with the pile closest to the acute corner of the structure.

- A simple frame element is sufficient to capture the behavior of the pile.

- The abutment-pile connection should be modeled as rigid, thus accounting for the worst possible condition.

- The demand imposed on the pile should be considered at the top of the pile rather than the top of the abutment.

Loading:

- The demand imposed on integral abutment bridges is a combination of thermal and shrinkage strains. The effects from both of these loads must be combined to determine the total demand for the supporting piles over the life of the structure.

- When modeling a structure, the assumed ultimate shrinkage value should be applied to the deck. Applying the full shrinkage amount to the entire superstructure (deck and girders) is over-conservative and not consistent with measured behavior.

- It is recommended that the European prediction model (CEB MC90) provides the best representation of the rate and magnitude of shrinkage for integral abutment bridges. A total strain of 500 $\mu\varepsilon$ is recommended for Indiana.

- The controlling temperature differential is the largest negative temperature differential. Shrinkage contracts the structure and combines with contraction from the negative temperature differential.

- When modeling a structure, temperature strains should be applied to the entire superstructure. It is sufficient to use average annual high and low ambient temperatures to determine the thermal load rather than extreme high and low temperatures.

Structural Model:

- Any analytical model should be sufficient to model the superstructure of an integral abutment bridge provided it accounts for the stiffness, continuity, and composite behavior of the superstructure.

- It is sufficient to model the interior supports as rollers assuming that integral or fixed interior supports are not to be used in the structure.

Soil:

- In regards to the demand displacement for the supporting piles, the soil behind the abutment does not impact the ultimate demand. Therefore, abutment springs are not required to calculate the controlling response and maximum displacements. Abutment springs, however, can be used if estimates of pressures behind the abutment are desired. For the structures investigated, passive pressures were not high enough that they would need consideration in design. For extremely long structures, the pressures may impact the design of the abutment and warrant consideration in analysis. Further investigation is needed regarding the development and magnitude of passive earth pressures.

- The soil surrounding the piles can be modeled using linear springs following the procedures described in Section 3.3.1.

- Pile-soil interaction can also be modeled by ignoring the soil springs and representing the pile as an equivalent column. The equivalent column results in a pile length approximately twice the depth of the inflection point. Chovichien (2004) provides guidance and estimates of the depth of inflection point for a large variety of piles and soil conditions. This procedure greatly reduces the difficulty in modeling integral abutment bridges.

CHAPTER 7. SUMMARY AND CONCLUSIONS

7.1. INTRODUCTION

In bridge design, an integral abutment bridge is created by monolithically connecting the superstructure with the substructure creating a jointless frame. This method of construction is preferred because the need for expansions joints and bearings is removed along with the various maintenance problems that are associated with them. The role of the expansion joints (allowing for expansion and contraction of the superstructure caused by volumetric strains imposed over time) is accommodated by the substructure, a single row of piles. While simple in concept, this design creates a complex soil-structure interaction problem. Traditionally, these structures have been designed based on engineering judgment with little or no attention to the behavior of integral construction. As long as the geometry of a proposed structure is within specified limits, design is not required to consider integral behavior. Typically, designers simply need to satisfy several design requirements, consider several simplified design assumptions, and use standard details especially for the abutments. Use of integral abutment bridges outside of the limits is considered on a case-by-case review and is some states not allowed. Because these structures provide significant advantages over that of traditional bridge structures, there is desire to increase the range of applicability.

Based on this interest, a significant amount of research has been conducted to understand the behavior of these structures. This research has aided in expanding the understanding of integral abutment bridges as well as increasing the geometric limitations imposed on these structures. Considerable work has been conducted to determine the lateral displacement and load capacity of standard sections of piles. Arsoy (2002), Chovichien (2004), and Talbott (2008) conducted experimental tests evaluating the lateral capacities of integral abutment piles. Greimann et al. (1984) and Greimann et al. (1987) conducted analytical experiments to determine appropriate methods to model the soil surrounding the piles. While these investigations, along with many others, helped to increase the understanding of integral abutment bridges, questions remain regarding certain aspects of their behavior. Specifically, questions remain regarding the

long-term lateral displacement demand that will be imposed on the supporting piles. In addition, the effects of skew on the lateral displacement demand of supporting piles are unknown.

The objective of this study was to address these two primary concerns, the long-term behavior and the effects of skew. Consequently, this study was divided into five different phases to evaluate these factors as outlined below:

1. Implementation of a field monitoring program of three integral abutment structures to observe and understand their behavior.

2. Analysis of the data collected from the field monitoring program to develop adequate analytical modeling techniques to represent the behavior of integral abutment structures,

3. Construction and testing of a quarter-scale, single span, 45° skew, integral abutment structure to increase understanding of the behavior of highly skewed structures,

4. Implementation of a parametric analysis to determine the effects of various characteristics of integral abutment bridges.

5. Development of design recommendations and guidelines.

7.2. RESEARCH PHASES

7.2.1. PHASE 1: FIELD MONITORING PROGRAM

A field monitoring program was implemented on three integral abutment bridges, Southbound I-65 over SR-25, SR-18 over the Mississinewa River, and US-231 over AEP Railway Spur. The objective of this phase was to measure the long-term in-service behavior. The structures were highly instrumented to measure movements of the abutments, lateral earth pressure, pile response, and temperatures to determine structural behavior when subjected to seasonal volumetric strains. Based on this phase of research, a number of conclusions as presented in Section 2.5 were developed.

7.2.2. PHASE 2: ANALYSIS OF FIELD RESULTS

Analytical models were developed and calibrated to match the behavior of two of the structures from the field monitoring program, SR-18 over the Mississinewa River and US-231 over AEP Railway Spur. The objective of this phase was to develop modeling techniques that accurately calculate longitudinal and transverse displacements of the abutments. Additionally, this phase was used to determine the driving force controlling the movements of integral

abutment bridges. The modeling techniques included varying the soil stiffness surrounding the abutment and piles, as well as varying the loading conditions. Based on this phase of research, a number of conclusions as presented in Section 3.6 were developed.

7.2.3. PHASE 3: EXPERIMENTAL INVESTIGATION

A quarter-scale integral abutment bridge with a 45° skew was constructed and tested to determine the behavior of highly skewed integral abutment bridges. Building off the conclusions from Phase 2, the objective of this phase was to increase the understanding of highly skewed structures. The experimental program included testing of a single laterally loaded pile and testing of a quarter-scale integral abutment bridge. The bridge was highly instrumented to monitor movement of the abutment, lateral deflection of the piles, and load required to expand and contract the structure. Additionally, the modeling techniques developed in Phase 2 were evaluated by comparing the calculated displacements to those measured by the experiments. Based on this phase of research, a number of conclusions as presented in Section 4.9 were developed.

7.2.4. PHASE 4: ANALYTICAL INVESTIGATION

Using the lessons learned from the first three phases, a parametric analysis was conducted. The objective of this phase was to determine the effect of various characteristic on the behavior of integral abutment bridges. The modeling techniques developed in Phase 2 were used to model a generic structure. The parametric study investigated the effects of length, skew, span length, temperature differential, shrinkage, pile section, pile orientation, and soil stiffness. Based on this phase of research, a number of conclusions as presented in Section 5.4 were developed.

7.2.5. PHASE 5: DESIGN RECOMMENDATIONS

The objective of this phase was to develop design recommendations to aid designers and facilitate the use of integral abutment bridges based on the findings of this study and lessons from additional investigations. The design recommendations have two primary aims: (1) provide designers with geometric limitations (length and skew) for integral abutment structures so that a design need not directly consider integral behavior, and (2) provide designers with modeling recommendations and guidelines so structures outside the limitations can be adequately modeled.

Based on this phase of research, recommended geometric limitations are provided in Section 6.4 while modeling guidelines are presented in Section 6.5.

7.3. CONCLUSIONS:

Based on the overall study, the following conclusions were made:

7.3.1. LONG-TERM BEHAVIOR

- Temperature differentials cause the cyclic behavior of the abutment movement.
- Lateral earth pressure reduces to approximately zero during phases of contraction indicating that a gap forms behind the abutment. Therefore, lateral earth pressure is not the cause of ratcheting.
- Concrete shrinkage of the deck causes net inward movement of the bridge (contraction) and is the cause of ratcheting.
- The maximum lateral pile demand occurs due to contraction. The demand is a combination of temperature change and concrete shrinkage. Therefore, the largest demand occurs for a bridge made integral on the hottest day of the year.
- The ratcheting of the abutment reduces in magnitude each year and will not continue for the entire life of the structure. A steady-state cyclic displacement occurs after a period of approximately seven years.

7.3.2. SKEW

- Skew of an integral abutment bridge causes rotation of the abutment and transverse movement of the structure.
- The largest longitudinal and transverse displacements occur at the acute corner. Therefore, this corner provides the greatest lateral demand on the piles.
- The transverse displacement occurs toward the acute side of the abutment.
- H-Piles should be oriented with the webs placed perpendicular to the centerline of the structure to minimize flexural forces.
- Skew has a minimal effect for values less than 30°. For structures with skews greater than 30°, the effect becomes significant.

7.4. <u>DESIGN RECOMMENDATIONS</u>

Based on the findings of this study, equations were developed to calculate the demand lateral displacement for piles of integral abutment bridges. The equations contain components of longitudinal and transverse displacement as a function of length and skew. The developed equations are presented in Equation (7.1) and Equation (7.2).

For $0 \leq \theta \leq 30$:

$$\Delta = \sqrt{\left(F\left(\varepsilon_{\Delta T} + \varepsilon_s\right)\frac{L}{2} + 0.006\theta \right)^2 + \left(0.01\theta\right)^2} \tag{7.1}$$

For $30 \leq \theta \leq 60$:

$$\Delta = \sqrt{\left(F\left(\varepsilon_{\Delta T} + \varepsilon_s\right)\frac{L}{2} + 0.011\theta - 0.16 \right)^2 + \left(0.03\theta - 0.6\right)^2} \tag{7.2}$$

where:

Δ = total demand deflection, in.

F = restraint reduction factor

= 0.6

$\varepsilon_{\Delta T}$ = strain due to temperature differential, in./in.

= $\alpha\Delta T$

α = coefficient of thermal expansion, 1/°F

= $5.5 \cdot 10^{-6} \, \frac{1}{°F}$

ΔT = maximum negative temperature differential (as a positive number), °F

ε_s = shrinkage strain, in./in.

= 500 $\mu\varepsilon$ recommended

L = total structural length, in.

θ = skew angle, degrees

Using these equations, two simplified bilinear design curves were developed for a negative temperature differential of 75 °F and 500 $\mu\varepsilon$ of shrinkage which is considered

appropriate for Indiana (Figure 7.1). The first curve represents an allowable lateral deformation of 2 in. for supporting piles, referred to as the zero damage limit. For the zero damage limit, no requirements beyond those provided by the current detailing and design requirements as provided by the INDOT Design Manual (2010) (applicable sections are provided in Appendix E) are needed. Specifically, both H-piles and 14 in. CFT piles are sufficient for accommodating the lateral deformation demand provided 24 in. of embedment is provided into the abutment. The second curve represents an allowable lateral deformation of 4 in. which corresponds to an allowable damage limit as defined by Talbott (2008). In addition to the requirements provided by the INDOT Design Manual (2010), confinement reinforcement must be provided as recommended by Talbott (2008). Also, the allowable damage limit has been confirmed only for HP sections and is not recommended at this time for steel-pipe piles.

For geometries outside these limits, modeling recommendations are provided in Section 6.5 to aid designers in the analysis of integral abutment bridges.
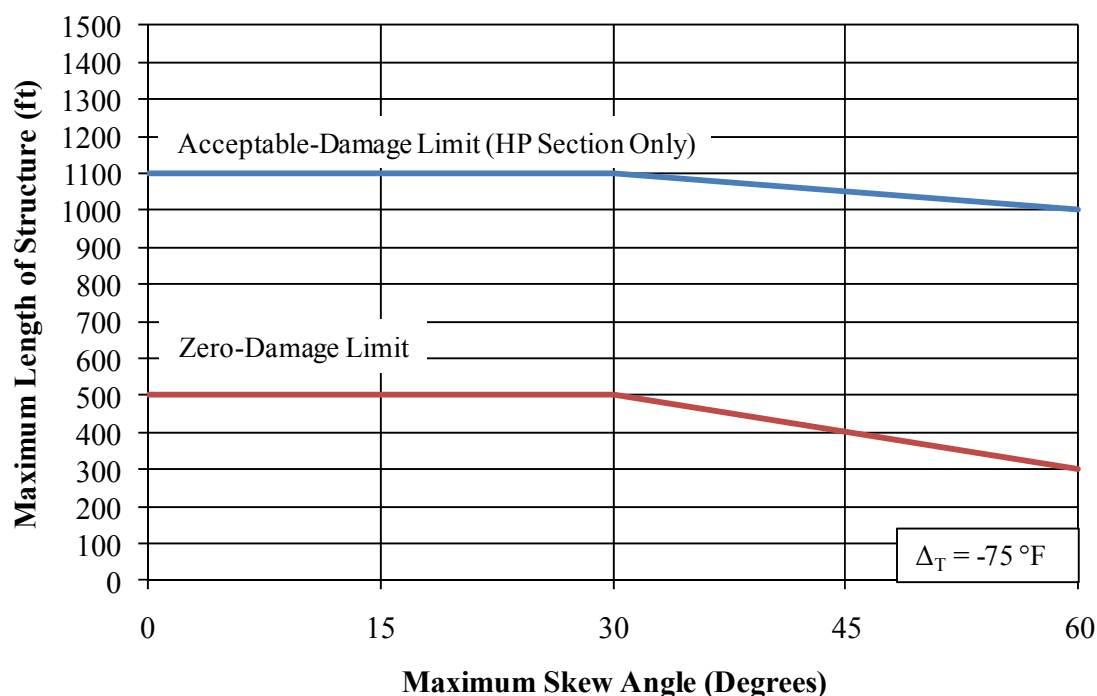
Figure 7.1: Recommended Design Curves for Integral Abutment Bridges.

7.5. FURTHER RESEARCH

Based on the findings from this study, several recommendations are provided regarding further research that should be conducted to extend the understanding of the behavior of integral abutment bridges.

- The current research provides limited information on the lateral deformation capacity of CFT piles. A full scale pile-abutment connection should be tested to determine the ultimate lateral deformation capacity of 14 in. CFT piles. Additionally, the confinement reinforcement details, as recommended by Talbott (2008), should be investigated for CFT piles.

- Adequate modeling techniques to represent the lateral earth pressure behind integral abutment bridges do not exist. Work is required to develop methods to analytically represent the effects of the backfill and in particular the stiffness of the soil. For extreme lengths of integral abutment bridges, the effects of passive earth pressure on the superstructure need to be understood.

- Based on the findings of this study, it is apparent that skew causes the abutment to rotate (plan view). An investigation should be conducted to investigate the effect of highly skewed structures on the behavior of the bridge deck. It is believed that rotation of the abutment will cause tensile stresses to occur at the corners of the deck requiring additional reinforcement. This may be above the current detailing requirements provided by AASTO for skewed structures.

LIST OF REFERENCES

1. AASHTO (2010), *AASHTO LRFD Bridge Design Specification, 5ᵗʰ Edition,* American Association of State Highway and Transportation Officials, Washington, D.C., 2010.

2. Abendroth, R.E., Greimann, L.F., Ebner, P.B. (1989), "Abutment Pile Design for Jointless Bridges," *Journal of Structural Engineering*, Vol. 115, No. 11, November 1989, pp. 2914-2929.

3. ACI 209 (2008), Guide for Modeling and Calculating Shrinkage and Creep in Hardened Concrete, American Concrete Institute (ACI) Committee 209, Farmington Hills, Michigan.

4. ACI 318 (2008), *Building Code Requirements for Structural Concrete (ACI318-08) and Commentary*, American Concrete Institute (ACI) Committee 318, Farmington Hills, Michigan.

5. Arsoy, S. et al. (1999), "The Behavior of Integral Abutment Bridges," Final Contract Report, Virginia Transportation Research Council, Charlottesville, Virginia, November 1999.

6. Arsoy, S., Duncan, J. M., and Barker, R. M. (2002), "Performance of Piles Supporting Integral Abutment Bridges," *Transportation Research Record: Journal of the Transportation Research Board*, Vol. 1808.

7. Brena, S. F., Bonczar, C. H., Civjan, S. A., Dejong, J. T., and Crovo, D. S. (2007), "Evaluation of Seasonal and Yearly Behavior of an Integral Abutment Bridge," *Journal of Bridge Engineering*, ASCE, Vol. 12, No. 3, May 2007, pp. 296- 305.

8. Burke, M. P. Jr. (1993), "The Design of Integral Concrete Bridges," *Concrete International: Design and Construction*, Vol. 15, No. 6, June 1993, pp. 37-42.

9. Chovichien, V. (2004), "The Behavior and Design of Piles for Integral Abutment Bridges." West Lafayette: Purdue University.

10. Coduto, D. P. (2001), *Foundation Engineering Principles and Practices, 2nd Edition*, Prentice Hall, New Jersey.

11. CSI, Inc. (2009), SAP2000 version 14. Berkeley, CA: Computers and Structures (CSI) Inc.

12. Douglas, D. J. and Davis, E. H. (1964), "The Movement of Buried Footings Due to Moment and Horizontal Load and the Movement of Anchor Plates," *Geotechnique: The International Journal of Soil Mechanics*, Vol. 14, No. 2, June 1964.

13. Duncan, M. J. and Mokwa, R. L. (2001), "Passive Earth Pressures: Thoeries and Tests," *Journal of Geotechnical and Geoenvironmental Engineering*, Vol. 127, No. 3, March 2001.

14. Durbin, K.O. (2001), "Investigation of the Behavior of an Integral Abutment Bridge," M.S. Thesis, Purdue University, West Lafayette, IN, 2001, 138 pp.

15. Famighetti, R. ed. (1997), *The World Almanac and Book of Facts*, Ed. 130, World Almanac Books, Mahwah, NJ, 976 pp.

16. Girton, D., Hawkinson, T., and Greimann, L. F. (1993), "Validation of Design Recommendations for Integral-Abutment Piles," *Journal of Structural Engineering*, ASCE, Vol. 117, No. 7, July 1991, pp. 2117 – 2134.

17. Greimann, L.F., Yang, P.S., and Wolde-Tinsae, A.M. (1984), "Design of Piles for Integral Abutment Bridges," Final Report, Department of Civil Engineering, Engineering Research Institute, Iowa State University, Ames, Iowa, August 1984, 260 pp.

18. Greimann, L.F., Yang, P.S., and Wolde-Tinsae, A.M. (1986), "Nonlinear Analysis of Integral Abutment Bridges," *Journal of Structural Engineering*, ASCE, Vol. 112, No. 10, 1986, pp. 2263-2280.

19. Greimann, L.F., et al. (1987), "Pile Design and Tests for Integral Abutment Bridges," Final Report, Department of Civil Engineering, Engineering Research Institute, Iowa State University, Ames, Iowa, December 1987, 302 pp.

20. Horvath, J. H. (2004), "Integral-Abutment Bridges: A Complex Soil-Structure Interaction Challenge," ASCE Geo Trans Conference Proceedings, Vol. 154, No 31.

21. INDOT Design Manual (2010), The Indiana Design Manual, Indiana Department of Transportation (INDOT).

22. Kunin, J. and Alampalli, S. (2000), "Integral Abutment Bridges: Current Practice in United States and Canada," *Journal of Performance of Constructed Facilities,* ASCE, Vol. 14, No. 3, August 2000, pp. 104-111.

23. Lawver, A., French, C., and Shield, C. K. (2000), "Field Performance of Integral Abutment Bridge," *Transportation Research Record: Journal of the Transportation Research Board*, Vol. 1740.

24. Potyondy, J. G. (1961), "Skin Friction Between Various Soils and Construction Materials." Geotechnique, London, Vol. 11, No. 1, pp. 339-353.

25. Reese, L.C. and Van Impe, W. F. (2001), *Single Piles and Pile Groups Under Lateral Loading*, A. A. Balkema, Rotterdam.

26. Rollins, K. M. and Cole, R. T. (2006), "Cyclic Lateral Load Behavior of Pile Cap and Backfill," Journal of Geotechnical and Geoenvironmental Engineering, Vol. 132, No. 9, September 2006.

27. Soubra, A. H. (2000), "Static and Seismic Earth Pressure Coefficients by Methods of Slices." Journal of Soil Mechanics and Foundations Division, ASCE, Vol. 99, No. 12, pp. 1043-1053.

28. Talbott, A. (2008), "Earthquake Resistance of Integral Abutment Bridges." West Lafayette: Purdue University.

29. Terzaghi, K. (1943), *Theoretical Soil Mechanics*, Wiley, New York.

30. Terzhaghi, K., Peck, R. B., and Mezri, G. (1996), S*oil Mechanics in Engineering Practice, 3rd Edition*, Wiley, New York.

31. Wasserman, E. P. and Walker, J. H. (1996), "Integral Abutments for Steel Bridges," Highway Structures Design Handbook, Tennessee Department of Transportation, Volume II, Chapter 5, American Iron and Steel Institute, October 1996.

32. Welch, R.C. and Reese, L.C. (1972), "Laterally Loaded Behavior of Drilled Shafts," Research Report No. 3-5-65-89, Center for Highway Research, the University of Texas at Austin, May 1972.

33. Wight, J. K. and MacGregor, J. G. (2009), *Reinforced Concrete Mechanics and Design, 5th Edition*, Pearson Education, Inc., New Jersey.

Appendix A

Construction plans
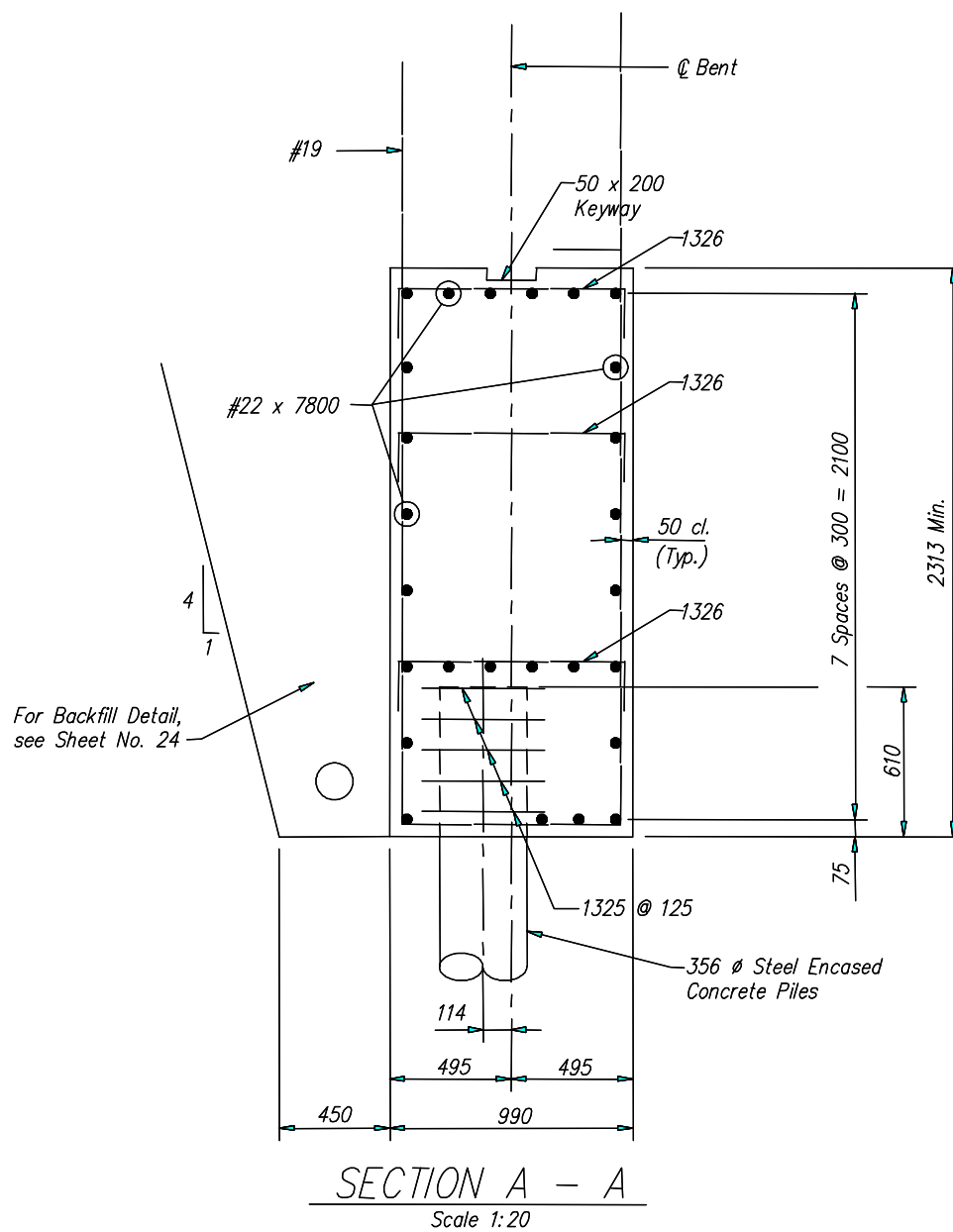
Figure A.1: End Bent Details of Bent 1 (I65 over US25)
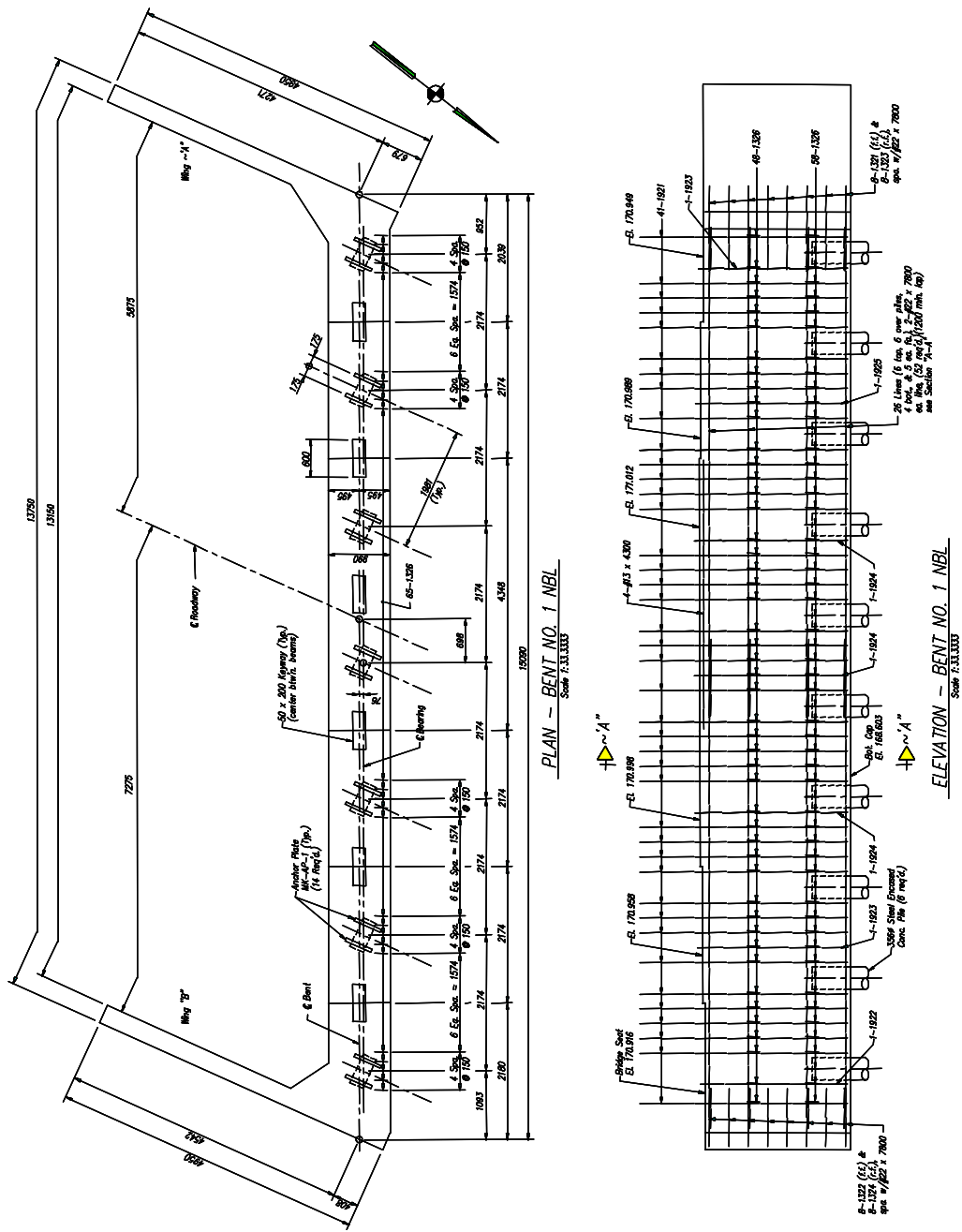
Figure A.2: Plan and Elevation Views of Bent 1 (I65 over US25)

Figure A.3: End Bent Details of Bent 1 (SR18 over Mississinewa River)
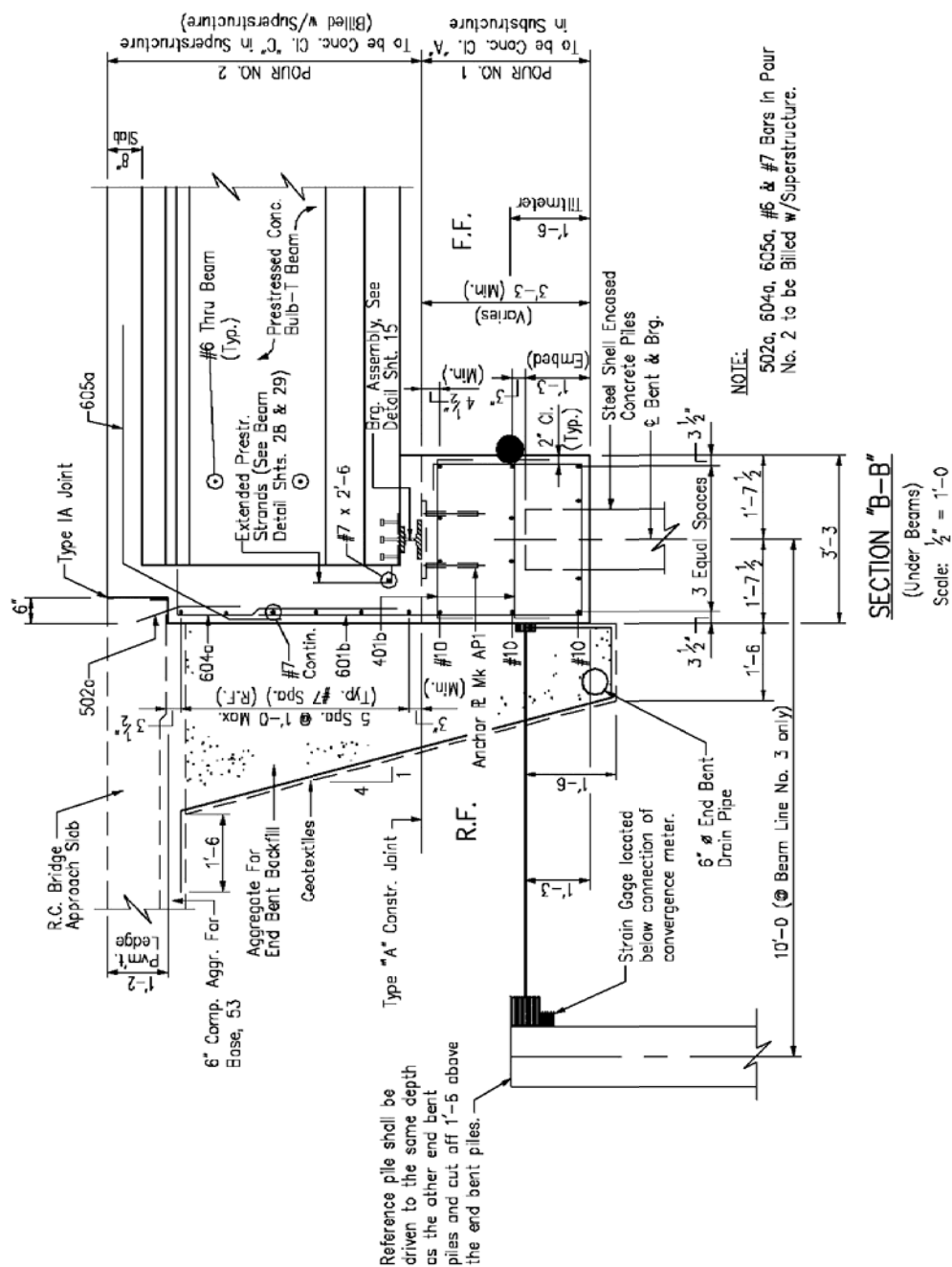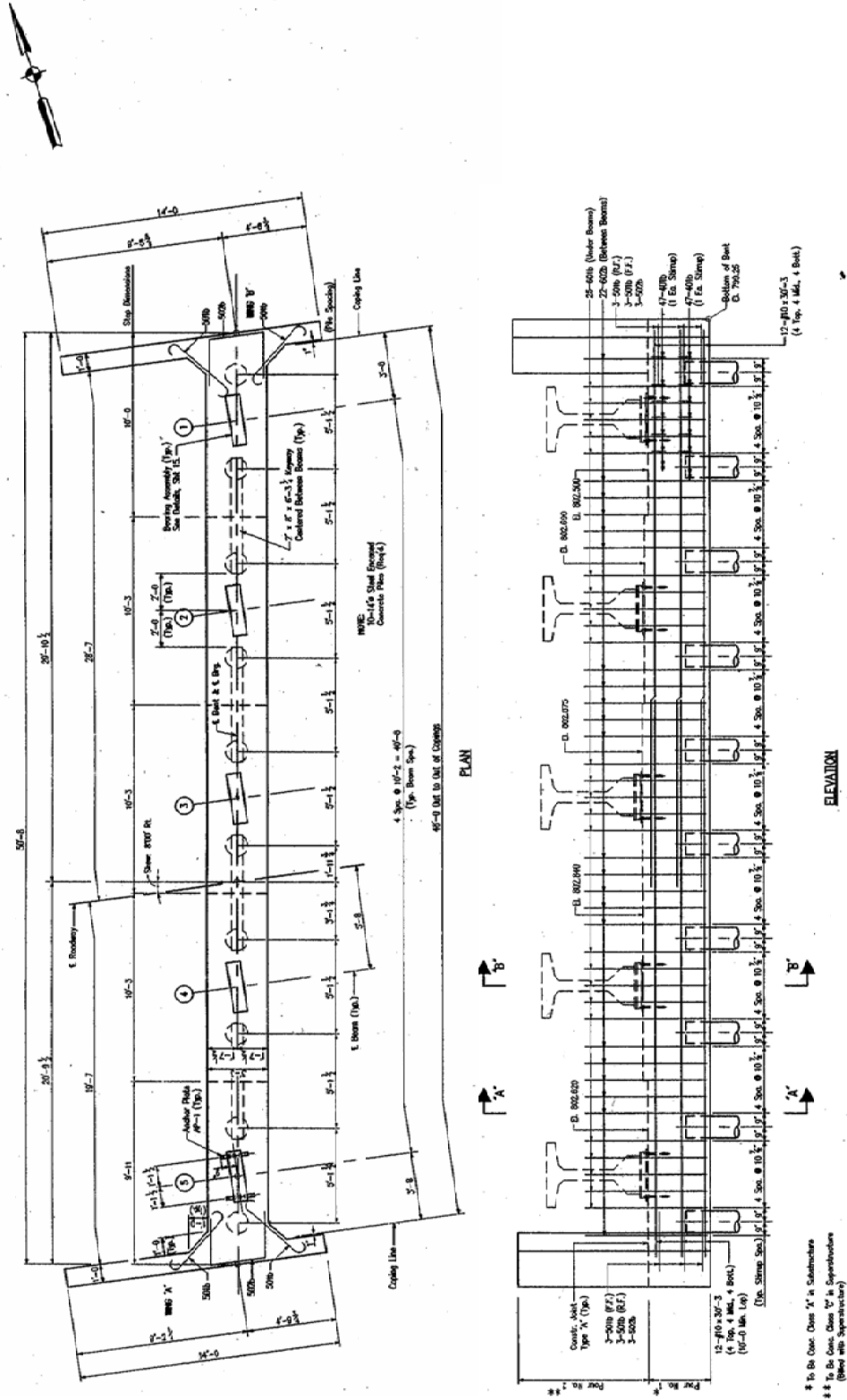
Figure A.4: Plan and Elevation Views of Bent 1 (SR18 over Mississinewa River)
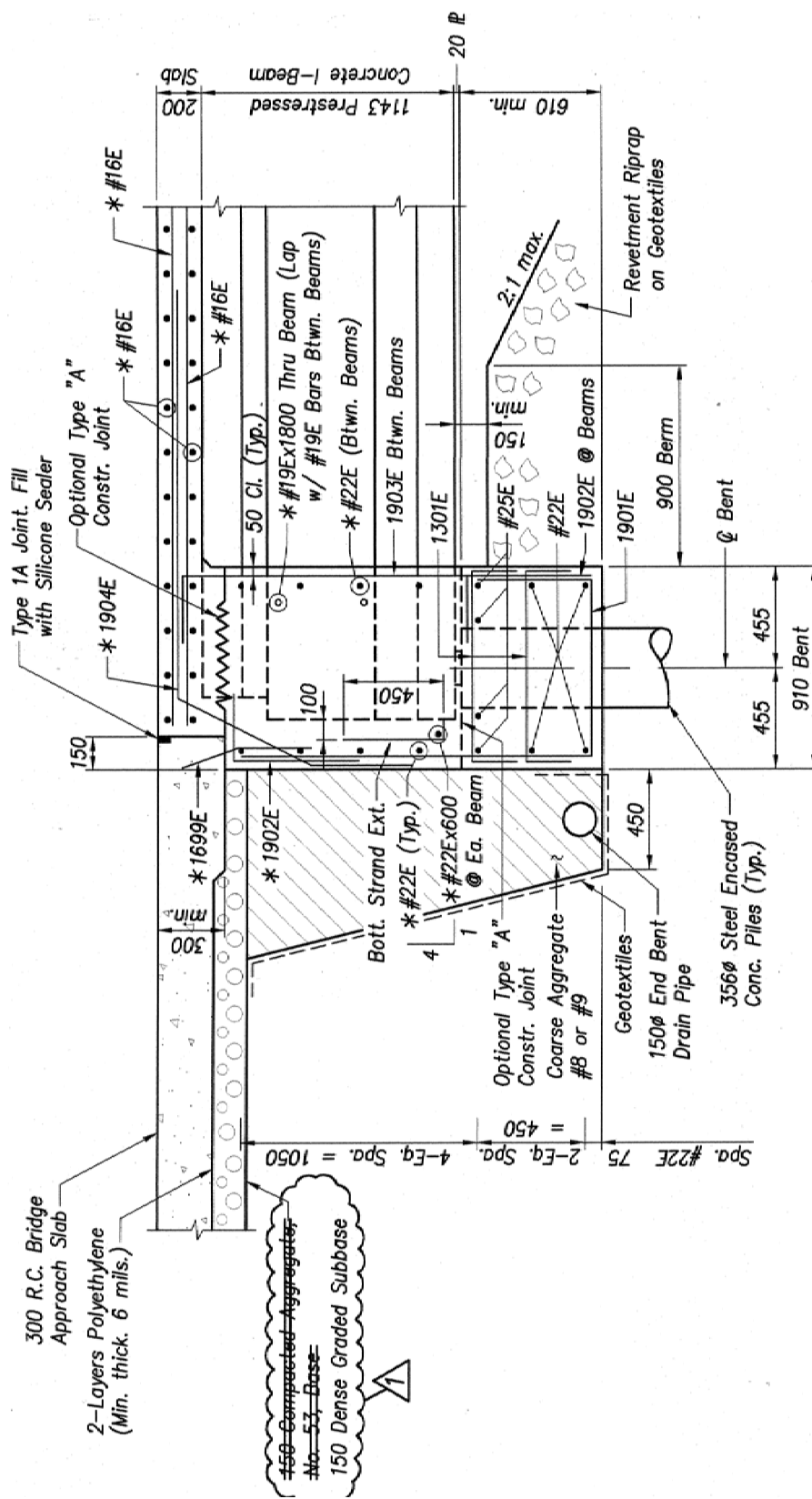
Figure A.5: End Bent Elevation View of Bent 4 (US231 over Railroad Supr)

Figure A.6: Plan and Elevation Views of Bent 4 (US231 over Railroad Supr)
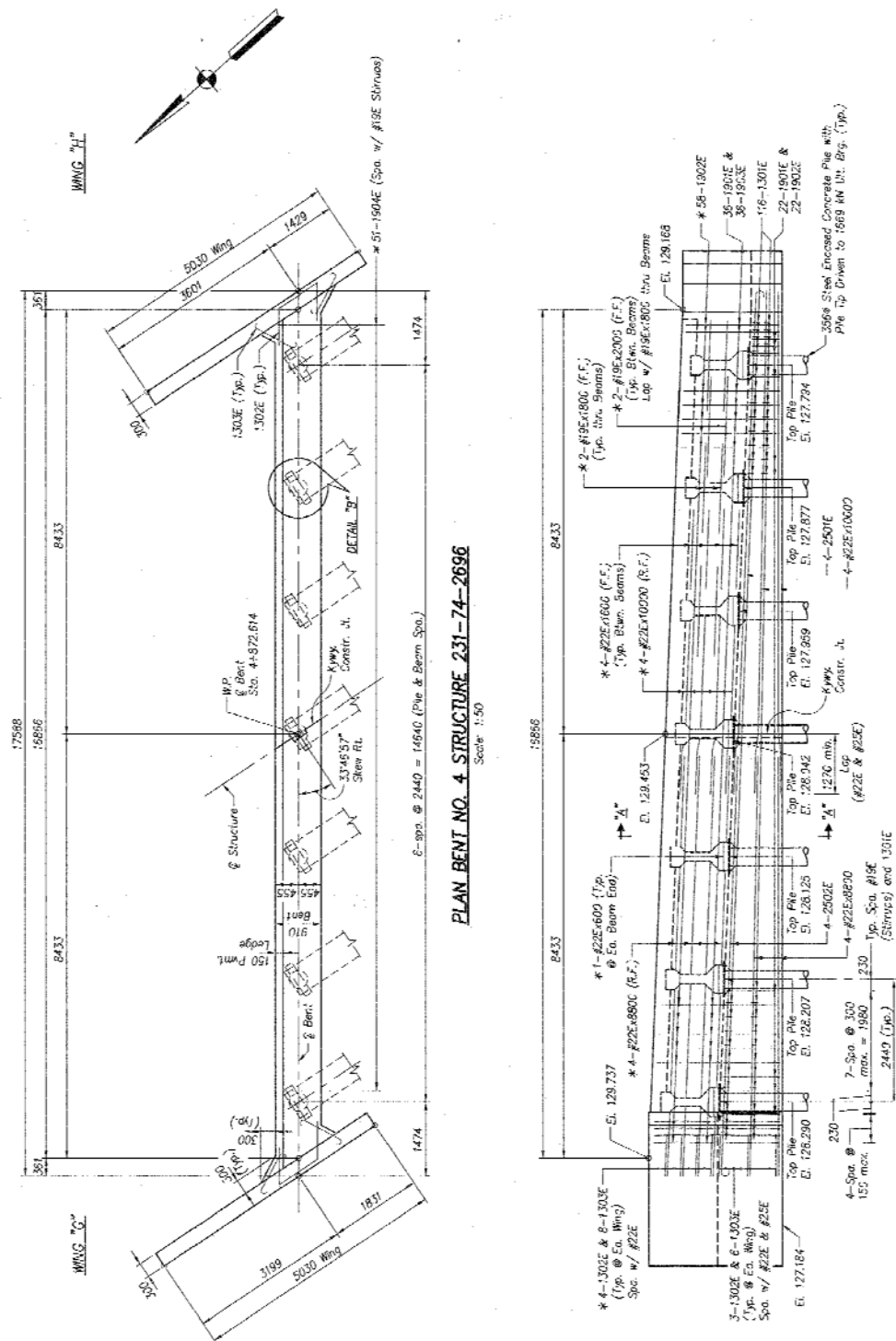
Appendix B

SR18 over The Mississinewa River Bridge Soil Borings

SOIL BORING LOG OF SR18 BRIDGE

DES. NO. 0013030 **PROJECT NO.** STP-132-5 (037) **ROAD NO.** SR18 **BORING NO.** TB-1

COUNTY: GRANT **STRU. #:** 18-27-4518

LOC: SR18 OVER MISSASSINEWA RIVER (SW CORNER) **STARTED:** 3-25-03 **COMPL:** 3-25-03

HOLE DIA: 8"

WEATHER: CLOUDY **TEMP:** 50 F **WATER ADDED:** NO **DEPTH WATER @ DRILL:** N/A
USED:

GROUND WATER @ DRILL: 33.5 **AT COMP:** DRY **AFTER 24 HRS:** N/A **HOLE CAVED TO:** 26.2

Bent 1

INTVL FT.	Blow count 0-6-12-18	Total Blow Count	% RC	FIELD
				0.0 -0.5 Asphalt
				0.5-1.4 Concrete
1.4 / 2.9	3-6-8	17	65	Tan, Stiff, Slightly Moist Silty Loam
3.5 / 5	6-8-9	23	90	Gray, Stiff, Slightly Moist Silty Clay Loam
5.5 / 10	5-7-8	20	70	Brown, Stiff, Slightly Moist Silty Loam + some sand + gravel
14 / 15	5-7-9	21	80	Tan, Stiff, Slightly Moist Silty Loam
19 / 20	4-6-6	16	65	Grayish Brown, Medium Stiff, Slightly Moist, Silty Clay Loam
24 / 25	4-5-6	15	100	Gray, Medium stiff, Slightly Moist Silty Loam
29 / 30	2-2-2	6	100	Gray, Soft, Moist Silty Loam
34 / 35	23-14-13	47	65	Gray, Soft Silty Loam
39 / 40	10-15-25	50	30	-
44 / 45	15-25-38	78	80	Gray, Hard, Dry Silty Loam

Figure B.1: Soil Boring TB-1 (SR-18)

INDOT DIVISION OF MATERIALS & TESTS GEOTECHNICAL SECTION FIELD LOG OF TEST BORINGS

SOIL BORING LOG OF SR18 BRIDGE

DES. NO. 0013030 PROJECT NO. STP-132-5 (037) ROAD NO. SR18 BORING NO. TB-2

COUNTY: GRANT STRU. #: 18-27-4518

LOC: SR18 OVER MISSASSINEWA RIVER (NE CORNER) STARTED: 3-26-03 COMPL: 3-26-03

HOLE DIA: 8"

WEATHER: SUNNY TEMP: 53 F WATER ADDED: NO DEPTH WATER @ DRILL: N/A

USED:

GROUND WATER @ DRILL: DRY AT COMP: DRY AFTER 24 HRS: N/A HOLE CAVED TO: 22.1

INTVL FT.	Blow count 0-6-12-18	Total Blow Count	% RC	FIELD
				0.0 -0.6 Asphalt
				0.6-1.2 Concrete
1.2 / 2.7	5-5-9	19	60	Brown, Stiff, Slightly Moist Silty Loam
3.5 / 8.0	11-9-8	28	20	Gray, Medium Dense, Slightly Moist Sandy Loam
8.5 / 10.0	5-5-6	16	65	Brown, Medium Stiff, Slightly Moist Slity Loam
13.5 / 15.0	4-2-2	8	80	Brown, Loose, Slightly Moist Sandy Loam
18.5 / 20.0	4-4-4	12	80	Tan, Loose, Slightly Moist Sand
23.5 / 25.0	5-5-9	19	70	Brown, Medium Dense, Moist Snad + some gravel
28.5 / 30.0	17-21-25	63	60	Gray, Hard, Slightly Moist Silty Loam
33.5 / 35.0	37-34-41	112	90	Gray, Hard, Dry Silty Clay Loam +Gravel

Figure B.2: Soil Boring TB-2 (SR-18)

Appendix C

US231 over Railroad Spur Soil Borings
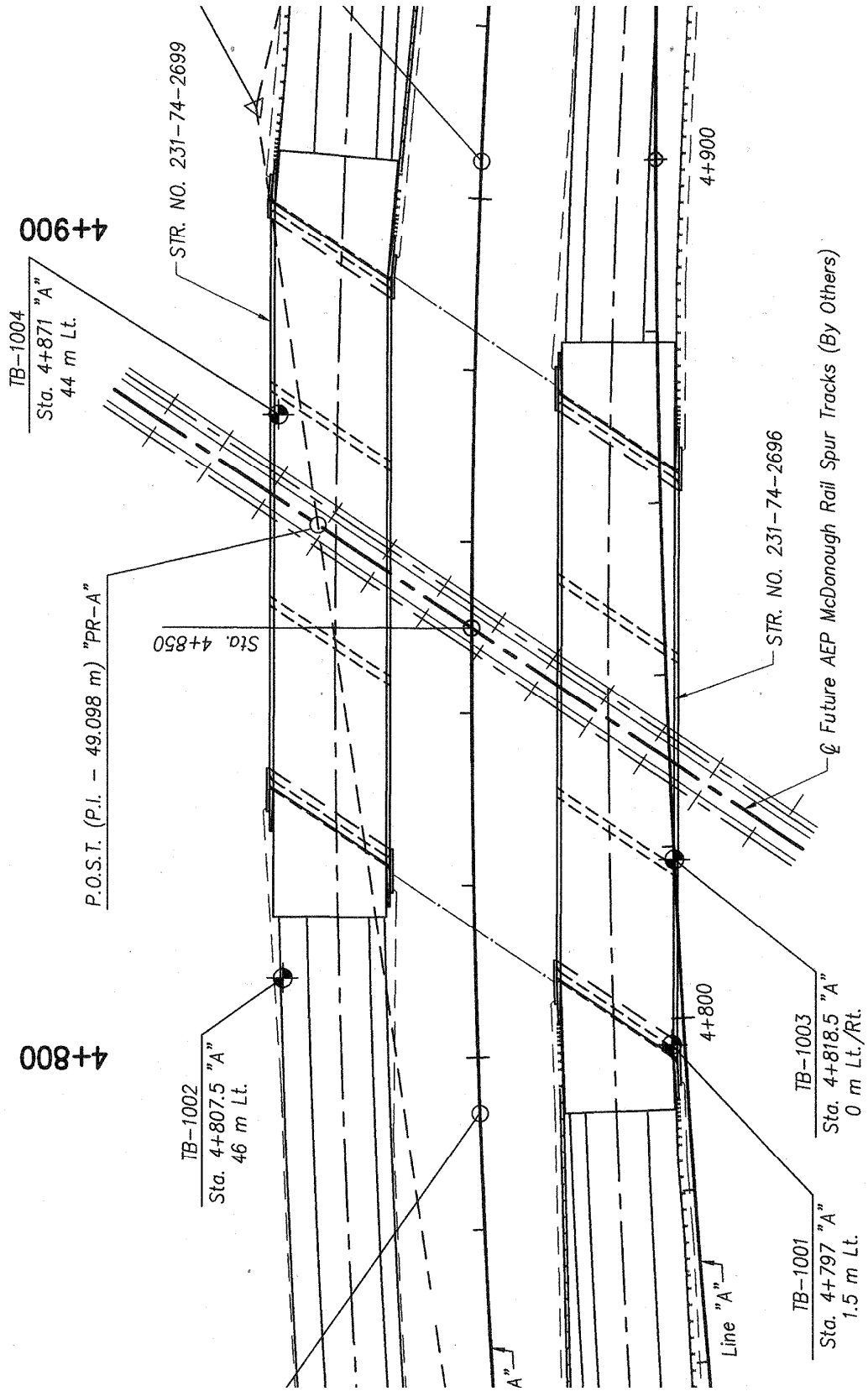
Figure C.1: Location of Soil Borings for US231 over Railway Spur

301

TB–1001
4+797 ”A”
1.5 m Lt.
118.0 m

SAMPLE		N	% Rec.	% Rqd.	DESCRIPTION
NO.	ELEV.				
	118.0				Surface El. 118.0
SS–1	117.7	7	100		Brown Clay Topsoil
SS–2		15	60		
SS–3		12	100		
SS–4		6	100		
SS–5		11	100		SILTY CLAY LOAM, medium stiff to stiff, moist, brown
SS–6	115.6 ▼	17	100		
SS–7		25	75		SILTY CLAY LOAM, medium stiff to stiff, moist, brown
SS–8	112.5	12	45		
SS–9		16	60		
SS–10		18	90		
SS–11		13	75		
SS–12		22	60		
SS–13		20	50		
SS–14		21	75		
SS–15		23	80		
SS–16		39	75		
SS–17		43	80		GRAVELLY SAND, medium dense to dense wet, brown to gray
SS–18	94.1	35	100		
1/RC			100		COMPLETELY WEATHERED SHALE, occasional sand seams, hard, gray
2/RC			100		
3/RC	93.6		100		
					SEVERELY WEATHERED SHALE, thin bedding
	93.0				horizontal discontinuity angle, soft, gray
					MODERATELY SEVERELY WEATHERED SILTSTONE, occasional clay shale seams, fine grained, thinly bedded, horizontal discontinuity angle,
	92.4				moderately hard, gray
					MODERATELY SEVERELY WEATHERED SHALE, thinly bedded horizontal discontinuity angle,
	92.1				soft, gray
					MODERATELY WEATHERED SHALE, very thinly bedded, horizontal discontinuity angle,
	90.2				medium to moderately hard, gray & black
					END OF BORING 27.8 m
					1/RC 24.0 – 24.7 m Rec. = 100%, Rqd. = 54%
					2/RC 24.7 – 26.2 m Rec. = 100%, Rqd. = 52%
					3/RC 26.2 – 27.8 m Rec. = 100%, Rqd. = 48%

Figure C.2: Soil Boring 1001 (US-231)

-header	**TB-1002**				
-header	**4+807.5 "A"**				
-header	**46 m Lt.**				
-header	**118.0 m**				

SAMPLE		N	% Rec.	% Rqd.	DESCRIPTION
NO.	ELEV.				
	118.0				Surface El. 118.0
SS-1	117.7	16	100		Brown Clay Topsoil
SS-2		11	100		
SS-3		9	100		
SS-4		8	100		SILTY CLAY LOAM, very stiff to stiff, moist, brown
SS-5	113.3	4	100		
SS-6		8	100		SILTY CLAY LOAM, medium stiff to soft, moist, brown
SS-7	111.0 ▼	17	100		
SS-8		14	100		
SS-9		22	100		
SS-10		13	100		
SS-11		14	100		
SS-12		20	100		
SS-13		17	100		
SS-14		14	100		
SS-15	97.6	20	100		GRAVELLY SAND, medium dense, wet, brown to gray
SS-16		59	100		
1/RC			88		COMPLETELY WEATHERED SANDSTONE/SILTSTONE, medium to fine grained, very dense, gray
2/RC	95.4		96		
3/RC			50		
4/RC	94.8		100		COMPLETELY WEATHERED CLAY SHALE, hard, gray
					SEVERELY WEATHERED SHALE, thinly bedded, horizontal discontinuity angle, soft to medium gray
	93.0				
					MODERATELY WEATHERED SILTSTONE, fine grained, thinly bedded, horizontal discontinuity angle, medium to moderately hard, gray
	92.5				
					MODERATELY WEATHERED SHALE, fine grained, thinly bedded, horizontal discontinuity angle, medium, gray
	91.8				
					END OF BORING 26.2 m
					1/RC 22.6 – 23.2 m Rec. = 88%, Rqd. = 0%
					2/RC 23.2 – 24.4 m Rec. = 96%, Rqd. = 44%
					3/RC 24.4 – 25.0 m Rec. = 50%, Rqd. = 50%
					4/RC 25.0 – 26.2 m Rec. = 100%, Rqd. = 49%

Figure C.3: Soil Boring 1002 (US-231)

TB−1003					
Sta. 4+818.5 "A"					
0 m Lt./Rt. (Centerline "A")					
117.9 m					

SAMPLE		N	% Rec.	% Rqd.	DESCRIPTION
NO.	ELEV.				
	117.9				Surface El. 117.9
SS-1	117.6	7	70		Brown Clay Topsoil
SS-2		8	100		
SS-3		13	100		SILTY CLAY LOAM, medium stiff to stiff,
SS-4		11	100		moist, brown
SS-5	114.9	7	100		
SS-6		5	100		SILTY CLAY LOAM, medium stiff to soft,
SS-7	110.6	▼ 16	70		brown
SS-8		17	70		
SS-9		18	45		
SS-10		15	80		
SS-11		8	50		
SS-12		21	75		
SS-13		17	35		
SS-14		26	75		
SS-15		23	75		
SS-16		19	90		GRAVELLY SAND, medium dense to dense,
SS-17	95.2	42	100		wet, brown to gray
	95.0				WEATHERED SHALE
					END OF BORING 22.9 m

Figure C.4: Soil Boring 1003 (US-231)

					TB−1004
					Sta. 4+871 "A"
					44 m Lt.
					118.2 m

SAMPLE		N	% Rec.	% Rqd.	DESCRIPTION
NO.	ELEV.				
	118.2				Surface El. 118.2
SS−1	117.9	16	100		Brown Clay Topsoil
SS−2		23	100		
SS−3		12	100		SILTY CLAY LOAM, very stiff to stiff, moist
SS−4		10	100		
SS−5	115.8	7	100		brown
SS−6		7	100		SILTY CLAY LOAM, medium stiff, moist, brown
SS−7	111.2	13	100		
SS−8		17	100		
SS−9		13	100		
SS−10		14	100		
SS−11		17	100		
SS−12		20	100		
SS−13		18	100		
SS−14		18	100		
SS−15	97.5	23	100		GRAVELLY SAND, medium dense, wet, brown, to gray
SS−16		67	75		COMPLETELY WEATHERED SHALE, hard, gray
SS−17	94.9	50	100		(visual)
1/RC				67	VERY SEVERELY TO SEVERELY WEATHERED SHALE,
2/RC				50	fine grained thinly bedded, horizontal
3/RC				71	discontinuity angle, soft, gray
	93.8				
					MODERATELY WEATHERED SILTSTONE, occasional
					limestone seams, fine grained, thinly bedded,
	93.4				horizontal discontinuity angle, hard, gray
					MODERATELY SEVERELY WEATHERED SHALE,
					fine grained, thinly bedded, horizontal
	92.3				discontinuity angle, medium, gray
					END OF BORING 25.9 m
					1/RC 22.9 − 23.3 m Rec. = 100%, Rqd. = 67%
					2/RC 23.3 − 25.3 m Rec. = 93%, Rqd. = 50%
					3/RC 25.3 − 25.9 m Rec. = 100%, Rqd. = 71%

Figure C.5: Soil Boring 1004 (US-231)

TB–1005					
4+868 "A"					
5 m Lt.					
117.6					

SAMPLE		N	% Rec.	% Rqd.	DESCRIPTION
NO.	ELEV.				
	117.6				Surface El. 117.6
SS-1	117.3	7	40		Brown Clay Topsoil
SS-2		4	80		
SS-3		12	100		
SS-4		7	100		
SS-5		5	100		SILTY CLAY LOAM, medium stiff to soft,
SS-6	115.2	7	100		moist, brown
SS-7		▼ 21	90		SILTY CLAY LOAM, medium stiff to soft,
SS-8	110.6	20	100		brown
SS-9		24	100		
SS-10		36	100		
SS-11		16	80		
SS-12		34	80		
SS-13		17	75		
SS-14		25	80		
SS-15		17	75		GRAVELLY SAND, medium dense to very dense
SS-16	96.3	10	100		wet, brown to gray
1/RC			43		
					COMPLETELY WEATHERED TO SEVERELY
					WEATHERED SHALE, fine grained, thinly bedded,
					horizontal discontinuity angle, very soft to
	93.6				soft, brownish gray to gray
					END OF BORING 24.0 m
					1/RC 22.9 – 24.0 m Rec. = 96%, Rqd. = 43%

Figure C.6: Soil Boring 1005 (US-231)

TB-1006
4+894 "A"
43 m Lt.
118.2 m

SAMPLE		N	% Rec.	% Rqd.	DESCRIPTION
NO.	ELEV.				
	118.2				Surface El. 118.2
SS-1	117.9	11	60		Brown Clay Topsoil
SS-2		17	100		
SS-3		14	100		SILTY CLAY LOAM, stiff to very stiff,
SS-4		7	100		moist, brown
SS-5	115.8	7	100		
SS-6		8	100		SILTY CLAY LOAM, medium stiff, moist, brown
SS-7	111.2	8	80		
SS-8		28	80		
SS-9		16	60		
SS-10		15	60		
SS-11		20	75		
SS-12		13	75		
SS-13		21	70		
SS-14		24	90		
SS-15		15	75		GRAVELLY SAND, loose to medium dense, wet, brown to gray
1/RC	97.5		100		COMPLETELY WEATHERED SHALE, occasional
2/RC			83		sandstone seams, soft, gray
3/RC			100		
4/RC	96.4		83		
5/RC			100		SEVERELY WEATHERED SHALE, fine grained, thinly bedded, horizontal discontinuity angle, soft to medium, gray
	93.8				
					MODERATELY WEATHERED SILTSTONE/SANDSTONE, fine to medium grained, thinly bedded, horizontal discontinuity angle, moderately hard to hard, gray
	93.4				
					END OF BORING 24.8 m
					1/RC 20.7 - 21.2 m Rec. = 100%, Rqd. = 36%
					2/RC 21.2 - 21.5 m Rec. = 83%, Rqd. = 0%
					3/RC 21.5 - 21.8 m Rec. = 100%, Rqd. = 0%
					4/RC 21.8 - 23.3 m Rec. = 83%, Rqd. = 67%
					5/RC 23.3 - 24.8 m Rec. = 100%, Rqd. = 73%

Figure C.7: Soil Boring 1006 (US-231)

Appendix D

Bowen Lab Soil Borings
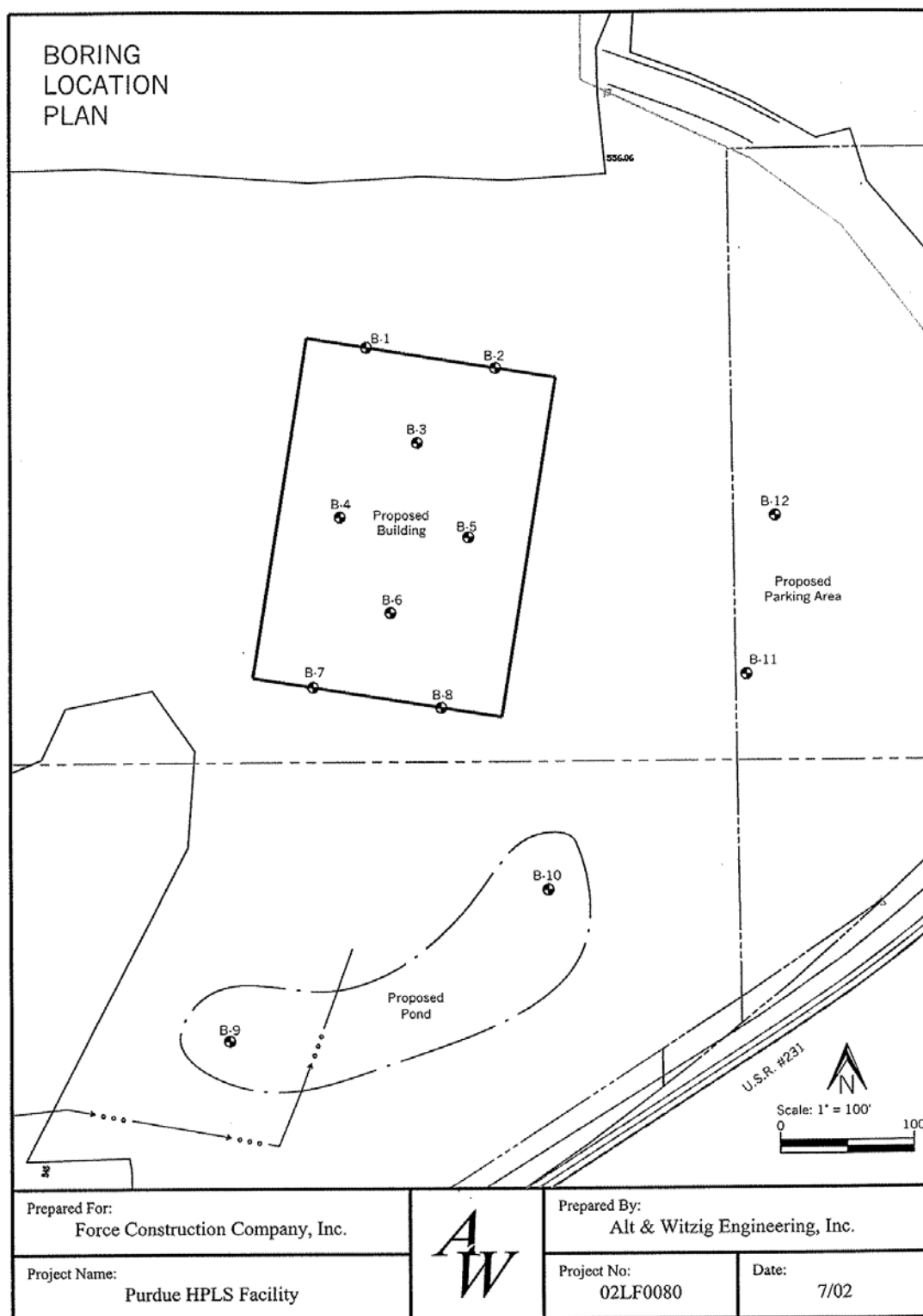
Figure D.1: Boring Location Plan for Bowen Laboratory

RECORD OF SUBSURFACE EXPLORATION

Alt & Witzig Engineering, Inc.

CLIENT	Purdue University
PROJECT NAME	Purdue HPLS Facility
LOCATION	West Lafayette, Indiana

Boring #	SB-1
Alt & Witzig File No.	02LF0080

DRILLING and SAMPLING INFORMATION

Date Started	6/24/2002
Date Completed	6/24/2002
Boring Method	HSA

Hammer Wt.	140 lbs.
Hammer Drop	30 in.
Spoon Sampler OD	2 in.

STRATA ELEV.

SOIL CLASSIFICATION

SURFACE ELEVATION 553.02

Strata Depth	Sample No.	Sample Type	Standard Penetration Test, N - Blows/foot	Qu - tsf Unconfined Compressive Strength	Pp - tsf Pocket Penetrometer	Moisture Content %
0.4	1	SS	18			19.0
1.5	2	SS	11		1.0	10.5
	3	SS	6		0.3	12.1
5.0	4	SS	3			17.0
	5	SS	17			22.4
8.0	6	SS	8			21.8
	7	SS	14	2.8		10.7
11.0	8	SS	29		1.0	22.3
	9	SS	16		0.3	21.1
	10	SS	19	1.6	1.0	24.2
		SS	17	0.8	1.0	20.9
		SS	18	2.3	1.3	13.7
19.0		SS	50/4"		1.5	18.9
21.0	14	SS	56			12.4
		SS	50/4""			9.9
		SS	50/3"			11.0
		SS	50/3""			8.3
27.0		SS	50/3"			8.3
	19	SS	50/3"			
	20	SS	50/3""			
31.0	21	SS	50/0"			

Soil classification / strata:
- Brown Clayey SILT with Organics (topsoil)
- Brown Sandy Silty CLAY with Gravel
- Dark Brown Silty CLAY with Gravel — 548.02
- Brown, Wet, Coarse, SAND and Gravel with a Trace of Clay
- Brown, Wet, Silty CLAY with a Trace of Gravel — 543.02
- Brown to Gray, Moist, Clayey SILT with a Trace of Gravel — 538.02
- Gray, Moist, Fine to Medium, Silty SAND with a Trace of Clay and Gravel — 533.02
- Gray, Wet, Sandy SILT with a Trace of Clay and Gravel and Sand Seams — 528.02
- Gray, Wet, Coarse, SAND and Gravel — 523.02
- Auger Refusal at 31 feet on an Apparent Boulder

Remarks: Caved at 9.0 feet

Depth Scale: 5, 10, 15, 20, 25, 30

Boring Method
HSA - Hollow Stem Augers
CFA - Continuous Flight Auger
DC - Driving Casing
MD - Mud Drilling

GROUNDWATER
At Completion 3.0 ft.
After hours ft.
Water on Rods 5.0 ft.

Sample Type
SS - Driven Split Spoon
ST - Pressed Shelby Tube
CA - Continuous Flight Auger
RC - Rock Core
CU - Cuttings

Figure D.2: Boring Log for Soil Boring 1

RECORD OF SUBSURFACE EXPLORATION

Alt & Witzig Engineering, Inc.

CLIENT	Purdue University	Boring #	SB-2
PROJECT NAME	Purdue HPLS Facility	Alt & Witzig File No.	02 LF 0080
LOCATION	West Lafayette, Indiana		

DRILLING and SAMPLING INFORMATION

Date Started	6/25/2002	Hammer Wt.	140 lbs.
Date Completed	6/25/2002	Hammer Drop	30 in.
Boring Method	HSA	Spoon Sampler OD	2 in.

STRATA ELEV.	SOIL CLASSIFICATION SURFACE ELEVATION 550.32	Depth Scale	Strata Depth	Sample No.	Sample Type	Ground Water	Standard Penetration Test, N - Blows/foot	Qu - tsf Unconfined Compressive Strength	Pp - tsf Pocket Penetrometer	Moisture Content %	Remarks
	Brown Clayey SILT with Organics (topsoil)		1.0	1	SS		1			57.0	
	Dark Brown Silty Sandy CLAY			2	SS		6		0.6	20.2	
				3	SS	▽	7		0.3	17.7	
545.32		5	6.0	4	SS		1			20.9	
	Brown, Dry, SILT		7.5	5	SS	O	12	2.3	1.8	24.1	
				6	SS		15			22.7	
540.32		10		7	SS		19		1.0		
	Brown to Gray Clayey SILT with a Trace of Gravel and intermittent Wet Sand Seams			8	SS		11	1.2	2.0	22.7	
				9	SS		14		1.0		
535.32		15		10	SS		14	1.6	0.5		
			17.0	11	SS		21			20.0	
				12	SS		50/5"			27.8	
				13	SS		68			21.6	
530.32		20		14	SS		50/2"			13.0	Driving on Boulders
				15	SS		50/3"				
	Gray, Wet, Medium, Silty SAND and GRAVELS			16	SS		'50/1"				
525.32		25		17	SS		50/1"				
				18	SS		50/2"				
				19	SS		50/1"				
520.32		30	30.0	20	SS		50/3"				
				21	SS		50				
	Gray Clayey SILT with a Trace of Gravel and intermittent Wet Sand Seams			22	SS		57		2.5	20.8	
				23	SS		43	4.5+	2.5	21.7	
515.32		35	36.0	24	SS		76		3.5	24.9	
	Boring Continued on Next Page										

Boring Method
HSA - Hollow Stem Augers
CFA - Continuous Flight Auger
DC - Driving Casing
MD - Mud Drilling

GROUNDWATER
▽ At Completion 5.0 ft.
▼ After hours ft.
O Water on Rods 8.0 ft.

Sample Type
SS - Driven Split Spoon
ST - Pressed Shelby Tube
CA - Continuous Flight Auger
RC - Rock Core
CU - Cuttings

Figure D.3: Boring Log for Soil Boring 2 (1/2)

RECORD OF SUBSURFACE EXPLORATION

Alt & Witzig Engineering, Inc.

CLIENT	Purdue University	Boring #	SB-2 (Cont.)
PROJECT NAME	Purdue HPLS Facility	Alt & Witzig File No.	02LF0080
LOCATION	West Lafayette, Indiana		

DRILLING and SAMPLING INFORMATION

Date Started	6/25/2002	Hammer Wt.	140	lbs.
Date Completed	6/25/2002	Hammer Drop	30	in.
Boring Method	HSA	Spoon Sampler OD	2	in.

STRATA ELEV.	SOIL CLASSIFICATION / SURFACE ELEVATION	Depth Scale	Strata Depth	Sample No.	Sample Type	Sampler Graphics	Ground Water	Standard Penetration Test, N - Blows/foot	Qu - tsf Unconfined Compressive Strength	Pp - tsf Pocket Penetrometer	Moisture Content %	Remarks
				25	SS			82	2.7	2.0	26.5	
				26	SS			84		4.3	22.9	
		40		27	SS			50/4"	0.7	4.0	22.2	
510.32				28	SS			65	1.7	1.8		
	Gray Clayey SILT with a Trace of Gravel and intermittent Wet Sand Seams			29	SS			44	1.6	2.0	17.7	
		45		30	SS			45	3.3	3.0	22.4	
505.32				31	SS			40	3.4	3.0	18.2	
				32	SS			50/3"			18.5	
				33	SS			50/4"			32.1	
500.32		50	51.0	34	SS			50/4"	4.7	3.3	19.7	
	Boring Terminated at 51.0 feet											

Boring Method	GROUNDWATER	Sample Type
HSA - Hollow Stem Augers	▽ At Completion ___ ft.	SS - Driven Split Spoon
CFA - Continuous Flight Auger	▼ After ___ hours ___ ft.	ST - Pressed Shelby Tube
DC - Driving Casing		CA - Continuous Flight Auger
MD - Mud Drilling	○ Water on Rods ___ ft.	RC - Rock Core
		CU - Cuttings

Figure D.4: Boring Log for Soil Boring 2 (2/2)

RECORD OF SUBSURFACE EXPLORATION

Alt & Witzig Engineering, Inc.

CLIENT	Purdue University	Boring #	SB-3
PROJECT NAME	Purdue HPLS Facility	Alt & Witzig File No.	02LF0080
LOCATION	West Lafayette, Indiana		

DRILLING and SAMPLING INFORMATION

Date Started	6/25/2002	Hammer Wt. 140	lbs.
Date Completed	6/25/2002	Hammer Drop 30	in.
Boring Method	HSA	Spoon Sampler OD 2	in.

STRATA ELEV.	SOIL CLASSIFICATION SURFACE ELEVATION 548.60	Depth Scale	Strata Depth	Sample No.	Sample Type	Sampler Graphics	Ground Water	Standard Penetration Test, N - Blows/foot	Qu - tsf Unconfined Compressive Strength	Pp - tsf Pocket Penetrometer	Moisture Content %	Remarks
	Brown Clayey SILT with Organics (topsoil)		1.0	1	SS			13		2.3	19.8	
				2	SS			7			14.2	
				3	SS			3			9.7	
543.60	Dark Brown, Moist to Wet, Sandy CLAY with Gravel	5		4	SS			1			15.9	
				5	SS			1			17.7	
				6	SS			7			19.0	
538.60		10	10.5	7	SS			21				
	Dark Brown, Wet, Coarse, Clayey SAND and GRAVEL		11.0	8	SS			11			21.4	
				9	SS			16		0.5	20.8	
533.60	Gray, Moist, SILT	15		10	SS			20			17.3	
				11	SS			17		3.0	15.3	
			17.5	12	SS			18		2.3	14.6	
				13	SS			67			22.1	
528.60		20		14	SS			62	3.2		15.8	
	Gray, Moist to Wet, Clayey SILT with Sand and Gravel and intermittent Wet Sand Seams			15	SS			72		4.5	7.4	
				16	SS			"50/2"		3.3	13.9	
523.60		25		17	SS			73			21.1	
			27.0	18	SS			15	3.8	2.5		
				19	SS			50				Driving on a Boulder
518.60		30		20	SS			42		4.0	22.3	
				21	SS			28	1.9	2.0	22.0	
	Gray SILT			22	SS			43	4.5	4.0		
				23	SS			60	4.5	4.0	18.1	
513.60		35	36.0	24	SS			50	4.5	4.0	17.5	
	Boring Continued on Next Page											

Boring Method	GROUNDWATER	Sample Type
HSA - Hollow Stem Augers	▽ At Completion 5.0 ft.	SS - Driven Split Spoon
CFA - Continuous Flight Auger	▼ After ___ hours ___ ft.	ST - Pressed Shelby Tube
DC - Driving Casing		CA - Continuous Flight Auger
MD - Mud Drilling	○ Water on Rods 9.0 ft.	RC - Rock Core
		CU - Cuttings

Figure D.5: Boring Log for Soil Boring 3 (1/2)

RECORD OF SUBSURFACE EXPLORATION

Alt & Witzig Engineering, Inc.

CLIENT	Purdue University	Boring #	SB-3 (Cont.)
PROJECT NAME	Purdue HPLS Facility	Alt & Witzig File No.	02LF0080
LOCATION	West Lafayette, Indiana		

DRILLING and SAMPLING INFORMATION

Date Started 6/25/2002 Hammer Wt. 140 lbs.
Date Completed 6/25/2002 Hammer Drop 30 in.
Boring Method HSA Spoon Sampler OD 2 in.

STRATA ELEV.	SOIL CLASSIFICATION / SURFACE ELEVATION	Depth Scale	Strata Depth	Sample No.	Sample Type	Standard Penetration Test, N - Blows/foot	Qu - tsf Unconfined Compressive Strength	Pp - tsf Pocket Penetrometer	Moisture Content %	Remarks
				25	SS	32				
				26	SS	48		2.5	20.7	
507.60		40		27	SS	35	3.3	3.5	19.1	
				28	SS	34	2.7	1.5	18.2	
	Gray Clayey SILT with a Trace of Gravel and intermittent Wet Sand Seams			29	SS	35	2.4	2.0	20.6	
		45		30	SS	35	2.3	2.0	24.1	
502.60				31	SS	37	2.7	2.0	20.3	
				32	SS	55	4.3	4.0	9.6	
				33	SS	57		4.5	12.6	
		50		34	SS	70	3.1	4.5	12.4	
497.60			51.0							
	Boring Terminated at 51.0 feet									

Boring Method
HSA - Hollow Stem Augers
CFA - Continuous Flight Auger
DC - Driving Casing
MD - Mud Drilling

GROUNDWATER
▽ At Completion ft.
▼ After hours ft.
○ Water on Rods ft.

Sample Type
SS - Driven Split Spoon
ST - Pressed Shelby Tube
CA - Continuous Flight Auger
RC - Rock Core
CU - Cuttings

Figure D.6: Boring Log for Soil Boring 3 (2/2)

RECORD OF SUBSURFACE EXPLORATION

Alt & Witzig Engineering, Inc.

CLIENT: Purdue University
PROJECT NAME: Purdue HPLS Facility
LOCATION: West Lafayette, Indiana

Boring #: SB-4
Alt & Witzig File No.: 02LF0080

DRILLING and SAMPLING INFORMATION

Date Started: 6/28/2002
Date Completed: 7/1/2002
Boring Method: HSA

Hammer Wt. 140 lbs.
Hammer Drop 30 in.
Spoon Sampler OD 2 in.

SOIL CLASSIFICATION
SURFACE ELEVATION 549.97

STRATA ELEV.	Soil Classification	Strata Depth	Sample No.	Sample Type	Standard Penetration Test, N - Blows/foot	Qu - tsf Unconfined Compressive Strength	Pp - tsf Pocket Penetrometer	Moisture Content %
	Brown Clayey SILT with Organics (topsoil)	1.0	1	SS	8			17.4
			2	SS	12			
			3	SS	9			10.2
544.97			4	SS	21			8.5
			5	SS	17			10.8
	Brown Silty Sandy CLAY with a trace of Sand, Gravel and Cobbles (Fill)		6	SS	24		0.3	10.5
539.97			7	SS	46			11.3
			8	SS	23			14.2
			9	SS	10			10.8
534.97			10	SS	14		0.5	17.3
	Brown Silty CLAY with a trace of Sand and Gravel	16.0	11	SS	44	3.2	3.0	19.9
		17.0	12	SS	16	1.1	2.5	18.1
	Gray SILT		13	SS	23	1.1	1.0	18.2
529.97		20.0	14	SS	50/2"			16.1
	Gray Silty CLAY	21.5	15	SS	41			
			16	SS	64			
	Gray wet medium coarse SAND and GRAVEL	25.0	17	SS	50/4"			10.4
524.97			18	SS	50/4"			13.8
	Gray Silty CLAY with a trace of Sand and Gravel	28.0	19	SS	70			10.8
519.97			20	SS	32	4.5+		19.8
			21	SS	47		4.0	37.6
	Gray Clayey SILT with a trace of Sand and Gravel		22	SS	37	4.9	1.8	18.3
			23	SS	36		4.0	20.7
514.97			24	SS	38	5.4	4.0	17.4
	Boring Continued on Next Page							

Boring Method
HSA - Hollow Stem Augers
CFA - Continuous Flight Auger
DC - Driving Casing
MD - Mud Drilling

GROUNDWATER
At Completion Dry ft.
After hours ft.
Water on Rods 24.0 ft.

Sample Type
SS - Driven Split Spoon
ST - Pressed Shelby Tube
CA - Continuous Flight Auger
RC - Rock Core
CU - Cuttings

Figure D.7: Boring Log for Soil Boring 4 (1/2)

RECORD OF SUBSURFACE EXPLORATION

Alt & Witzig Engineering, Inc.

CLIENT	Purdue University
PROJECT NAME	Purdue HPLS Facility
LOCATION	West Lafayette, Indiana

Boring #	SB-4 (Cont.)
Alt & Witzig File No.	02LF0080

DRILLING and SAMPLING INFORMATION

Date Started	6/28/2002	Hammer Wt.	140	lbs.
Date Completed	7/1/2002	Hammer Drop	30	in.
Boring Method	HSA	Spoon Sampler OD	2	in.

STRATA ELEV.	SOIL CLASSIFICATION / SURFACE ELEVATION	Depth Scale	Strata Depth	Sample No.	Sample Type	Sampler Graphics	Ground Water	Standard Penetration Test, N - Blows/foot	Qu - tsf Unconfined Compressive Strength	Pp - tsf Pocket Penetrometer	Moisture Content %	Remarks
				25	SS			22	4.5+	3.0	18.6	
				26	SS			82	3.0	3.0	19.7	
		40		27	SS			48	3.4	2.5		
509.97				28	SS			70	5.9	3.5	18.0	
	Gray Clayey SILT with a trace of Sand and Gravel			29	SS			59	3.9	3.0	16.5	
		45		30	SS			43	1.9	2.5	17.4	
504.97				31	SS			63		1.8	16.2	
				32	SS			31	2.6	2.3	18.6	
				33	SS			51	4.5+	4.0	13.6	
		50		34	SS			47	4.7	4.0	12.9	
	Boring Terminated at 51.0 feet		51.0									

Boring Method
HSA - Hollow Stem Augers
CFA - Continuous Flight Auger
DC - Driving Casing
MD - Mud Drilling

GROUNDWATER
▽ At Completion Dry ft.
▼ After hours ft.
○ Water on Rods 24.0 ft.

Sample Type
SS - Driven Split Spoon
ST - Pressed Shelby Tube
CA - Continuous Flight Auger
RC - Rock Core
CU - Cuttings

Figure D.8: Boring Log for Soil Boring 4 (2/2)
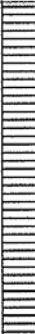
RECORD OF SUBSURFACE EXPLORATION

Alt & Witzig Engineering, Inc.

CLIENT **Purdue University**
PROJECT NAME **Purdue HPLS Facility**
LOCATION **West Lafayette, Indiana**

Boring # **SB-5**
Alt & Witzig File No. **02LF0080**

DRILLING and SAMPLING INFORMATION

Date Started **6/27/2002** — Hammer Wt. **140** lbs.
Date Completed **6/27/2002** — Hammer Drop **30** in.
Boring Method **HSA** — Spoon Sampler OD **2** in.

STRATA ELEV.	SOIL CLASSIFICATION — SURFACE ELEVATION 548.05	Depth Scale	Strata Depth	Sample No.	Sample Type	Sampler Graphics	Ground Water	Standard Penetration Test, N - Blows/foot	Qu - tsf Unconfined Compressive Strength	Pp - tsf Pocket Penetrometer	Moisture Content %	Remarks
	Brown Clayey SILT with Organics (topsoil)		0.5	1	SS			8		2.0	21.1	
				2	SS			50/1"			12.8	Driving on a Boulder
543.05				3	SS			50/0"			9.2	Driving on a Boulder
	Brown Silty Sandy CLAY with a Trace of Gravel	5		4	SS			50/3"			12.6	Driving on a Boulder
				5	SS			35				
				6	SS			50/3"			10.3	Driving on a Boulder
538.05		10	10.5	7	SS			38				
				8	SS	▽		25				
	Brown, Dry, Fine, SAND			9	SS	○		59				
533.05		15	14.0	10	SS			47				Driving on a Boulder
				11	SS			49				
	Gray, Wet, Coarse, Silty SAND and GRAVEL with a Trace of Clay			12	SS			61			15.9	
			19.0	13	SS			26				
528.05		20		14	SS			20		1.0		
	Gray Clayey SILT with intermittent Wet Sand Seams			15	SS			54				
			23.0	16	SS			42			21.5	
523.05		25		17	SS			70				
	Gray, Wet, Medium to Fine, SAND with a Trace of Gravel			18	SS			41				
			28.0	19	SS			47				
518.05		30		20	SS			40	4.5	3.0	20.3	
				21	SS			30		3.8	19.7	
	Gray Clayey SILT			22	SS			63		4.5	12.4	
				23	SS			53	4.7	3.5	16.4	
513.05		35	36.0	24	SS			50/4"	4.5	3.8	14.3	
	Boring Continued on Next Page											

Boring Method
HSA - Hollow Stem Augers
CFA - Continuous Flight Auger
DC - Driving Casing
MD - Mud Drilling

GROUNDWATER
▽ At Completion **12.0** ft.
▼ After ___ hours ___ ft.
○ Water on Rods **13.0** ft.

Sample Type
SS - Driven Split Spoon
ST - Pressed Shelby Tube
CA - Continuous Flight Auger
RC - Rock Core
CU - Cuttings

Figure D.9: Boring Log for Soil Boring 5 (1/2)

RECORD OF SUBSURFACE EXPLORATION

Alt & Witzig Engineering, Inc.

CLIENT	Purdue University
PROJECT NAME	Purdue HPLS Facility
LOCATION	West Lafayette, Indiana

Boring # SB-5 (Cont.)
Alt & Witzig File No. 02LF0080

DRILLING and SAMPLING INFORMATION

Date Started	6/27/2002	Hammer Wt. 140	lbs.
Date Completed	6/27/2002	Hammer Drop 30	in.
Boring Method	HSA	Spoon Sampler OD 2	in.

STRATA ELEV.	SOIL CLASSIFICATION / SURFACE ELEVATION	Depth Scale	Strata Depth	Sample No.	Sample Type	Sampler Graphics	Ground Water	Standard Penetration Test, N - Blows/foot	Qu - tsf Unconfined Compressive Strength	Pp - tsf Pocket Penetrometer	Moisture Content %	Remarks
	Gray, Wet, Coarse, SAND and GRAVELS			25	SS			50/4"				
				26	SS			50/4"				
		40	40.0	27	SS			68		4.0	15.3	
509.05				28	SS			58	4.5	4.0	15.6	
				29	SS			52		2.3	18.7	
		45		30	SS			48	3.3	2.5	14.8	
504.05	Gray Clayey SILT with intermittent Wet Sand Seams			31	SS			56	4.5	3.5	13.7	
				32	SS			50/4"	4.1	3.8	14.9	
				33	SS			64	4.7	3.0	13.9	
		50		34	SS			80	5.4	3.8	14.0	
499.05			51.0									
	Boring Terminated at 51.0 feet											

Boring Method
HSA - Hollow Stem Augers
CFA - Continuous Flight Auger
DC - Driving Casing
MD - Mud Drilling

GROUNDWATER
▽ At Completion ____ ft.
▼ After ____ hours ____ ft.
◯ Water on Rods ____ ft.

Sample Type
SS - Driven Split Spoon
ST - Pressed Shelby Tube
CA - Continuous Flight Auger
RC - Rock Core
CU - Cuttings

Figure D.10: Boring Log for Soil Boring 5 (2/2)

RECORD OF SUBSURFACE EXPLORATION

Alt & Witzig Engineering, Inc.

CLIENT	Purdue University	Boring #	SB-6
PROJECT NAME	Purdue HPLS Facility	Alt & Witzig File No.	02LF0080
LOCATION	West Lafayette, Indiana		

DRILLING and SAMPLING INFORMATION

Date Started	6/25/2002	Hammer Wt.	140	lbs.
Date Completed	6/25/2002	Hammer Drop	30	in.
Boring Method	HSA	Spoon Sampler OD	2	in.

STRATA ELEV.	SOIL CLASSIFICATION SURFACE ELEVATION 541.64	Depth Scale	Strata Depth	Sample No.	Sample Type	Sampler Graphics	Ground Water	Standard Penetration Test, N - Blows/foot	Qu - tsf Unconfined Compressive Strength	Pp - tsf Pocket Penetrometer	Moisture Content %	Remarks
	Brown, Dry, Fine, SAND			1	SS			16				
				2	SS			17				
				3	SS			19				
536.64		5		4	SS			21				
			7.5	5	SS			25				
				6	SS			23				
531.64	Brown, Moist to Wet, Fine to Medium, SAND	10		7	SS			50/4"				
			12.0	8	SS			50/0"				
				9	SS			5			18.4	
526.64		15		10	SS			13			22.0	
				11	SS			15			20.3	
				12	SS			5			19.2	
				13	SS			16			16.9	
521.64		20		14	SS			22			16.0	
				15	SS			36			18.3	
	Gray Clayey SILT with a Trace of Gravel and intermittent Wet Sand Seams			16	SS			44			20.2	
516.64		25		17	SS			47	1.9	1.5	21.3	
				18	SS			55	2.4	1.5	18.2	
				19	SS			65	1.9	1.5	20.7	
511.64		30		20	SS			41			20.2	
				21	SS			35	2.2	3.5	18.0	
				22	SS			34	1.9	2.3	16.6	
				23	SS			28	1.9	2.0	24.5	
506.64		35	36.0	24	SS			35	1.9	1.5	18.8	
	Boring Continued on Next Page											

Boring Method
HSA - Hollow Stem Augers
CFA - Continuous Flight Auger
DC - Driving Casing
MD - Mud Drilling

GROUNDWATER
▽ At Completion 3.0 ft.
▼ After hours ft.
○ Water on Rods 7.5 ft.

Sample Type
SS - Driven Split Spoon
ST - Pressed Shelby Tube
CA - Continuous Flight Auger
RC - Rock Core
CU - Cuttings

Figure D.11: Boring Log for Soil Boring 6 (1/2)

RECORD OF SUBSURFACE EXPLORATION

Alt & Witzig Engineering, Inc.

CLIENT	Purdue University		Boring #	SB-6 (Cont.)
PROJECT NAME	Purdue HPLS Facility		Alt & Witzig File No.	02LF0080
LOCATION	West Lafayette, Indiana			

DRILLING and SAMPLING INFORMATION

Date Started	6/25/2002	Hammer Wt. 140	lbs.
Date Completed	6/25/2002	Hammer Drop 30	in.
Boring Method	HSA	Spoon Sampler OD 2	in.

STRATA ELEV.	SOIL CLASSIFICATION / SURFACE ELEVATION	Depth Scale	Strata Depth	Sample No.	Sample Type	Sampler Graphics	Ground Water	Standard Penetration Test, N - Blows/foot	Qu - tsf Unconfined Compressive Strength	Pp - tsf Pocket Penetrometer	Moisture Content %	Remarks
				25	SS			35	3.4	2.0		
				26	SS			37			18.2	
		40		27	SS			39			21.8	
501.64				28	SS			49	1.9	1.5	15.7	
	Gray Clayey SILT with a Trace of Gravel and intermittent Wet Sand Seams			29	SS			48	3.0	3.0	14.0	
		45		30	SS			40			18.9	
496.64				31	SS			55	3.9		11.7	
				32	SS			40			15.3	
		50		33	SS			28		3.0	28.0	
491.64			51.0	34	SS			24			28.5	
	Boring Terminated at 51.0 feet											

Boring Method
HSA - Hollow Stem Augers
CFA - Continuous Flight Auger
DC - Driving Casing
MD - Mud Drilling

GROUNDWATER
▽ At Completion ft.
▼ After hours ft.
○ Water on Rods ft.

Sample Type
SS - Driven Split Spoon
ST - Pressed Shelby Tube
CA - Continuous Flight Auger
RC - Rock Core
CU - Cuttings

Figure D.12: Boring Log for Soil Boring 6 (2/2)

RECORD OF SUBSURFACE EXPLORATION
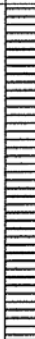
Alt & Witzig Engineering, Inc.

CLIENT	Purdue University	Boring #	SB-7
PROJECT NAME	Purdue HPLS Facility	Alt & Witzig File No.	02LF0080
LOCATION	West Lafayette, Indiana		

DRILLING and SAMPLING INFORMATION

Date Started	6/24/2002	Hammer Wt.	140	lbs.
Date Completed	6/24/2002	Hammer Drop	30	in.
Boring Method	HSA	Spoon Sampler OD	2	in.

STRATA ELEV.	SOIL CLASSIFICATION / SURFACE ELEVATION 541.51	Depth Scale	Strata Depth	Sample No.	Sample Type	Sampler Graphics	Ground Water	Standard Penetration Test, N - Blows/foot	Qu - tsf Unconfined Compressive Strength	Pp - tsf Pocket Penetrometer	Moisture Content %	Remarks
	Brown Clayey SILT with Organics (topsoil)		3.0	1	SS			22				
	Brown, Dry, Fine, SAND w Concrete & Asphalt fragment			2	SS			33				
536.51	Brown, Dry, Fine, SAND	5		3	SS		▽	21				
				4	SS			13				
			6.5	5	SS			11				
	Brown, Wet, Fine, SAND			6	SS		O	10				
531.51		10		7	SS			16				
			11.0	8	SS			36				
				9	SS			40				
	Brown, Wet, Fine to Coarse, Silty SAND with Cobbles and Clay Seams			10	SS			28			22.1	
526.51		15		11	SS			19				
	Gray, Wet, Sandy CLAY		17.0	12	SS			11				
	Gray SILT		18.0	13	SS			8			8.8	
521.51		20	19.5	14	SS			30		4.0	6.8	
	Gray Clayey SILT with a Trace of Sand and Gravel			15	SS			50/3'''		4.0	7.7	
			24.0	16	SS			38			25.3	
516.51		25		17	SS			36	4.5	4.3	18.7	
				18	SS			35		4.3	20.7	
				19	SS			37		4.3	17.2	
511.51	Gray Clayey SILT	30		20	SS			37				
				21	SS			35		4.0	20.7	
				22	SS			58		4.0	13.2	
				23	SS			21		4.5	12.7	
506.51		35	36.0	24	SS			48		3.5	14.3	
	Boring Continued on Next Page											

Boring Method	GROUNDWATER	Sample Type
HSA - Hollow Stem Augers	▽ At Completion 4.0 ft.	SS - Driven Split Spoon
CFA - Continuous Flight Auger	▼ After ___ hours ___ ft.	ST - Pressed Shelby Tube
DC - Driving Casing	O Water on Rods 9.0 ft.	CA - Continuous Flight Auger
MD - Mud Drilling		RC - Rock Core
		CU - Cuttings

Figure D.13: Boring Log for Soil Boring 7 (1/2)

RECORD OF SUBSURFACE EXPLORATION

Alt & Witzig Engineering, Inc.

CLIENT	Purdue University
PROJECT NAME	Purdue HPLS Facility
LOCATION	West Lafayette, Indiana

Boring # SB-7 (Cont.)
Alt & Witzig File No. 02LF0080

DRILLING and SAMPLING INFORMATION

Date Started 6/24/2002 Hammer Wt. 140 lbs.
Date Completed 6/24/2002 Hammer Drop 30 in.
Boring Method HSA Spoon Sampler OD 2 in.

STRATA ELEV.	SOIL CLASSIFICATION / SURFACE ELEVATION	Depth Scale	Strata Depth	Sample No.	Sample Type	Sampler Graphics	Ground Water	Standard Penetration Test, N - Blows/foot	Qu - tsf Unconfined Compressive Strength	Pp - tsf Pocket Penetrometer	Moisture Content %	Remarks
				25	SS			51		4.5	15.6	
				26	SS			40	5.4	3.5	16.6	
		40		27	SS			44		4.5	13.4	
501.21				28	SS			40				
	Gray Clayey SILT			29	SS			42	1.8	3.5	14.2	
		45		30	SS			38	3.9	3.0	16.0	
496.21				31	SS			35			16.7	
			48.0	32	SS			52	4.1	2.8	16.0	
	Gray Clayey SILT with Wet Sand and Gravel Seams	50		33	SS			64		2.5	16.0	
	Boring Terminated at 51.0 feet		51.0	34	SS			76			21.9	

Boring Method
HSA - Hollow Stem Augers
CFA - Continuous Flight Auger
DC - Driving Casing
MD - Mud Drilling

GROUNDWATER
▽ At Completion ___ ft.
▼ After ___ hours ___ ft.
○ Water on Rods ___ ft.

Sample Type
SS - Driven Split Spoon
ST - Pressed Shelby Tube
CA - Continuous Flight Auger
RC - Rock Core
CU - Cuttings

Figure D.14: Boring Log for Soil Boring 7 (2/2)

RECORD OF SUBSURFACE EXPLORATION

Alt & Witzig Engineering, Inc.

CLIENT	Purdue University	Boring #	SB-8
PROJECT NAME	Purdue HPLS Facility	Alt & Witzig File No.	02LF0080
LOCATION	West Lafayette, Indiana		

DRILLING and SAMPLING INFORMATION

Date Started	6/28/2002	Hammer Wt. 140 lbs.	
Date Completed	7/1/2002	Hammer Drop 30 in.	
Boring Method	HSA	Spoon Sampler OD 2 in.	

STRATA ELEV.	SOIL CLASSIFICATION / SURFACE ELEVATION 539.84	Depth Scale	Strata Depth	Sample No.	Sample Type	Sampler Graphics	Ground Water	Standard Penetration Test, N - Blows/foot	Qu - tsf Unconfined Compressive Strength	Pp - tsf Pocket Penetrometer	Moisture Content %	Remarks
	Brown, Dry to Wet, Fine, SAND with a Trace of Gravel			1	SS			7				
				2	SS			13				
534.84		5		3	SS			12				
				4	SS			13				
			7.0	5	SS			15				
				6	SS		O	16				
529.84		10		7	SS			16				Caved at 10.5 feet
				8	SS			14				
				9	SS			14				
524.84		15	15.0	10	SS			23				
	Brown Clayey SILT		17.0	11	SS			17	1.9	2.5	23.6	
				12	SS			15	0.7		21.1	
519.84		20		13	SS			14				
				14	SS			5				
	Gray, Wet, Medium, Silty SAND with Gravel			15	SS			20				
				16	SS			43				
514.84		25		17	SS			69				
				18	SS			50/4""				
			28.5	19	SS			40				
509.84		30		20	SS			37				
	Gray, Wet, Coarse to Medium, SAND and GRAVEL			21	SS			50/3"				
				22	SS			50/3"				
				23	SS			50/5"				
504.84		35	36.0	24	SS			45				
	Boring Continued on Next Page											

Boring Method
HSA - Hollow Stem Augers
CFA - Continuous Flight Auger
DC - Driving Casing
MD - Mud Drilling

GROUNDWATER
▽ At Completion Dry ft.
▼ After hours ft.
O Water on Rods 8.5 ft.

Sample Type
SS - Driven Split Spoon
ST - Pressed Shelby Tube
CA - Continuous Flight Auger
RC - Rock Core
CU - Cuttings

Figure D.15: Boring Log for Soil Boring 8 (1/2)

RECORD OF SUBSURFACE EXPLORATION

Alt & Witzig Engineering, Inc.

CLIENT	Purdue University
PROJECT NAME	Purdue HPLS Facility
LOCATION	West Lafayette, Indiana

Boring #	SB-8 (Cont.)
Alt & Witzig File No.	02LF0080

DRILLING and SAMPLING INFORMATION

Date Started	6/28/2002	Hammer Wt. 140	lbs.
Date Completed	7/1/2002	Hammer Drop 30	in.
Boring Method	HSA	Spoon Sampler OD 2	in.

STRATA ELEV.	SOIL CLASSIFICATION / SURFACE ELEVATION	Depth Scale	Strata Depth	Sample No.	Sample Type	Sampler Graphics	Ground Water	Standard Penetration Test, N - Blows/foot	Qu - tsf Unconfined Compressive Strength	Pp - tsf Pocket Penetrometer	Moisture Content %	Remarks
	Gray, Wet, Coarse to Medium, SAND and GRAVEL			25	SS			89				
				26	SS			50/3"				
		40		27	SS			50/4"				
499.80			41.5	28	SS			81	4.5	4.5	12.7	
	Gray Clayey SILT with a Trace of Sand and Gravel			29	SS			50/4"				
		45		30	SS			56		4.5	12.2	
494.80				31	SS			57	4.5	4.3	15.7	
				32	SS			41	4.1	4.0	23.9	
			49.0	33	SS			50/4""				
	Gray, Wet, Fine, SAND with a Trace of Gravel	50	51.0	34	SS			35				
	Boring Terminated at 51.0 feet											

Boring Method
HSA - Hollow Stem Augers
CFA - Continuous Flight Auger
DC - Driving Casing
MD - Mud Drilling

GROUNDWATER
▽ At Completion ___ ft.
▼ After ___ hours ___ ft.
○ Water on Rods ___ ft.

Sample Type
SS - Driven Split Spoon
ST - Pressed Shelby Tube
CA - Continuous Flight Auger
RC - Rock Core
CU - Cuttings

Figure D.16: Boring Log for Soil Boring 8 (2/2)

RECORD OF SUBSURFACE EXPLORATION

Alt & Witzig Engineering, Inc.

CLIENT **Purdue University**
PROJECT NAME **Purdue HPLS Facility**
LOCATION **West Lafayette, Indiana**

Boring # **SB-9**
Alt & Witzig File No. **02LF0080**

DRILLING and SAMPLING INFORMATION

Date Started **7/2/2002**   Hammer Wt. **140** lbs.
Date Completed **7/2/2002**   Hammer Drop **30** in.
Boring Method **HSA**   Spoon Sampler OD **2** in.

STRATA ELEV.	SOIL CLASSIFICATION SURFACE ELEVATION 545.19	Depth Scale	Strata Depth	Sample No.	Sample Type	Sampler Graphics	Ground Water	Standard Penetration Test, N - Blows/foot	Qu - tsf Unconfined Compressive Strength	Pp - tsf Pocket Penetrometer	Moisture Content %	Remarks
								39				
				2	SS			20				
540.19	Brown, Fine to Medium Coarse, SAND and Gravel	5		3	SS		▽	17				
				4	SS			7				
				5	SS			5				
			9.0	6	SS			5				
535.19		10		7	SS		○	6				
				8	SS			9				
				9	SS			9				
530.19	Brown, Wet, Coarse, SAND and Gravel	15		10	SS			12				
				11	SS			19				
				12	SS			37				
				13	SS			29				
525.19		20	21.0	14	SS			18				
	Boring Terminated at 21 feet											

Boring Method
HSA - Hollow Stem Augers
CFA - Continuous Flight Auger
DC - Driving Casing
MD - Mud Drilling

GROUNDWATER
▽ At Completion **5.0** ft.
▼ After ___ hours ___ ft.
○ Water on Rods **11.0** ft.

Sample Type
SS - Driven Split Spoon
ST - Pressed Shelby Tube
CA - Continuous Flight Auger
RC - Rock Core
CU - Cuttings

Figure D.17: Boring Log for Soil Boring 9

RECORD OF SUBSURFACE EXPLORATION

Alt & Witzig Engineering, Inc.

CLIENT **Purdue University**
PROJECT NAME **Purdue HPLS Facility**
LOCATION **West Lafayette, Indiana**

Boring # **SB-10**
Alt & Witzig File No. **02LF0080**

DRILLING and SAMPLING INFORMATION

Date Started **7/2/2002**
Date Completed **7/2/2002**
Boring Method **HSA**

Hammer Wt. **140** lbs.
Hammer Drop **30** in.
Spoon Sampler OD **2** in.

STRATA ELEV.	SOIL CLASSIFICATION SURFACE ELEVATION 543.39	Depth Scale	Strata Depth	Sample No.	Sample Type	Sampler Graphics	Ground Water	Standard Penetration Test, N - Blows/foot	Qu - tsf Unconfined Compressive Strength	Pp - tsf Pocket Penetrometer	Moisture Content %	Remarks
								7				
				2	SS			18				
538.39				3	SS			21				
	Brown, Dry, Fine to Medium, SAND and Gravel	5		4	SS			20				
				5	SS			34				Caved at 6.0 feet
				6	SS			35				
533.39		10	10.5	7	SS		O	24				
				8	SS			23				
				9	SS			20				
528.39		15		10	SS			12				
	Brown, Wet, Coarse, SAND and Gravel			11	SS			25				
				12	SS			22				
				13	SS			34				
523.39		20	21.0	14	SS			33				
	Boring Terminated at 21 feet											

Boring Method
HSA - Hollow Stem Augers
CFA - Continuous Flight Auger
DC - Driving Casing
MD - Mud Drilling

GROUNDWATER
▽ At Completion ____ ft.
▼ After ____ hours ____ ft.
◯ Water on Rods **10.0** ft.

Sample Type
SS - Driven Split Spoon
ST - Pressed Shelby Tube
CA - Continuous Flight Auger
RC - Rock Core
CU - Cuttings

Figure D.18: Boring Log for Soil Boring 10

RECORD OF SUBSURFACE EXPLORATION

Alt & Witzig Engineering, Inc.

CLIENT **Purdue University**

PROJECT NAME **Purdue HPLS Facility**

LOCATION **West Lafayette, Indiana**

Boring # **SB-11**

Alt & Witzig File No. **02LF0080**

DRILLING and SAMPLING INFORMATION

Date Started **7/1/2002** Hammer Wt. **140** lbs.

Date Completed **7/1/2002** Hammer Drop **30** in.

Boring Method **HSA** Spoon Sampler OD **2** in.

STRATA ELEV.	SOIL CLASSIFICATION SURFACE ELEVATION 544.92	Depth Scale	Strata Depth	Sample No.	Sample Type	Sampler Graphics	Ground Water	Standard Penetration Test, N - Blows/foot	Qu - tsf Unconfined Compressive Strength	Pp - tsf Pocket Penetrometer	Moisture Content %	Remarks
	Brown Clayey SILT with Gravel and Brick (FILL)		0.5					16				
	Brown, Dry, Fine, SAND with Gravel		1.0	2	SS			8				
	Brown, Wet, Medium Coarse, SAND and Gravel		2.5	3	SS			6				
	Brown, Wet, Fine to Coarse, SAND and Gravel		4.0									
539.92		5		4	SS			7				
	Brown, Wet, Medium to Fine, SAND			5	SS			5				
			7.5									
	Brown Clayey SILT		8.5	6	SS			7				
534.92		10		7	SS			12				Caved at 10.0 feet
				8	SS		O	15				
				9	SS			14				
529.92	Gray, Moist, Clayey SILT	15		10	SS			18				
				11	SS			26				
				12	SS			38			14.5	
				13	SS			16		0.5	20.9	
524.92		20		14	SS			12	0.1	1.5	18.8	
			21.0									
	Boring Terminated at 21 feet											

Boring Method	GROUNDWATER	Sample Type
HSA - Hollow Stem Augers	▽ At Completion ft.	SS - Driven Split Spoon
CFA - Continuous Flight Auger	▼ After hours ft.	ST - Pressed Shelby Tube
DC - Driving Casing	O Water on Rods 11.5 ft.	CA - Continuous Flight Auger
MD - Mud Drilling		RC - Rock Core
		CU - Cuttings

Figure D.19: Boring Log for Soil Boring 11

RECORD OF SUBSURFACE EXPLORATION

Alt & Witzig Engineering, Inc.

CLIENT **Purdue University**
PROJECT NAME **Purdue HPLS Facility**
LOCATION **West Lafayette, Indiana**

Boring # **SB-12**
Alt & Witzig File No. **02LF0080**

DRILLING and SAMPLING INFORMATION

Date Started **7/1/2002**   Hammer Wt. **140** lbs.
Date Completed **7/1/2002**   Hammer Drop **30** in.
Boring Method **HSA**   Spoon Sampler OD **2** in.

STRATA ELEV.	SOIL CLASSIFICATION SURFACE ELEVATION 550.55	Depth Scale	Strata Depth	Sample No.	Sample Type	Sampler Graphics	Ground Water	Standard Penetration Test, N - Blows/foot	Qu - tsf Unconfined Compressive Strength	Pp - tsf Pocket Penetrometer	Moisture Content %	Remarks
	Brown Clayey SILT with Organics (topsoil)		0.4					15				
	Light Brown SAND		0.5									
	Brown Silty CLAY with Gravel		1.5	2	SS			52				
	Brown, Dry, Fine, SAND with Gravel		2.0	3	SS			21				
545.55	Brown, Dry, Fine, SAND	5	5.5	4	SS			26				
	Brown, Moist, SILT with a Trace of Clay		7.0	5	SS			28				
				6	SS			19				
540.55		10		7	SS			24				
				8	SS			26				
				9	SS			18				
	Gray, Moist, Clayey SILT			10	SS			20				
535.55		15		11	SS			47		2.5	20.9	
				12	SS			12		0.5	19.2	
				13	SS			16			19.3	
530.55		20	21.0	14	SS			15			18.8	
	Boring Terminated at 21 feet											

Boring Method
HSA - Hollow Stem Augers
CFA - Continuous Flight Auger
DC - Driving Casing
MD - Mud Drilling

GROUNDWATER
▽ At Completion **Dry** ft.
▼ After ____ hours ____ ft.
○ Water on Rods **Dry** ft.

Sample Type
SS - Driven Split Spoon
ST - Pressed Shelby Tube
CA - Continuous Flight Auger
RC - Rock Core
CU - Cuttings

Figure D.20: Boring Log for Soil Boring 12

Appendix E

INDOT Design Manual: Selected Recommendations for Integral abutment Bridges

Selections from INDOT Design Manual:

67-1.01 Integral End Bent

67-1.01(01) General
Traditionally, bridges have been designed with expansion joints or other structural releases that allow the superstructure to expand and contract relatively freely with changing temperatures and other geometric effects. Integral end bents eliminate expansion joints in the bridge deck, which reduce both the initial construction costs and subsequent maintenance costs. The use of integral end bents is very effective in accommodating the horizontal seismic forces of Seismic Performance Zone 1 or 2. Minimum support-length requirements need not be investigated for an integral-end-bent bridge.

67-1.01(02) Usage for a New Structure
Integral end bents should be used for a new structure in accordance with the geometric limitations provided in Figure 67-1A.

67-1.01(03) Usage for an Existing Structure
For an existing bridge without integral end bents, the design criteria shown in Figure 67-1A should be used when evaluating the conversion to an integral-end-bent structure. For additional information, see Section 72-3.04.

67-1.01(04) General Design Criteria
The following requirements must be satisfied.
1. Backfill. Each integral end bent for a beam or girder type superstructure should be backfilled with coarse aggregate, under the pay item, aggregate for end bent backfill. Each reinforced concrete slab bridge end bent should be backfilled with flowable backfill material. The INDOT *Standard Drawings* provide backfill details for both concrete slab and beam or girder type structures. The total estimated quantity of flowable backfill or aggregate for end bent backfill should be shown on the Layout Sheet.

2. Bridge Approach. A reinforced-concrete bridge approach, anchored to the end bent with epoxy coated #5 bars spaced at 1'-0" centers, should be used at each integral end bent regardless of the traffic volume. The bars should extend out of the pavement ledge as shown in Figures 67-1B and 67-1C. Two layers of polyethylene sheeting should be placed between the reinforced-concrete bridge approach and the subgrade. A rigid reinforced-concrete bridge approach is necessary to prevent compaction of the backfill behind the end bent.

3. Bridge-Approach Joint. A 2-ft wide terminal joint or pavement relief joint should be used at the roadway end of the reinforced-concrete bridge approach if a portion of the adjacent pavement section is concrete. A joint is not required if the entire adjacent pavement section is asphalt.

4. Wingwall Configuration. Wingwalls should extend parallel to the centerline of roadway. This configuration reduces the loads imposed upon the bridge structure due to passive earth pressure from the end bent backfill.

5. Wingwall Connection. The connection between the wingwall and the end bent cap should be treated as described below. The wingwall should not extend more than 10 ft behind the rear face of the cap. If longer extensions are necessary, force effects in the connection between the wingwall and cap, and in the wingwall itself, should be investigated, and adequate reinforcing steel should be provided.

6. Interior Diaphragms for Steel Structure. Where steel beams or girders are used, an interior diaphragm should be placed within 10 ft of the end support to provide beam stability prior to and during the deck pour.

67-1.01(05) Superstructure and Interior Substructure Design Criteria

Although each end of the superstructure is monolithically attached to an integral end bent, the rotation permitted by the piles is sufficiently high, and the attendant end moment sufficiently low, to justify the assumption of a pinned-end condition for design. The following design assumptions should be considered.

1. Ends. The ends of the superstructure are free to rotate and translate longitudinally.

2. Passive Earth Pressure. The restraining effect of passive earth pressure behind the end bents should be neglected when considering superstructure longitudinal force distribution to the interior piers.

3. Interior Pile Bents. All longitudinal forces from the superstructure are to be disregarded when designing an interior pile bent or a thin-wall pier on a single row of piles.

4. Shears and Moments. Force effects in the cap beam may be determined on the basis of a linear distribution of vertical pile reactions. For minimum reinforcement, the cap should be treated as a structural beam.

67-1.01(06) Design Requirements
An integral end bent may be constructed using either of the following methods.

1. Method A. The superstructure beams are placed on and attached directly to the end-bent piling. The entire end bent is then poured at the same time as the superstructure deck. This is the preferred method.

2. Method B. The superstructure beams are set in place and anchored to the previously cast in-place end-bent cap. The concrete above the previously cast-in-place cap should be poured at the same time as the superstructure deck.

Optional construction joints may be placed in the end bent cap to facilitate construction. The optional joint below the bottom of beam may be used regardless of bridge length. The optional construction joint at the pavement-ledge elevation shown in Figures 67-1B and 67-1C allows the contractor to pour the reinforced-concrete bridge approach with the bridge deck. Regardless of the method used, the end bent should be in accordance with the following:

1. Width. The width should not be less than 2.5 ft.

2. Cap Embedment. The embedment of piles into the cap should be 2 ft. The embedded portion should not be wrapped with polystyrene.

3. Beam Attachment. The beams should be physically attached to the piling if using Method A, or to the cast-in-place cap if using Method B.

4. Beam Extension. The beams should extend at least 1.67 ft into the bent, as measured along the centerline of the beam.

5. Concrete Cover. Concrete cover beyond the farthest most edge of the beam at the rear face of the bent should be at least 4 in. This minimum cover should also apply to the pavement ledge area. The top flanges of steel beams and prestressed I-beams may be coped to meet this requirement. Where the 4-in. minimum cover cannot be maintained within a 2.5-ft cap, the cap should be widened.

6. Stiffener Plates. Steel beams or girders should have 5/8-in. stiffener plates welded to both sides of their webs and to the flanges over the supports to anchor the beams into the concrete. A minimum of three holes should be provided through the webs of steel beams or girders. Two holes should be provided through prestressed I-beam webs near the front face of the bent, to allow #6 bars to be inserted to further anchor the beam to the cap. Box beams should have two threaded inserts placed in each side face for anchorage of #7 threaded bars.

7. Reinforcement. The minimum size of stirrups should be #6 spaced at a maximum of 1'- 0". Longitudinal cap reinforcing should be #7 at 1'-0" maximum spacing along both faces of the bent. All reinforcing steel should be epoxy coated.

8. Corner Bars. Corner bars should extend from the rear face of the cap into the top of the deck at not more than 1'-0" spacing as shown in Figures 67-1B and 67-1C.

67-1.01(07) Plan Details
Section 62-3.0 includes suggested details for integral end bents with a reinforced concrete slab bridge. Figures 67-1B and 67-1C show suggested details for integral end bents with a structural members bridge. Other reinforcing and connection details should be considered and used where they are structurally sound and afford a definite advantage if compared to those shown in the Figures.

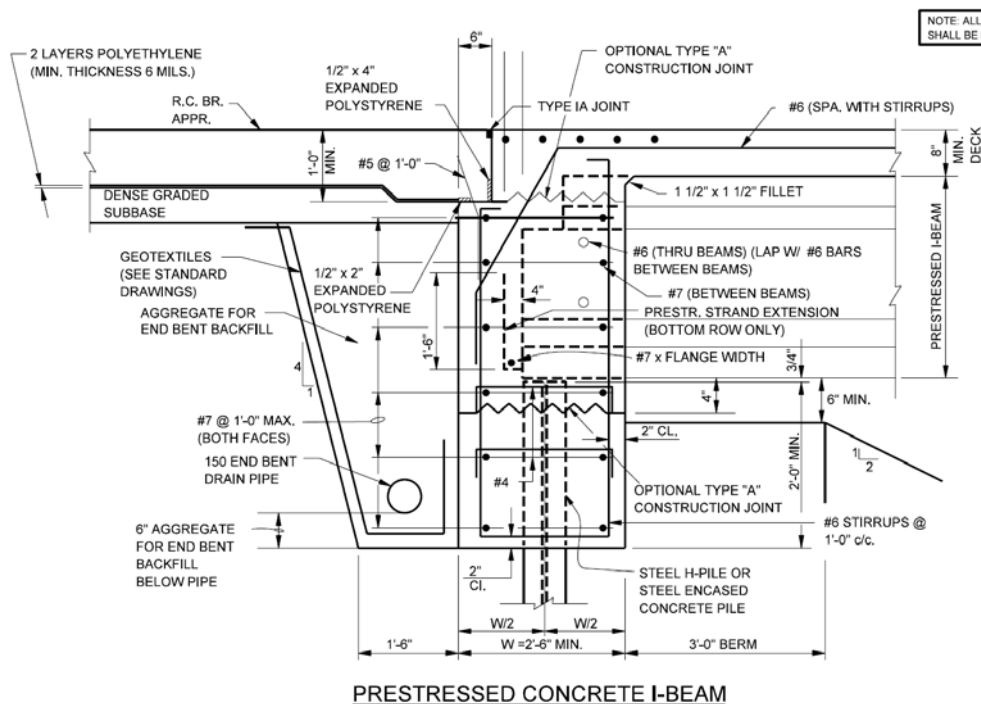| Structure Type	Highway Alignment Across Bridge	Maximum Skew	Maximum Bridge Length	Maximum to Zero Point
Reinforced Concrete Slab	No Restrictions	No Restrictions	500 ft *	250 ft *
Structural Steel	Tangent Only **	30 deg ***	500 ft *	250 ft *
Prestressed Concrete	No Restrictions	30 deg ***	500 ft *	250 ft *

Notes:

*   *The maximum length indicated may be increased, subject to approval by the Structural Services Office manager, if a rational analysis of induced pile loads indicates that the piles are not overloaded. Two rational analysis methods are described in the Iowa Department of Transportation report,* Pile Design and Tests for Integral Abutment Bridges*. See Section 67-1.03(03) for an alternative analysis in lieu of the above criteria.*

**   *The horizontal alignment may be curved as long as curved beams are not used.*

***   *A skew of greater than 30 deg but equal to or less than 45 deg will be permitted if the maximum bridge length does not exceed 250 ft, or if the maximum to zero point does not exceed 125 ft.*
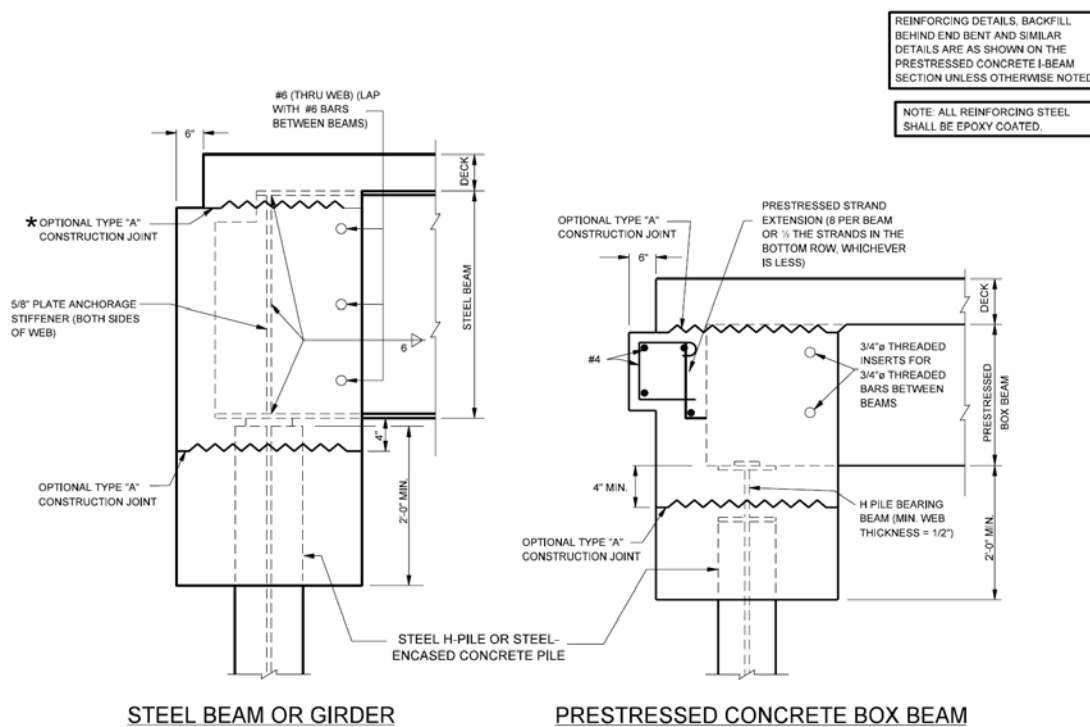
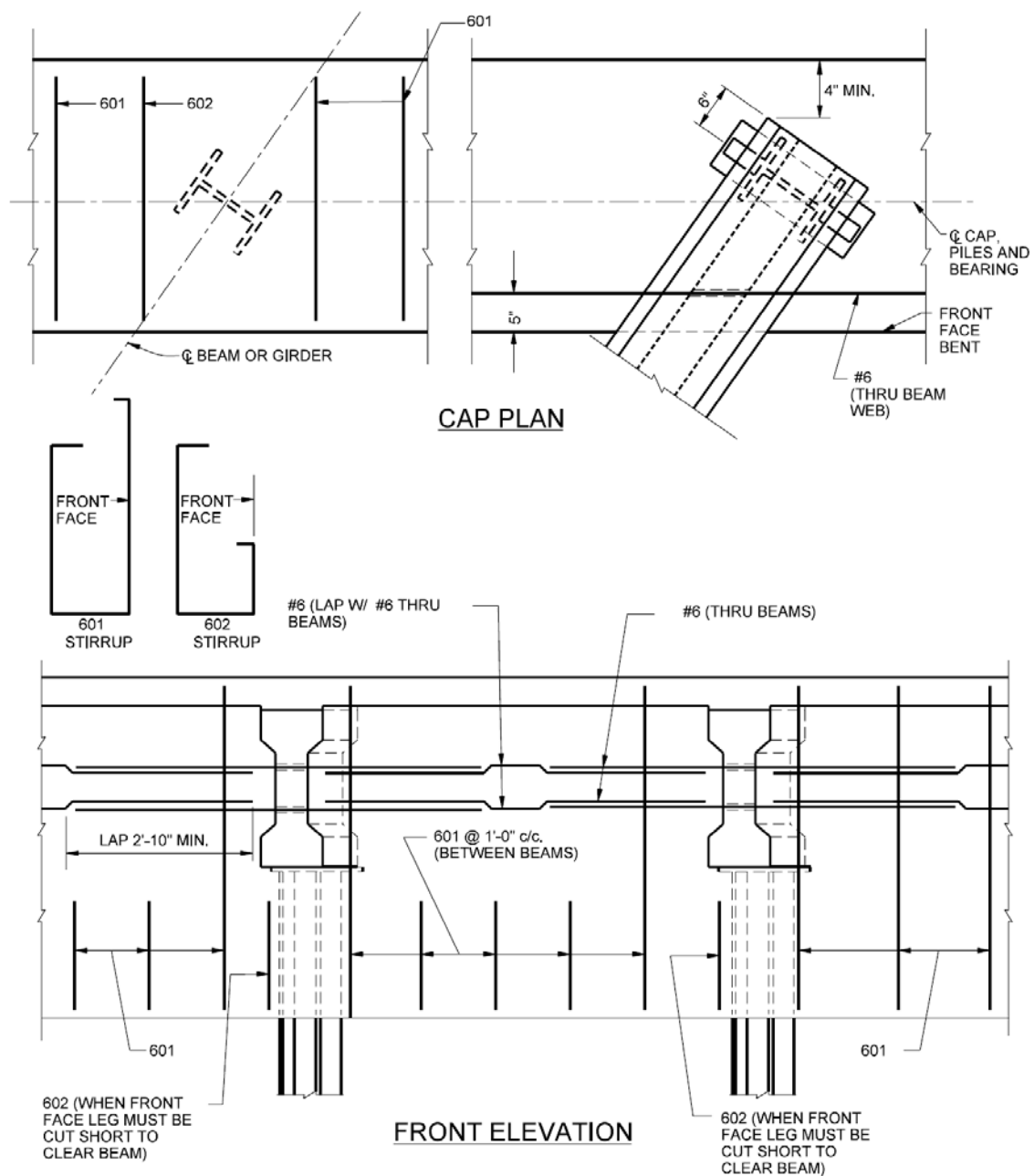**USE OF INTEGRAL END BENTS**

Figure 67-1A

PRESTRESSED CONCRETE I-BEAM

SUGGESTED INTEGRAL END BENT DETAILS
(Beams Attached Directly to Piling, Method A)

Figure 67-1B
(Page 1 of 4)

REINFORCING DETAILS, BACKFILL BEHIND END BENT AND SIMILAR DETAILS ARE AS SHOWN ON THE PRESTRESSED CONCRETE I-BEAM SECTION UNLESS OTHERWISE NOTED.

NOTE: ALL REINFORCING STEEL SHALL BE EPOXY COATED.

#6 (THRU WEB) (LAP WITH #6 BARS BETWEEN BEAMS)

6"

DECK

STEEL BEAM

★ OPTIONAL TYPE "A" CONSTRUCTION JOINT

5/8" PLATE ANCHORAGE STIFFENER (BOTH SIDES OF WEB)

6

OPTIONAL TYPE "A" CONSTRUCTION JOINT

4"

2'-0" MIN.

STEEL H-PILE OR STEEL-ENCASED CONCRETE PILE

STEEL BEAM OR GIRDER

OPTIONAL TYPE "A" CONSTRUCTION JOINT

6"

PRESTRESSED STRAND EXTENSION (8 PER BEAM OR ⅓ THE STRANDS IN THE BOTTOM ROW, WHICHEVER IS LESS)

DECK

#4

3/4"ø THREADED INSERTS FOR 3/4"ø THREADED BARS BETWEEN BEAMS

PRESTRESSED BOX BEAM

4" MIN.

OPTIONAL TYPE "A" CONSTRUCTION JOINT

H PILE BEARING BEAM (MIN. WEB THICKNESS = 1/2")

2'-0" MIN.

PRESTRESSED CONCRETE BOX BEAM

SUGGESTED INTEGRAL END BENT DETAILS
(Beams Attached Directly to Piling, Method A)

Figure 67-1B
(Page 2 of 4)

601

601 602

4" MIN.

6"

C CAP,
PILES AND
BEARING

5"

FRONT
FACE
BENT

#6
(THRU BEAM
WEB)

C BEAM OR GIRDER

CAP PLAN

FRONT
FACE

FRONT
FACE

601
STIRRUP

602
STIRRUP

#6 (LAP W/ #6 THRU
BEAMS)

#6 (THRU BEAMS)

LAP 2'-10" MIN.

601 @ 1'-0" c/c.
(BETWEEN BEAMS)

601

601

602 (WHEN FRONT
FACE LEG MUST BE
CUT SHORT TO
CLEAR BEAM)

FRONT ELEVATION

602 (WHEN FRONT
FACE LEG MUST BE
CUT SHORT TO
CLEAR BEAM)

SUGGESTED INTEGRAL END BENT DETAILS
(Beams Attached Directly to Piling, Method A)

Figure 67-1B
(Page 3 of 4)

CONCRETE BOX BEAM
END VIEW

CONCRETE BOX BEAM
SIDE VIEW

CONCRETE I-BEAM
SIDE VIEW

CONCRETE I-BEAM
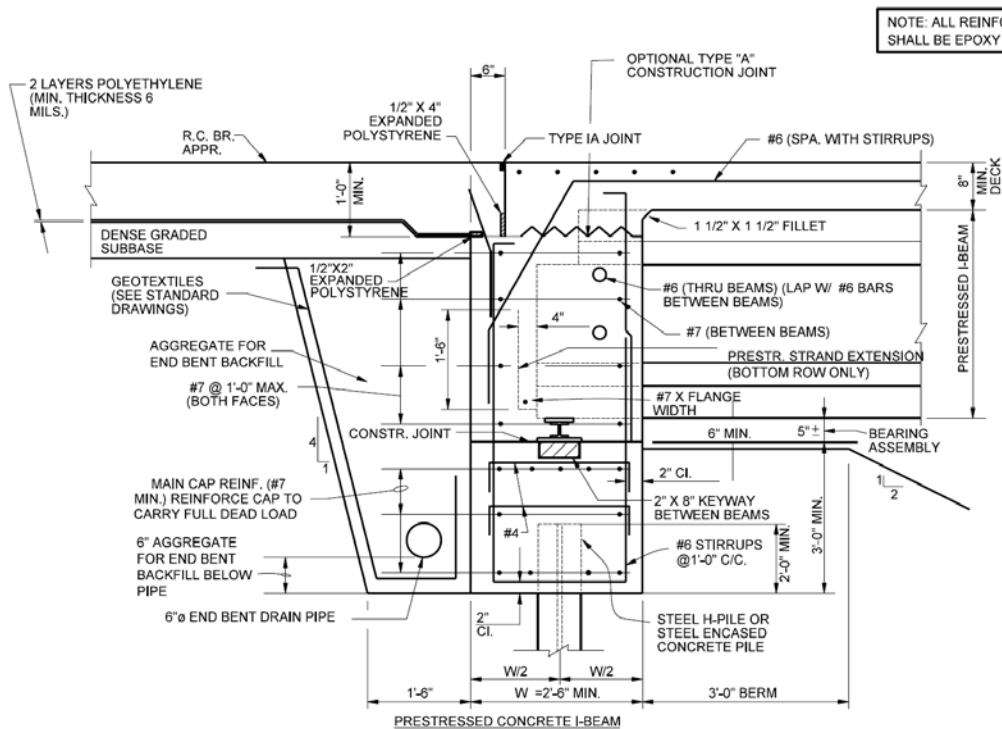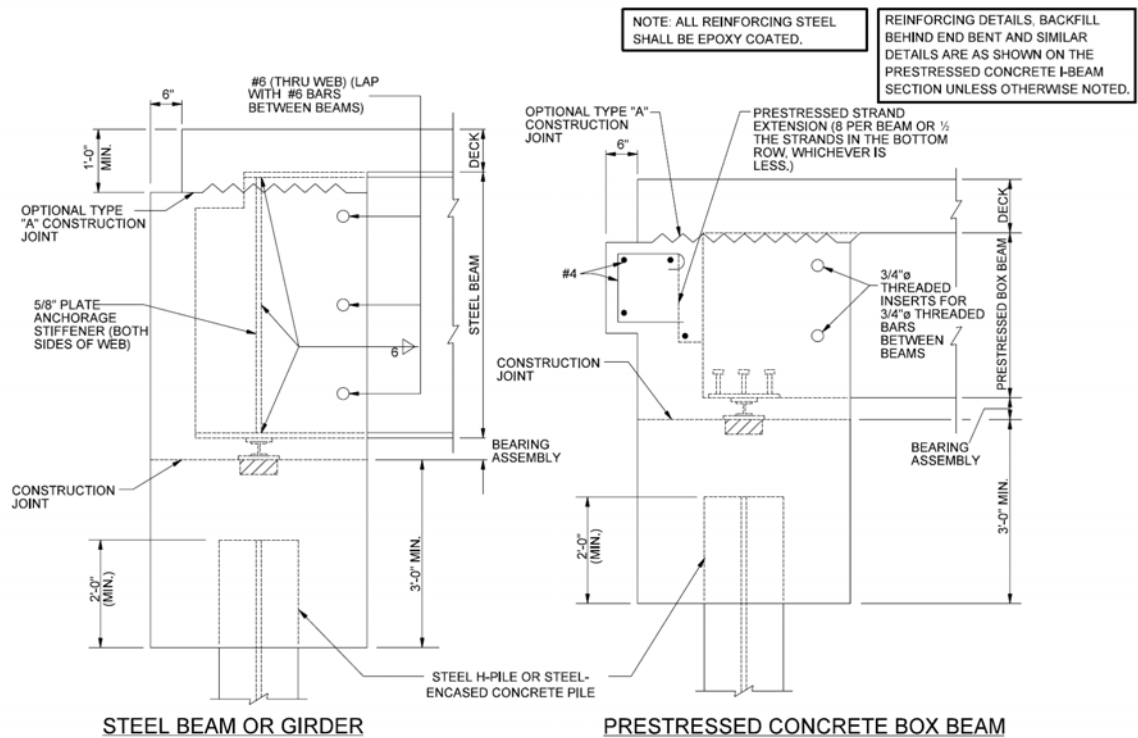END VIEW

STEEL I-BEAM
END VIEW

SUGGESTED INTEGRAL END BENT DETAILS
(Beams Attached Directly to Piling, Method A)
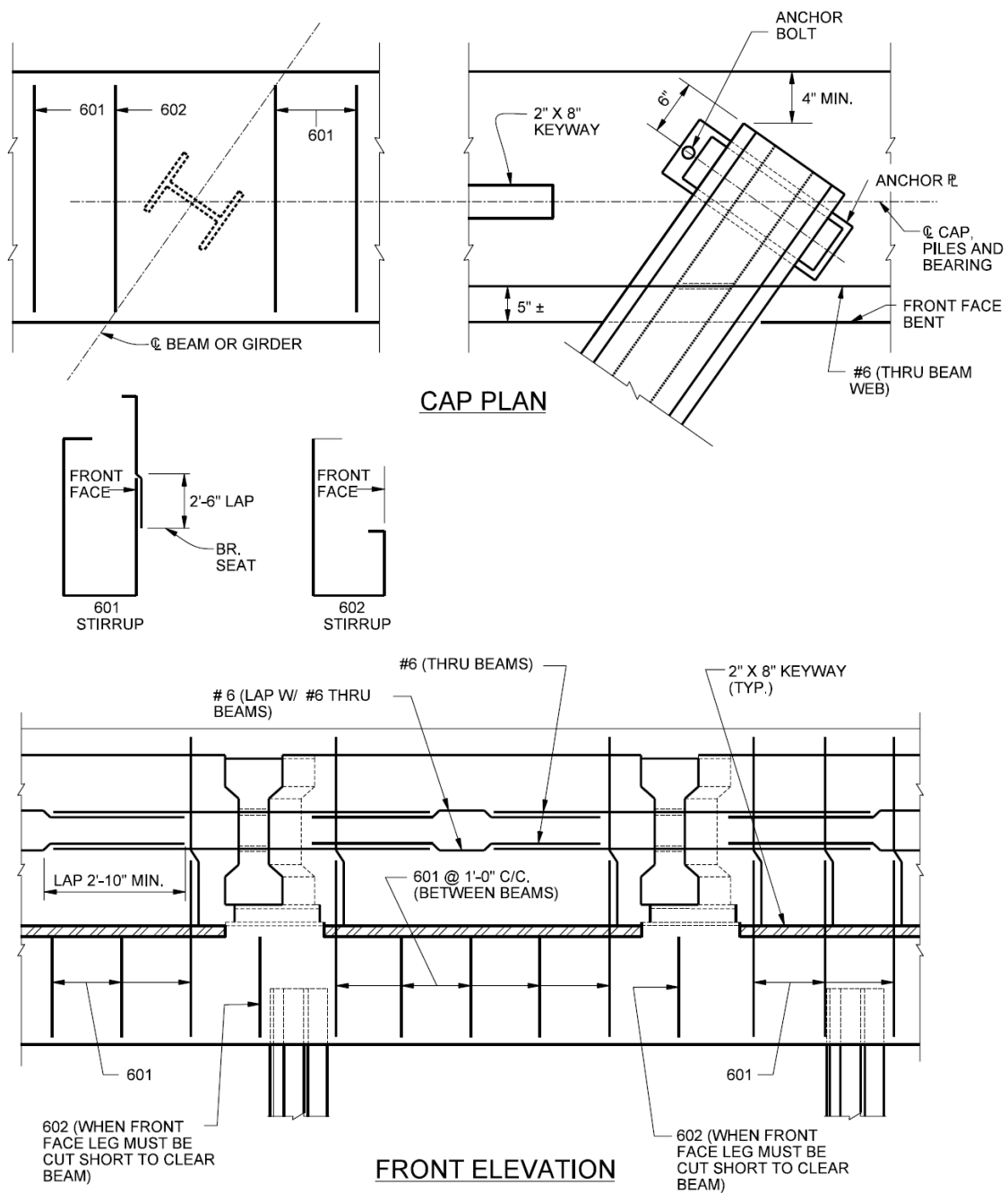
Figure 67-1B
(Page 4 of 4)

SUGGESTED INTEGRAL END BENT DETAILS
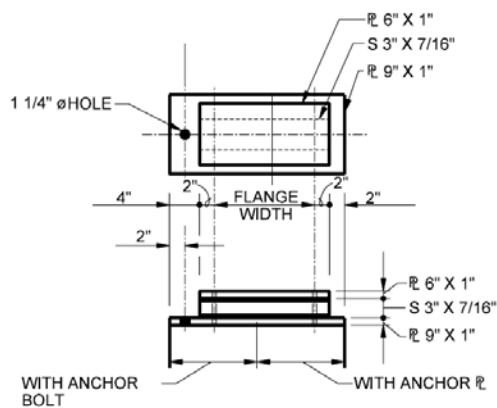(Beams Attached to Concrete Cap, Method B)

Figure 67-1C
(Page 1 of 4)

SUGGESTED INTEGRAL END BENT DETAILS
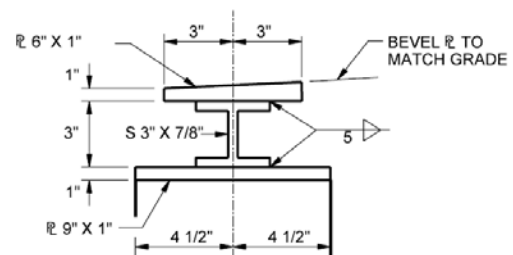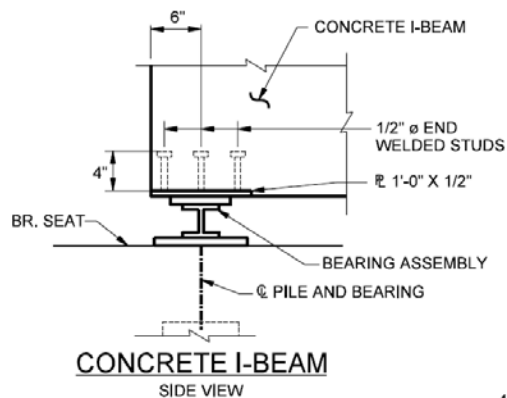(Beams Attached to Concrete Cap, Method B)
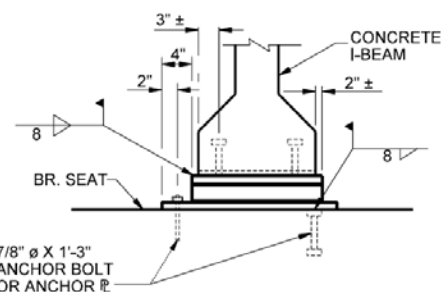
Figure 67-1C
(Page 2 of 4)

ANCHOR
BOLT

4" MIN.

6"

2" X 8"
KEYWAY

ANCHOR ℄

℄ CAP,
PILES AND
BEARING

℄ BEAM OR GIRDER

5" ±

FRONT FACE
BENT

#6 (THRU BEAM
WEB)

CAP PLAN

FRONT
FACE

2'-6" LAP

BR.
SEAT

FRONT
FACE

601
STIRRUP

602
STIRRUP

#6 (THRU BEAMS)

2" X 8" KEYWAY
(TYP.)

6 (LAP W/ #6 THRU
BEAMS)

LAP 2'-10" MIN.

601 @ 1'-0" C/C,
(BETWEEN BEAMS)

601

601

602 (WHEN FRONT
FACE LEG MUST BE
CUT SHORT TO CLEAR
BEAM)

602 (WHEN FRONT
FACE LEG MUST BE
CUT SHORT TO CLEAR
BEAM)

FRONT ELEVATION

SUGGESTED INTEGRAL END BENT DETAILS
(Beams Attached to Concrete Cap, Method B)

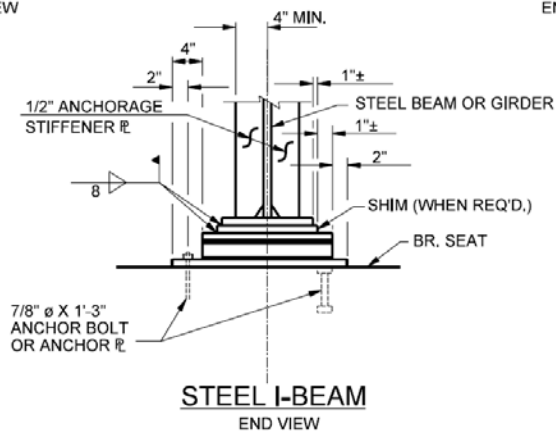Figure 67-1C
(Page 3 of 4)

BEARING ASSEMBLY
TOP / SIDE VIEW

BEARING ASSEMBLY
END VIEW

CONCRETE I-BEAM
SIDE VIEW

CONCRETE I-BEAM
END VIEW

STEEL I-BEAM
END VIEW

SUGGESTED INTEGRAL END BENT DETAILS
(Beams Attached Directly to Concrete Cap, Method B)

Figure 67-1C
(Page 4 of 4)